



National Library  
of Canada

Bibliothèque nationale  
du Canada

Canadian Theses Service

Service des thèses canadiennes

Ottawa, Canada  
K1A 0N4

## NOTICE

The quality of this microform is heavily dependent upon the quality of the original thesis submitted for microfilming. Every effort has been made to ensure the highest quality of reproduction possible.

If pages are missing, contact the university which granted the degree.

Some pages may have indistinct print especially if the original pages were typed with a poor typewriter ribbon or if the university sent us an inferior photocopy.

Reproduction in full or in part of this microform is governed by the Canadian Copyright Act, R.S.C. 1970, c. C-30, and subsequent amendments.

## AVIS

La qualité de cette microforme dépend grandement de la qualité de la thèse soumise au microfilmage. Nous avons tout fait pour assurer une qualité supérieure de reproduction.

S'il manque des pages, veuillez communiquer avec l'université qui a conféré le grade.

La qualité d'impression de certaines pages peut laisser à désirer, surtout si les pages originales ont été dactylographiées à l'aide d'un ruban usé ou si l'université nous a fait parvenir une photocopie de qualité inférieure.

La reproduction, même partielle, de cette microforme est soumise à la Loi canadienne sur le droit d'auteur, SRC 1970, c. C-30, et ses amendements subséquents.

UNIVERSITY OF ALBERTA

HORIZONTAL WELL STRATEGIES FOR STEAMFLOODING OIL  
FORMATIONS WITH A COMMUNICATING WATER ZONE

BY

HELEN LI-HUA CHANG



A THESIS

SUBMITTED TO THE FACULTY OF GRADUATE STUDIES AND RESEARCH  
IN PARTIAL FULFILLMENT OF THE REQUIREMENTS FOR THE DEGREE  
OF MASTER OF SCIENCE

IN

PETROLEUM ENGINEERING

DEPARTMENT OF MINING, METALLURGICAL AND PETROLEUM  
ENGINEERING

EDMONTON, ALBERTA

FALL, 1990



National Library  
of Canada

Bibliothèque nationale  
du Canada

Canadian Theses Service    Service des thèses canadiennes

Ottawa, Canada  
K1A 0N4

The author has granted an irrevocable non-exclusive licence allowing the National Library of Canada to reproduce, loan, distribute or sell copies of his/her thesis by any means and in any form or format, making this thesis available to interested persons.

The author retains ownership of the copyright in his/her thesis. Neither the thesis nor substantial extracts from it may be printed or otherwise reproduced without his/her permission.

L'auteur a accordé une licence irrévocable et non exclusive permettant à la Bibliothèque nationale du Canada de reproduire, prêter, distribuer ou vendre des copies de sa thèse de quelque manière et sous quelque forme que ce soit pour mettre des exemplaires de cette thèse à la disposition des personnes intéressées.

L'auteur conserve la propriété du droit d'auteur qui protège sa thèse. Ni la thèse ni des extraits substantiels de celle-ci ne doivent être imprimés ou autrement reproduits sans son autorisation.

ISBN 0-315-64988-7

UNIVERSITY OF ALBERTA

RELEASE FORM

NAME OF AUTHOR: Helen Li-Hua Chang

TITLE OF THESIS: Horizontal Well Strategies for Steamflooding Oil Formations With a Communicating Water Zone

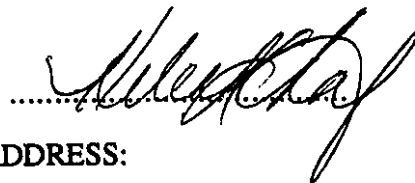
DEGREE FOR WHICH THESIS WAS PRESENTED : MASTER OF SCIENCE

YEAR THE DEGREE WAS GRANTED : FALL, 1990

Permission is hereby granted to the UNIVERSITY OF ALBERTA LIBRARY to reproduce single copies of this thesis and to lend or sell such copies for private, scholarly or scientific research purposes only.

The author reserves other publication rights, and neither the thesis nor extensive extracts from it may be printed or otherwise reproduced without the author's written permission.

(SIGNED) .....



PERMANENT ADDRESS:

31426 Springhill Place

Clearbrook, B.C., Canada

V2T 4K1

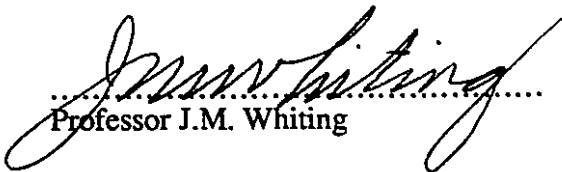
DATED :

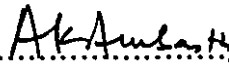
*August 7, 1990*

UNIVERSITY OF ALBERTA  
FACULTY OF GRADUATE STUDIES AND RESEARCH

The undersigned certify that they have read and recommend to the Faculty of Graduate Studies and Research, for acceptance, a thesis entitled HORIZONTAL WELL STRATEGIES FOR STEAMFLOODING OIL FORMATIONS WITH A COMMUNICATING WATER ZONE submitted by HELEN LI-HUA CHANG in partial fulfillment of the requirements for the degree of MASTER OF SCIENCE in PETROLEUM ENGINEERING.

  
.....  
Professor S.M. Farouq Ali (Supervisor)

  
.....  
Professor J.M. Whiting

  
.....  
Professor A.K. Ambastha

  
.....  
Professor J.D. Scott (External Examiner)

  
.....  
Professor W.S. Tortike

DATED : June 7, 90.....

*To My Parents for their Boundless Support  
and Faith in Me*

## Abstract

In Alberta and Saskatchewan, many heavy oil formations have a communicating high water saturation zone, which makes it difficult to employ steamflooding as an oil recovery method. In view of the remarkable success of steam injection for heavy oil recovery, it is important to seek techniques for using steam in such marginal reservoirs. This was the underlying objective of the research reported here.

The approach employed was essentially experimental, with theoretical interpretations using classical methods. A heavy oil reservoir in Saskatchewan, the Aberfeldy reservoir in Lloydminster, was selected as the prototype for the scaled model steamflooding experiments. One-quarter of an eight hectare five-spot was constructed using low pressure scaling principles.

Base case waterfloods and steamfloods were established for reference. Gas and solvent additives were investigated for homogeneous and bottom water formations, with a view to divert steam early from the water zone. The effect of solvent slug size on recovery was also investigated for a thin bottom water case.

Steam injection experiments were conducted in four combinations of vertical and horizontal wells (injectors and producers) using two bottom water thicknesses in the one-quarter of a five-spot. The use of a small volume of solvent with steam was also examined.

Temperature measurements and theoretical analyses were used to interpret the results obtained. The experimental findings suggest that there is an optimal bottom water thickness, below which formation heating by conduction is far more useful than use of gas or solvent additives. An optimal bottom water thickness value was determined to be between 7-10% of gross formation thickness. The application of horizontal injectors and producers in marginal reservoirs subjected to steamfloods seems to be the best strategy in the light of this work.

## **Acknowledgements**

Extreme gratitude is expressed towards Dr. S.M. Farouq Ali for his endless support and overwhelming generosity. His expertise and guidance has made this study an immensely rewarding experience. It has been a great privilege and honour to have studied under such a distinguished individual. The memories of the time together at the University will always be cherished by the author.

Special thanks are extended to Mr. Rex Matthias for his invaluable assistance in conducting the experiments, and to Mrs. Sara Thomas for her continual support and words of encouragement.

Thanks are also expressed to the technical staff of the Mining, Metallurgical and Petroleum Engineering Department for their expertise and advice, particularly, Mr. Bob Smith, Mr. Rob Stefaniuk, Mr. Jacques Gibeau and Mr. John Czuroski.

Sincere appreciation is extended to Dr. K.W.A. Miller, Mr. Jon Peggs and Mr. T.R. Vonde, Husky Oil Operations Ltd., for providing the information on the Aberfeldy reservoir, which served as the prototype.

The financial assistance of CANMET/Energy, Mines and Resources is gratefully acknowledged, especially, Dr. Albert E. George for his technical assistance and ideas.



## Table of Contents

<u>Chapter</u>	<u>Page</u>
1. Introduction .....	1
2. Statement of the Problem .....	2
Experimental Objectives .....	2
Theoretical Objectives .....	2
3. Literature Review .....	3
Physical Model Studies of Steamflooding .....	3
Unscaled Physical Models .....	3
Scaled Physical Models .....	4
High Pressure Models .....	4
Low Pressure Models .....	6
Steamflooding in the Presence of Bottom Water .....	7
Horizontal Well Applications .....	8
Background .....	9
The Productivity of Horizontal Wells .....	11
Homogeneous and Isotropic Reservoirs .....	11
The Influence of Anisotropy .....	11
Water Coning and Cresting .....	12
Well Flow Behaviour .....	14
Early Time Flow Geometry of a Horizontal Well .....	14
Late Time Flow Geometry of a Horizontal Well .....	17
Gravity Drainage .....	19
Well Patterns .....	21
Applications of Horizontal Wells to Steamflood Processes .....	24
Recovery Using Solvents in Conjunction with Steam .....	25

4. Scaling Parameters and Calculations .....	27
Development of Scaling Parameters for the Low Pressure Model .....	27
Unscaled Parameters .....	27
Scaling Procedures .....	29
Calculation of Parametric Values for the Aberfeldy Low Pressure Model .....	32
Prototype and Model Correlations .....	32
Length Scale Selection .....	33
Model Pressure Scaling .....	33
Model Temperature Scaling .....	37
Time Scale Determination .....	38
Flow Rate Scaling .....	39
Scaling of Steam Quality .....	40
Scaling of Model Oil Viscosity .....	42
Scaling of Model Permeability .....	42
Scaling of Vertical Wells .....	43
Derivation of Scaling Criteria for Steam Injection with Gas as an Additive .....	45
5. Experimental Apparatus and Procedure .....	50
Experimental Apparatus .....	50
Physical Model .....	50
Vertical and Horizontal Wells .....	55
Porous Media .....	57
Model Cart, Rail System and Cold Storage Compartment .....	57
Fluid Injection System .....	57
Fluid Collection System .....	58
Data Acquisition System .....	62
Model Fluids .....	65
Selection of Model Oil for the Aberfeldy Reservoir .....	65

Solvent Selection .....	65
Preparation of the Experimental Model .....	67
Model Packing Procedure .....	67
Fluid Saturation Process .....	69
Preparation of a Bottom Water Model .....	71
Creation of a Gas Zone .....	71
Conducting Experiments in the Model .....	72
Waterflood .....	72
Steamflood in a Homogeneous Model .....	73
Solvent-Steamflood .....	73
Bottom Water Runs .....	73
Gas Injection Runs .....	73
Apparatus Cleanup .....	74
Data Analysis .....	74
6. Discussion .....	76
Presentation of Results .....	76
Steam Quality .....	81
Steamfloods in a Homogeneous Model .....	83
Waterflood followed by a Steamflood .....	91
Gas Injection Runs .....	91
Prior to a Conventional Waterflood .....	95
Prior to a Hot Waterflood .....	95
Effect of a Gas Zone on Steamflood Recovery .....	95
Thick Bottom Water .....	99
Thin Bottom Water .....	99
Steamflood in the Presence of Bottom Water .....	103
Solvent-Steamfloods .....	103

Results of Solvent-Steamfloods .....	108
Horizontal-Vertical Well Strategies .....	117
Horizontal Producer-Vertical Injector .....	119
Horizontal Producer-Horizontal Injector .....	124
Vertical Producer-Horizontal Injector .....	124
Comparison of the Reservoir Situations .....	133
Homogeneous Case .....	133
Thin Bottom Water .....	135
Thick Bottom Water .....	135
Application of Horizontal-Vertical Well Strategies in Solvent-	
Steamfloods .....	138
Summary of Horizontal-Vertical Well Strategies .....	144
Reproducibility of Results .....	144
7. Conclusions .....	147
8. Recommendations For Further Studies .....	149
References.....	151
Appendix A .....	155
Appendix B .....	160
Appendix C .....	176
Appendix D .....	180
Appendix E .....	203

## List of Tables

<u>Table</u>	<u>Page</u>
3.1 List of Horizontal Well Projects for Heavy Oil Reservoirs.....	10
4.1 Scaling Parameters for Steam Processes .....	30
4.2 Scaling Parameters for the Aberfeldy Reservoir.....	34
4.3 Prototype and Model Scaling Values.....	36
4.4 Scaling Set for Steam Processes.....	44
4.5 Constraints and Constitutive Relationships.....	46
4.6 Similarity Groups from Inspectional Analysis.....	48
5.1 Temperature vs. Oil Viscosity Data for Prototype and Ideal Model Oil.....	65
6.1 Summary of Experiments Conducted.....	78
6.2 Data Comparison with Run 79 and Run 67 (Ref.46) .....	86
E.1 Run 70A: Waterflood prior to a Steamflood in a Homogeneous Model .....	204
E.2 Run 70B: Steamflood following a Waterflood in a Homogeneous Model.....	205
E.3 Run 71: Gas Injection followed by a Waterflood in a Homogeneous Model.....	206
E.4 Run 72A: Waterflood in a Homogeneous Model.....	207
E.5 Run 72B: N <sub>2</sub> Injection followed by Hot Water Injection in a Homogeneous Model which was Initially Waterflooded.....	208
E.6 Run 73: Steamflood in a Homogeneous Model.....	209
E.7 Run 74: Steam Injection of a Homogeneous Model using a Vertical Injector and a Horizontal Producer .....	210
E.8 Run 75: Steam Injection of a Homogeneous Model using a Horizontal Injector and a Horizontal Producer .....	211
E.9 Run 76: Steam Injection of a Homogeneous Model using a Horizontal Injector and a Vertical Producer.....	212
E.10 Run 77: Steam Injection of a Homogeneous Model using a Vertical Injector and a Vertical Producer.....	213
E.11 Run 78: Solvent-Steamflood in a Bottom Water Model.....	214

E.12	Run 78: Solvent-Steamflood in a Homogeneous Model.....	215
E.13	Run 82: Solvent-Steamflood in a Bottom Water Model.....	216
E.14	Run 83: Solvent-Steamflood in a Bottom Water Model.....	217
E.15	Run 84: Solvent-Steamflood in a Bottom Water Model.....	218
E.16	Run 85: Continuous Steamflood in a Bottom Water Model .....	219
E.17	Run 86: Steam Injection of a Homogeneous Model using a Vertical Injector and a Horizontal Producer .....	220
E.18	Run 87: Steam Injection of a Bottom Water Model using a Vertical Injector and a Horizontal Producer .....	221
E.19	Run 90: Steam Injection of a Bottom Water Model using a Vertical Injector and a Vertical Producer.....	222
E.20	Run 91: Solvent-Steamflood in a Bottom Water Model using a Vertical Injector and a Horizontal Producer .....	223
E.21	Run 92: Solvent-Steamflood in a Bottom Water Model using a Horizontal Injector and a Horizontal Producer .....	224
E.22	Run 93: Solvent-Steamflood in a Bottom Water Model using a Horizontal Injector and a Vertical Producer.....	225
E.23	Run 94: Solvent-Steamflood in a Bottom Water Model using a Vertical Injector and a Vertical Producer.....	226
E.24	Run 95: Steam Injection of a Thick Bottom Water Model subsequent to N <sub>2</sub> Gas Injection .....	227
E.25	Run 96: Steam Injection of a Thin Bottom Water Model subsequent to N <sub>2</sub> Gas Injection .....	228
E.26	Run 97: Steam Injection of a Bottom Water Model using a Vertical Injector and a Horizontal Producer .....	229
E.27	Run 98: Steam Injection of a Bottom Water Model using a Horizontal Injector and a Horizontal Producer .....	230
E.28	Run 99: Steam Injection of a Bottom Water Model using a Horizontal Injector and a Vertical Producer.....	231
E.29	Run 100: Steam Injection of a Bottom Water Model using a Vertical Injector and a Vertical Producer.....	232
E.30	Run 101: Steam Injection of a Bottom Water Model using a Horizontal Injector and a Horizontal Producer .....	233

E.31	Run 102: Steam Injection of a Bottom Water Model using a Horizontal Injector and a Vertical Producer.....	234
E.32	Run 104: A Continuous Steamflood in a Homogeneous Model .....	235
E.33	Run 105A: A Continuous Waterflood in a Homogeneous Model .....	236
E.34	Run 105B: A Continuous Steamflood in a Homogeneous Model following a Waterflood (Run 105A).....	237
E.35	Run 106: Solvent-Steamflood in a Bottom Water Model using a Horizontal Injector and Horizontal Producer (Solvent Injected from a Horizontal Well) .....	238
E.36	Run 107: A Continuous Steamflood in a Homogeneous Model .....	239

## List of Figures

<b>Figure</b>	<b>Page</b>
3.1 Water Coning Toward a Vertical Well and Cresting Toward a Horizontal Well.....	13
3.2 Schematic of Potential Flow to a Horizontal Well.....	15
3.3(a) Intermediate-Time Linear Flow.....	18
3.3(b) Late-Intermediate-Time Linear Flow.....	18
3.3(c) Late-time linear flow.....	18
3.4 Steam Assisted Gravity Drainage Concept Applied to a Horizontal Well Pair.....	20
3.5 Steam Zone Growth Above Adjacent Horizontal Wells.....	20
3.6 Different Well Configuration Schemes for Steam Assisted Gravity Drainage.....	22
3.7 A Schematic Diagram of Various Horizontal Well Configurations.....	23
5.1 A Schematic Diagram of the Apparatus.....	51
5.2 A Schematic Diagram of the Thermocouple Positions.....	56
5.3 A Schematic Diagram of the Produced Fluid Collection System.....	60
5.4 Viscosity vs. Temperature Profiles for the Ideal and Actual Selected (Faxam-100) Model Oil.....	66
5.5 Viscosity of the Mixture of Faxam-100 and Heavy Virgin Naphtha vs. HVN Solvent Concentration.....	68
5.6 The Wygal Particle Distributor.....	70
6.1 Overview of Experimental Runs.....	77
6.2 Cumulative Production/Cumulative Injection (CP/CI) vs. Cumulative Pore Volume Injected for Run 104—Steamflood in a Homogeneous Model.....	84
6.3 Cumulative Production/Cumulative Injection (CP/CI) vs. Cumulative Pore Volume Injected for Runs 67 (Ref. 51) and 79—7% BW, 10 HVN.....	87
6.4 Production History for Run 77: Base Case Steamflood in a Homogeneous Model using a Vertical Injector and a Vertical Producer.....	88



6.5	Top View Temperature Profiles for Run 77—Steamflood using a Horizontal-Vertical Well Combination in a Homogeneous Model .....	89
6.6	Injector to Producer Profile for Run 77 at 0.50 PV .....	90
6.7	Production History for Run 105: Waterflood in a Homogeneous Model, followed by a Continuous Steamflood .....	92
6.8	Top View Temperature Profiles for Run 105A—Waterflood.....	93
6.9	Top View Temperature Profiles for Run 105B—Steamflood following a Waterflood.....	94
6.10	Production History for Run 71: Gas (N <sub>2</sub> ) Injection in a Homogeneous Model prior to a Conventional Waterflood.....	96
6.11	Production History for Run 72: Waterflood in a Homogeneous Model, followed by N <sub>2</sub> Injection and then, by a Hot Waterflood.....	97
6.12	Top View Temperature Profiles for Run 72B—Gas Injection prior to a Hot Waterflood.....	98
6.13	Production History for Steamfloods in 50% Bottom Water—Run 95 (Pre-Injection of N <sub>2</sub> Gas) and Run 100 (Continuous Steamflood, No Gas) .....	100
6.14	Top View Temperature Profiles for Run 95—Gas Injection prior to a Steamflood in a Thick (50%) Bottom Water Model .....	101
6.15	Top View Temperature Profiles for Run 100—Steamflood using a Horizontal-Vertical Well Combination in a Thick (50%) Bottom Water Model.....	102
6.16	Production History for Steamfloods in 10% Bottom Water—Run 96 (Pre-Injection of N <sub>2</sub> Gas) and Run 90 (Continuous Steamflood, No Gas).....	104
6.17	Top View Temperature Profiles for Run 96—Gas Injection prior to a Steamflood in a Thin (10%) Bottom Water Model.....	105
6.18	Top View Temperature Profiles for Run 90—Steamflood using a Horizontal-Vertical Well Combination in a Thin (10%) Bottom Water Model.....	106
6.19	Cumulative Oil Recoveries for Steamfloods using a Vertical Producer and a Vertical Injector as a function of Bottom Water Thickness .....	107
6.20	Production History for Run 83: No Solvent Injection in a Bottom Water Model, 7% BW, prior to a Continuous Steamflood .....	109
6.21	Top View Temperature Profiles for Run 83—No Solvent Steamflood in a Thin (7%) Bottom Water Model .....	110
6.22	Production History for Run 78: Solvent, 10% PV, Injection in a Bottom Water Model, 7% BW, prior to a Continuous Steamflood .....	111

6.23	Top View Temperature Profiles for Run 78—Solvent (10% PV) Steamflood in a Thin (7%) Bottom Water Model .....	112
6.24	Production History for Run 84: Solvent, 20% PV, Injection in a Bottom Water Model, 7% BW, prior to a Continuous Steamflood .....	113
6.25	Top View Temperature Profiles for Run 84—Solvent (20% PV) Steamflood in a Thin (7%) Bottom Water Model .....	114
6.26	Production History for Run 82: Solvent, 30% PV, Injection in a Bottom Water Model, 7% BW, prior to a Continuous Steamflood .....	115
6.27	Top View Temperature Profiles for Run 82—Solvent (30% PV) Steamflood in a Thin (7%) Bottom Water Model .....	116
6.28	Comparison of Cumulative Oil Recoveries from Continuous Solvent-Steamfloods in Bottom Water Situations, 7% BW, as a function of Solvent Slug Size .....	118
6.29	Cumulative Oil Recoveries for Steamfloods using a Horizontal Producer and a Vertical Injector as a function of Bottom Water Thickness .....	120
6.30	Top View Temperature Profiles for Run 74—Steamflood using a Horizontal-Vertical Well Combination in a Homogeneous Model .....	121
6.31	Top View Temperature Profiles for Run 87—Steamflood using a Horizontal-Vertical Well Combination in a Thin (10%) Bottom Water Model.....	122
6.32	Top View Temperature Profiles for Run 97—Steamflood using a Horizontal-Vertical Well Combination in a Thick Bottom (50%) Water Model.....	123
6.33	Cumulative Oil Recoveries for Steamfloods using a Horizontal Producer and a Horizontal Injector as a function of Bottom Water Thickness.....	125
6.34	Top View Temperature Profiles for Run 75—Steamflood using a Horizontal-Vertical Well Combination in a Homogeneous Model.....	126
6.35	Top View Temperature Profiles for Run 101—Steamflood using a Horizontal-Vertical Well Combination in a Thin (10%) Bottom Water Model.....	127
6.36	Top View Temperature Profiles for Run 98—Steamflood using a Horizontal-Vertical Well Combination in a Thick Bottom (50%) Water Model.....	128
6.37	Cumulative Oil Recoveries for Steamfloods using a Vertical Producer and a Horizontal Injector as a function of Bottom Water Thickness.....	129
6.38	Top View Temperature Profiles for Run 76—Steamflood using a Horizontal-Vertical Well Combination in a Homogeneous Model .....	130

6.39	Top View Temperature Profiles for Run 102—Steamflood using a Horizontal-Vertical Well Combination in a Thin (10%) Bottom Water Model.....	131
6.40	Top View Temperature Profiles for Run 99—Steamflood using a Horizontal-Vertical Well Combination in a Thick Bottom (50%) Water Model.....	132
6.41	Instantaneous and Cumulative Oil Production as a function of Cumulative PV Injected for Steamfloods in Homogeneous Models .....	134
6.42	Instantaneous and Cumulative Oil Production as a function of Cumulative PV Injected for Steamfloods in Thin (10%) Bottom Water Formations.....	136
6.43	Instantaneous and Cumulative Oil Production as a function of Cumulative PV Injected for Steamfloods in Thick (50%) Bottom Water Formations ...	137
6.44	Instantaneous and Cumulative Hydrocarbon Production as a function of Cumulative PV Injected for Solvent-Steamfloods in Thin (10%) Bottom Water Formations .....	139
6.45	Top View Temperature Profiles for Run 91—Solvent (10% PV)-Steamflood using a Horizontal-Vertical Well Combination in a Thin (10%) Bottom Water Model.....	140
6.46	Top View Temperature Profiles for Run 92—Solvent (10% PV)-Steamflood using a Horizontal-Vertical Well Combination in a Thin (10%) Bottom Water Model .....	141
6.47	Top View Temperature Profiles for Run 93—Solvent (10% PV)-Steamflood using a Horizontal-Vertical Well Combination in a Thin (10%) Bottom Water Model .....	142
6.48	Top View Temperature Profiles for Run 94—Solvent (10% PV)-Steamflood using a Horizontal-Vertical Well Combination in a Thin (10%) Bottom Water Model.....	143
6.49	Solvent Injection Strategies for Steamfloods using a Horizontal Producer and a Horizontal Injector (10%BW, 10% HVN) .....	145
6.50	Comparison of the Various Injection-Production Strategies on Ultimate Oil Recovery, for the Different Bottom Water Cases Investigated .....	146
B.1	A Plot of Refractive Index vs. %NaCl.....	166
B.2	A Schematic of the Metrabyte Data Acquisition Unit.....	171
D.1	Cable Schematics for Macintosh Computer to Modem/Plotter.....	191
D.2	A Schematic of the Top View of the Aberfeldy Model Showing the Coordinate Systems used for the DISSPLA Data Files .....	201

## List of Photographic Plates

<b>Plate</b>	<b>Page</b>
5.1 Overall View of Low Pressure Apparatus.....	52
5.2 View of Apparatus in Operation.....	53
5.3 The Scaled Model of the Aberfeldy Reservoir.....	54
5.4 Internal View of the Boiler.....	59
5.5 Fluid Collection System.....	61

## NOMENCLATURE

a	half of the major axis of drainage ellipse, [L]
A'	area for heat loss to overburden associated with reservoir volume $V_b$ , [ $L^2L^{-3}$ ]
B	formation volume factor, [ $L^3L^{-3}$ ]
b	half of the minor axis of drainage ellipse, [L]
C	specific heat, [ $L^2t^{-2}T^{-1}$ ]
c	shape parameter of the water oil contact
$C_{ij}$	concentration of component j in phase i, mass fraction
D	height above datum, m; $D=D(x)$ , [L]
d	distance of the summit of the water crest to the top of the reservoir, or diameter, [L]
$f_s$	steam quality, dimensionless
g	acceleration due to gravity, [ $Lt^{-2}$ ]
h	enthalpy per unit mass, [ $L^2t^{-2}$ ]
h	thickness of formation, [L]
k	permeability, [ $L^2$ ]
$k_h$	thermal conductivity, [ $MLt^{-3}T^{-1}$ ]
$k_r$	relative permeability, dimensionless
L	length or distance, [L]
$L_v$	latent enthalpy per unit mass, [ $L^2t^{-2}$ ]
m	arbitrary variable, or mass [M]
p	pressure, [ $ML^{-1}t^{-2}$ ]
q	flow rate, [ $L^3t^{-1}$ ]
$\bar{q}$	conductive heat flux, [ $M/t^3$ ]
$q^*$	injection/production rate, [ $L^3t^{-1}$ ]
$q_H$	flow rate into a horizontal well, [ $L^3t^{-1}$ ]
$q_h$	heat loss rate, [ $ML^2t^{-3}$ ]

$r$	radius, [L]
$r_e$	drainage radius, [L]
$r_w$	effective radius of model well, [L]
$r_w$	effective wellbore radius, [L]
$S$	saturation, mass fraction
$T$	temperature, [T]
$t$	time, [t]
$\bar{u}$	volumetric flux (Darcy velocity), [L $t^{-1}$ ]
$U$	internal energy, [L $^2t^{-2}$ ]
$w$	mass flow rate, [M $t^{-1}$ ]
$x, y, z$	coordinates

### **Greek Symbols**

$\alpha$	thermal diffusivity, [L $^2t^{-1}$ ]
$\Delta p$	pressure drop, [ML $^{-1}t^{-2}$ ]
$\Delta r$	half of horizontal well length, [L]
$\Phi$	potential function, [ML $^{-1}t^{-2}$ ]
$\phi$	porosity, dimensionless
$\mu$	fluid viscosity, [ML $^{-1}t^{-1}$ ]
$\rho$	density, [ML $^{-3}$ ]
$\theta$	parameter
$\omega$	slit width, [L]
$\psi$	streamline function, [ML $^{-1}t^{-2}$ ]

## **Subscripts**

a	aqueous phase
c	cap or base rock
D	dimensionless quantity
g	vapour phase
H	horizontal well
i	initial
is	steam injection rate
j	phase (oil, water or steam)
m	model
o	oil or oleic phase
ob	overburden
or	residual oil saturation to steam
p	prototype
R	reference variable used to obtain a dimensionless quantity
r	reservoir rock, except with k
s	steam
sat	saturation temperature or pressure
sc	calculated steam temperature
ss	superheated steam
t	total interval
V	vertical well
w	water (unless otherwise specified)
wc	irreducible water

## Chapter 1

### Introduction

Many heavy oil formations in the Lloydminster area of Saskatchewan and in eastern Alberta are not suitable for thermal recovery methods, such as steamflooding, cyclic steam stimulation, and in situ combustion. Approximately 85% of Saskatchewan's thin, heavy oil formations are classified as "marginal reservoirs". These reservoirs are characterized by relatively thin pay sections (6-13 m) and underlying high water saturation zones. The water sand, which is often in communication with the oil zone, can be either a transition zone or else a zone of high water saturation that can approach 100%. Under these conditions, low oil recovery and poor sweep are expected due to excessive vertical heat losses and steam scavenging effects by the bottom water zone. As marginal reservoirs constitute a major portion of the heavy oil reserves in Canada, it is essential to establish a viable recovery technique for such reservoirs.

The main focus of this research was to incorporate vertical and horizontal well combinations in the steamflood process of a marginal oil reservoir in Lloydminster, Saskatchewan. The experiments were conducted in a scaled physical model of the Aberfeldy heavy oil reservoir. Other recovery schemes included the applications of a gas additive and a solvent slug, and were investigated under various reservoir conditions, such as the homogeneous (no bottom water), thin bottom water (10%), and thick bottom water (50%) cases. The present research discusses the results of the above experiments, suggesting strategies which may permit the economic production of a marginal heavy oil reservoir.



## Chapter 2

### Statement of the Problem

The specific objectives of this research were to employ horizontal well strategies for steamflooding heavy oil formations with a communicating water zone, using experimental and theoretical methods, which are outlined as follows:

#### Experimental Objectives

1. Improved experimental design:
  - a) Modification of the boiler unit to improve steam quality;
  - b) Design and installation of a data acquisition system for recording and analyzing experimental data;
  - c) Design and construction of a produced fluid collection system; and
  - d) Converting the existing walk-in cooler to a freezer in order to create bottom water in situ.
2. Methods for steamflooding thin, heavy oil formation, with and without bottom water:
  - a) Gas injection; and
  - b) Solvent Injection.
3. Horizontal well strategies for steamflooding marginal reservoirs:
  - a) No bottom water;
  - b) Thin bottom water; and
  - c) Thick bottom water.

#### Theoretical Objectives

1. Derivation of steamflooding scaling criteria with gas as the only additive and the evaluation of gas runs in light of these criteria.
2. Interpretation of selected runs.

## Chapter 3

### Literature Review

Extensive reviews of theoretical and experimental studies of steamflooding for oil recovery have been conducted. This review presents laboratory studies of the steam drive process, horizontal well applications and case histories of horizontal well technology, and the incorporation of solvent into steam injection. Scaling methods will also be covered briefly.

#### Physical Model Studies of Steamflooding

Physical models, which can be unscaled or scaled, are used to predict the performance of a proposed recovery scheme in the reservoir under investigation. They are especially useful for studying new processes whose mechanisms are not fully understood. They are used to complement numerical studies by validating the predictions of the mathematical models or obtaining process parameters for the simulator. Farouq Ali and Redford<sup>1</sup> presented a review of various approaches to scaling steam injection processes.

#### **Unscaled Physical Models**

Unscaled models are relatively simple, and are selected on the basis of the recovery method being studied. Their dimensions are often limited by the physical constraints on the laboratory equipment. Sometimes, they are referred to as “elemental models” since the materials used and the operating procedures represent the specific conditions of the field at some point in its life. Unscaled experiments give an understanding of the dominant recovery mechanisms such as diffusion, dispersion, gravity segregation and rate dependence. As an example, Watts and Hutchinson<sup>2</sup> showed from their unscaled Asphalt Ridge tar sands model that optimum oil recovery occurred when intermediate quality steam was injected, instead of a high quality steam or a hot waterflood.

## **Scaled Physical Models**

Scaled models are desirable because their results may be directly applied for field predictions. The principle of similarity, the basis of scaled physical models, expresses the spatial and temporal configuration of a physical system by means of dimensionless ratios within the system. There are four types of similarity: (i) geometric (dimensions are similar), (ii) mechanical (static—geometric similarity is preserved when deforming forces are applied to a static body, kinematic—ratio of time is constant, or dynamic similarity—ratio of forces is constant), (iii) thermal (ratio of thermal conductivities are similar) and (iv) chemical (ratios of chemical properties, such as chemical composition, potentials, and concentrations are constant). Since it is impossible to satisfy all scaling criteria simultaneously, engineering judgement is often used to relax some of the criteria, leading to a reduced set of similarity groups.

## **High Pressure Models**

Scaled models can be divided into two categories: high pressure and low pressure. High pressure models scale rock-fluid interactions, temperature dependence of rock properties, emulsions, steam distillation, gas solubility, compressibility, and fluid properties<sup>3,4</sup> more accurately than low pressure models, which are constrained to operate at lower temperatures, and thus, must use rocks and fluids different from those in the reservoir.

Huygen<sup>5</sup> developed a high pressure model (400-4020 kPa) representing one half of a five-spot, which used the field crude oil and crushed Berea sandstone. Only heat flow was considered in the scaling calculations. He studied the effects of oil viscosity, initial oil saturation, and distillation residue on oil recovery.

Pujol and Boberg's<sup>6</sup> multidimensional steam injection scaling criteria are widely used for the design of high pressure models. They showed that unscaled capillary pressures had a negligible effect on oil recovery for oils with a very low ratio of capillary to

viscous forces. Hence, accurate scaling of capillary pressure was not required for viscous crudes. However, optimistic recoveries were obtained when capillary pressures were unscaled for medium viscosity oils ( $\mu < 10,000$  mPa·s).

Pursley<sup>7</sup> applied Pujol and Boberg's<sup>6</sup> high pressure scaling criteria to his Cold Lake model (3450 kPa). He investigated the effects of reservoir heterogeneities, such as the presence of a gas cap, bottom water, presence of vertical flow barriers (tight or low permeability streaks). He also studied the effects of process variable, such as pattern size, steam quality and steam additives, on steam drive performance. It should be noted that Pujol and Boberg's<sup>6</sup> scaling criteria do not allow for steam additives.

Lo<sup>8</sup> constructed an intermediate pressure model (100 kPa) of a seven-spot pattern for the Lloydminster heavy oil. He based his model on Pujol and Boberg's<sup>6</sup> analysis, but scaled mobility rather than permeability. Scaling mobility permits greater flexibility in selecting model materials, but fails to scale oil viscosity, as done by Stegemeier, Laumbach and Volek<sup>9</sup>. Subsequently, Singhal<sup>10</sup> included the ratio of enthalpies of vapour-to-liquid water in the previously used groups to match steam quality.

To satisfy the similarity groups for scaling geometry, viscous forces and gravitational forces, Pujol and Boberg<sup>6</sup> required that the pressure drop in the model be different from that in the field. They overcame this obstacle by selecting a porous medium for the model different from that found in the prototype. Kimber, Puttagunta and Farouq Ali<sup>3</sup> presented new scaling criteria, which allowed the same fluids and same porous medium to be used to scale steam or steam processes for horizontal reservoirs. As a consequence of satisfying other scaling requirements, they relaxed some of the geometric scaling groups. They compared the relative merits of their approach with those previously published in literature, both analytically (inspectional and dimensional analysis)<sup>3</sup> and experimentally<sup>11,12</sup> (steamflooding scaled physical models representing one-eighth of a five-spot pattern).

### Low Pressure Models

Low pressure models are designed to operate at subatmospheric pressures and low temperatures. Better scaling of the Clausius-Clapeyron relationship (steam saturation pressure-saturation temperature relation) in low pressure models result in a more accurate representation of temperature and velocity distributions than a high pressure model. Unlike high pressure models, low pressure models often require a fluid with different properties from that of the prototype to satisfy all the relevant criteria. The low pressure scaling approach requires considerable skill in satisfying a multitude of criteria, with both the operating conditions and rock and fluids being totally different from those in the prototype.

Simulation of models operating in the vacuum range was first described by Stegemeier et al.<sup>9</sup> whose low pressure scaling criteria have been the basis of several studies. They conducted extensive steam injection experiments in two dipping reservoirs, the Mt. Poso and the Midway Sunset fields.

Prats<sup>13</sup> used the Stegemeier et al.<sup>9</sup> approach to model the Peace River oil sand. He found that vacuum models appeared to be the most suitable for simulating vaporization phenomena associated with pressure blowdown in the pressure cycling process. Proctor<sup>14</sup> applied the same approach to investigate several aspects of steamflooding thin, heavy oil reservoirs with a communicating water saturation zone. His three-dimensional physical model represented one-quarter of a five-spot in the Aberfeldy reservoir.

Doscher and Lechtenberg<sup>4</sup> took a slightly different approach than Stegemeier et al.<sup>9</sup> in developing their low pressure scaling criteria for their Kern River model. They derived the similarity groups by the integral approach, developed by Yortsos and Gavalas<sup>15,16</sup>, as opposed to the differential approach developed by Stegemeier et al.<sup>9</sup>. Yortsos and Gavalas<sup>15,16</sup> used the integral form of the thermal energy and latent heat balance to determine the upper bounds of the steam zone for multidimensional reservoirs. Although the integral approach caused distorted saturation and temperature distributions, Doscher and

Lechtenberg<sup>4</sup> noted that process phenomena, such as oil recovery, oil-steam ratio, efficiency and override are of an integral nature. Hence, they concluded that the integral approach was a more accurate representation of recovery process than the differential method.

### **Steamflooding in the Presence of Bottom Water**

Relatively few studies have been conducted on heavy oil reservoirs in the presence of bottom water. The first instance where steam was injected into an underlying water sand was in the case of the Slocum field in northeast Texas. However, in spite of the high oil saturation (65%), the large quantities of steam required for the process reduced the profitability of the project<sup>17</sup>.

Prats<sup>13</sup> modelled the Peace River reservoir (200 000 mPa•s), which is characterized by an underlying water zone containing a large oil saturation (55%). In the laboratory experiments, a modified steam injection scheme consisted in using the steam to heat the basal zone. The recovery process involved pressurizing the zone, producing some oil, blowing it down to the steam zone, and finally, conducting a steamflood in the oil zone.

Pursley<sup>7</sup> used a scaled model of the Cold Lake reservoir (100 000 mPa•s) to examine the effect of steam injection into a thin bottom water layer (15% PV) and an overlying gas zone (2.5% PV). It was concluded that the tendency of steam override was responsible for the high recovery obtained in the bottom water model because it enabled steam to contact a greater portion of the sand. Further, a steam drive through a basal sand appeared to be feasible only if the vertical permeability was high and if heating close to the base of the oil sand could be affected.

Ehrlich<sup>18</sup>, and Huygen and Lowry<sup>19</sup> performed steamflooding experiments through a simulated bottom water layer in scaled laboratory models of the Wabasca formation ( $5 \times 10^6$  mPa•s). Their conclusions agreed with those of Prats<sup>13</sup>; high recovery was a result of conduction heating of bitumen due to steam flow through the bottom water zone.

In all instances<sup>7,18,19</sup>, bottom water provided the initial injectivity path for steam in viscous oil sands.

Doscher and Huang<sup>20</sup> investigated the steamflood performance through a thin bottom water zone (15% of total pay). Their studies indicated that while steam initially advanced through the basal sand, continued injection caused the oil to drain down and be carried through the water zone. Eventually, with continued steam injection, steam override occurred. Contrary to previous studies, increasing steam injection rate did not result in a monotonic increase in oil-steam ratio at any given recovery factor. Doscher and Huang<sup>20</sup> concluded that there was a critical injection rate, above and below which steam-drive performance deteriorated.

Proctor, George and Farouq Ali<sup>21</sup> studied steam injection strategies for thin bottom water reservoirs in a scaled physical model. They showed that the effect of bottom water was small for some minimum bottom water thickness (10% of gross thickness). Kasraie and Farouq Ali<sup>22</sup> used a numerical model to examine heavy oil recovery in the presence of bottom water. They concluded that thick water zones delayed the steamflood response and consequently reduced process profitability.

### **Horizontal Well Applications**

This review of horizontal well technology for producing heavy oils and oil sands discusses the reservoir engineering aspects of horizontal wells, which are relevant to this investigation. Special emphasis is placed on the productivity of horizontal wells in homogeneous and isotropic reservoirs as well as the influence of anisotropy on productivity. The use of horizontal wells in bottom water zones is examined as it offers a means of delaying water coning effects. Horizontal well flow behaviour is analyzed for early and late time flow geometry. The steam assisted gravity drainage process, when employed with horizontal wells, gives substantially higher recoveries than from vertical wells. Finally, optimum horizontal-vertical well patterns are investigated.

## Background

In recent years, interest in horizontal wells has been rekindled (see Table 3.1). Horizontal wells have been proposed for conventional recovery from tight reservoirs where production from horizontal wells exceeds that from vertical wells due to their greater reservoir contact. They are particularly effective when vertical fractures are present, in thin pay sections where water or gas coning is a problem, and in soft formations, such as chalk, which are liable to collapse. Horizontal wells may have great potential in the recovery of bitumen and heavy oil in Alberta and Saskatchewan. Satisfactory steam injection rates are only feasible at formation parting pressures because of the low injectivity of steam in oil sands. However, while high pressure steam injection is acceptable for a cyclic steam stimulation process, it may be detrimental for a subsequent steamflood. Horizontal wells may offer a non-fracture alternative to the steam fracturing technology.

Theoretical and laboratory studies as well as reported field successes indicate that horizontal wells will likely be more effective than vertical wells in certain situations. A horizontal well contacts a much greater portion of the reservoir, and hence, the production rate from a horizontal well may be two to five times greater<sup>23</sup> than a vertical well. Horizontal wells operate with lower local fluid velocities in the reservoir while still providing adequate productivity due to the vast area which is exposed to the reservoir. This results in less sand transport into the well and reduced coning of gas or water when a gas cap or a bottom water zone is present, respectively.

The negative aspects of horizontal wells include high drilling and completion costs, 1.5 to 2 times greater<sup>24</sup> than conventional vertical wells, and their inability to produce zones separated by impermeable layers via a single wellbore. Horizontal wells are ineffective in thick (150 to 180 m) reservoirs with low vertical permeability<sup>23</sup>. Of nearly 150 horizontal wells drilled worldwide, only the ones in Table 3.1, less than 10% of the



**Table 3.1: List of Horizontal Well Projects for Heavy Oil Recovery**

<u>Year</u>	<u>Field</u>	<u>Company</u>	<u>Process</u>	<u>Comments</u>
1937	Yarega, USSR		Steam	First horizontal well. Mine assisted steam. (Same horizontal well was used for injection and production.)
1978/83/89	Rospo Mare, Italy	Elf Aquit. (& Institut Français du Petrole in 1978/83)	Primary	Offshore in Italy.
1979	Fort McMurray, Alberta	Texaco	Steam	Wells drilled from a single drill pad using a slant rig. (Same horizontal well was used for injection and production.)
1979/89	Cold Lake, Alberta	Esso Resources Canada Ltd.	Steam	Steam assisted gravity drainage process. (Horizontal producer.)
1984	Cold Lake, Alberta	Esso Resources Canada Ltd.	Steam	Longest recorded horizontal well. Cyclic steam process. (Horizontal producer.)
1987	Fort McMurray, Alberta	AOSTRA	Steam	Underground Test Facility (UTF). Steam assisted gravity drainage. (Two separate horizontal wells for injection and production.)
1987/89	North Tangleflags, Saskatchewan	Sceptre Resources and Murphy Oil	Steam	Thermal EOR in gas cap/bottom water area. (Horizontal producer.)
1988	Kern River, California	Dietrich Corp.	Steam	Steam inj./oil recovery lateral holes drilled radially from a central shaft parallel to and a few feet above the base of the heavy oil column. (Horizontal injector.)
1988	Medicine Hat, Alberta	Alberta Energy Co. (AEC)	Primary	14° API oil.
1988	Pelican Lake, Alberta	Gulf	Steam	14° API oil.
1988/89	Pelican Lake, Alberta	CS Res.	Steam	Long radius well.
1988/89	Winter, Saskatchewan	CS Res.	Primary	Long radius well.
1989	Suffield, Alberta	AEC	Primary	Water coning inherent.
1989	Winter, Saskatchewan	Saskoil	Primary	Field was not previously waterflooded.
1989	Plover Lake	Saskoil	Primary	Horizontal steam producer, vertical injector proposed.
1989	Provost, Alberta	Pan Canadian Petroleum	Primary	N/C
1989	Provost, Alberta	Renaissance Energy	Primary	N/C

wells drilled to-date, were located in heavy oil formations. Thus, the experience with horizontal wells for heavy oil production is limited.

## **The Productivity of Horizontal Wells**

### Homogeneous and Isotropic Reservoirs

One advantage of horizontal wells is that their productivity may be greater than conventional vertical wells. The productivity of a conventional well is a function of permeability and thickness. Thus, low productivities result from either low formation permeability or low values of formation thickness or both. Horizontal wells can compensate for these problems in heterogeneous reservoirs because they have a greater chance of penetrating a favourable geological structure, such as vertical fractures.

### **The Influence of Anisotropy**

In many reservoirs, the vertical permeability is less than the horizontal permeability. A decrease in vertical permeability can be detrimental for a horizontal well because it will result in an increase in the vertical flow resistance and a decrease in oil production rates. Conversely, if the vertical permeability is greater than the horizontal permeability, then there will be a decrease in vertical flow resistance and an increase in oil production. Muskat<sup>25,26</sup> accounted for reservoir anisotropy by modifying the vertical coordinate as  $z' = h\sqrt{k_H/k_V}$  and defining the average or isotropic equivalent reservoir permeability as  $\sqrt{k_H k_V}$ . This modification leads to an elliptical wellbore. It has been shown that replacing the elliptical wellbore by a circular wellbore has a negligible effect on wellbore productivity. Giger, Reiss and Jourdan<sup>26</sup> did not recommend using horizontal wells when  $k_V/k_H$  was less than one. However,  $k_V/k_H$  values greater than one indicated that vertical fractures were present in the reservoir, thereby suggesting favourable productivity conditions for horizontal wells.

### **Water Coning and Cresting**

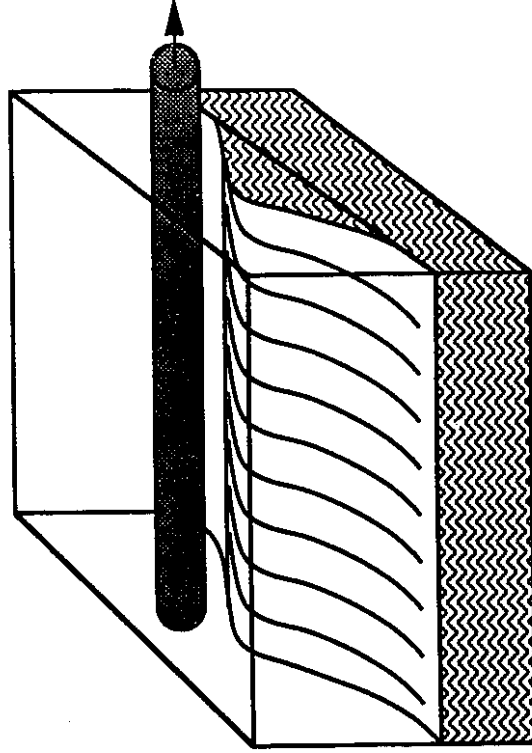
Production with horizontal wells offers a new approach to reduce the effect of water coning during oil production. Regardless of the method of production, there is always a “critical velocity” which when exceeded can lead rapidly to the entry of gas or water into the well when producing in the presence of a bottom water or gas cap zone, respectively.

Water coning, as shown in Figure 3.1, is due to pressure gradients resulting from the production of fluid from the reservoir. If a water-oil contact exists in the producing interval, these pressure gradients will induce water to rise in the immediate vicinity of a vertical well which acts as a single point in a horizontal plane. The tendency of the water to cone is partially offset by gravitational forces because water has a higher specific gravity than oil. Thus, a balance exists between the gravity forces arising from the difference in the specific gravities of water and oil, and the pressure gradients causing the flow of fluids into the wellbore. When the pressure gradient exceeds the gravitational force, water coning occurs with increased water production.

Horizontal wells, which extend parallel to the initial oil-water contact, reduce coning tendencies by generating more favourable flow conditions and shallower pressure gradients and thus, reduce coning tendency. Horizontal wells exhibit better performance because they require a much smaller pressure drawdown as compared to vertical wells to produce oil at the same rate. Horizontal wells exhibit an approximately linear pressure gradient from the wellbore to the drainage radius. However, water may rise in horizontal wells in the form of crests instead of cones. Water cresting is shown in Figure 3.1.

Giger<sup>27</sup> determined the shape of the water-oil contact (WOC) created by the development of a water crest in an oil column during production with a horizontal well. He showed that the shape of the water-oil contact is an ellipse with a horizontal tangent close to its sides. Below the well, the shape of the water crest is represented by a branch of a parabola; this is also the case far from the well.

Horizontal Well



Vertical Well

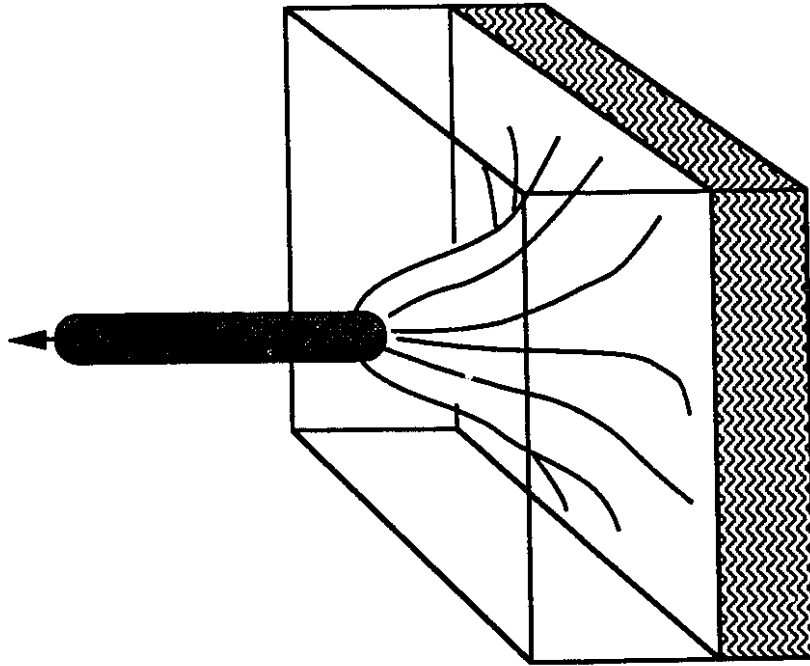


Figure 3.1: Water Coning Toward a Vertical Well and Cresting Toward a Horizontal Well.

Giger<sup>27</sup> also defined the critical flow rate,  $q_c$ , as the rate which will cause water to enter the wellbore. He showed that  $q_c$  will continue to approach the production rate until a time,  $t_c$ , at which it is equal to the production rate. At this time, water begins to appear in the production. To prevent water production, the production rate of the horizontal well must be gradually reduced with time so that the production rate will always be less than the critical flow rate.

## **Well Flow Behaviour**

### Early Time Flow Geometry of a Horizontal Well

While horizontal drainholes and horizontal wells have been available for numerous years, only recent advances in horizontal drilling have made it economically feasible and technically possible to drill in various formations. As shown previously in Table 3.1, the Russians were the first to apply horizontal well technology to heavy oil formations. Borisov<sup>28</sup> was one of the earliest researchers, who studied the flow potentials of horizontal and highly-deviated wells. In his study, he proposed formulae to determine the production rates of single and multiple groups of deviated wells for various well configurations.

Joshi<sup>23</sup> found that a horizontal well of length  $L$  has an ellipsoid drainage pattern, as shown in Figure 3.2(a). Joshi<sup>23</sup> presented equations for early time horizontal well flow geometry, that is, until the first pressure transient reaches the upper or lower reservoir flow boundaries. Figures 3.2(b) and (c) schematically represent the method Joshi<sup>23</sup> used to simplify this problem. He subdivided the three-dimensional ellipsoid problem into two, two-dimensional problems: flow into a horizontal well in a horizontal plane and flow in a vertical plane. It is observed that the radius of the reservoir drained by this flow regime is approximately equal to one-half of the reservoir height. Joshi<sup>23</sup> used the potential theory presented by Muskat<sup>25</sup> in Figure 3.2(d) for flow from an infinite reservoir into a finite line source to obtain the solution.

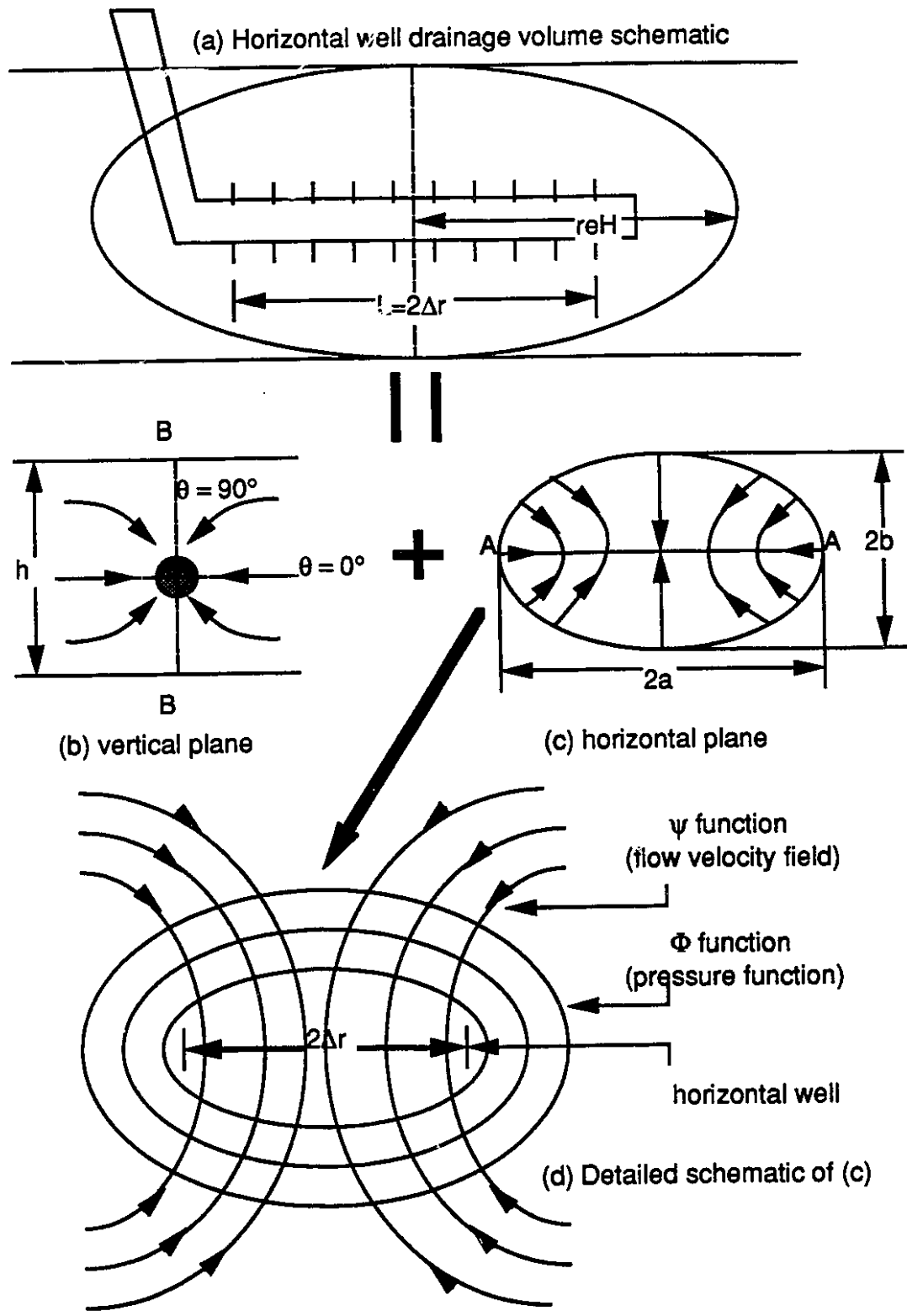


Figure 3.2: Schematic of Potential Flow to a Horizontal Well. (Modified from Ref. 23)

Figures 3.2(c) and (d) show a schematic diagram of flow to a horizontal well in the x-y plane at early times. Joshi<sup>23</sup> presents the equations for the equipotential function ( $\Phi$ ) which is represented by ellipses and the streamline function ( $\psi$ ) which is expressed by hyperbolas:

$$w(z) = \Phi + i\psi = \cosh^{-1}\left(\frac{z}{\Delta r}\right) \quad (3.1)$$

where:

$$z = x + iy \quad (3.2)$$

$$\Phi = \cosh^{-1} H^* \quad (3.3)$$

$$\psi = \cos^{-1} H^* \quad (3.4)$$

$$H^* = \left[ \frac{x^2 + y^2 + \Delta r^2 \pm \sqrt{(x^2 + y^2 + \Delta r^2)^2 - 4\Delta r^2 x^2}}{2\Delta r^2} \right]^{1/2} \quad (3.5)$$

He then gave the equation for flow into a horizontal plane:

$$q_1 = \frac{2\pi k_o \Delta p / \mu}{\ln \left[ \frac{a + \sqrt{a^2 - \Delta r^2}}{\Delta r} \right]} \quad (3.6)$$

From Figure 3.2(b), which schematically demonstrates flow in a vertical plane (x-z), Joshi<sup>23</sup> obtained:

$$w(z) = \Phi + i\psi = q \left[ \left( \frac{\pi r}{h} \right) \cos \theta - \ln \left( \frac{\pi r}{h} \right) \right] + iq \left[ \left( \frac{\pi r}{h} \right) \sin \theta - \theta \right] \quad (3.7)$$

The flow into a horizontal well in the vertical plane is given as

$$q_2 = \frac{2\pi k_o \Delta p / \mu}{\ln \left[ \frac{h}{2r_w} \right]} \quad (3.8)$$

Joshi<sup>23</sup> multiplied the two flow equations (Equations 3.6 and 3.8) by the reservoir height, h, and used an electric analog to calculate flow resistance in the horizontal and vertical

planes. He added the horizontal and vertical flow resistances to obtain the equation for flow into a horizontal well in the early time flow regime:

$$q_h = \frac{\left( \frac{2\pi k_o h \Delta p}{\mu B_o} \right)}{\ln \left( \frac{a + \sqrt{a^2 - (L/2)^2}}{L/2} \right) + \frac{h}{L} \ln \left( \frac{h}{2r_w} \right)} \quad (3.9)$$

for  $L > h$  and  $\frac{L}{2} < 0.9 r_{eH}$ .

where

$$a = \frac{L}{2} \left[ \frac{1}{2} + \sqrt{\frac{1}{4} + \frac{1}{\left( \frac{0.5L}{r_{eH}} \right)^4}} \right]^{0.5} \quad (3.10)$$

In a recent study of extended reach and horizontal wells, Economides and Nolte<sup>29</sup> presented Joshi's<sup>23</sup> flow equation, perhaps because of its simplicity and popularity. Giger<sup>26,30</sup> also obtained his equations for the steady-state flow into a horizontal well and the productivity index of horizontal wells based on Muskat's<sup>25</sup> potential flow theory.

### Late Time Flow Geometry of a Horizontal Well

Figure 3.3(c) depicts the flow geometry in the final flow period (flow at earlier times is illustrated in Figures 3.3(a) and 3.3(b)) at which time flow lines are almost completely linear everywhere outside the well. This flow regime is known as plane parallel flow and is caused by the pressure response in the reservoir in response to the effects of the lateral boundaries. It should be noted, however, that radial flow still dominates in the immediate vicinity of the wellbore.

It has been determined that if the length of the horizontal well is significantly larger than the height of the reservoir ( $L/h \gg 1$ ), then the production from a horizontal well can be considered to be equivalent to the production from a fully penetrating vertical fracture<sup>23,31</sup>.



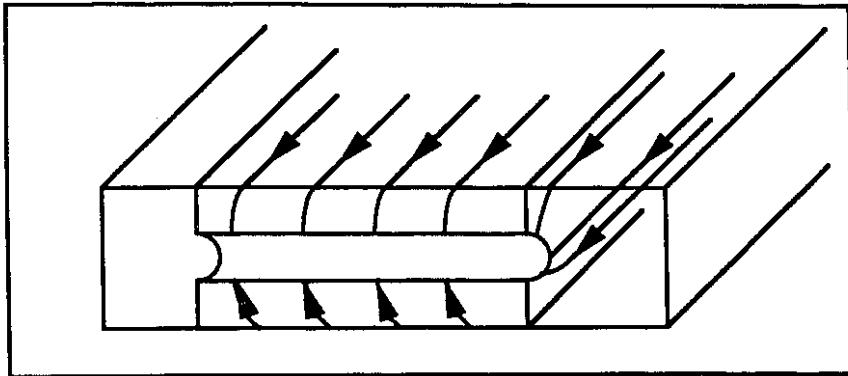


Figure 3.3 (a): Intermediate-Time Linear flow.

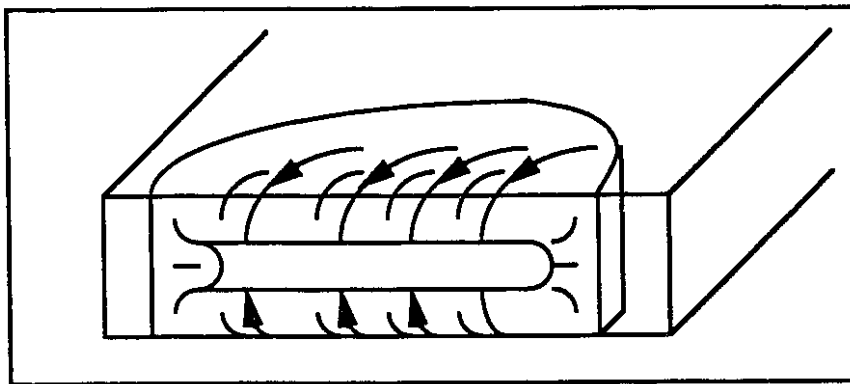


Figure 3.3 (b): Late-Intermediate-Time Linear flow.

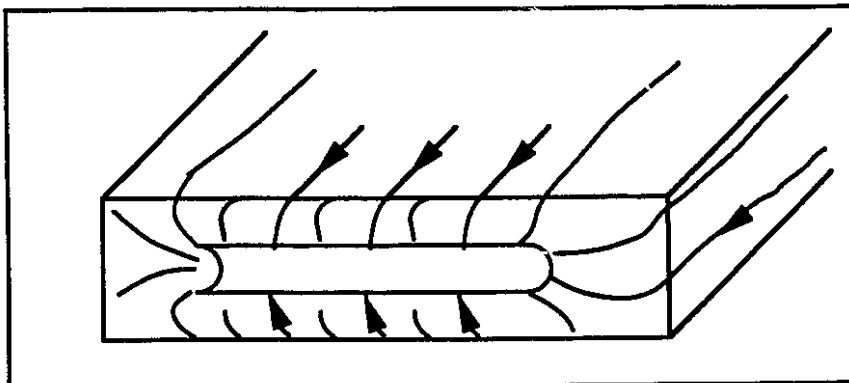


Figure 3.3 (c): Late-Time Linear Flow.  
(Modified from Ref. 31)

## Gravity Drainage

In cyclic steam stimulation, the dominant production mechanism is the pressure gradient between the reservoir and the production well. In steamflooding, oil production rates are governed by the pressure gradient between the injection and production wells. However, in steam assisted gravity drainage, the only pressure drop is due to the gravity head between the injection and production wells. Oil production is controlled solely by gravity drainage and the rate of gravity drainage is enhanced by a reduction in oil viscosity resulting from steam heating. The steam assisted gravity drainage concept (SAGD) as introduced by Butler and associates<sup>32,33</sup> will be discussed as it relates to horizontal wells.

Figure 3.4 shows a horizontal well pair located near the bottom of an oil column with the injection well above the production well. The wells are placed as close as possible to each other in order to minimize the pressure gradient and maximize the gravity head between them. Steam is introduced into the upper injection well, which is located at the base of the reservoir. Oil viscosity is reduced as steam rises and heats the surrounding formation. The heavier condensates and the heated oil will flow to the lower production well as a result of the gravity drainage mechanism. The pressure within the steam zone will essentially remain constant. The steam zone will continue to grow upwards and sideways as the oil is produced. Butler, McNab and Lo<sup>32</sup> reported that the rate of upward growth rate was larger than the sideways rate. However, the upwards growth would eventually be limited by the top of the reservoir at which time sideways growth would become the critical consideration, and steam forms a single layer above the oil zone. Figure 3.5 represents the expected growth of steam zone above adjacent horizontal wells. Steam assisted gravity drainage permits a high process efficiency and thus, increased recovery due to improved sweep efficiency. Furthermore, hot oil is produced as soon as it is displaced from the formation, which differs from cyclic steam stimulation and steam drives. Favourable

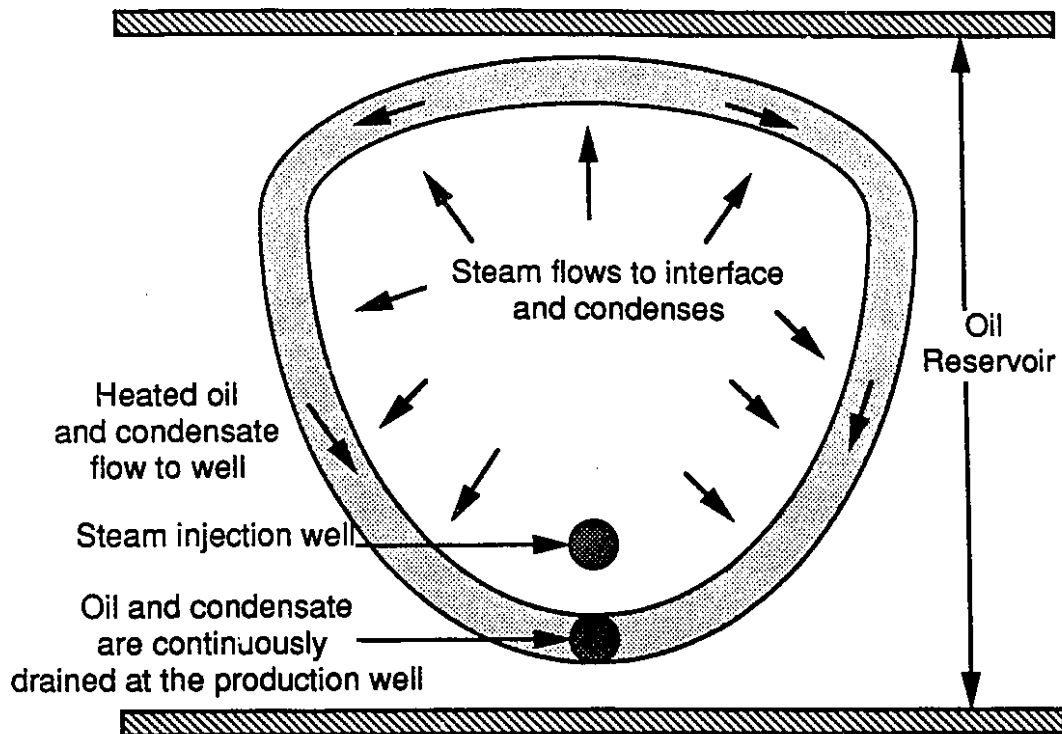


Figure 3.4: Steam assisted gravity drainage concept applied to a horizontal well pair.  
(Modified from Ref. 32)

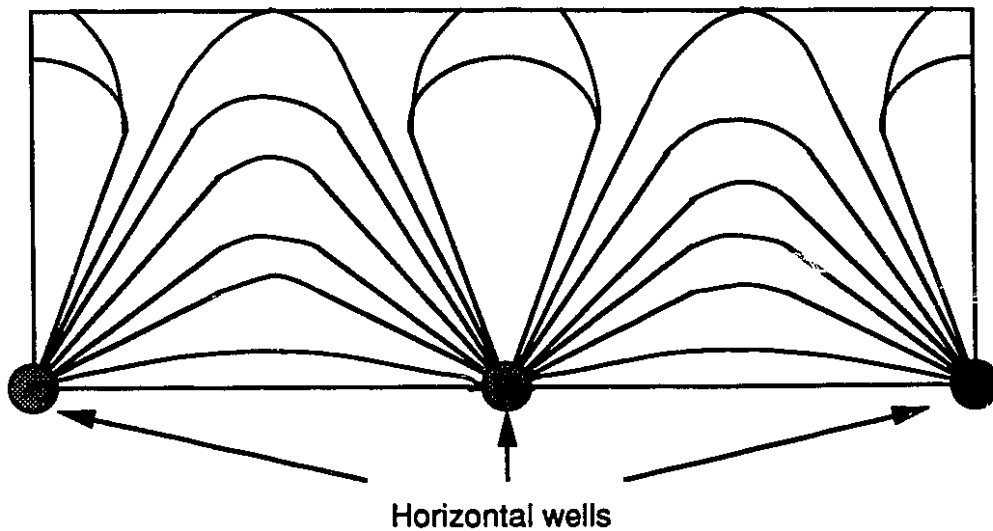


Figure 3.5: Steam growth chamber above adjacent horizontal wells.  
(Modified from Ref. 32)

relative permeability conditions for oil flow are created as a result of the creation of independent flow paths for oil, condensed water and steam. In addition, steam injection can be stopped and reinitiated without any significant loss in the recovery efficiency in the event of early steam breakthrough.

The negative aspects of gravity drainage are that it requires a relatively thick oil column ( $\approx 15$  m) and it may be hindered in zones separated by thick, continuous shale layers. In the latter case, horizontal wells may have to be drilled in each layer that is to be drained. Also, SAGD is not applicable for mobile oils and was not investigated in this study.

Butler and Stephens<sup>33</sup> developed a semi-analytical solution to calculate oil production and oil-steam ratios (OSR) for parallel horizontal wells. Joshi<sup>34</sup> studied two possible well configuration schemes for field applications which are shown in Figure 3.6. Joshi's<sup>34</sup> results indicated that the optimum well scheme for reservoirs with non-continuous shale barriers is Scheme II (Figure 3.6) with vertical injectors and a horizontal producer.

### Well Patterns

Steam override is a common phenomenon in steam injection processes. Steam rises to the formation top, and sweeps the upper portion of the reservoir. The lower portion is primarily swept by condensate. Consequently, high oil saturation zones in the lower portion of the reservoir can remain after a steamflood. Horizontal wells used in combination with vertical wells provide a way to improve the overall sweep efficiency and help to drain such high oil saturation zones. The following discussion on well configurations is based on numerical simulation studies.

Figure 3.7 represents two horizontal well configurations studied by Gussis<sup>35</sup>. The first pattern (Scheme I), a line drive, considers a series of injection and production wells at the base of the reservoir. Scheme II places the injectors at the bottom and the producers at

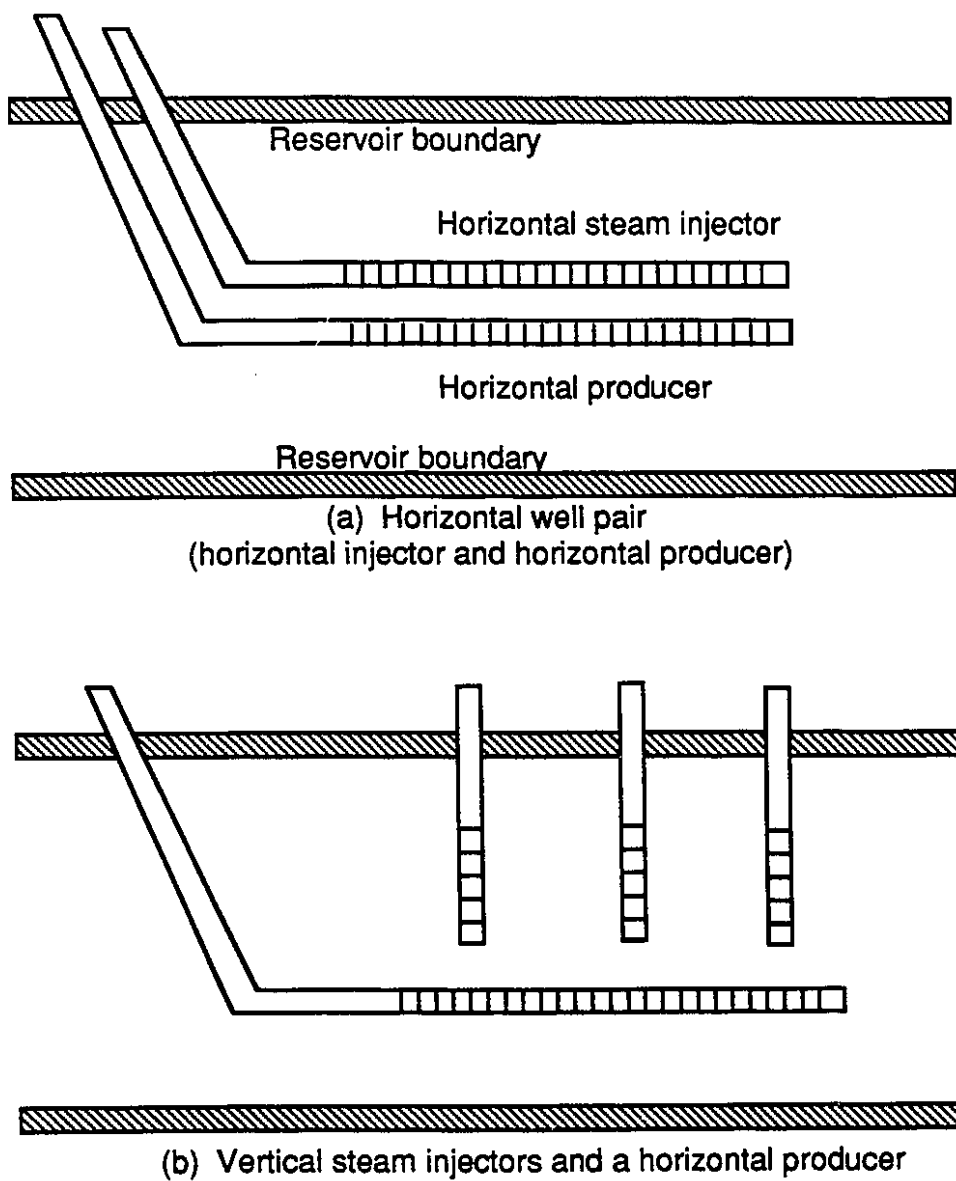


Figure 3.6: Different Well Configuration Schemes for Steam Assisted Gravity Drainage.  
(Modified from Ref. 34)

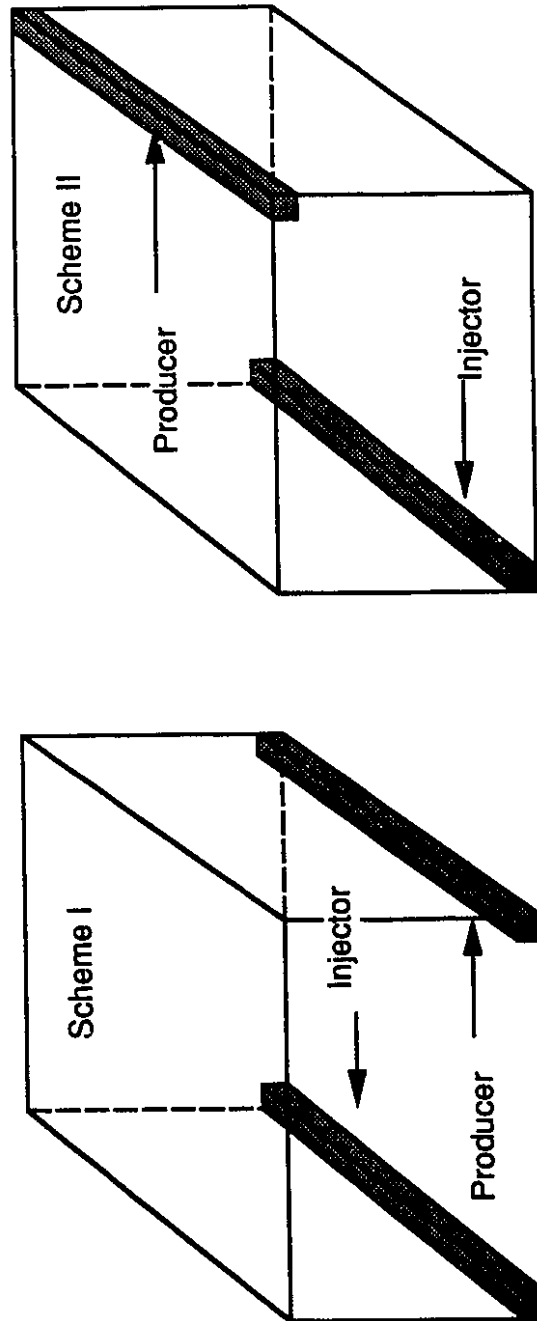


Figure 3.7: A Schematic Diagram of Various Horizontal Well Configurations.  
(Modified from Ref. 35)

the top of the reservoir simulating a zig-zag line drive. Pattern II loses too much heat to the overburden near the top of the reservoir. It was concluded, strictly from a recovery standpoint, that Scheme I produced the best results. This was the scheme used for the horizontal well steam injection experiments in the present study for the Aberfeldy reservoir.

### **Applications of Horizontal Wells to Steamflood Processes**

The selection of oil sand recovery processes is influenced by the formation depth. Shallow formations may be exploited by surface mining techniques, such as the Syncrude and Suncor operations, while deep formations may require in situ methods, as in the case of Esso Resources, who employ horizontal wells with cyclic steaming. However, there are intermediate areas in the Athabasca oil sands which are too deep for mining and too shallow for in situ methods. The Underground Test Facility (UTF), as initiated by the Alberta Oil Sands Technology and Research Authority (AOSTRA), investigates thermal recovery processes (SAGD, and the Heated Annulus Steam Drive or HAS Drive) in the McMurray oil sands formation ( $5 \times 10^6$  mPa·s). One of the primary objectives of this pilot was to develop the shaft and tunnel access concept (SATAC). Three horizontal well pairs were drilled at the base of the column from an underground tunnel system constructed in the Devonian limestone underlying the oil sands. Preliminary results from the pilot indicated that horizontal wells and gravity drainage processes could revolutionize in situ bitumen and heavy oil production by substantially lowering recovery costs than conventional cyclic steam stimulation methods<sup>36</sup>.

Because reservoir conditions at the Kern River field were unfavourable for conventional oil recovery processes or novel oil-mining techniques, such as the UTF, a horizontal-well steam pilot was proposed. It appeared to be an appropriate adjunct to the previous primary and steam-soak operations. Eight horizontal wellbores spaced at  $45^\circ$  increments were drilled radially at the base of the heavy oil column (18 to 20 °API) from a vertical shaft located at the center of the pilot area<sup>37</sup>. Conventional vertical wells were

drilled within each of the eight horizontal well sectors. The horizontal wells were first preheated with steam slugs to initiate oil production. Next, steam was injected vertically and oil was recovered through the horizontal wells. However, as a result of low oil recovery (2.5% of OOIP), which was attributed to low vertical permeability, and unfavourable project economics, the pilot was terminated.

The Tangleflags North Steamflood Pilot involved drilling a 500 m horizontal wellbore to recover the heavy oil (12-13° API) from the Lloydminster area<sup>37,38,39</sup>. A gas cap above and a water table below the reservoir resulted in poor oil production by conventional vertical wells. Horizontal wells offered a feasible alternative to gas or water coning. The pilot, which began in June 1987, was operated for six months without steam and subsequently for 18 months with steam. Two vertical steam injection wells were used in conjunction with a horizontal producer completed at the oil-water contact<sup>39</sup>. It is anticipated that oil recovery will increase from less than 1%, by primary methods, to 50% through a horizontal production well<sup>40</sup>.

### Recovery Using Solvents in Conjunction with Steam

It has been reported previously<sup>41,42</sup> that heavy oil recovery can be improved by injecting a small amount of solvent. The recovery mechanism of an effective solvent on steam recovery processes consists of several factors which improve the sweep by creating a mobile transition zone. When the solvent mixes with the oil, a transition zone of lower-viscosity fluid is created between the steam and heavy oil. As the mobility ratio of the displacing and displaced fluid is improved, viscous fingering is suppressed and sweep efficiency improves. Shu and Hartman<sup>42</sup> found that lighter solvents (CO<sub>2</sub>, ethane or other gases) promoted earlier oil recovery, whereas medium solvents (naphtha) provided the greatest increase in total production. Further, heavy solvents (C<sub>16</sub> to C<sub>20</sub> range) did not improve oil recovery. Oracheski, Farouq Ali and George<sup>41</sup> confirmed the success of



injecting a small naphtha slug prior to steam injection. Shu and Hartman<sup>42</sup> suggested that co-injection of solvents with steam would increase the transition zone and hence, recovery.

Farouq Ali and Snyder<sup>43</sup> investigated the recovery of bitumen using a solvent in a two-dimensional, vertical tar pack. Naphtha injection prior to steam injection in a homogeneous pack was used to develop initial channels for steam flow. This was highly effective in a homogeneous model, but ineffective in the presence of a high permeability channel. Naphtha only entered the permeable channel and did not contact the tar pack. Also, formation plugging caused by asphaltene flocculation during naphtha injection occurred only when large volumes were injected. Using a three-dimensional model, Farouq Ali and Abad<sup>44</sup> found that bitumen recovery depended on the solvent type and slug size, and on the placement of the solvent in the sandpack. Smaller solvent slugs injected through the *production* well were found to be more effective than injection through the injection well.

## Chapter 4

### Scaling Parameters and Calculations

The development of scaled physical models is based on the recognition that dimensional similarities between prototype and model systems exert control over the geometrical, mechanical, thermal and chemical phenomena occurring. This concept of dimensional similarity, as applied by Stegemeier et al.<sup>9</sup> through the principle of inspectional analysis, was used in the development of the scaling parameters. The development of the parametric scaling principles required corresponding model and prototype similarities at the physical and dynamic points within the system. The following chapter discusses the techniques used to implement this scaling method and also presents examples of its application.

#### Development of Scaling Parameters for the Low Pressure Model

##### **Unscaled Parameters**

Scaled physical laboratory models, like numerical models, are developed under certain physical constraints which unfortunately lead to approximations and simplifications in the final product. These simplifications are necessary to achieve greater ease in the handling of the problem and are based on the best current understanding of the process dynamics. Hence, as a result of the simplifications required to match the scaled model and field prototype, it is impossible to satisfy all of the similarity parameters simultaneously. Consequently, a reduced number of parameters known as scaling parameters were generated.

The parameters which were not scaled between the model and prototype systems in this study are:

1. steam distillation of the crude oil;
2. capillary pressure and relative permeability;

3. thermal expansion and compression of the reservoir fluids and matrix;
4. the extent of emulsification and its mechanism;
5. specifications corresponding to the injection and production of a horizontal well (such as pressure drop in the vicinity of and within the wellbore, skin factor, most desirable perforation intervals); and
6. effects of asphaltene flocculation.

For strict scaling, the relative permeability and capillary pressure relationship would have to be the same functions of saturation in both the model and prototype. Unfortunately, they cannot be scaled in an unconsolidated bead pack because of the large difference in the respective grain sizes. They could thus have a significant effect on the displacement processes. Prats<sup>13</sup> stated that the failure to scale relative permeability resulted in the inability to determine the three-phase curves for the prototype under the anticipated operating conditions. In spite of this limitation, Prats<sup>13</sup> produced favourable correlations between the Peace River scaled physical model and prototype. Pujol and Boberg<sup>6</sup> and Demetre<sup>42</sup> proved numerically and experimentally that capillary pressure scaling was not required for a prototype with a high viscosity crude oil. Demetre<sup>45</sup> showed that the breakthrough recovery, at large mobility ratios, was only a weak function of the capillary number provided that the displacement is stable.

The scaling of the parameters stated above could be more readily addressed by a high pressure system where pressure, temperature, fluid and matrix components could be made to approach the values at which the processes occur in practice. However, the success of vacuum model studies imply that the listed phenomena have only a second order effect on the mechanical processes involved in the production of viscous crude oils resulting from steamflood process. It is noted that while these phenomena may not be actively scaled, they may occur and/or exist during the steam drive process.

## Scaling Procedures

The procedure that Stegemeier et al.<sup>9</sup> used to obtain the scaling parameters in Table 4.1 for modelling the steam drive processes was to:

1. formulate the governing equations (partial differential, constraint, constitutive and auxiliary equations) in dimensionless form ( $m_D$ ) by dividing the dimensional variables ( $m$ ) by a suitable reference quantity ( $m_R$ ). Thus:

$$m_D = \frac{m}{m_R} \quad (4.1)$$

2. identify the set of similarity parameters by inspectional analysis; and
3. obtain a set of scaling parameters by combining and modifying, using engineering judgement, the similarity parameters which could be matched between the scaled model and field prototype.

Stegemeier et al.<sup>9</sup> made the following assumptions when deriving the scaling criteria in Equations (4.2) to (4.17) for the low pressure model:

1. three phases consisting of oleic, aqueous and steam phase (no volatile hydrocarbons) may exist;
2. there is no partitioning into or out of the oil phase (dead oil assumption);
3. rock compressibility and thermal expansion are negligible;
4. Darcy's and Fourier's equations are valid;
5. capillary pressure effects are negligible;
6. the system is in local thermodynamic equilibrium;
7. kinetic energy, potential energy and dissipation energy are negligible compared with the thermal energy;
8. the enthalpy and internal energy are linear functions of temperature and are approximately equal for the oleic phase and aqueous phase;
9. the difference between the steam enthalpy and internal energy can be neglected;

**Table 4.1: Scaling Parameters for Steam Processes**

<u>Number</u>	<u>Scaling Parameter</u>	<u>Name of Scaling Parameter</u>
1.	$\frac{P_R}{\rho_R g_R L_R}$	Poiseuille Number divided by Stokes number
2.	$\left( \frac{f_{sR} L_{vt}}{C_R T_R} + 1 \right) \times A^*$	Modified Jacob Number + 1
3.	$\frac{f_{sR} \mu_{sR} \rho_R}{\mu_R \rho_{sR}}$	Ratio of steam pressure gradient to oil pressure gradient
4.	$\frac{k_{hr} t_R}{\phi_R S_R \rho_R C_R L_R^2} \times A^*$	Fourier Number or Peclet Number
5.	$\frac{\phi_{\lambda} S_R \mu_R L_R}{k_R \rho_R g_R t_R}$	Stokes Number
6.	$\frac{w_R t_R}{\rho_R \phi_R S_R L_R^3}$	Poiseuille Number divided by Modified Poiseuille Number

\* Subscript 'R' denotes the reference variable used to obtain a dimensionless term.

\*\* When  $\phi \Delta S$  is not matched, A takes on a value between unity and  $\phi_R S_R \left( \frac{\rho_R C_R}{\rho_{cR} C_{cR}} \right)$ .

~ If reservoir heating or heat production predominates, use unity.

~ If cap and base rock heating predominates, then use  $\phi_R S_R \left( \frac{\rho_R C_R}{\rho_{cR} C_{cR}} \right)$ .

(Modified from Ref. 9)

10. the time rate of change of the specific steam enthalpy in the steam zone is negligible;
11. the internal energy of the rock is a linear function of temperature;
12. the saturated steam temperature is the maximum temperature at any location;
13. relative permeabilities depend exclusively on the saturations;
14.  $S_{ors}$  and  $S_{wc}$  are constant and uniform throughout the model;
15. critical saturation for steam flow is assumed to be zero; and
16. the changes in the density of the immobile water and residual oil are negligible.

Using the above assumptions and applying the conservation of mass balance to the oil phase, denoted by the subscript 'o', yielded:

$$\phi \frac{\partial(\rho_o S_o)}{\partial t} + \nabla \cdot (\rho_o \bar{u}_o) = 0 \quad (4.2)$$

The continuity equation for water, including both liquid and vapour (steam) phases denoted by subscript 'w' for water in the liquid phase and 's' for the vapour, was:

$$\phi \frac{\partial(\rho_w S_w)}{\partial t} + \nabla \cdot (\rho_w \bar{u}_w) + \phi \frac{\partial(\rho_s S_s)}{\partial t} + \nabla \cdot (\rho_s \bar{u}_s) = 0 \quad (4.3)$$

From the assumption that Darcy's equation was valid, the following equation was written for any species j, where j=o, w, or s (z-coordinate is positive downward):

$$\bar{u}_j = -\frac{kk_{rj}}{\mu_j} (\nabla p - \rho_j \bar{g}) \quad (4.4)$$

The conservation of energy for the reservoir was expressed by

$$\begin{aligned} & [(1-\phi)\rho_r C_r + \phi(\rho_o C_o S_o + \rho_w C_w S_w)] \frac{\partial T}{\partial t} + L_v \left[ \phi \frac{\partial(\rho_s S_s)}{\partial t} + \nabla \cdot (\rho_s \bar{u}_s) \right] \\ & + (\rho_o C_o \bar{u}_o + \rho_w C_w \bar{u}_w) \cdot \nabla T + \rho_s \bar{u}_s \cdot \nabla h_s + \nabla \cdot \bar{q} = 0 \end{aligned} \quad (4.5)$$

Conductive heat flux is given by the Fourier equation:

$$\bar{q} = -k_h \nabla T \quad (4.6)$$

When all the saturations were present, the constraint equation became

$$S_o + S_w + S_s = 1 \quad (4.7)$$

The functional form of Clausius-Clapeyron relationship at saturated conditions, where pressure and temperature are mutually dependent, can be written as:

$$P_{sat} = P_{sat}(T_{sat}) \quad (4.8)$$

The remaining constitutive equations, required to describe the dependence of the material properties in the reservoir system on the thermodynamic state variables, were expressed in their functional forms as

$$\phi = \phi(x, y, z) \quad (4.9)$$

$$\rho_j = \rho_j(p, T) \quad (4.10)$$

$$k = k(x, y, z) \quad (4.11)$$

$$k_{rj} = k_{rj}(S) \quad (4.12)$$

$$\mu_j = \mu_j(T) \quad (4.13)$$

$$h_s = h_s(T) \quad (4.14)$$

$$L_v = L_v(T) \quad (4.15)$$

$$k_h = k_h(x, y, z) \quad (4.16)$$

$$\rho_r = \rho_r(x, y, z) \quad (4.17)$$

where  $S$  denotes phase saturation dependence.

### **Calculation of Parametric Values for the Aberfeldy Low Pressure Model**

#### **Prototype and Model Correlations**

The design of the vacuum model involved the selection of representative values that were typical of the Aberfeldy heavy oil reservoir, chosen as the prototype. The calculations

used to scale the prototype data to model values are expressed in this section. A summary of the Aberfeldy prototype and model values is given in Table 4.2.

### Length Scale Selection

Since it was assumed that the model element of symmetry and the prototype are geometrically similar, the scaling factor was defined as the ratio of the dimensions of the model and prototype. The length scale,  $\gamma(L)$ , for a prototype with a production well pressure of 100 psia or less was dependent on the temperature-pressure relationships and the physical constraints placed on the model size. Stegemeier et al.<sup>9</sup> recommended that the best match between the pressure-temperature correlation for saturated steam could be achieved by making  $\gamma(L)$  as small as possible and thus, the model as large as possible within the practical limitations of cost and time to prepare the model. In addition, the increased probability of leaks and the necessity for larger structural requirements for larger models, were also considered. Hence, the selection of the length scale was somewhat arbitrary.

The model used in the study represented one-quarter of an eight hectare five-spot in the Aberfeldy heavy oil reservoir. The prototype length,  $L_p$ , for the 2 ha section was determined to be 141.4 m corresponded to 32 inches (81.3 cm) in the model,  $L_m$ . Since the prototype and model were geometrically similar, the length scale was calculated as

$$\frac{L_p}{L_m} = \gamma(L) = 173.99 \quad (4.18)$$

Applying the length scale in three dimensions, the model thickness representing the prototype thickness of 11 m was 6.3 cm (2.5 in).

### Model Pressure Scaling

The most difficult relationship to match is the Clausius-Clapeyron temperature-pressure relation. The result of not scaling the Clausius-Clapeyron relation is that the



**Table 4.2: Scaling Parameters for the Aberfeldy Reservoir**

<u>Aberfeldy Field Property</u>	<u>Prototype Value</u>	<u>Model Value</u>
Well Spacing	8 hectare (20 acre), 5-spot	1/4 of 5-spot
Depth of Reservoir	522.4 m	—
Net Pay Thickness	11 m	6.32 cm
Gross Pay	Varies from 10 to 13 m	6.32 cm
Porosity	31%	32.1%
Permeability	2000 md	5390.2 d
Thermal Conductivity	0.002077 kW/m•K (1.2 BTU/hr•ft•°F)	0.003266 kW/m•K
Heat Capacity	2.2217 kJ/kg•K	2.3824 kJ/kg•K
Initial Fluid Saturations	$S_o = 0.75$ $S_w = 0.23$ $S_g = 0.02$	$S_o = 0.85$ $S_w = 0.10$ $S_g = 0.05$
Steamflood Residual Oil Saturation	$S_{or} = 0.15$	$S_{or} = 0.05$
Oil Viscosity	1275 mPa•s at 23.9°C 560 mPa•s at 32.2°C 90 mPa•s at 65.6°C 12.5 mPa•s at 135.0°C 1.29 mPa•s at 301.7°C	9257 mPa•s at 3.2°C 243 mPa•s at 22.9°C
Water Viscosity	0.891 mPa•s at 25.8°C	0.891 mPa•s at 25.8°C
Gas Viscosity	0.013 mPa•s at 23.3°C 0.016 mPa•s at 134.4°C	—
Solvent Viscosity	0.46 mPa•s at 25.0°C	0.46 mPa•s at 25.0°C
Specific Gravity of Gas	0.55	—
Initial Reservoir Temperature	23.3°C	3.0°C
Initial Reservoir Pressure	3.45 MPa	0.0267 MPa
Steam Injection Pressure	1.9 MPa	—
Steam Injection Rate	100 - 150 m <sup>3</sup> /D	247.49 cm <sup>3</sup> /min
Steam Quality	0.70 (Actually $f_{st}$ is 0.80 to 0.85, but a lower value was used to compensate for wellbore heat loss)	0.093
Solvent Injection Rate	80.81 m <sup>3</sup> /D	200 cm <sup>3</sup> /min
Pressure Range	Upper Range: fracture gradient of reservoir Lower Range: bottom hole production pressure (0.345 MPa (50 psia) back pressure)	Lower Range: 0.006895 MPa (1 psia)

temperature and pressure will not correspond at all points within the steam zone. This problem is overcome by operating the model at subatmospheric pressure levels and low temperatures. Thus, for typical prototype length scales of 100 to 200 and pressures as low as 0.345 MPa (50 psia), the best match can be obtained by selecting the lowest possible value of model production pressure. From a practical standpoint, the lowest pressure that can be maintained is limited by the vapour pressure and the physical constraints of the vacuum pump is approximately 1 psia.

From the parametric equality:

$$\gamma(\Delta p) = \frac{(p - p_p)_p}{(p - p_m)_m} = \frac{\rho_p g_p L_p}{\rho_m g_m L_m} \quad (4.19)$$

where:  $\frac{L_p}{L_m} = \gamma(L) = 173.99$

$$\gamma(\rho_r) = \frac{\rho_p}{\rho_m} = 0.9 \quad (4.20)$$

$$\gamma(g_r) = \frac{g_p}{g_m} = 1.0 \quad (4.21)$$

$$(pp)_m = 0.345 \text{ MPa (50 psia)} \quad (4.22)$$

$$(pp)_p = 6.895 \text{ kPa (1 psia)} \quad (4.23)$$

where  $p_p$  denotes production well pressure.

Table 4.3 is obtained by substituting the identities in equations (4.18) and (4.20) through (4.23) into equation (4.19) to obtain the model pressure relation as a function of the prototype pressure, where  $p_m$  and  $p_p$  are in MPa:

Table 4.3: Prototype and Model Scaling Values

Prototype Values										Model Values									
P (MPa)	Ts (C)	hw (kJ/kg)	CwΔT (kJ/kg)	Lv (kJ/kg)	p (kg/m <sup>3</sup> )	μs (cp)	P (MPa)	Ts (C)	Tsc (C)	hw (kJ/kg)	CwΔT (kJ/kg)	Lv (kJ/kg)	p (kg/m <sup>3</sup> )	μs (cp)	fs	μom/μop (cp/cp)	wa/wt	hss (kJ/kg)	
*	*	*	*	*	*	**	Eq.4.24	*	Eq.4.27	*	*	*	*	**	Eq.4.37	Eq.4.39	Eq.4.38	**	
3.45	241.73	1045.6	949.1	1757.9	19.220	0.0175	0.0267	66.39	65.48	277.9	265.3	2342.8	0.170	0.0112	0.070	8.02	0.8734	2723.5	
3.00	233.90	1008.4	911.9	1795.7	14.997	0.0173	0.0239	63.83	63.24	267.2	254.6	2349.1	0.153	0.0111	0.073	7.33	0.8744	2723.8	
2.50	223.99	962.1	865.6	1841.0	12.508	0.0169	0.0207	60.84	60.40	254.1	241.5	2356.7	0.134	0.0110	0.077	7.44	0.8756	2724.1	
2.00	212.42	908.8	812.3	1890.7	10.037	0.0165	0.0175	56.97	57.10	238.5	225.9	2365.8	0.113	0.0109	0.081	7.56	0.8775	2724.4	
1.50	198.32	844.9	748.4	1947.3	7.589	0.0160	0.0143	52.40	53.06	220.9	208.3	2376.0	0.094	0.0107	0.087	7.47	0.8792	2724.7	
1.00	179.91	762.8	666.3	2015.3	5.143	0.0153	0.0111	47.85	47.80	199.1	186.6	2388.6	0.073	0.0106	0.093	7.17	0.8809	2725.1	
0.50	151.86	640.2	543.7	2108.5	2.667	0.0143	0.0079	41.13	39.77	172.3	159.7	2404.0	0.054	0.0103	0.107	6.07	0.8777	2725.4	
0.345	138.36	582.0	485.5	2149.7	0.532	0.0138	0.0069	38.45	35.91	161.1	148.5	2410.4	0.046	0.0102	0.116	1.60	0.8736	2725.5	

\* "Fundamentals of Classical Thermodynamics", 3rd Ed., SI Version by G.J. Van Wylen and R.E. Sonntag (1985), Ref. 46

where: p = steam density=1/specific volume of steam

\*\* μs = (0.2T+81.97)\*10\*\*<sup>-4</sup> where T in °F, μs in cp and T(°F) = 9/5T(°C)+32, Ref. 47

$$\frac{(p - 0.345 \text{ MPa})_p}{(p - 0.006895 \text{ MPa})_m} = 0.9 \times 1.0 \times 173.2$$

which reduces to:  $p_m = 0.004692 + 0.006386p_p$  (4.24)

### Model Temperature Scaling

To obtain the best match between the model and prototype oil viscosity curves, it is desirable to make the model temperature range as large as possible and hence, the initial model temperature as low as possible. However, from a practical standpoint, the minimum initial model temperature  $(T_i)_m$  is about 3°C since cooling below this range would have resulted in localized freezing of the model.

Stegemeier et al.<sup>9</sup> recommend selecting a value in the middle of the pressure range when calculating the temperature difference ratio since the majority of oil production will occur when these temperatures are significant. This is further supported by the fact that a poor fit is achieved for the pressure-temperature relation for saturated steam in the lower pressure range.

From the relation:

$$\frac{(\Delta T)_p}{(\Delta T)_m} = \frac{(T_p - T_R)_p}{(T_m - T_R)_m} = \frac{(T_s - T_R)_p}{(T_s - T_R)_m} \quad (4.25)$$

and using the midrange prototype and model temperatures from Table 4.3:

$$(T_R)_p = 23.3^\circ\text{C}$$

$$(T_R)_m = (T_i)_m = 3.0^\circ\text{C}$$

$$(T_s)_p = 212.42^\circ\text{C (at 2.0 MPa)}$$

$$(T_s)_m = 56.97^\circ\text{C (at 0.0175 MPa)}$$

substitution leads to 
$$\frac{\Delta T_p}{\Delta T_m} = \frac{212.42^\circ\text{C} - 23.3^\circ\text{C}}{56.97^\circ\text{C} - 3.0^\circ\text{C}}$$

which yields the identity 
$$\frac{\Delta T_p}{\Delta T_m} = 3.5 \quad (4.26)$$

To have the properly scaled proportion of energy stored as internal energy, this ratio must be constant over the temperature range. Thus,

$$\frac{(T_p - 23.3^\circ\text{C})_p}{(T_m - 3.0^\circ\text{C})_m} = 3.5$$

Or, 
$$T_m = 0.286T_p - 3.657 \quad (4.27)$$

As noted from Table 4.3, the calculated values,  $T_{SC}$ , do not correspond exactly with the saturation temperatures,  $T_s$ . Stegemeier et al.<sup>9</sup> state that better scaling is achieved by allowing the error to occur at lower temperatures.

### Time Scale Determination

Using the dimensionless parameter (4) in Table 4.1 and assuming that the heating of the cap and base rock predominates such that  $A^* = \phi_R S_R (\rho_R C_R / \rho_{cR} C_{cR})$ , Stegemeier et al.<sup>9</sup> developed the following time scale ratio:

$$\frac{t_m}{t_p} = \left( \frac{k_{hp}}{k_{hm}} \right) \left( \frac{\rho_{cm} C_{cm}}{\rho_{cp} C_{cp}} \right) \left( \frac{L_m}{L_p} \right)^2 \quad (4.28)$$

where  $k_{hm} = k_{\text{granite}} = 0.003266 \text{ kW/m}\cdot\text{K} (2.81 \text{ kcal}/(\text{m}\cdot\text{hr}\cdot^\circ\text{C}))$

$k_{hp} = k_{\text{sandstone}} = 0.002077 \text{ kW/m}\cdot\text{K}$

$\rho_{cm} C_{cm} = 2.3824 \text{ kJ/kg}\cdot\text{K}$  (granite cap block)

$\rho_{cp} C_{cp} = 2.1803 \text{ kJ/kg}\cdot\text{K}$  (sandstone cap block)

$$\frac{L_p}{L_m} = 173.99$$

The density-specific heat products for the cap rock and the reservoir matrix were assumed to be approximately equal:

$$\rho_{cm}C_{cm} = \rho_{cp}C_{cp} \text{ and } \rho_m C_m = \rho_p C_p \quad (4.29)$$

Therefore, the substitution of the variables into equation (4.28) yields

$$\frac{t_m}{t_p} = \left( \frac{0.002077 \text{ kW / m} \cdot \text{K}}{0.003266 \text{ kW / m} \cdot \text{K}} \right) \left( \frac{\rho_{cm} C_{cm}}{\rho_{cp} C_{cp}} \right) \left( \frac{1}{173.99} \right)^2 = 2.1007 \times 10^{-5}$$

For  $t_m$  in minutes and  $t_p$  in years, the final form of the time ratio is:

$$\frac{t_m}{t_p} = 2.1007 \times 10^{-5} \times 365.25 \text{ D / yr} \times 24 \text{ hr / D} \times 60 \text{ min / hr}$$

$$\frac{t_m}{t_p} = 11.05 \text{ min / yr} \quad (4.30)$$

### Flow Rate Scaling

Stegemeier et al.<sup>9</sup> used parameter (6) in Table 4.2 to scale the injection and production rates:

$$\frac{w_m}{w_p} = \left( \frac{\rho_{om}}{\rho_{op}} \right) \left( \frac{L_m}{L_p} \right)^3 \left( \frac{\phi_m \Delta S_m}{\phi_p \Delta S_p} \right) \left( \frac{t_p}{t_m} \right) \quad (4.31)$$

where from (4.18), (4.20) and (4.28):

$$\frac{L_p}{L_m} = 173.99$$

$$\gamma(\rho_r) = \frac{\rho_p}{\rho_m} = 0.9$$

$$\frac{t_m}{t_p} = 2.1007 \times 10^{-5}$$

and  $\phi_m = 0.321$  (in accordance with the specifications of the Wygal<sup>48</sup> particle distributor) (4.32)

$$\phi_p = 0.31 \quad (4.33)$$

$$\Delta S_m = 0.85 \quad (\text{scaling assumption}) \quad (4.34)$$

$$\Delta S_p = 1 - S_{or} - S_{wc} = 1 - 0.15 - 0.23 = 0.62 \quad (4.35)$$

Substitute identities (4.18), (4.29) and (4.31) to (4.34) into equation (4.30):

$$\frac{w_m}{w_p} = \left( \frac{1}{0.9} \right) \left( \frac{1}{173.99} \right)^3 \left( \frac{0.321 \times 0.85}{0.21 \times 0.625} \right) \left( \frac{1}{2.1007 \times 10^{-5}} \right) = 0.143 \times \left( \frac{10^6 \text{ cm}^3}{24 \text{ hr} / D \times 60 \text{ min} / \text{hr}} \right) \frac{1}{\text{m}^3 / D}$$

which reduces to:

$$\frac{w_m}{w_p} = 9.8995 \frac{\text{cm}^3 / \text{min}}{\text{m}^3 / D} \quad (4.36)$$

Since the model simulates one quarter of the total prototype injection rate of  $100 \text{ m}^3/D$ , the total steam injection rate,  $q_{ism}$ , for this study was determined to be  $247.49 \text{ cm}^3/\text{min}$  as follows:

$$q_{ism} = \frac{1}{4} \times 100 \text{ m}^3 / D \times 9.8995 \frac{\text{cm}^3 / \text{min}}{\text{m}^3 / D} = 247.49 \text{ cm}^3 / \text{min}$$

### Scaling of Steam Quality

When using parameter (2) in Table 4.2 to determine the model steam quality, Stegemeier et al.<sup>9</sup> assumed that cap and base rock heat predominates, which is often the case in steam drive processes in thin reservoirs, so  $A^* = \phi_R S_R (\rho_R C_R / \rho_{cR} C_{cR})$ :

$$f_{sm} = \left( \frac{C_w \Delta T}{L_v} \right)_m \left\{ \left( \frac{f_s L_v}{C_w \Delta T} + 1 \right)_p \times \left[ \left( \frac{\phi_p \Delta S_p}{\phi_m \Delta S_m} \right) \left( \frac{\rho_p C_p}{\rho_m C_m} \right) \left( \frac{\rho_{cm} C_{cm}}{\rho_{cp} C_{cp}} \right) \right] - 1 \right\} \quad (4.37)$$

The model steam quality was then calculated for all corresponding pressures in Table 4.3 using the constants as already described in (4.29), and (4.32) to (4.35) with  $f_s = 0.70$  for the prototype.

#### Example 4.1:

All the sample calculations, unless otherwise specified, pertain to the last row of data in Table 4.3 corresponding to  $p_p = 0.345$  MPa (50 psia) and  $p_m = 0.006895$  MPa (1 psia).

$$f_{sm} = \left( \frac{148.53 \text{ kJ/kg}}{2410.39 \text{ kJ/kg}} \right)_m \left\{ \left( \frac{0.7 \times 2149.7 \text{ kJ/kg}}{485.48 \text{ kJ/kg}} + 1 \right)_p \times \left[ \left( \frac{0.31 \times 0.62}{0.321 \times 0.85} \right) (1)(1) \right] - 1 \right\} = 0.1163$$

To complete the scaling of steam quality, the proportions of injected water ( $w_a$ ) and superheated steam ( $w_{ss}$ ) were calculated. The quality and hence, water proportions was a function of the enthalpy of steam from the steam generator at 120°C, the temperature of the feed water (generally taken at the room temperature at 23°C) and the heat loss from the metal lines. The heat balance is formed by equating the enthalpy rate of the two inlet water streams mixed together ( $w_{wt} = w_a + w_{ss}$ ) to the enthalpy rate of wet steam injected into the model plus the heat losses.

$$\frac{w_a}{w_{wt}} = \frac{w_a}{w_a + w_{ss}} = \frac{h_{ss} - f_s L_v - C_w \Delta T - q_h / w_{wt}}{h_{ss} - h_{wa}} \quad (4.38)$$

The heat loss ( $q_h$ ) was assumed to be zero.



**Example 4.2:**

$$\frac{w_s}{w_{wt}} = \frac{2725.5 \text{ kJ/kg} - (0.1163 \times 2410.39 \text{ kJ/kg}) - 148.53 \text{ kJ/kg} - 0}{2725.5 \text{ kJ/kg} - 96.518 \text{ kJ/kg}} = 0.8736$$

**Scaling of Model Oil Viscosity**

It is important that oil production after steam breakthrough be scaled by matching the pressure gradient in the steam zone and oil. Thus, the oil viscosity was scaled according to parameter (3) in Table 4.2:

$$\frac{\mu_{om}}{\mu_{op}} = \left( \frac{f_{sm}}{f_{sp}} \right) \left( \frac{\mu_{sm}}{\mu_{sp}} \right) \left( \frac{\rho_{sp}}{\rho_{sm}} \right) \left( \frac{\rho_{om}}{\rho_{op}} \right) \quad (4.39)$$

**Example 4.3:**

Substituting the data from Table 4.3 and identities  $f_s = 0.70$  and (4.20) into equation (4.39) yields:

$$\frac{\mu_{om}}{\mu_{op}} = \left( \frac{0.116}{0.70} \right) \left( \frac{0.0102}{0.0138} \right) \left( \frac{0.532}{0.046} \right) \left( \frac{1}{0.9} \right) = 1.60$$

**Scaling of Model Permeability**

Stegemeier et al.<sup>9</sup> scaled the model permeability using Stokes Number (Parameter Number 5) in Table 4.1:

$$\frac{k_m}{k_p} = \left( \frac{\phi_m \Delta S_m}{\phi_p \Delta S_p} \right) \left( \frac{L_m}{L_p} \right) \left( \frac{\mu_m}{\mu_p} \right) \left( \frac{\rho_{op}}{\rho_{om}} \right) \left( \frac{t_p}{t_m} \right) \quad (4.40)$$

Equation (4.40) shows that  $k_m/k_p$  is temperature dependent since  $\mu_m/\mu_p$  is a function of temperature. However, since  $k_m/k_p$  cannot be a function of temperature, a single representative value of  $\mu_m/\mu_p$  must be selected to determine a single value for the model permeability. As previously noted, the  $\mu_m/\mu_p$  ratio is significant only when steam pressures are low. This occurs after steam breakthrough and around the vicinity of the

production well. Consequently, Stegemeier et al.<sup>9</sup> suggested that the lower portion of Table 4.3 should be weighted heavily. Substituting an average value of  $\mu_m/\mu_p$  taken at a 1.00 MPa prototype pressure, and the constants defined in (4.18), (4.20), (4.30), (4.32) to (4.35) into Equation (4.40) yields:

$$\frac{k_m}{k_p} = \left( \frac{0.321 \times 0.85}{0.31 \times 0.62} \right) \left( \frac{1}{173.99} \right) (7.71)(0.9) \left( \frac{1}{2.1007 \times 10^{-5}} \right) = 2695.08$$

Since the permeability of the prototype,  $k_p$ , is 2 darcies,

$$k_m = k_p \times 2695.08 = 2 \text{ darcies} \times 2695.08$$

Thus,  $k_m = 5390.17 \text{ darcies}$  (4.41)

### Scaling of Vertical Wells

As a result of the small size of the model with a length scale of 173.99 and the large size of the glass beads, it was impractical to geometrically scale the vertical wells directly. This was primarily due to the mechanical problems encountered in constructing a small diameter well as well as the probability that the well size would lose significance when the diameter of the beads in the porous medium approached or exceeded the model diameter. Stegemeier et al.<sup>9</sup> introduced the 'slit' well concept where the effective radius of the slit was a function of the bead pack arrangement in front of the slit and the slit width,  $\omega$ :

$$\omega = 2\pi r_m \quad (4.42)$$

where  $\omega$  = slit width and  $r_m$  = the effective radius of the model well.

This study assumed that the diameter of the prototype well was 6 inches. Using this assumption and substituting it into equation (4.18), the model well width was determined to be 0.108" as described below:

$$L_m = \frac{L_p}{173.99} = \frac{6''}{173.99} = 0.0345'' = d_m$$

Thus, since the model well radius is  $r_m = 0.01725''$ , the slit width was calculated from equation (4.42):

$$\omega = 2\pi(0.01725'') = 0.108'' \quad (4.43)$$

Table 4.4 summarizes the scaling set used for the Aberfeldy model.

### Derivation of Scaling Criteria for Steam Injection with Gas as an Additive

Scaling criteria for steam injection with an inert gas as the only additive present with the steam was derived by inspectional analysis for a one dimensional system, not necessarily horizontal. The assumptions used to develop the scaling criteria were based on the following series of assumptions:

1. gas is present with steam;
2. the additive may be present in the oleic and vapour phases only, but not in the aqueous phase, which consists only of water;
3. the vapour phase consists of both steam and the gas additive;
4. the solubility of the gas in oil is zero; and
5. diffusion and dispersion effects are neglected.

Define  $C_{ij}$  as the concentration of phase  $i$  in component  $j$ . Assume this is a three phase system, consisting of the oleic (o), aqueous (a) and vapour (g) phases. The three components are oil (o), water (w) and additive (gas). Table 4.5 lists the constraints and constitutive relationships used in the derivation.

Using the above assumptions and applying the conservation of mass to the oil equation yields:

$$\nabla \cdot \left[ \frac{\rho_o k_o}{\mu_o} (\nabla p_o + \rho_o g \nabla D) \right] + q_o^* = \frac{\partial}{\partial t} (\phi S_o \rho_o) \quad (4.44)$$

**Table 4.4: Scaling Set for Steam Processes**

Length Scale:  $\frac{L_p}{L_m} = \gamma(L) = 173.99$  (4.18)

Pressure Relation:  $p_m = 0.004692 + 0.006386p$  (4.24)

Temperature Relation:  $T_m = 0.286T_p - 3.65$  (4.27)

Time Scale:  $\frac{t_m}{t_p} = 11.05 \text{ min / yr}$  (4.30)

Steam Quality: 
$$f_{sm} = \left( \frac{C_w \Delta T}{L_v} \right)_m \left\{ \left( \frac{f_s L_v}{C_w \Delta T} + 1 \right)_p \times \left[ \left( \frac{\phi_p \Delta S_p}{\phi_m \Delta S_m} \right) \left( \frac{\rho_p C_p}{\rho_m C_m} \right) \left( \frac{\rho_{cm} C_{cm}}{\rho_{cp} C_{cp}} \right) \right] - 1 \right\}$$
 (4.32)

$$\frac{w_s}{w_{wt}} = \frac{w_s}{w_s + w_m} = \frac{h_m - f_s L_v - C_w \Delta T - q_b / w_{wt}}{h_m - h_{ws}}$$
 (4.33)

Viscosity Ratio:  $\frac{\mu_{cm}}{\mu_{cp}} = \left( \frac{f_m}{f_{sm}} \right) \left( \frac{\mu_{sm}}{\mu_{sp}} \right) \left( \frac{\rho_{sp}}{\rho_{sm}} \right) \left( \frac{\rho_{cm}}{\rho_{cp}} \right)$  (4.34)

Injection and Production Rates:  $\frac{w_m}{w_p} = 9.8995 \frac{\text{cm}^3 / \text{min}}{\text{m}^3 / \text{D}}$  (4.36)

Permeability  $k_m = 5390.17 \text{ darcies}$  (4.41)

Slit Width  $\omega = 0.108''$  (4.43)

**Table 4.5: Constraints and Constitutive Relationships**

<u>Constraints</u>	<u>Constitutive Relationships</u>
$S_o + S_w + S_g = 1$	$\rho_o = \rho_o(p_o, T)$
$C_{ga} + C_{gw} = 1$	$\rho_w = \rho_w(p_w, T)$
$p_g = p_o + p_{cgo}(S_o, S_w)$	$\rho_g = \rho_g(p_g, T, C_{ga}, C_{gw})$
$p_w = p_o - p_{cow}(S_o, S_w)$	$\mu_o = \mu_o(p_o, T)$
$C_{gw} = K_{w gw}(p, T, C_{gw})$	$\mu_w = \mu_w(p_w, T)$
$C_{ga}/C_{gw} = K_{gaw}(p, T, C_{ga}, C_{gw})$	$\mu_g = \mu_g(p_g, C_{ga}, C_{gw})$
	$k_o = k_o(S_o, S_w, S_g)$
	$k_w = k_w(S_o, S_w, S_g)$
	$k_g = k_g(S_o, S_w, S_g)$
	$h_o = h_o(p, T)$
	$h_w = h_w(p, T)$
	$h_g = h_g(p, T)$
	$h_r = h_r(T)$
	$k_{hr} = k_{hr}(T)$
	$k_{hob} = k_{hob}(T)$
	$\phi = \text{constant}$
	$\rho_r = \text{constant}$
	$g = \text{constant}$
	$D = D(x, y, z)$
	$U_o = U_o(p, T, h_o)$
	$U_w = U_w(p, T, h_w)$
	$U_g = U_o(p, T, h_g, C_{ga}, C_{gw})$
	$U_r = U_r(T)$

Similarly, the material balance equation for water, including both the aqueous and vapour phase, can be written as:

$$\begin{aligned} \nabla \cdot \left[ \frac{\rho_w k_w}{\mu_w} (\nabla p_w + \rho_w g \nabla D) \right] + \nabla \cdot \left[ \frac{C_{gw} \rho_g k_g}{\mu_g} (\nabla p_g + \rho_g g \nabla D) \right] + q_w^* + C_{gw}^* q_g^* \\ = \frac{\partial}{\partial t} (\phi S_w \rho_w + \phi S_g C_{gw} \rho_g) \end{aligned} \quad (4.45)$$

The continuity equation for the gas additive is:

$$\nabla \cdot \left[ \frac{C_{ga} \rho_g k_g}{\mu_g} (\nabla p_g + \rho_g g \nabla D) \right] + C_{ga}^* q_g^* = \frac{\partial}{\partial t} (\phi S_g C_{ga} \rho_g) \quad (4.46)$$

Applying the law of conservation to the energy term yields:

$$\begin{aligned} \nabla \cdot (k_{tr} \nabla T) + \nabla \cdot \left[ \frac{\rho_o k_o h_o}{\mu_o} (\nabla p_o + \rho_o g \nabla D) \right] \\ + \nabla \cdot \left[ \frac{\rho_w k_w h_w}{\mu_w} (\nabla p_w + \rho_w g \nabla D) \right] \\ + \nabla \cdot \left[ \frac{\rho_g k_g h_g}{\mu_g} (\nabla p_g + \rho_g g \nabla D) \right] \\ + q_h^* - q_l^* \\ = \phi \frac{\partial}{\partial t} (\rho_o S_o U_o + \rho_w S_w U_w + \rho_g S_g U_g) + (1 - \phi) \rho_r \frac{\partial U_r}{\partial t} \end{aligned} \quad (4.47)$$

The expanded forms of the oil, water, additive and energy balances are presented in Appendix A. Table 4.6 is a summary of the scaling criteria for steam injection with a gas additive, derived by inspectional analysis.

Dimensional analysis may be employed if the differential equation is not known. The objective is to express the variable of interest as a function of other variables. Buckingham's Pi Theorem is used to obtain the final relationships, with the particular variable embedded in a dimensionless group. This group is subsequently expressed as a

**Table 4.6: Similarity Groups from Inspectional Analysis**

$$\frac{\rho_{oR} g_R D_R}{\rho_{oR}}, \frac{H}{L}, \frac{W}{L}, \frac{D}{L}, \frac{\rho_{wR}}{\rho_{gR}}, \frac{\rho_{oR}}{\rho_{gR}}, \frac{q_{gR}^{\cdot}}{q_{wR}^{\cdot}}, \frac{q_{gR}^{\cdot}}{q_{oR}^{\cdot}}, \frac{q_{oR}^{\cdot}}{q_{gR}^{\cdot}}$$

$$\frac{\mu_{gR} k_{oR}}{\mu_{oR} k_{gR}}, \frac{\mu_{wR} k_{oR}}{\mu_{oR} k_{wR}}, \phi_R, \frac{U_{oR}}{h_{oR}}, \frac{U_{wR}}{h_{oR}}, \frac{U_{gR}}{h_{oR}}, \frac{h_{wR}}{h_{oR}}, \frac{h_{gR}}{h_{oR}}$$

$$\frac{q_{hR}^{\cdot}}{h_{oR} q_{oR}^{\cdot}}, \frac{\rho_{rR} U_{rR}}{\rho_{oR} h_{oR}}, \frac{k_{ch} \rho_{oR} C_{ob} \rho_{ob}}{k_{hob} \phi_R S_{oR} \mu_{oR}}, \frac{S_{oR}}{S_{oR}}, \frac{S_{wR}}{S_{wR}}$$

$$\frac{P_{oR}}{P_{oR}}, \frac{P_{oR}}{P_{gR}}, \frac{P_{oR}}{P_{gR}}, \frac{P_{cpor}}{P_{gR}}, \frac{P_{cowR}}{P_{wR}}, \frac{\alpha_{rR}}{\alpha_{obR}}, \frac{T_{rR}}{T_R}$$

product of powers of other dimensionless groups composed of the variables involved. Given  $n$  separate variables and  $k$  principal dimensions (mass, length, time, temperature, force, and heat), a complete set of relationships will consist of  $n-k$  dimensionless groups<sup>48</sup>. Inspectional analysis normalizes differential equations by making independent variables dimensionless, and carrying out a judicious rearrangement of these variables. However, as it is impossible to describe all process phenomena with differential equations, inspectional analysis will not give all the groups. Hence, it is advisable to also derive the similarity groups by dimensional analysis to obtain a complete set of dimensionless groups.



## Chapter 5

### Experimental Apparatus and Procedure

This chapter describes the apparatus, materials and procedures used in this study. This section summarizes the experimental procedures, such as packing and fluid saturation, used when preparing and operating homogeneous, bottom water and gas injection models. Appendix B provides detailed information about the laboratory apparatus and procedures. Appendix C lists the suppliers of the materials used in this study.

#### Experimental Apparatus

The apparatus used in this study consisted of the following essential components: the model cart and rail system, solvent and steam injection equipment, produced fluids collection unit, and cold storage component. Figure 5.1 is a schematic illustration of the scaled physical model and its accompanying equipment. Plates 5.1 and 5.2 present an overall view of the experimental apparatus including the cap and base rocks clamped in place on the scaled physical model.

#### **Physical Model**

The model used in this study was designed to represent one-quarter of an eight hectare (20 acre) five spot pattern having the dimensions of 281.55 m x 281.55 m x 11 m (thick) in the Aberfeldy heavy oil reservoir. Plate 5.3 is a photograph of the scaled physical model, which was a custom built fibreglass tray filled with glass beads that simulated the porous medium. Four vertical slit wells were constructed, according to the description of the scaled vertical wells used by Stegemeier et al., in each corner of the fibreglass model. Granite blocks were placed above and below the model to act as the overburden and underburden.

Because the model was to be designed with the length scale factor of 173.99, the fibreglass tray was constructed with the dimensions of 81.28 cm (32 in) x 81.28 cm (32 in) x 6.35 cm (2.5 in thick). To satisfy the low pressure scaling criteria, the experiments were

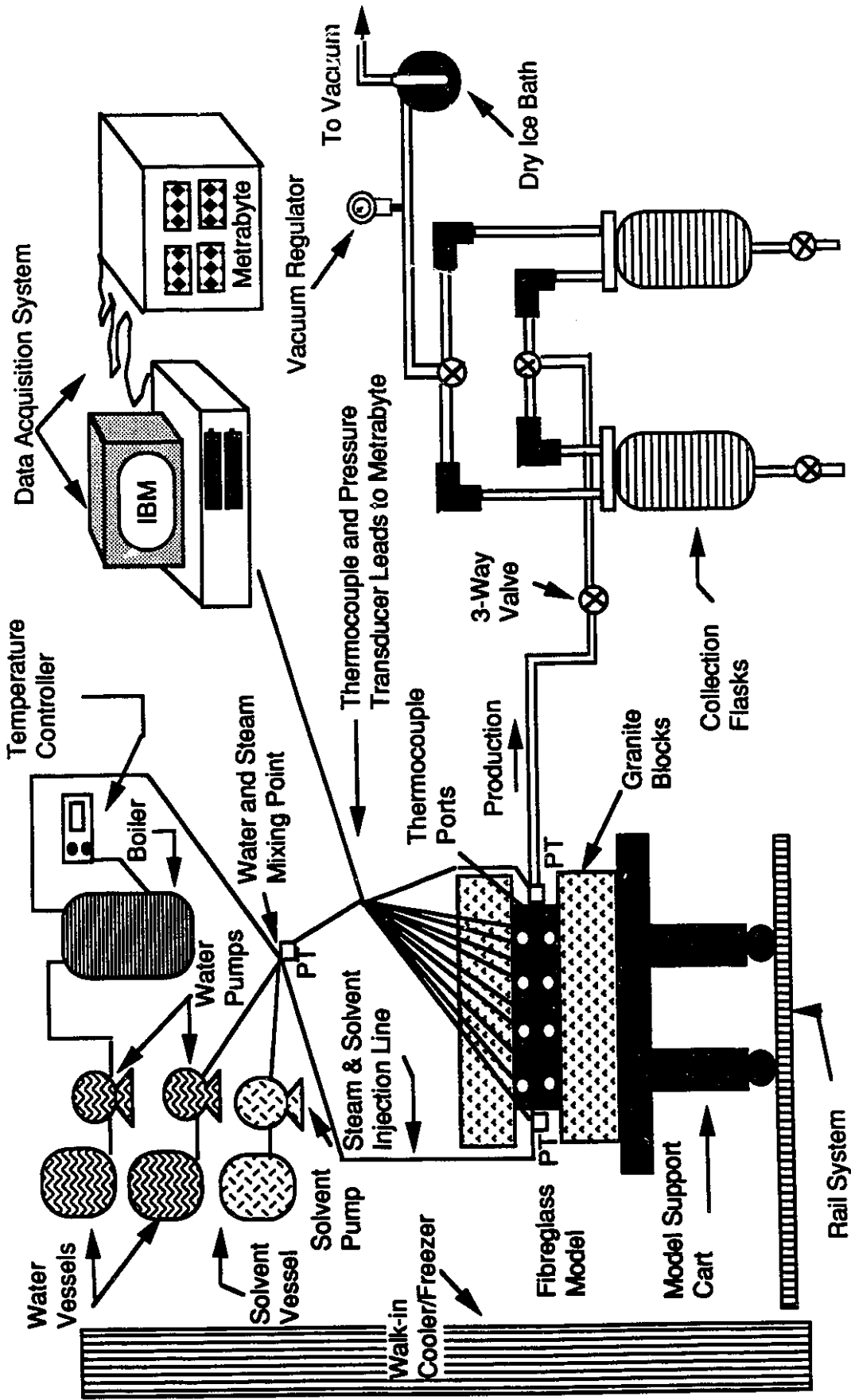


Figure 5.1: Schematic Diagram of Apparatus

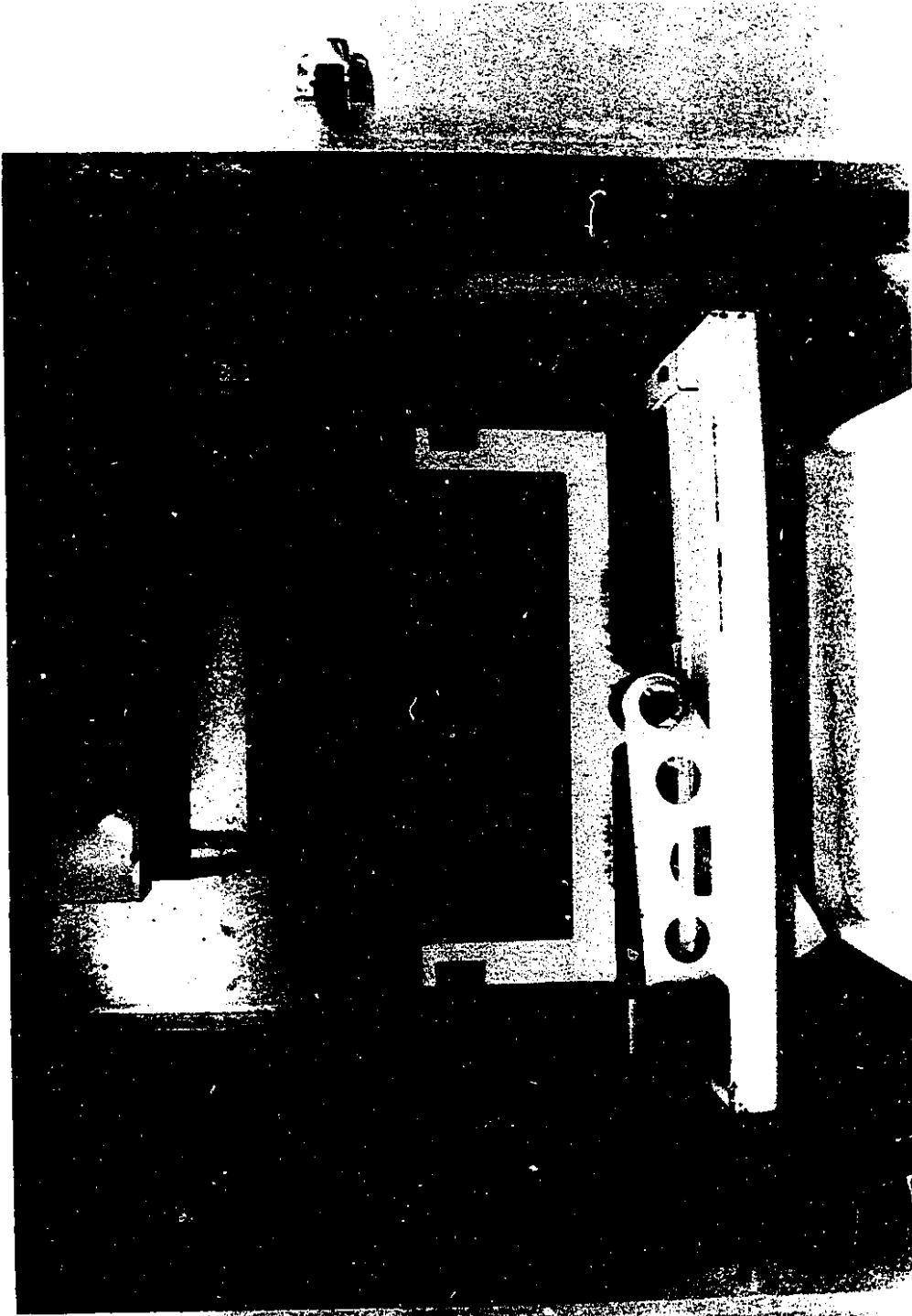


Plate 5.1: Overall View of the Low Pressure Apparatus.



Plate 5.2: View of Apparatus in Operation.

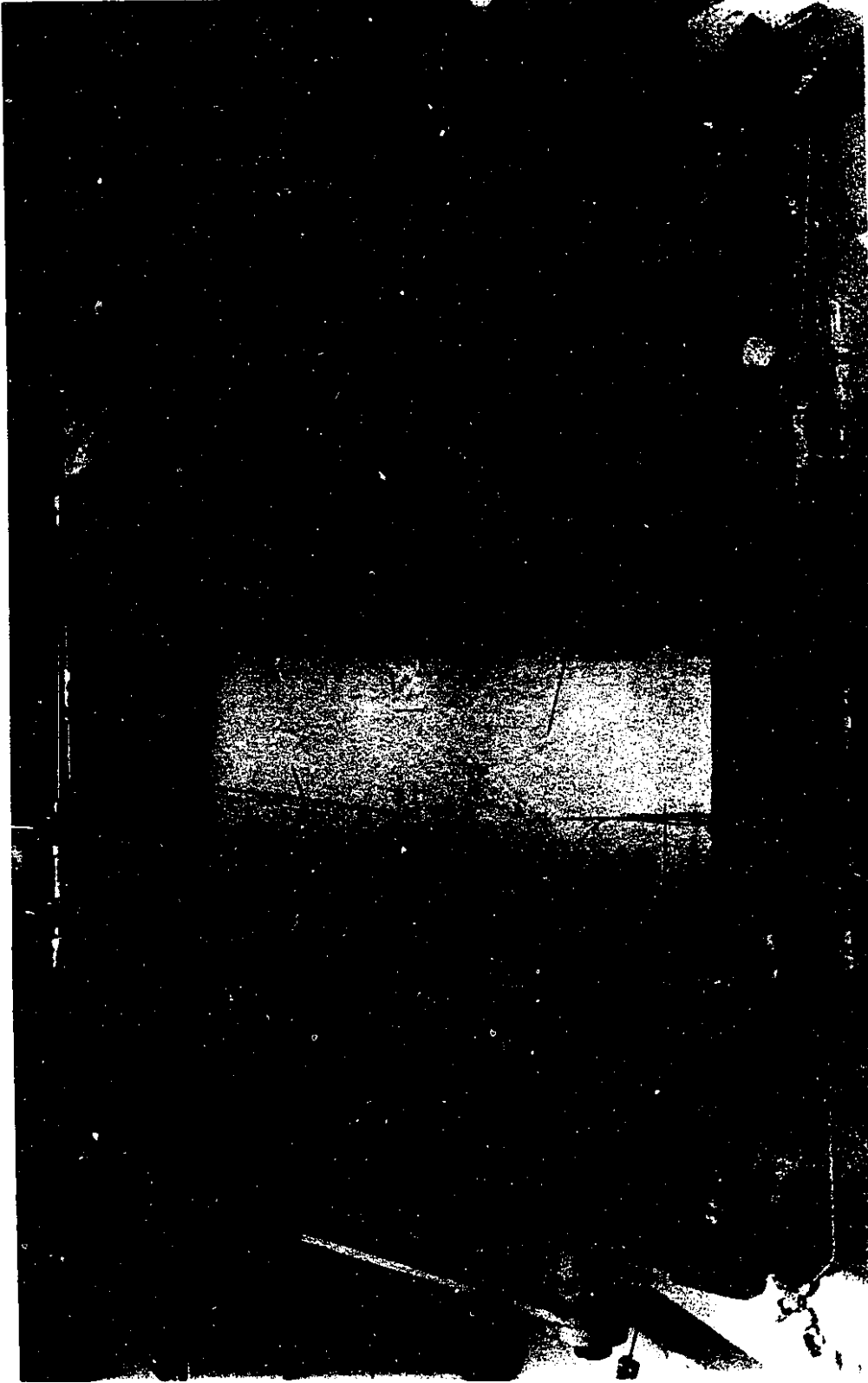


Plate 5.3: The Scaled Model of the Aberfeldy Reservoir

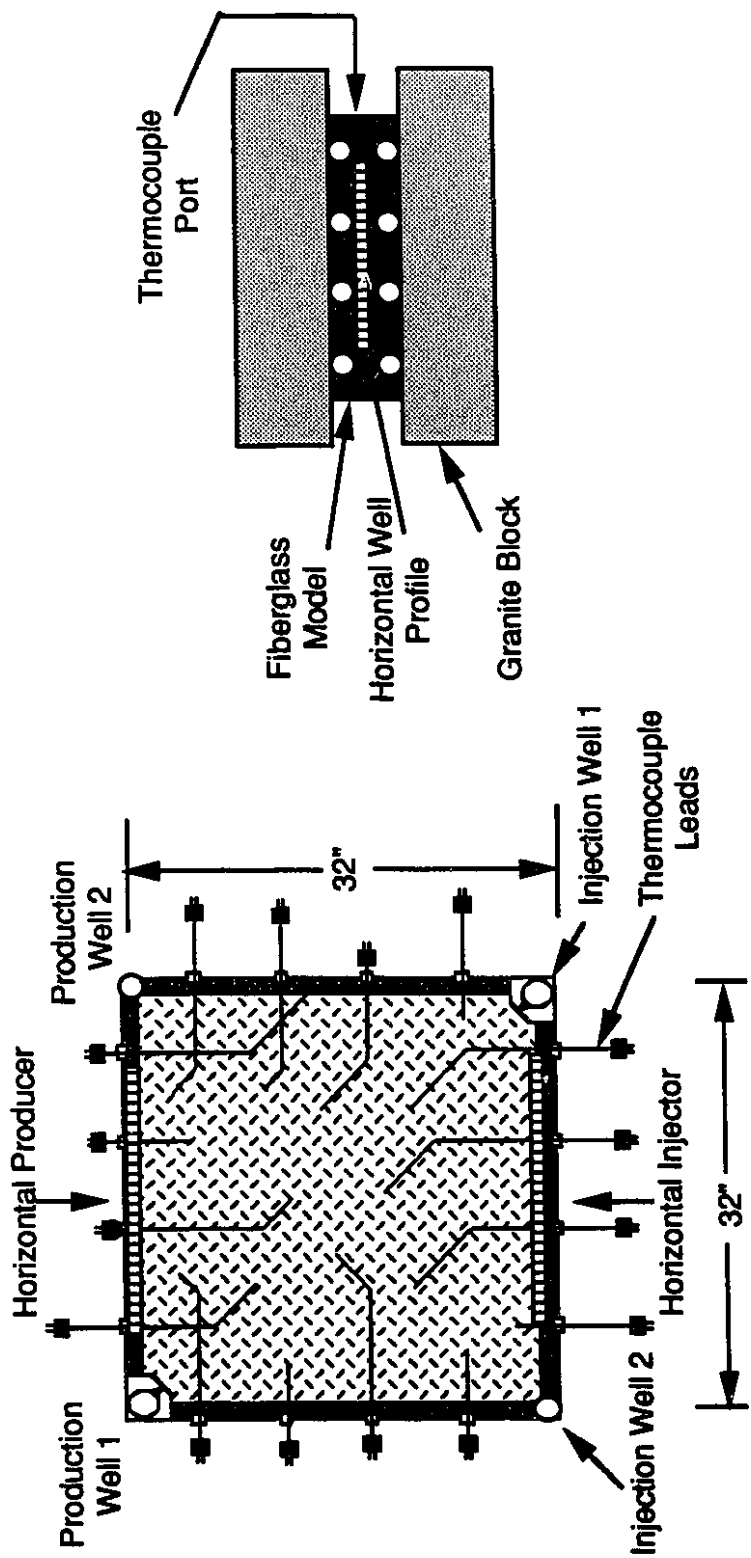
performed under vacuum conditions which involved applying severe loads over a large surface area. Therefore, it was required to select a material with a low heat transfer coefficient that could withstand a high degree of loading. Fibreglass was selected as the model material since it not only satisfied the conditions, but was also inexpensive and relatively easy material to machine.

The cap and base rocks of the model were made of two granite blocks each weighing 1100 pounds and having the dimensions of 91.44 cm (36 in) x 91.44 cm (36 in) x 21.59 cm (8.5 in thick). These blocks were used to simulate the heat transfer characteristics of the overburden and underburden of the Aberfeldy reservoir. The sides of the fibreglass tray were covered with cellular Neoprene to minimize heat loss from the lateral “no flow” boundaries of the model.

### **Vertical and Horizontal Wells**

Figure 5.2 shows the detailed internal features of the model, including the location of temperature sensors and well positions. Scaled aluminum slit wells were machined in each corner of the model to simulate vertical wells. The effective radius of each slit well was a function of the slit width and the arrangement of the bead pack directly in front of the slit. The wells were also designed to permit the insertion of a gate device which would enable the preferential selection of injection and production intervals.

Horizontal wells were represented by perforations machined into two sides of the model. Each well was 16 inches long and located between two vertical wells on each side of the model. Because the wells were unscaled, skin factor or pressure transients within the horizontal wellbore were not considered. However, the wells were designed to meet the material balance specification, by considering constant injection and production rates, such that the total flow capacity of one horizontal well was equivalent to that of its scaled vertical counterpart.



**Top View**

This view illustrates the approximate positions of the top thermocouple layer and the two horizontal wells as defined by a series of perforations along the side of the model.

**Side View**

This view shows the relative position of the upper and lower thermocouples and horizontal well.

Figure 5.2: Schematic Diagram of Thermocouple Positions

### **Porous Medium**

To obtain a model permeability of 4200 darcies and hence, satisfy the scaling criteria, a glass bead pack having an average bead diameter of 3 mm (6-8 U.S. mesh) was selected as the porous medium. For economic reasons, the glass beads were cleaned and dried after each experiment for reuse in future runs. The beads can be seen in their containment unit in Plate 5.1.

### **Model Cart, Rail System and Cold Storage Compartment**

A cold storage compartment was built to enable the model to be cooled to an initial temperature of 3°C that was required to fulfill the model temperature scaling criteria. The cooler was converted to a freezer to permit the creation of bottom water. The custom built walk-in cooler/freezer had the dimensions of 8 ft x 10 ft x 7 ft and is shown in Plate 5.1 along with the Wygal<sup>48</sup> particle distributor, glass beads, and bead drier.

The entire model, including the two granite blocks, rested on top of a support cart which was set on castors. This facilitated the movement of the model which was rolled in and out of the cold storage compartment on the accompanying tracks. The upper granite block was placed on top of the fibreglass tray with a hydraulic hoist system. A shaft, connecting the rack and pinion system to a gear box, was welded to the support cart. The gear box was used to tilt the 2200 pound model to a maximum angle of 45° with respect to the horizontal. Tilting the model frame permitted uniform model saturation by gravity flow. Dipping reservoirs can also be simulated using the existing equipment.

### **Fluid Injection System**

The steam injection equipment consisted of two Milroyal controlled volume pumps and a low pressure boiler. To generate the desired steam quality, a stream of superheated steam was mixed with room temperature water. One of the Milroyal pumps transported degassed, distilled water at room temperature to the water-steam mixing point while the



other pumped superheated steam generated from the boiler. The boiler electrically converted room temperature feed water to superheated steam. It consisted of an oil bath with seven heating rods and 80 ft (24.38 m) of 1/4" diameter stainless steel tubing coiled inside the unit as can be seen in Plate 5.4. The boiler coil was divided into two subcoils each 40 ft length—the inner coil pre-heated the water and the outer one converted the water to superheated steam.

Solvent was injected into the model by a Milroyal pump at 200 cc/min. It was hoped that this relatively high injection rate would create more distinct and extensive solvent channels in the oil zone. This would provide a more conductive path for the steam to travel within the oil zone.

### **Fluid Collection System**

The collection system, shown in Figure 5.3 and Plate 5.5, was developed to enable a single operator to extract large instantaneous samples of produced fluids without assistance. The unit consisted of a hydraulic pump, a mercury manometer, two plastic vacuum trap collection containers, each equipped with a chilling coil and a fluid level indicator tube, a circulating pump for the condenser coolant, a sized discharge system, a vacuum line to evacuate the container, and a dry ice bath.

Although each vacuum trap was capable of collecting a maximum sample size of 4000 cc, 2000 cc samples were taken using 2000 cc graduated cylinders to generate more data samples for the experimental analysis. A hydraulic suction pump was used to generate a vacuum and extract the samples. Under standard experimental conditions, it maintained a constant vacuum of 68 cm of mercury for a fully evacuated system. The vacuum was monitored during the run by an adjoining mercury manometer.

Since the traps were opaque and the samples were produced as a frothy mixture, it was impossible to monitor the volume of production using an electrical probe. Clear vacuum tubing was used to visually monitor the fluid level in each cylinder and hence, the

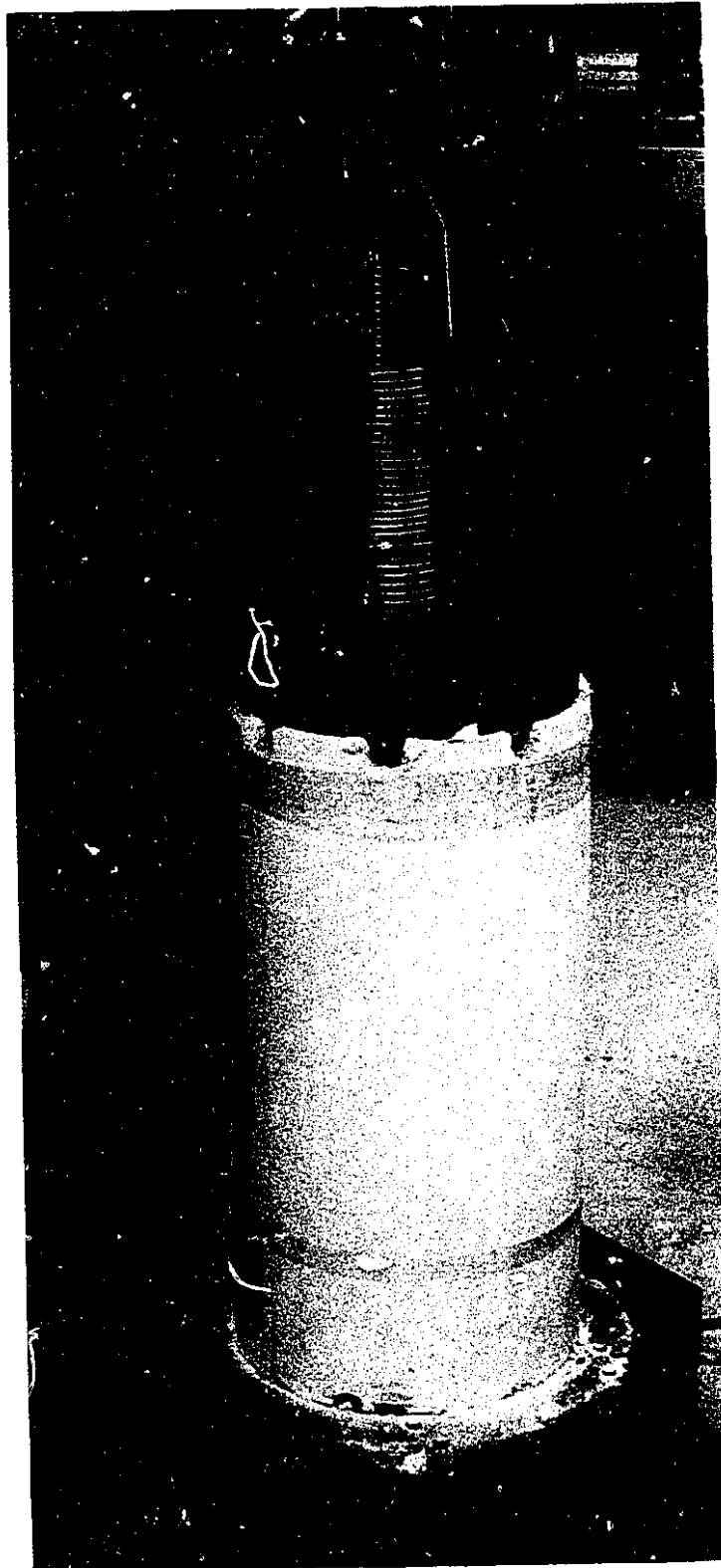


Plate 5.4: Internal View of the Boiler.

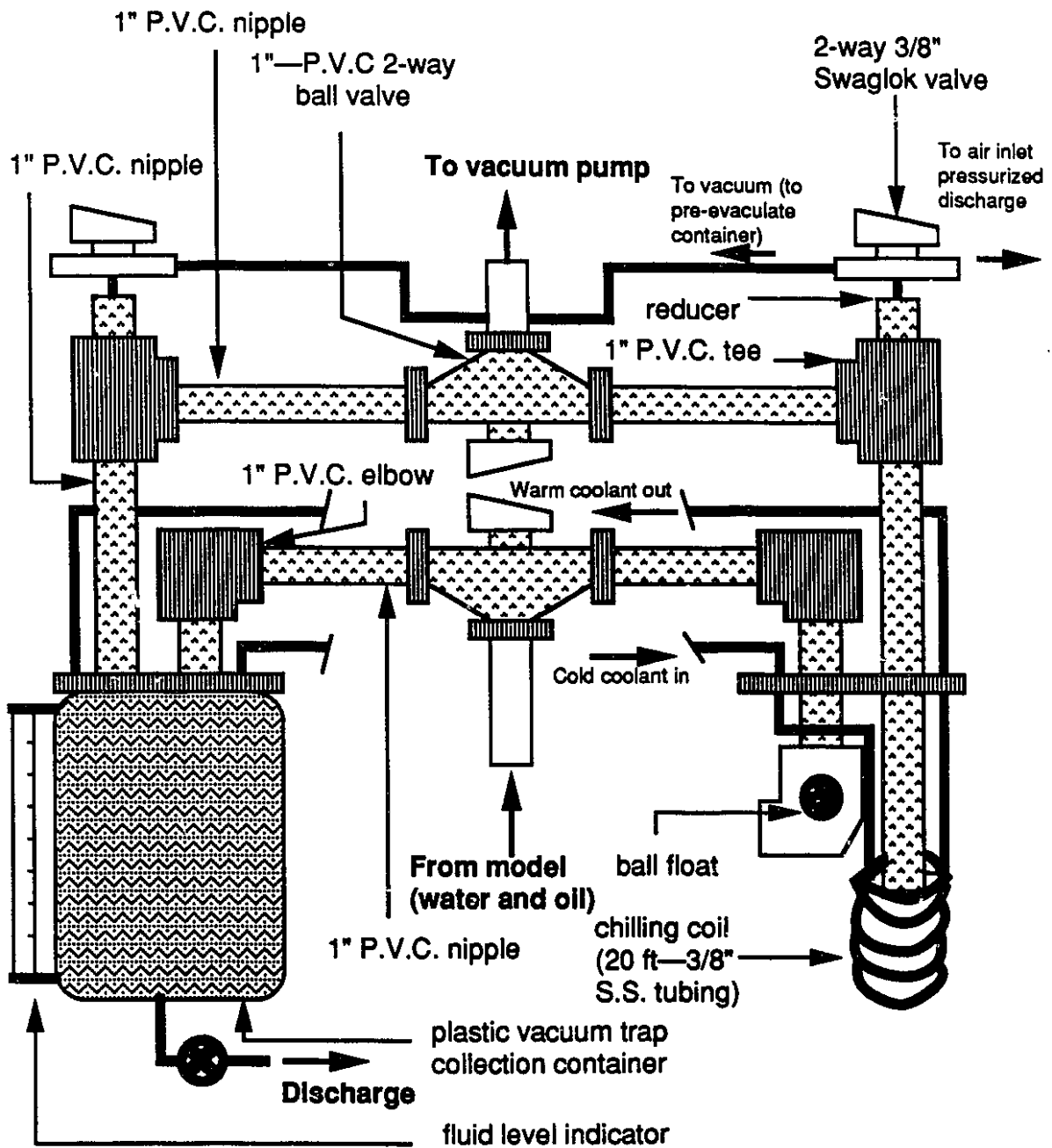


Figure 5.3: A schematic diagram of the produced fluid collection system

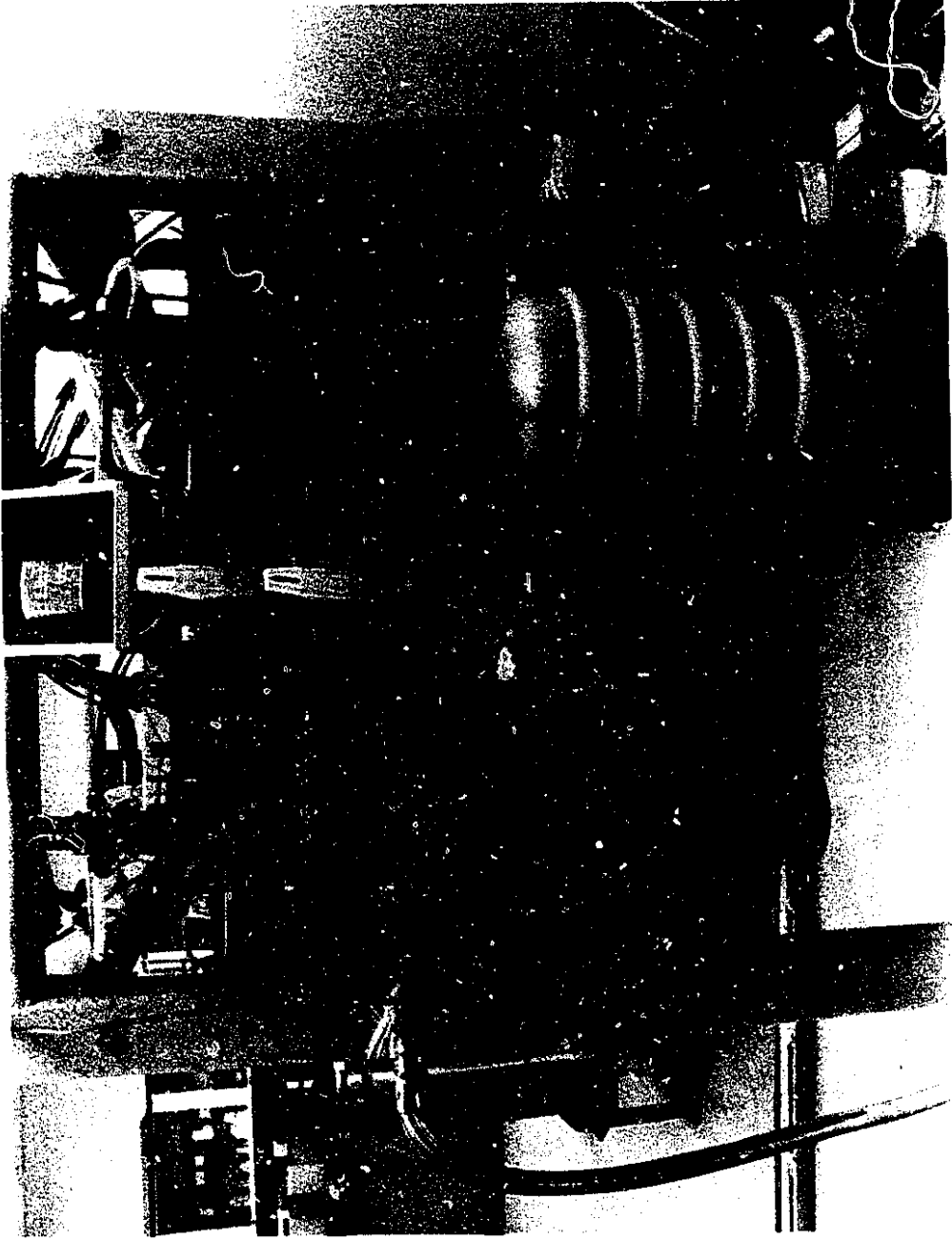


Plate 5.5: Fluid Collection System.

quantity of production. Under low pressure vacuum conditions, some vaporization of produced fluids may occur. Thus, chilling coils consisting of 20 ft of 3/8" stainless steel tubing were installed in each trap to recirculate antifreeze coolant, using a circulating pump. The coils were used in order inhibit the vaporization of produced samples and were built inside the containers.

The flasks were designed to enable each flask to operate independently of the other. Because of the high viscosity of the hydrocarbon in the initial phase of the experiment, a pressurized discharge was built into each flask. The purpose of this inlet was to inject air at approximately 1 psig into the container to shorten the length of time required to drain each collection container. If more than 1 psig of pressure was applied, it would propel the plastic container away from the plastic fittings and valves. Thus, a flexible cable was added to enclose the entire containment unit (plastic container, fitting and valves) as a safety precaution. To maintain a vacuum, each container was pre-evacuated using the negative pressure outlet prior to sample collection by turning the 2-way valve towards the vacuum source. Finally, a carbon dioxide dry bath was installed at the downstream of the collection unit to gather any produced vapours that had passed through the condensers in the flasks.

### **Data Acquisition System**

An extensive data acquisition network, consisting of thirty-seven thermocouple channels and four pressure transducers, was installed at selected locations within the fibreglass model. The model was machined to permit a maximum of thirty-two type-J thermocouples to be strategically installed in two layers inside the model, with sixteen in each layer. Additionally, five type-J thermocouples were used to measure the injection and production temperatures at various locations as well as the temperature of the mixing point. However, because these points of injection and production are situated close to metal fittings and connection, ungrounded thermocouples were chosen instead to prevent any

grounding effects from occurring. The transducers were placed adjacent to each well to monitor the inlet and outlet pressures.

During this study, three data acquisition systems were used to collect and process the experimental data with the aid of an IBM PC: Megadac 2000, Process I/O System and Metrabyte. Megadac was succeeded by the Process I/O, which, in turn, was replaced by the Metrabyte system. Metrabyte was used for the majority of the experiments. More detailed information regarding the operation and installation of Megadac and Metrabyte are provided in Appendix B.

The Megadac 2000 data acquisition unit had the potential to monitor 128 input channels as quickly as 2000 samples per second or as slowly as one sample per second. In all experiments, the scan time was set as one scan every thirty seconds. The Megadac 2000 data acquisition system broke down prior to the initiation of Run 70B. Because of the high repair cost and extensive amount of repairs needed for the Megadac unit as well as the modifications required for the Megadac software package, Optim Users Software, another acquisition system was selected.

The new system was developed by the Department of Chemical Engineering at the University of Alberta and was modified specifically for the purposes of this research project. The *Process I/O System* is based on a Digital Equipment Corporation (DEC) LSI 11/03 microcomputer using an Adac Corporation Model 1113AD with 2 Model 1113EX boards to provide low level analog input. Thirty two channels of input were available, configured as thermocouple type input or  $\pm 100$  millivolt input. If a channel was configured as a thermocouple type, cold junction compensation was performed on the board.

The I/O operating system used on the LSI 11/03 was the DEC RT11 system. The program to perform the input and prepare the data for storage on an IBM PC was written in Parallel Pascal which was a product from Interactive Technology Incorporated. The program used to receive the data from the LSI 11/03 was written under DOS in Modula-2 as implemented in the M2SDS development system. This system was chosen because

equipment repairs and software revision could be performed quickly at the University of Alberta whereas the only place to service the Megadac 2000 is in Maryland, U.S.A. The new system could be adapted to the existing IBM personal computer in the laboratory with a series of thermocouple jack panels built to satisfy the total number of thermocouple inputs.

Based on the results from 70B, the Process I/O system was assessed to be a poor replacement for the old Megadac data acquisition unit. It was inflexible to any alterations; each time slight modifications to the equipment were implemented, such as the addition of another thermocouple lead, the data collection program had to be completely rewritten in Modula-2. The Process I/O lacked expansion capability reading only 32 thermocouple temperature values simultaneously. It was unable to handle any more input channels for future experiments, such as heat flux transducers or additional thermocouples or other modifications to the system. The system was undependable, since it ran on an eight inch disk and an obsolete computer unit which had to be replaced twice in the duration of the run. "Black box" calculations used to process and generate the data were also questionable. Therefore, the unit was returned at the end of the trial period due to a lack of experimental confidence in the Process I/O System.

After investigating other data acquisition units including a Macintosh computer package, a DAS-8 board, four EXP-16 multiplexers and the Labtech Notebook Software from the Metrabyte Corporation was purchased. The advantages of this system were its versatility, expansion capability, equipment repair accessibility and the supplemental software package. Labtech Notebook package processed all raw thermocouple (mV) and pressure transducer (mV) measurements and converted them into real values of temperature and pressure ( $^{\circ}\text{C}$  and kPa) and time (seconds). Because the experimental data was stored in ASCII file format, it could be analyzed in a spreadsheet program, such as Lotus 1-2-3 or Symphony, directly through Labtech Notebook.

## Model Fluids

### Selection of Model Oil for the Aberfeldy Reservoir

Choosing the upper limit values of the viscosity relationships between the model oil and the Aberfeldy prototype oil as previously stated in Table 4.3 in Chapter 4, an average ratio of model oil viscosity to prototype oil viscosity ( $\mu_{oM}/\mu_{oP}$ ) was determined to be 7.26. The ideal viscosity of the model oil was then calculated at different model temperatures using both the viscosity and the temperature relationship between the model and prototype in equation 4.39 and is shown in Table 5.1.

*Table 5.1: Temperature vs. Oil Viscosity Data for Prototype and Ideal Model Oil.*

<u>Prototype Temperature (°C)</u>	<u>Prototype Oil Viscosity (mPa·s)</u>	<u>Model Temperature (°C)</u>	<u>Ideal Model Oil Viscosity (mPa·s)</u>
23.9	1275	3.2	9256.5
32.2	560	5.6	4065.6
65.6	90	15.1	653.4
135.0	12.5	35.0	90.75
301.7	1.29	82.6	9.37

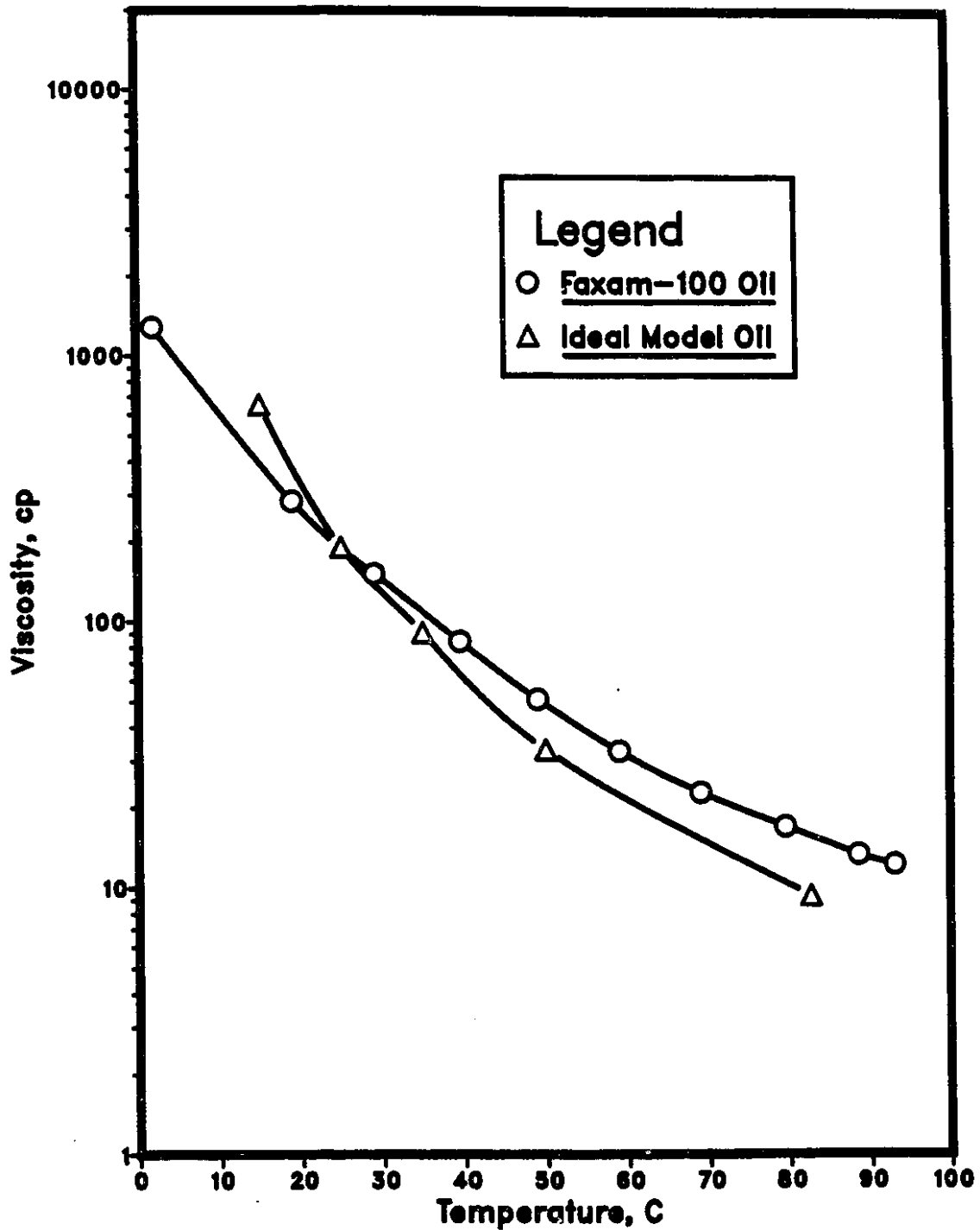
Figure 5.4 is a viscosity-temperature profile plot of the refined MCT 30 base oil called Faxam-100, which was selected as the actual model oil. Faxam-100 was chosen because its curve best matched that for the ideal Aberfeldy oil. The model temperature range in the experiments was 3° to 80°C approximately.

### Solvent Selection

Following an extensive viscosity investigation, Heavy Virgin Naphtha solvent (HVN) was selected for the steamflood investigations conducted in the low pressure model. The chemical properties of the Heavy Virgin Naphtha, primarily the initial boiling



Figure 5.4: Viscosity vs. Temperature Profiles for the Ideal and Actual selected (Faxam-100) Model Oil.



point of 61.0°C, caused the partial vaporization of the solvent to occur during the steamflood process which had an average upper temperature range of 80° to 100°C. This phenomenon produced favourable results since the partial vaporization of the Heavy Virgin Naphtha enhanced the mobilization of the oil as a consequence of the diffusion of the solvent vapour into the oil ahead of the solvent bank.

Figure 5.5 is a plot of viscosity versus HVN solvent concentration. Other properties of Heavy Virgin Naphtha are:

$$\rho_{\text{HVN}} = 0.7320 \text{ g/cc}$$

$$\text{API gravity} = 61.7^\circ \text{ API}$$

$$\text{Initial Boiling Point} = 61^\circ \text{C}$$

$$\text{Final Boiling Point} = 131.5^\circ \text{C}$$

### Preparation of the Experimental Model

#### **Model Packing Procedure**

A “particle distributor” was used to pack the model with glass beads since traditional tamping and vibrating methods were not feasible for the large irregularly shaped fibreglass model. The concept of a distributor matrix was first introduced by Currie and Gregory, and was later modified by Wygal<sup>48</sup>. According to Wygal<sup>48</sup>, the particle distributor produced mechanically stable packs with uniform properties throughout that could be accurately reproduced, while tamping and vibrating procedures generated non-uniform or unstable particle packs.

The success of the particle distributor occurred as a result of the hitting action of the beads falling onto the pack surface. It was observed that the beads strike the pack singly after being distributed through a series of sieves. Part of their kinetic energy was transferred to the surface beads which were thereby knocked into more stable positions. As the bead pack grew, Wygal<sup>48</sup> stated that the surface appeared to be fluid and alive for a depth of two or three particle diameters.

**Figure 5.5: Viscosity of the Mixture of Faxam-100 and Heavy Virgin Naphtha vs. HVN Solvent Concentration.**

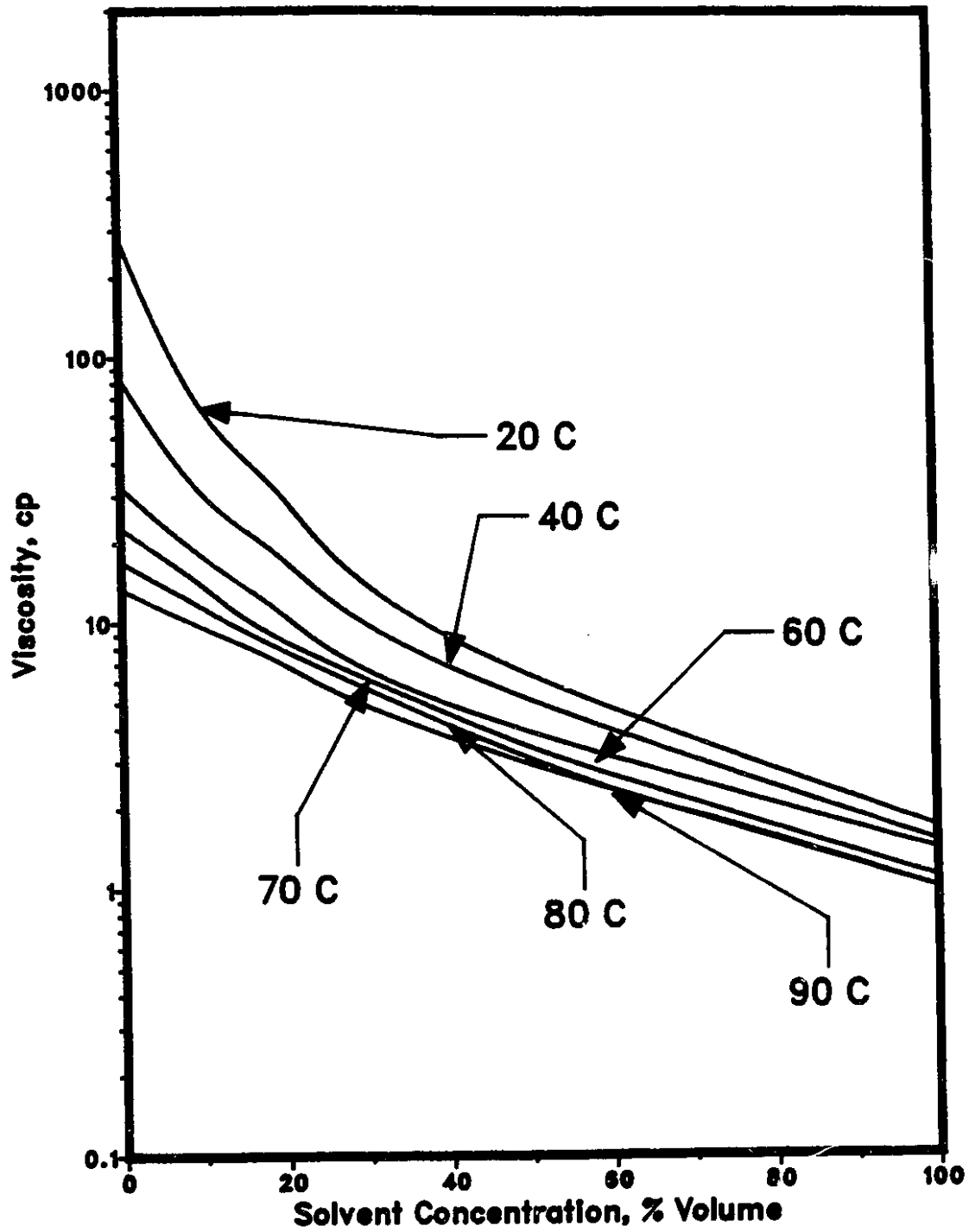


Figure 5.6 is a schematic diagram of the Wygal<sup>48</sup> particle distributor constructed for this study. It consisted of a 32" x 32" x 26" plywood frame, a metering board and five wire mesh screens each with 5/8" openings that were offset from each other. The model was packed by supplying a continuous supply of the glass beads at a constant rate to the orifices on the metering board until the model was filled. The particle distributor was removed and excess beads were trimmed off the model surface. Average model porosities ranged from 32% for a homogeneous model to 35% for a bottom water model, which was partially packed by hand.

### **Fluid Saturation Process**

After the model was packed with glass beads, a thin layer of silicone sealant was applied to the edges of the fibreglass model being careful not to cover the slit wells. A 3' x 3' x 1/8" thick sheet of Celtite Neoprene was then positioned on top of the tray and the top granite block was lowered and clamped onto the model. The entire apparatus was tilted and evacuated for saturation since saturating from the lower to upper end creates a more efficient gravity stabilized front.

A total of six saturation ports, three on each opposing side of the model, were machined into the model to enhance saturation efficiency. The model fluids entered the apparatus from downdip and were pulled upward due to the vacuum at the updip end. Initially, degassed, distilled water saturated the model. The pore volume was determined as the volume of water taken into the system from which the porosity could be determined. Next, the model was saturated with Faxam-100 oil in the same manner used for water saturation. The total volume of water displaced during oil saturation was equivalent to the initial oil saturation. The volume of water remaining after no more water was produced was referred to as the irreducible water saturation. When the quick connect fittings were removed at the injection and production ends, a vacuum was maintained within the model as was confirmed by a vacuum regulator.

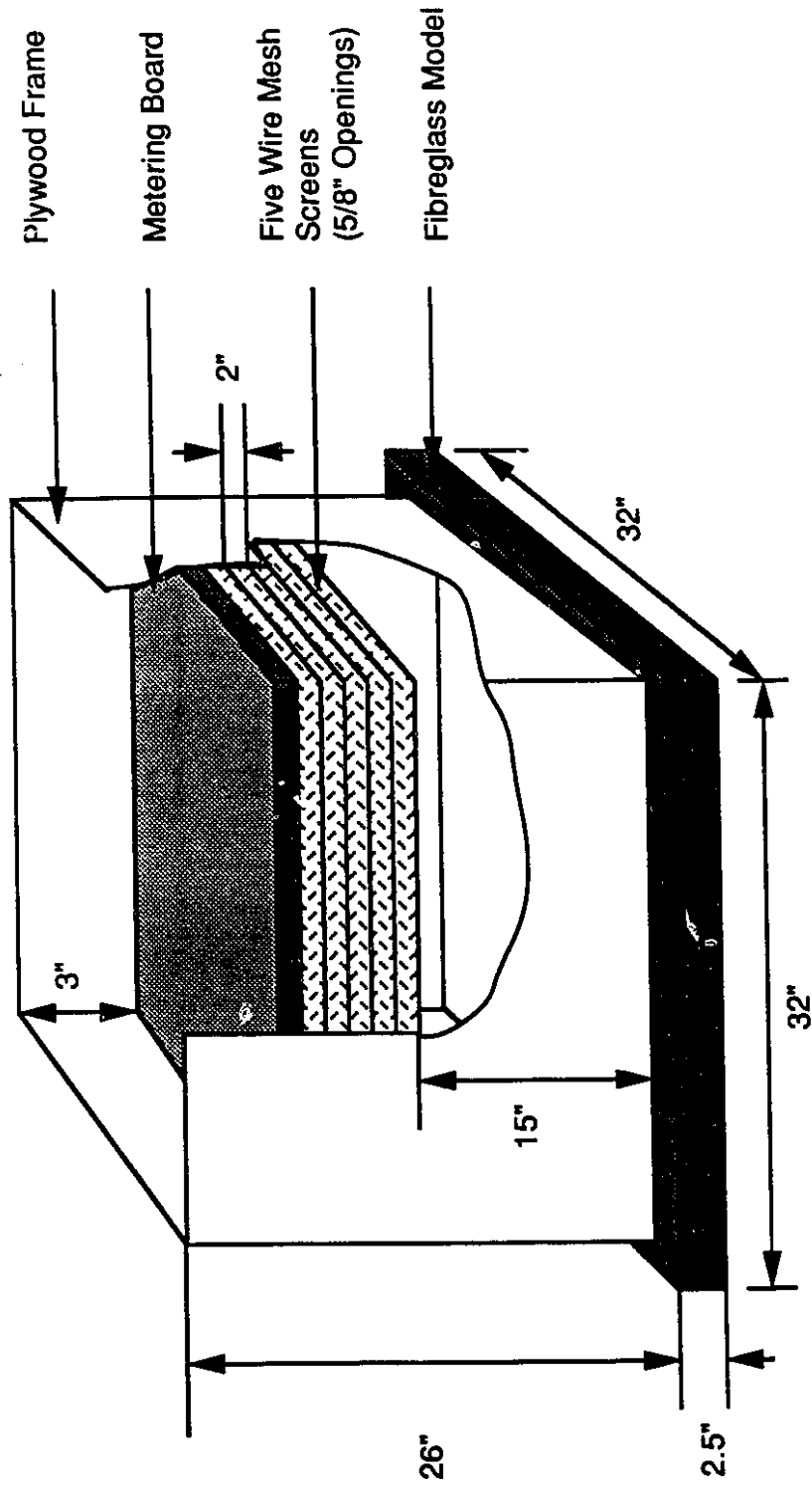


Figure 5.6: The Wygal Particle Distributor

### **Preparation of a Bottom Water Model**

Since this experimental study investigated marginal reservoirs containing a bottom water zone, a method was devised to create a bottom water zone and is discussed in Appendix B. Approximately two days were required to prepare a bottom water model.

A predetermined volume of 5% (by weight) sodium chloride solution, which corresponded to a percentage of the gross model thickness, was poured into the empty fibreglass tray. Glass beads were then sprinkled by hand with the aid of a beaker to cover the brine solution. Another thin layer of beads was added to compensate for the expansion of water due to freezing. The model was then pushed, along with a 50 litre tub of clean, dry glass beads, into the walk-in cooler/freezer until the bottom water layer was completely frozen.

Once the bottom water layer was frozen, the remainder of the model was packed with cold glass beads using the Wygal<sup>48</sup> particle distributor and any excess was trimmed off. The model was then saturated in the usual manner as quickly as possible to minimize the thawing of the bottom water layer. The refractive indices of the produced water solutions were measured to determine the quantity of bottom water lost due to melting, using the lever rule. Thus, the volume of bottom water remaining after saturation could be determined.

### **Creation of a Gas Zone**

A gas zone was created by injecting a small quantity of inert nitrogen gas into the model prior to the experiment. Gas injection was expected to improve oil recovery by diverting the injected fluid away from the bottom water zone and into the oil zone and hence, mitigate the heat scavenging effects of bottom water. Nitrogen gas was injected at 1 psig for a period of one prototype year (11.5 minutes). A larger injection pressure was avoided since it would break the vacuum seal.

### **Conducting Experiments in the Model**

Once the homogeneous model was packed and saturated, it was pushed into the walk-in cooler/freezer and cooled overnight to 3°C. For the bottom water model, it was necessary to allow the model to thaw out completely before it could be cooled. The injection vessels were filled with distilled water and degassed using a vacuum pump while the model was cooling in preparation for the experimental run.

Prior to each experiment, the chilling system in the fluid collection unit was turned on to cool the coils and the collection flasks were evacuated. The Labtech Notebook data acquisition software was then loaded into the computer. The model was rolled out of the cooler/freezer and the thermocouple cables were connected to the thermocouples inside the fibreglass tray. Broken thermocouples or cable short circuits were detected when the cold junction cable value was displayed on the computer by Labtech. Furthermore, the pressure transducers could be checked and calibrated with the aid of Labtech. Labtech was then reloaded in preparation of the run, dry ice was added to the dry ice bath, the production line was connected to the desired outlet port, either the vertical or horizontal producer, and the experiment was ready to proceed.

It was crucial to record the time at the beginning and conclusion of the injection of different fluids (water, steam or gas) from Labtech to determine the lag time between fluid hook up and total injection length. To provide experimental consistency, 2000 cc samples were collected from the vacuum traps in graduated cylinders and labelled chronologically. Each run lasted for approximately two hours during which two pore volumes of fluid were injected (2 PV cumulative volume injected). Fluid injection rates could be adjusted by the controller on the Milroyal pump.

### **Waterflood**

Because steam was not required for a waterflood run, it was not necessary to pre-heat the boiler. Degassed, distilled water at room temperature was pumped through the

injection line to flush out any trace fluids from previous experiments. The injection line was inserted into the desired inlet port either the vertical or horizontal injector. Water was then injected into the model and the produced samples were collected.

### **Steamflood in a Homogeneous Model**

For a steam injection run, the oil bath was pre-heated in the boiler to the desired temperature. Feed water was pumped through the boiler to convert it to superheated steam, which was mixed with room temperature water in proper proportions to form the required steam quality. This time, the injection line was flushed with steam before connecting to the inlet.

### **Solvent-Steamflood**

In solvent-steamfloods, the only variation was that the solvent Milroyal pump was used to initially inject a specified volume of Heavy Virgin Naphtha into the model prior to steam injection. The steam Milroyal pump was attached, the injection line was flushed with steam and the steamflood commenced in the usual manner. The volume of solvent recovered in each sample was determined from the refractive index of the sample, but the solvent concentration changed due to evaporation over a short period of time. Therefore, the refractive index of the samples was measured immediately after they were taken or if it was desired to record the information later, the cylinders were sealed with an impermeable material.

### **Bottom Water Runs**

For bottom water runs, like solvent-steamfloods, the volume of bottom water production was inferred using the refractive indices of the produced samples.

### **Gas Injection Runs**

For gas injection runs, an inert gas cylinder was connected to the model using plastic tubing. In all cases, nitrogen was injected at a constant pressure of 1 psig which



was monitored using a pressure regulator. Since the injection pressure was greater than atmospheric pressure, a slight drop in the vacuum occurred at the production end and could be seen in a decrease in the level of mercury in the manometer during gas injection.

### **Apparatus Cleanup**

At the conclusion of the experiment, the aluminum clamps and the top block were removed. The Neoprene sheet was peeled off the model, shaken to remove any attached beads, and then disposed in a waste container. The glass beads were carefully removed to avoid damaging the thermocouples. Any broken thermocouples were replaced and the bent ones were repositioned. A degreasing agent followed by a laboratory detergent was applied by hand to the glass beads to remove all hydrocarbon residues (Faxam-100 oil and Heavy Virgin Naphtha solvent) and water. The glass beads were placed into two 3-ft stainless steel cylinders set on risers. Any water would drain through an outlet line attached at the bottom of the cylinder. The beads were then dried by connecting the cylinders to air inlets and forcing air to flow through the beads.

Excess silicone sealant was scraped off the tray using a chisel. A degreasing solution, followed by Varsol and acetone were applied to the tilted fibreglass model. After the waste was drained using a siphon, the traces of the cleaning agents were removed by using laboratory wipers. Plastic cylinders were washed with dishwashing detergent while glass ones were cleaned using the laboratory detergent. Thus, the model was ready for the next experiment.

### **Data Analysis**

Following each experiment, the data was recalled from Labtech Notebook and analyzed by a data spreadsheet program, such as Lotus 1-2-3 or Microsoft Excel. All pertinent data including porosity, initial fluid saturations, fluid recoveries, initial model temperature and cumulative pore volume injected were summarized in an experimental

table. The following variables were then correlated as a function of cumulative pore volume: % oil in sample, % cumulative oil recovery (%OOIP), % solvent in sample, % cumulative solvent recovery and average effluent temperature. Temperature top and cross-section profiles were constructed, where applicable, at 0.25, 0.50, 1.0 and 1.5 PV of steam injected, using the programs in Appendix D.

## Chapter 6

### Discussion

This chapter discusses the experimental results underscoring the importance of steam quality control in the steamflood process, and analyzes the following types of experiments: waterflooding, gas injection, steamflooding in the presence of bottom water, solvent-steamflooding, and horizontal-vertical well strategies. Corresponding tables and figures for each experiment appear throughout the discussion as appropriate. Temperature profiles were obtained for all thermal experiments and these are included as contours. Detailed experimental results are given in the tables for all runs in Appendix E.

### Presentation of Results

A total of thirty-eight experiments were conducted in the scaled physical model of the Aberfeldy reservoir during this study. Thirty-five of these experiments were successfully completed, while three were prematurely terminated because of mechanical failures and system limitations. The following section discusses steam injection experiments of several types in thin, heavy oil formations in the low pressure apparatus: continuous steamfloods and waterfloods under a variety of reservoir conditions (with and without bottom water, and with a gas additive), solvent-steamfloods, and horizontal-vertical well strategies.

The experiments, as illustrated schematically in Figure 6.1, were divided into three main categories: waterflood, steamflood and solvent-steamflood. Pertinent model properties, such as porosity and initial fluid saturations, as well as recovery results are summarized for all runs in Table 6.1. To avoid confusion with the horizontal well experiments, discussed later, all runs, unless otherwise specified, were conducted using a vertical producer and a vertical injector well pair, representing one-quarter of a five-spot pattern.

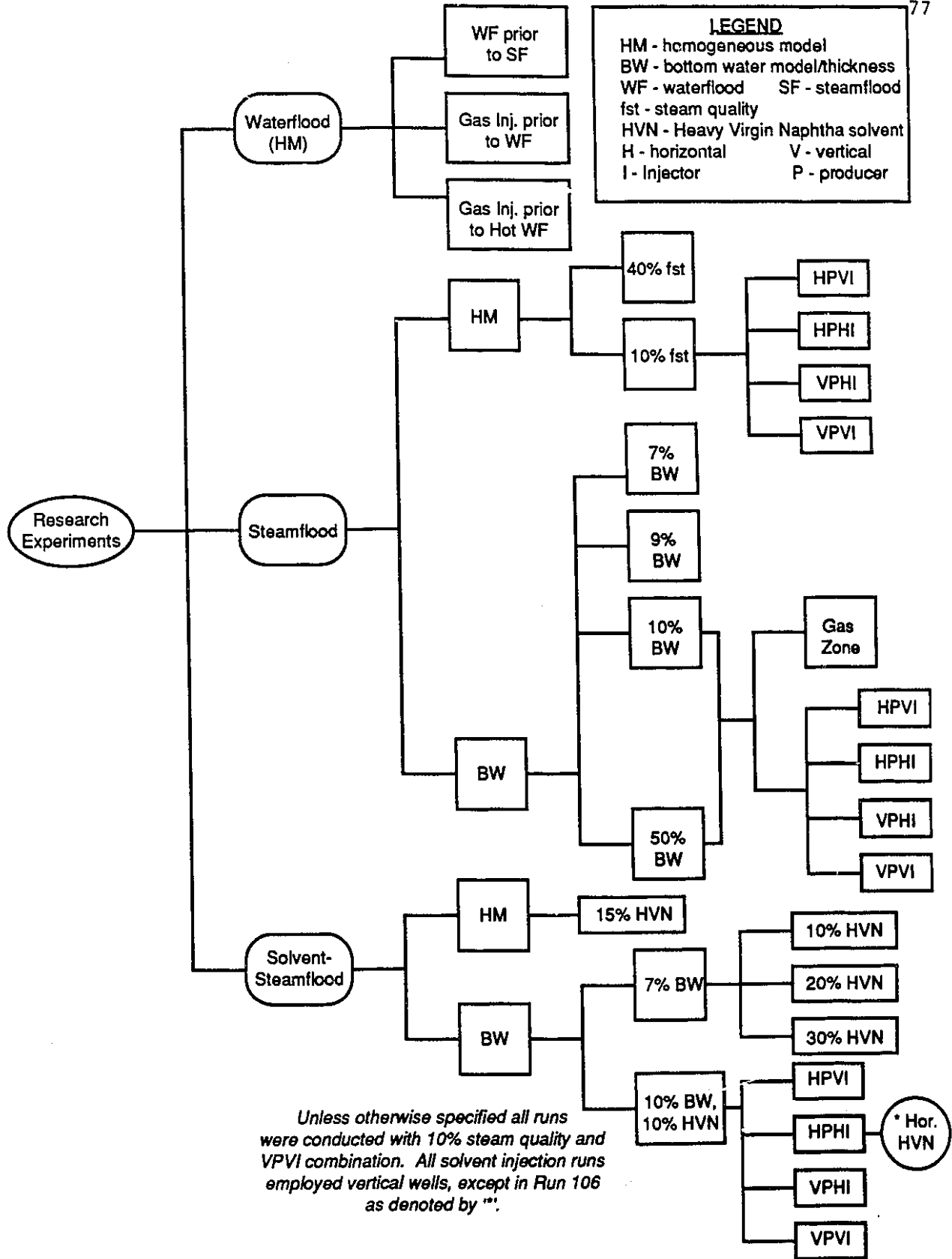


Figure 6.1: Overview of Experimental Runs

Table 6.1

## Summary of Experiments Conducted

(Explanations at the end of the table)

Run No.	Model Type	Type of Process	Porosity (%)	Soi (%)	Swi (%)	Bottom Water (% gross thickness)	Solvent Slug Size (PV)	Cum. Rec. (%OOIP)	Solvent Rec. (%)	Cum. FV Inj. (PV)
70A	HM	W/F prior to SF	31.7	87.9	12.1	--	--	27.69	--	2.09
70B	HM	SF following W/F	31.7	59.8	40.2	--	--	7.70	--	2.10
71	HM	Gas inj. prior to W/F	34.2	90.2	9.8	--	--	19.51	--	2.04
72A	HM	W/F	33.6	89.2	10.8	--	--	19.67	--	1.54
72B	HM	Gas inj. prior to hot W/F	33.6	71.7	28.3	--	--	33.82	--	1.61
73	HM	SF (fst = 40%)	32.1	93.2	6.8	--	--	53.31	--	2.09
74	HM	SF: vert.inj. & hor.prod.	32.0	91.1	8.9	--	--	48.45	--	2.05
75	HM	SF: hor.inj. & hor.prod.	33.8	91.5	8.5	--	--	60.89	--	2.12
76	HM	SF: hor.inj. & vert. prod.	33.9	90.6	9.4	--	--	53.91	--	2.16
77	HM	SF: vert. inj. & vert.prod.	32.4	92.2	7.8	--	--	57.40	--	2.14
78	BW	Solvent-steamflood	34.8	79.7	20.3	7.59	0.11	52.92	99.20	2.07
79	HM	Solvent-steamflood	32.5	90.9	9.1	--	0.15	57.51	99.93	2.13
80	BW	Solvent-steamflood	33.3	74.6	25.4	7.05	0.20	46.21	94.09	2.19
81	BW	Repeat of Run 80	33.1	91.1	8.9	8.12	0.19	48.46	99.95	2.13
82	BW	Solvent-steamflood	33.0	90.8	9.2	7.15	0.28	54.31	99.95	2.14
83	BW	SF	33.4	91.2	8.8	7.00	--	56.60	--	2.06
84	BW	Repeat of Run 80	32.4	85.3	14.7	7.67	0.19	52.05	100.00	2.12
85	BW	SF	32.9	81.2	18.8	9.10	--	49.18	--	2.02
86	HM	Repeat of Run 74	33.8	90.9	9.1	--	--	51.87	--	2.10
87	BW	SF: vert.inj. & hor.prod.	32.7	78.9	21.1	9.94	--	53.56	--	1.99
88	BW	*--SF: hor.inj. & hor.prod.	32.1	79.6	20.4	9.93	--	65.59	--	1.90
89	BW	*--SF: hor.inj. & vert. prod.	32.3	82.7	17.3	9.88	--	51.60	--	2.19
90	BW	SF: vert. inj. & vert.prod.	34.0	83.6	16.4	8.50	--	47.32	--	2.10

SF: vert.inj. &amp; hor.prod.

\*--SF: hor.inj. &amp; hor.prod.

\*--SF: hor.inj. &amp; vert. prod.

SF: vert. inj. &amp; vert.prod.

Table 6.1 (continued)

Run No.	Model Type	Type of Process	Porosity (%)	Soi (%)	Swi (%)	Bottom Water (% gross thickness)	Solvent Slug Size (PV)	Cum. Rec. (%OOIP)	Solvent Rec. (%)	Cum. PV Inj. (PV)
91	BW	SSF: vert.inj. & hor.prod.	33.9	82.9	17.1	9.20	0.10	49.87	95.00	2.04
92	BW	SSF: hor.inj. & hor.prod.	34.2	84.0	16.0	8.84	0.10	67.49	79.64	2.19
93	BW	SSF: hor.inj. & vert. prod.	32.6	84.4	15.6	9.96	0.10	56.65	84.96	2.18
94	BW	SSF: vert. inj. & vert.prod.	33.5	80.8	19.2	10.41	0.09	52.12	87.71	2.10
95	BW	SF with a gas zone	30.1	53.3	46.7	49.71	--	32.81	--	2.18
96	BW	SF with a gas zone	32.8	82.6	17.4	10.38	--	50.22	--	2.08
97	BW	SF: vert.inj. & hor.prod.	31.3	50.2	49.8	48.51	--	32.40	--	2.22
98	BW	SF: hor.inj. & hor.prod.	31.9	49.8	50.2	49.81	--	40.55	--	2.11
99	BW	SF: hor.inj. & vert. prod.	32.0	44.8	55.2	54.85	--	38.44	--	2.07
100	BW	SF: vert. inj. & vert.prod.	30.5	50.5	49.5	49.18	--	32.69	--	2.23
101	BW	Repeat of Run 88	33.2	81.6	18.4	10.04	--	64.54	--	2.09
102	BW	Repeat of Run 89	33.7	79.9	20.1	10.00	--	47.04	--	2.09
103	HM	*--SF (Repeat of Run 77)	32.2	91.3	8.7	--	--	N/A	--	N/A
104	HM	SF (Repeat of Run 77)	32.8	90.5	9.5	--	--	57.80	--	2.13
105A	HM	W/F prior to S/F	33.4	92.7	7.3	--	--	18.39	--	1.84
105B	HM	SF following W/F	33.4	75.7	24.3	--	--	42.84	--	2.01
106	BW	†--SSF:hor.inj.&hor.prod.	34.4	78.7	21.3	11.70	0.10	61.98	86.29	2.06
107	HM	††--SF	32.8	84.6	15.4	--	--	59.84	--	2.00

**Key to Abbreviations:**

HM: Homogeneous Model  
 BW: Bottom Water Model  
 SF: Continuous Steamflood (vert. inj. & vert. prod.)  
 SSF: Solvent-Steamflood  
 W/F: Waterflood

vert. inj.: Vertical Injector  
 vert.prod: Vertical Producer  
 hor.inj.: Horizontal Injector  
 hor.prod: Horizontal Producer

\*--Misrun

**Notes on Unsuccessful Runs:**

Run 88: Computer hard drive failure; computer was replaced.  
 Run 89: Improper scanning due to error in software package resulting from using another computer.  
 Run 103: Experimental use of vacuum grease as a sealant unsuccessful.

†-- Solvent slug was injected from a horizontal well in Run 106. In the other solvent-steamflood runs, solvent was injected from a vertical well regardless of the well configurations used for steam.  
 ††-- Repeat of base case steamflood in a homogeneous model following steam generator modifications.

Initial water and steam runs were conducted in a homogeneous (in the following discussion, this will imply no bottom water) model to establish a series of base experiments for future analysis. Waterflood runs, which were the simpler type of experiments, were the first group of experiments conducted. Even these experiments took as long as any of the steamflooding experiments, the average turnaround time being about two weeks. Several scenarios incorporating steam and gas additives with the waterflood were investigated.

Next, steamfloods were performed in both homogeneous and bottom water models for four horizontal-vertical well combinations in one-quarter of a five-spot pattern: horizontal producer-vertical injector (HPVI), horizontal producer-horizontal injector (HPHI), vertical producer-horizontal injector (VPHI), and vertical producer-vertical injector (VPVI). Horizontal-vertical well steamflood strategies were investigated for thin bottom water (10% of gross model thickness) and thick bottom water (50% of gross model thickness) formations. Additional runs incorporating an inert gas additive and varying bottom water thicknesses were also studied.

Finally, the runs examining the application of small solvent slugs in steamfloods were conducted. The effect of a solvent slug on steamflooding thin, bottom water formations was studied. As an adjunct to the horizontal-vertical well study, a small slug (10% PV) of Heavy Virgin Naphtha (HVN) solvent was injected through a vertical well prior to steam injection in the presence of thin bottom water. The effect of injecting the solvent horizontally was also investigated for the HPHI 10% bottom water case.

### Steam Quality

The crucial variable, which governs the outcome of any successful steamflood, in the laboratory or field, is the steam quality. Substantial heat loss from the fluid lines or improper mixing of feedwater and superheated steam can reduce the quality to zero. This is especially critical in low pressure experiments because the scaled steam quality is low to



begin with — 5-15%. The obvious consequence of reducing a steamflood to hot waterflood is reflected by low ultimate oil recovery. In the present vacuum model, because of the low steam quality (10%) derived from the scaling procedure, correct steam quality is essential. Any fluctuations in the superheated steam temperature from the generator as a result of atmospheric pressure fluctuations or heat loss that occurs while the fluid is transported from the steam mixing point to the injection point, can easily decrease the quality from 10% to zero, with further cooling of the condensate below the saturation temperature.

All the exposed lines were insulated with rigid neoprene hose. It was determined from thermocouple readings that the temperature drop between the generator and the mixing point for the low pressure model was 40°C. Hence, the boiler was set to 160°C to compensate for the heat loss from the lines and thus, enabled precise mixing of 120°C superheated steam with 23°C water. It was calculated that the heat loss occurring from the mixing point to the injection point in the model, reduced the quality by 5 percentiles. Thus, the fluid flow rates were calculated from the revised  $w_g/w_t$  quantity for 15% quality.

Steam quality was calculated both mathematically and determined experimentally. Fluid temperatures were measured using thermocouples located at the boiler, the feedwater vessel, the mixing point and the injection point. Hence, using the steam properties in a heat balance, steam quality was calculated. The quality, defined as the mass fraction of steam vapour in a water-steam system, was also measured physically. A mixture of superheated steam and feedwater was pumped through the flow line and the resulting liquid was collected in a graduated cylinder. The mass fraction of vapour was determined by difference between this volume and the CWE (cold water equivalent) flow rate of wet steam over the same period. It was believed that the major source of error in this method was that the measured wet steam volume was larger than expected. This was because its volume also included the steam condensate produced as a result of cooling in the lines. Consequently, the measured quality would be lower than the actual steam quality.

However, several trials showed that the condensation effect was not as significant as earlier believed, since the experimental results closely coincided with the calculated values.

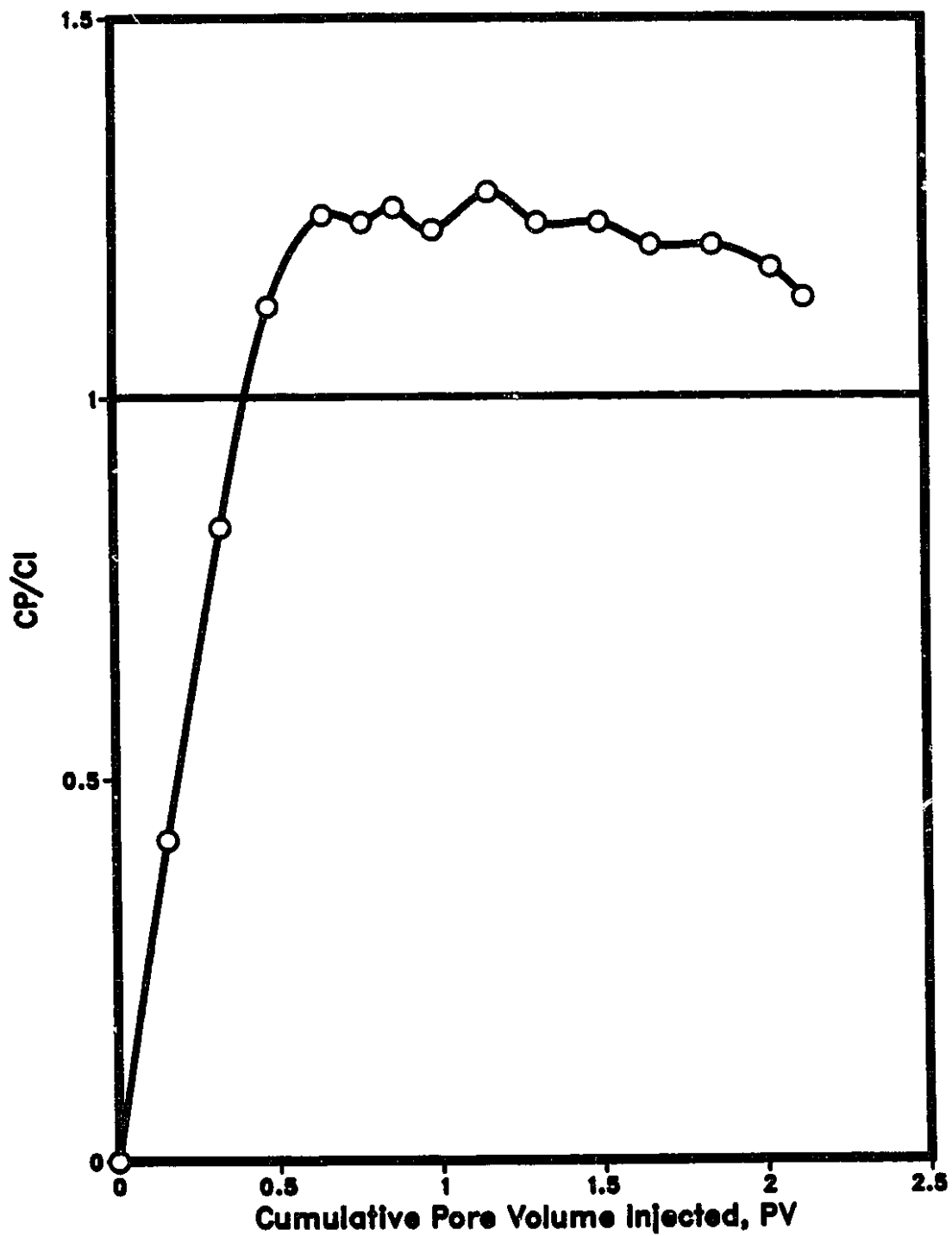
### Steamfloods in a Homogeneous Model

The simplest thermal recovery method, the hot water drive, involves only two phases: oil and water. At any given time, the temperature at the injection point is equal to the fluid temperature. Temperature decreases away from the injection point until it eventually reaches the original reservoir temperature.

An additional gas phase enables steam processes to exhibit better sweep and displacement efficiencies. The presence of a gas phase causes lighter crude components to be distilled and carried as hydrocarbon components in the gas phase. The performance is due to the presence and condensing effects of the condensing vapour. The viscosity of the crude at the condensation front, where the steam and condensable hydrocarbons condense, will be reduced. Three steamfloods (Runs 77, 104, 107) were conducted in a homogeneous model to serve as a basis for comparison and to test the reproducibility of the experiments.

To further verify that a steam drive, as contrasted with a hot water drive, was the primary recovery process in the model, a plot of the ratio of cumulative production to cumulative injection (CP/CI) vs. cumulative pore volumes injected was constructed for Run 104, given in Figure 6.2. Initially, as steam is injected into the cold formation, the cumulative production is less than the cumulative injection due to the low mobility of the viscous crude. As the formation is heated and the steam zone expands, steam distillation effects cause the cumulative production to exceed the cumulative injection. The rise in the curve is indicative of the premises of the Marx-Langenheim theory<sup>49</sup>, which assumes that the latent heat of the injected steam is greater than the rate of its consumption. However, Mandl-Volek<sup>50</sup> stated that at some critical time, this ceases to be so and allowance must be made for the convective heat transport by hot water ahead of the condensation front, which

**Figure 6.2: Cumulative Production/Cumulative Injection, (CP/Ci) vs. Cumulative Pore Volume Injected for Run 104 – Steamflood In a Homogeneous Model.**



is shown by the decline in the curve. Eventually, as the formation is allowed to return to the initial temperature, the oil volume will decrease and the hot waterflood process will dominate. Thus, the curve approaches a CP/CI ratio of one.

As an illustration of the importance of steam quality, Table 6.2 compares the results of Run 79, solvent-steamflood in a homogeneous model, with its hot water counterpart, Run 67<sup>51</sup>. The most noticeable difference is that the ultimate oil recovery from the steamflood (56%) is 30 percentiles more than that for the hot waterflood (26%). The steam drive process, as seen from Figure 6.3, is even more evident in Run 79 than in Run 104 discussed previously. In a hot waterflood, there is clearly no steam zone, assuming that pressure control is precise enough to preclude flash steam formation. Consequently, CP/CI is always unity for Run 67<sup>51</sup>. The small anomaly at the beginning of the Run 67 CP/CI curve can be attributed to the dissolved gas coming out of solution from the crude as a result of the increase in temperature, which also occurs in waterfloods.

Only one of the base case steamfloods, Run 77, will be discussed in this section. Figure 6.4 presents a concise overview of the results. The oil production rate is high initially and declines with time, resulting in an ultimate recovery of 57% at 2.0 PV steam injected (CWE). The produced water-oil ratio approached a constant value of 7 after 1.5 PV of cumulative steam injection. It was shown experimentally that this water-oil ratio remained approximately constant even after 3.5 PV injection. It was also noted from the top view temperature profiles in Figure 6.5 that the average model temperature was 60°C after approximately 1.5 PV of steam was injected. It was decided to terminate all experiments at 2.0 PV of steam injection since there did not appear to be any significant changes in temperature or oil recovery thereafter. On average, oil recovery only increased between 8-10 percentiles after a total of 3.0-3.5 PV of steam was injected. The time constraints and high operation costs did not warrant steam injection exceeding 2.0 PV. The cross-section profile at 0.5 PV in Figure 6.6 showed steam override, with excessive

**Table 6.2**

**Data Comparison with Run 79 and Run 67 (Ref.51).**

*(Steamflood in a Homogeneous Model, 15% PV Solvent)*

	Run 79				Run 67			
	Cum. PV Inj.	Cum. Inj.	Cum. Prod.	C.Prod/ C.Inj.	Cum. PV Inj.	Cum. Inj.	Cum. Prod.	C.Prod/ C.Inj.
HC Pore Volume:	0.00	0	0	0	0.00	0	0	0
Pore Volume:	0.10	1400	1920	1.37	0.07	980	980	1
Bulk Volume:	0.14	1932	3580	1.85	0.16	2205	2205	1
Porosity:	0.18	2500	5445	2.18	0.27	3795	3795	1
Initial Oil Saturation:	0.28	3864	7245	1.88	0.41	5715	5715	1
Initial Water Saturation:	0.40	5455	9345	1.71	0.55	7745	7745	1
Type of Oil Used:	0.50	6818	11225	1.65	0.69	9680	9680	1
Initial Model Temperature:	0.62	8409	13105	1.56	0.83	11720	11720	1
Total Flow Rate of Steam:	0.74	10114	15100	1.49	0.97	13700	13700	1
Steam Quality, fst:	0.87	11819	17140	1.45	1.12	15730	15730	1
Solvent Flow Rate:	0.98	13410	18960	1.41	1.26	17760	17760	1
Steam Volume Injected:	1.12	15341	20995	1.37	1.41	19785	19785	1
Solvent Volume Injected:	1.25	17046	22795	1.34	1.55	21770	21770	1
Net Oil Recovery:	1.39	18978	24725	1.30	1.70	23935	23935	1
Solvent Recovery:	1.54	21023	26785	1.27	1.85	25990	25990	1
Final Oil Saturation:	1.68	22955	28785	1.25	2.00	28105	28105	1
	1.81	24774	30565	1.23	2.14	30105	30105	1
	1.98	27046	32645	1.21				
	2.13	29092	34525	1.19				

**Run 67**

13030 cc  
 14080 cc  
 42005 cc  
 33.5%  
 92.5%  
 7.5%  
 Faxam-100  
 3°C  
 242.8 cc/min  
 N/A  
 200 cc/min  
 32160 cc (2.14 PV)  
 2100 cc (0.15 PV)  
 25.90%  
 97.00%  
 68.60%

**Run 79**

12410 cc  
 13655 cc  
 42005 cc  
 32.5%  
 90.9%  
 9.1%  
 Faxam-100  
 Initial Model Temperature: 3°C  
 Total Flow Rate of Steam: 227.28 cc/min  
 0.10  
 200.00 cc/min  
 29092 cc (2.13 PV)  
 2200 cc (0.15 PV)  
 57.51%  
 99.93%  
 38.62%

**Figure 6.3: Cumulative Production/Cumulative Injection, (CP/CI) vs. Cumulative Pore Volume Injected for Runs 67 (Ref. 51) and 79 – 7%BW, 10% HVN.**

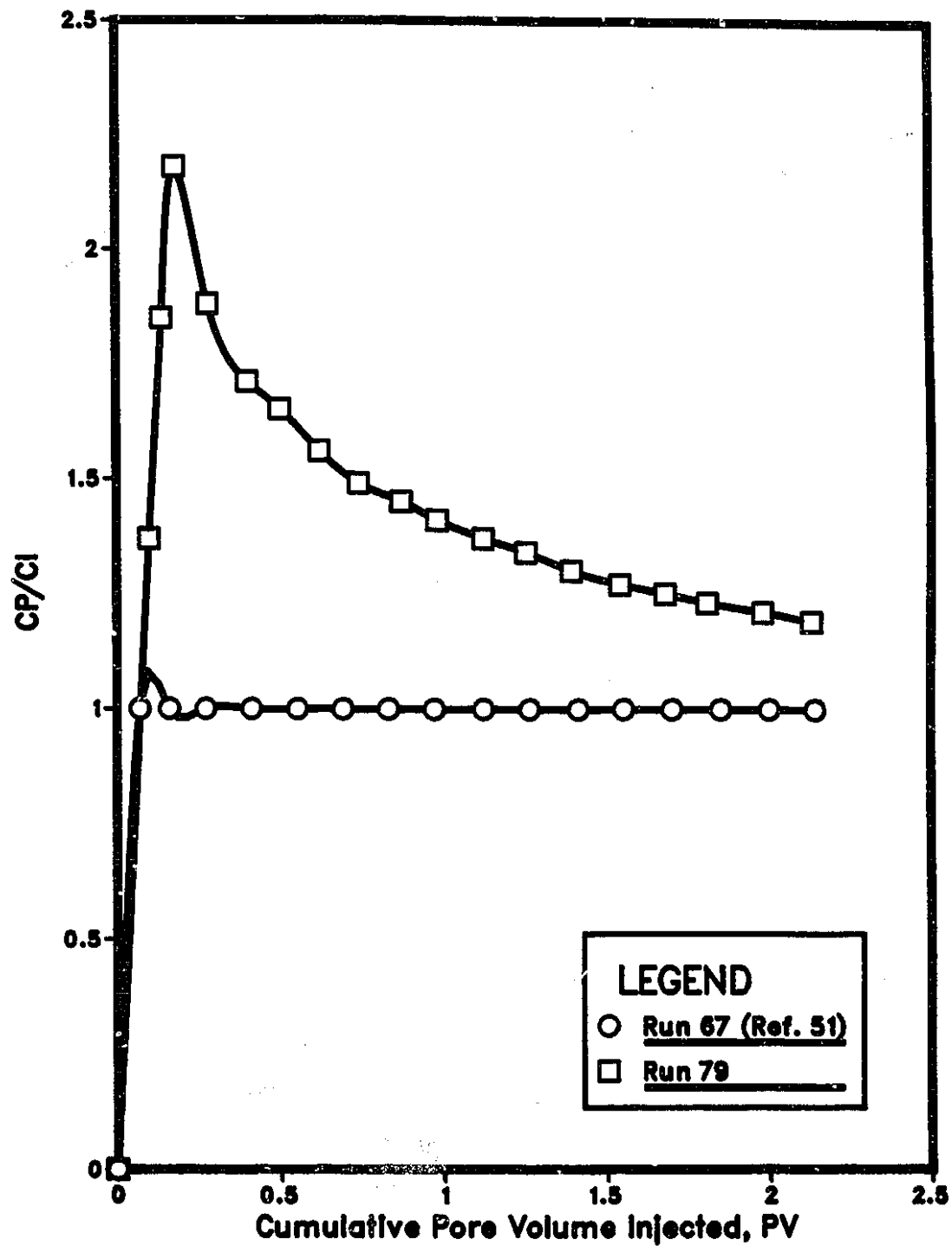


**Figure 6.4: Production History for Run 77: Base Case Steamflood in a Homogeneous Model using a Vertical Injector and a Vertical Producer.**

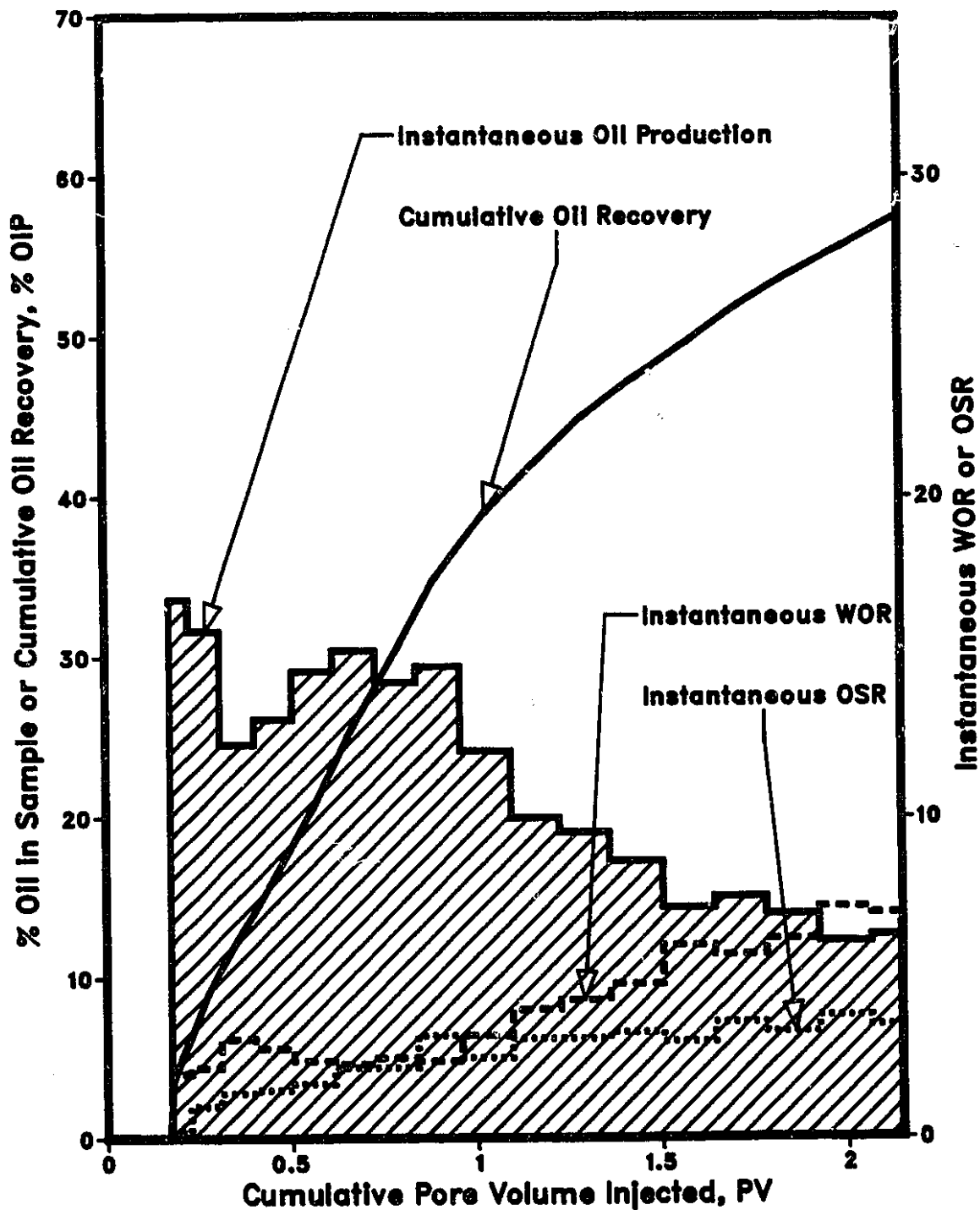


Figure 6.5: Top View Temperature Profiles for Run 77—Steamflood using a Horizontal-Vertical Well Combination in a Homogeneous Model.

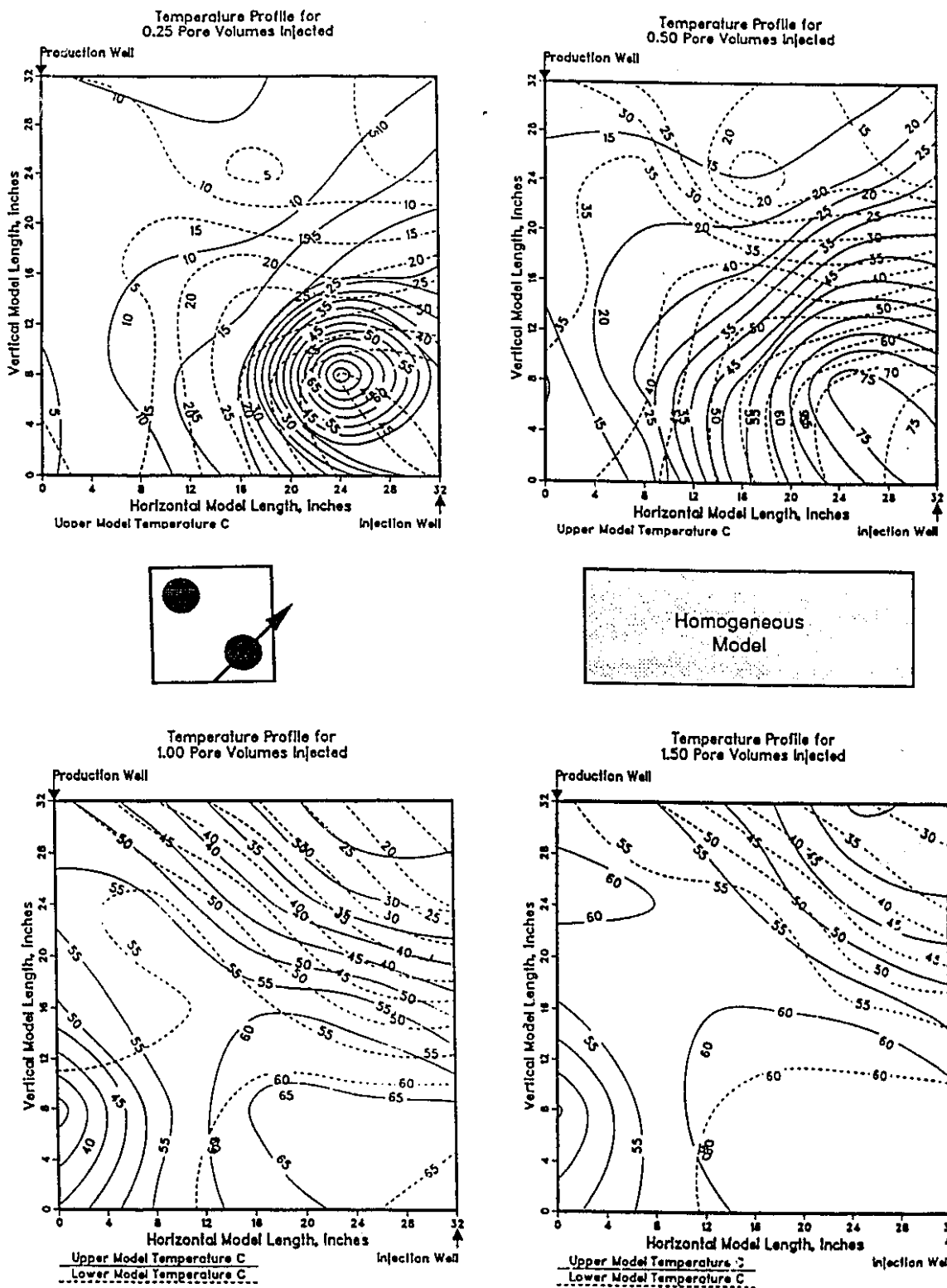
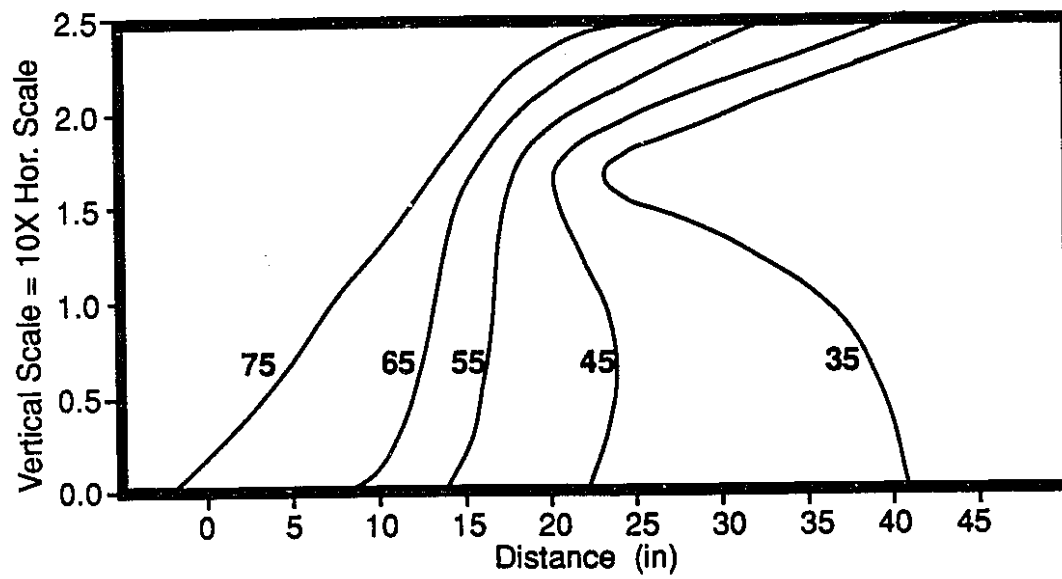




Figure 6.6: Injector to Producer Profile for Run 77 at 0.50 PV.



steam/steam condensate production and very low oil production, primarily by condensate segregation.

### Waterflood followed by a Steamflood

The next series of experiments examined the process of steamflooding a previously waterflooded reservoir. In Run 70A, a homogeneous reservoir was waterflooded, followed by a subsequent steamflood in Run 70B. This strategy is of particular interest for waterflooded reservoirs in Saskatchewan, which yield less than 5% by primary recovery, and between 5 and 10% by secondary (waterflood) recovery methods. To test experimental reproducibility, these runs were repeated (Runs 105A and 105B). Since the results were similar, only Run 105 will be considered.

In Run 105A, water was injected until a water-oil ratio (WOR) of approximately 15 was achieved, which is typical of many field operations. The ultimate recovery by waterflooding was only 18%. A steamflood was then initiated in Run 105B. Figure 6.7 shows the gradual increase in oil production upon steam injection and a cumulative oil recovery of 61% after 2.0 PV of steam was injected. While steam segregation and preferential flow through the path of least resistance are mutually opposing effects, the dominant factor controlling steam flow was segregation. Figures 6.8 and 6.9 show that the injected steam followed the high water saturation channels on the top of the formation and also showed override.

### Gas Injection Runs

By injecting a small slug of an inert gas prior to steamflooding, it is expected that the gas would create flow channels in the upper portion of the model, thereby creating a more conductive path for the injected fluid. This is particularly effective in the case of a bottom water zone where heat scavenging is a problem. The gas channels should divert the injected fluid away from the bottom water. Thus, gas injection could offer a means of increasing initial reservoir injectivity for a waterflood.

**Figure 6.7: Production History for Run 105: Waterflood in a Homogeneous Model, followed by a Continuous Steamflood.**

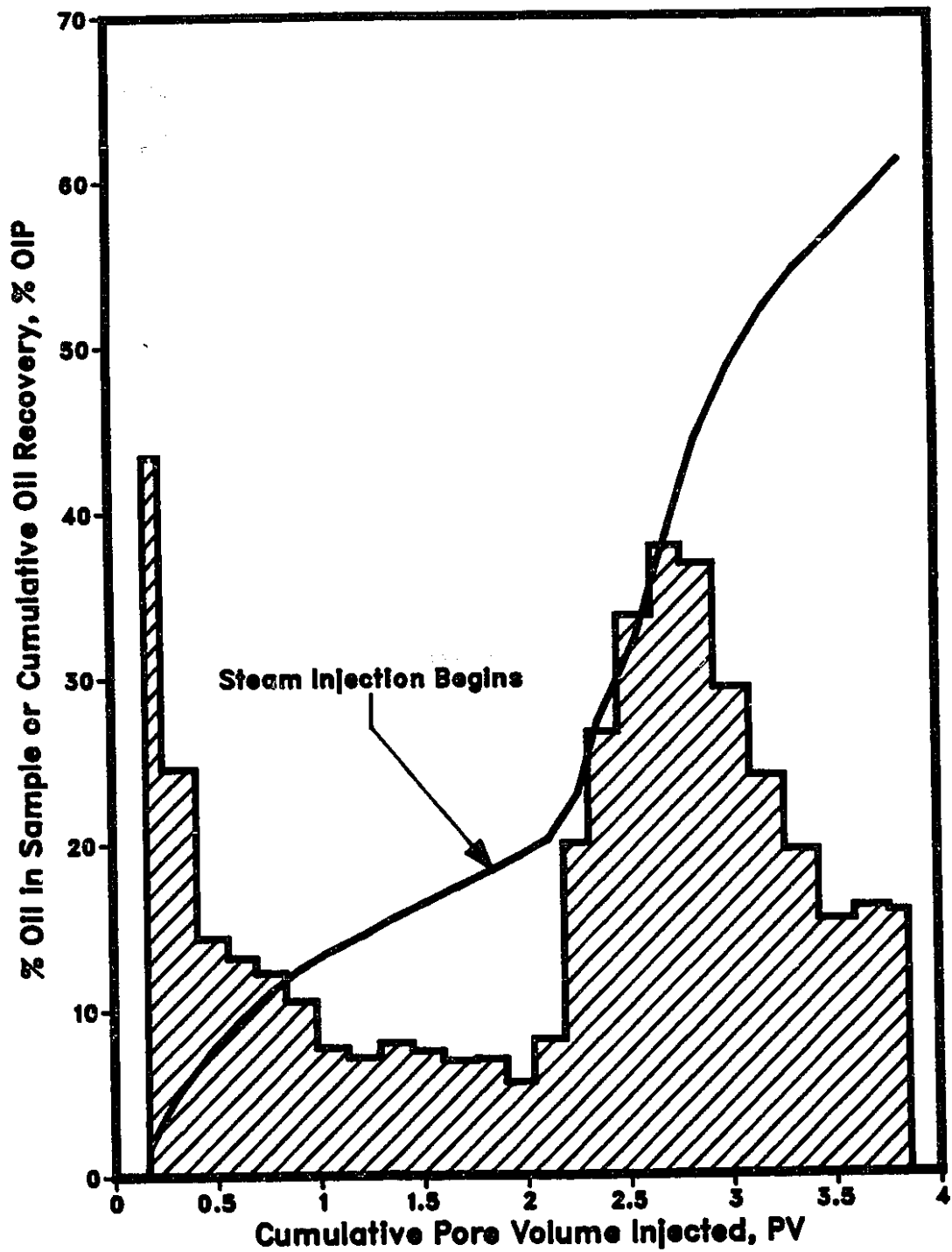


Figure 6.8: Top View Temperature Profiles for Run 105A-Waterflood (WOR of 15)

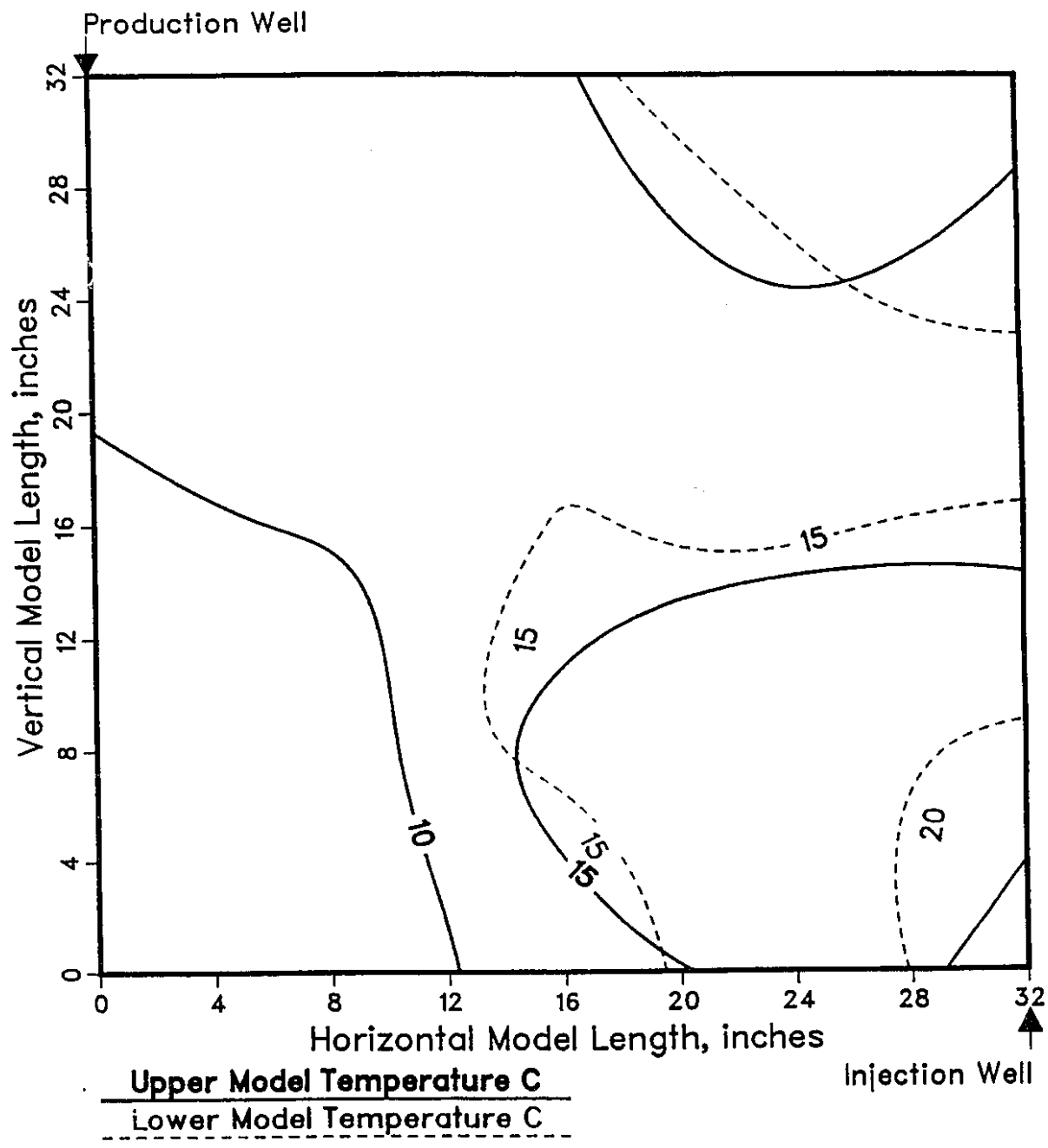
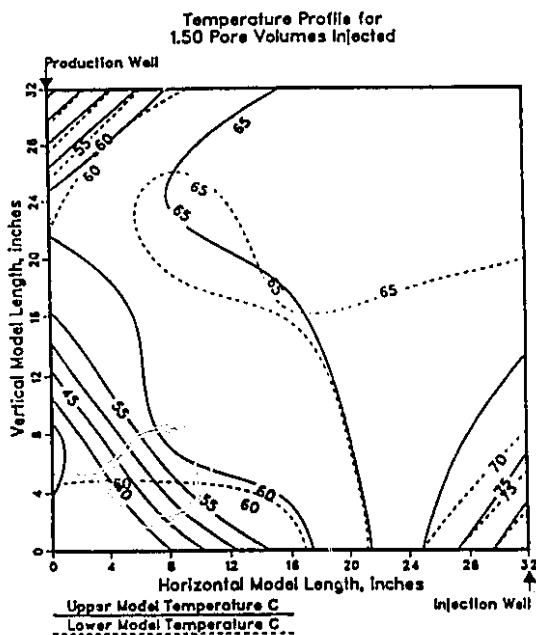
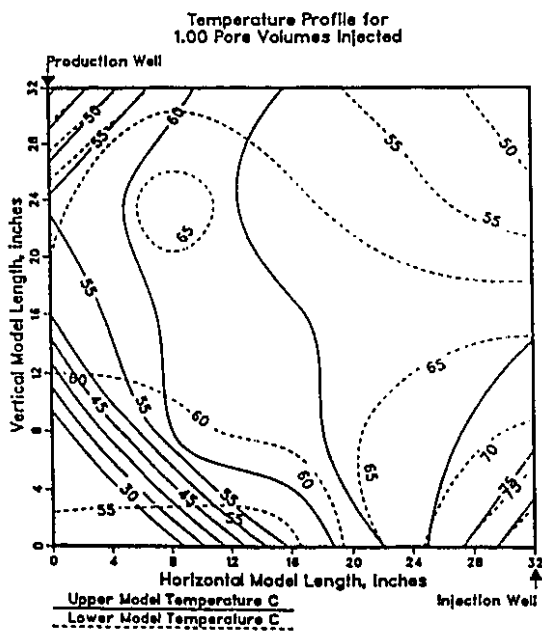
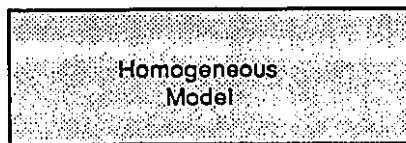
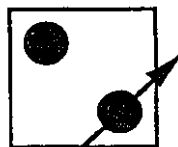
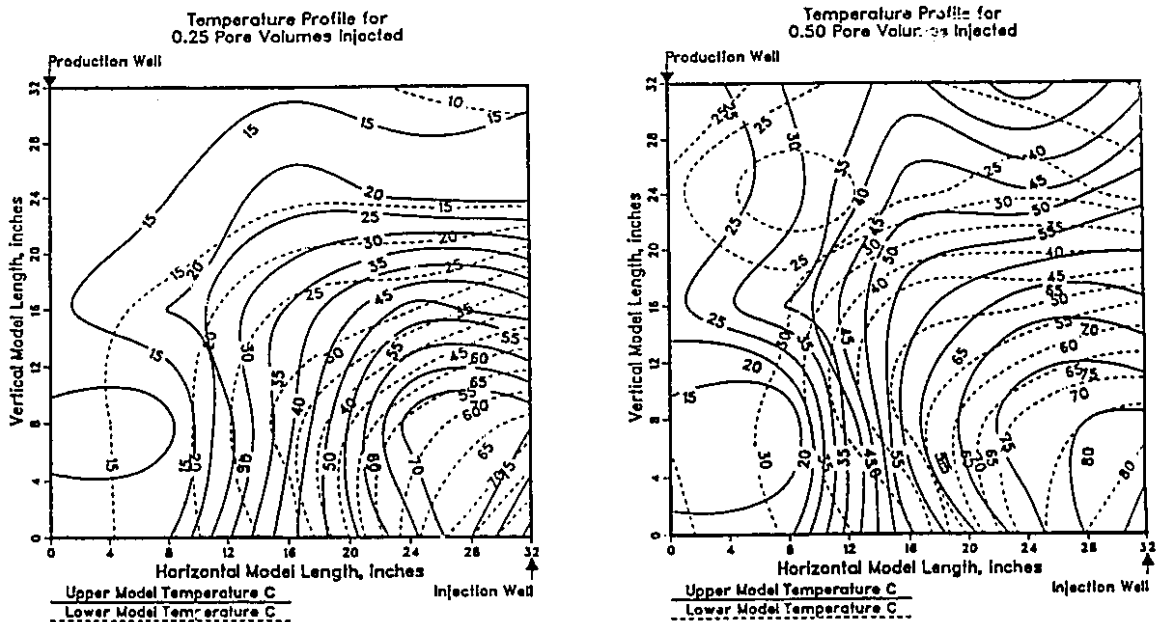


Figure 6.9: Top View Temperature Profiles for Run 105B—Steamflood following a Waterflood.



### **Prior to a Conventional Waterflood**

Nitrogen was selected because of its inert nature, availability and low cost. Nitrogen gas was injected for one prototype year (approximately 11.5 minutes) at 7 kPa (1 psig). Injection pressure was monitored regularly to ensure that it did not exceed 7 kPa. Pressures above this level were sufficient to lift the model and break the vacuum seal.

In Run 71, gas injection in a homogeneous pack resulted in an initial gas saturation of approximately 3%. The initial gas saturation was equivalent to the volume of fluid displaced during the gas injection. Results of this run indicate that gas injection prior to waterflooding did not improve oil recovery as can be seen in Figure 6.10. Only 19% of the original oil in place was recovered at a WOR of 20 compared to 18% for the waterflood in Run 105A with no gas injection.

### **Prior to a Hot Waterflood**

Gas injection subsequent to a waterflood may produce preferential channels in addition to the ones created by water. Hot water at 70°C was then injected for 1.5 PV until a constant WOR was obtained. Hot water was chosen because its higher sensible heat would improve ultimate recovery, without the complexity of a steamflood. Again, as seen in Figure 6.11, gas injection did not seem to alter the recovery curves in spite of the hot water drive. The cumulative recovery increased by 13% with the initiation of a hot waterflood in a homogeneous model. Figure 6.12 shows significantly lower temperature contours, on average 25°C less, than those produced from steam drives. The lower thermocouple contours showed that a layer of cold water was flowing in the lower portion of the pack.

### **Effect of a Gas Zone on Steamflood Recovery**

The effect of gas on steam injection processes in the presence of bottom water was examined in the next two runs. Nitrogen gas was injected using the procedure described

**Figure 6.10: Production History for Run 71: Gas (N<sub>2</sub>) Injection in a Homogeneous Model prior to a Conventional Waterflood.**

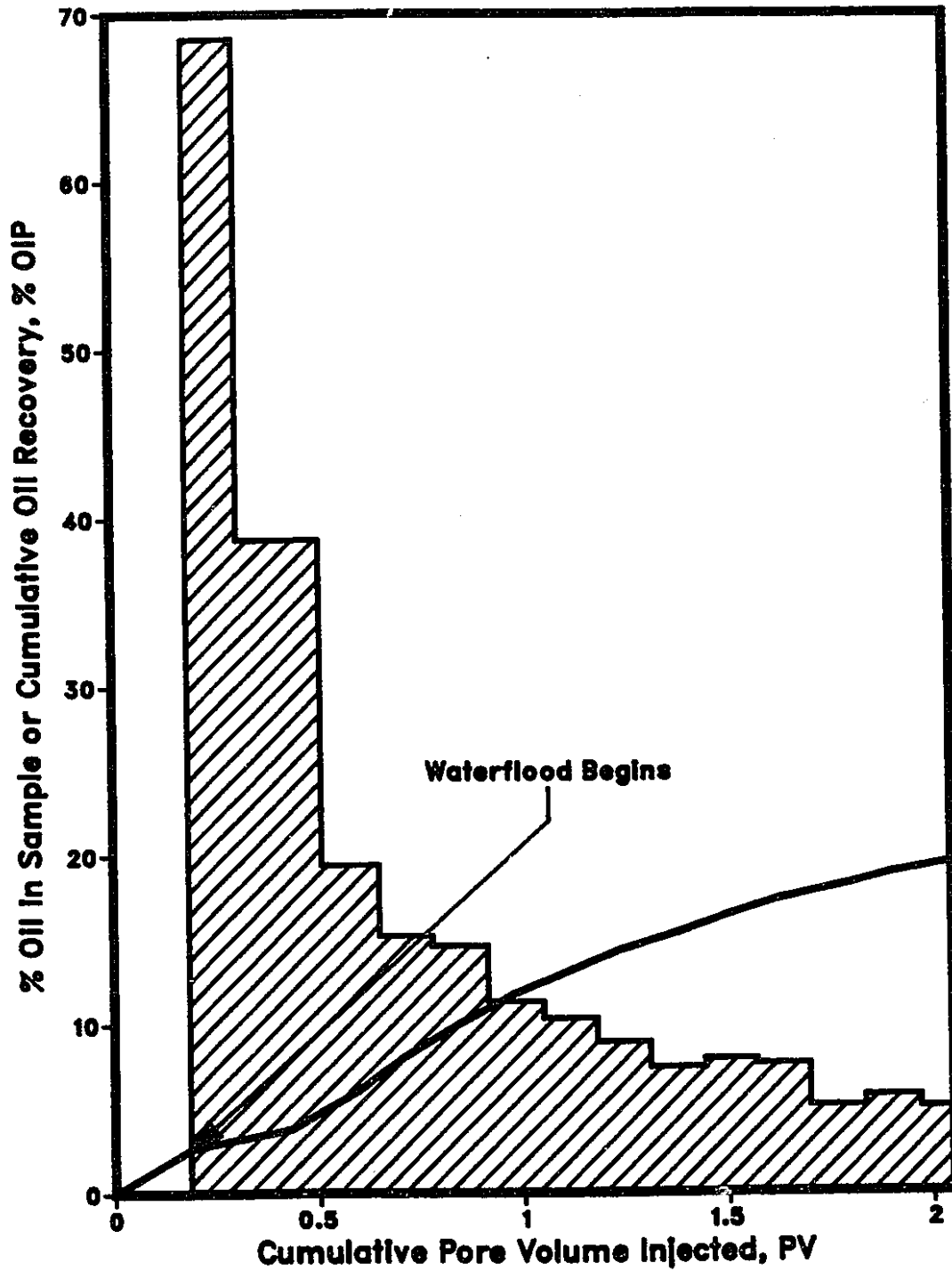


**Figure 6.11: Production History for Run 72: Waterflood in a Homogeneous Model, followed by N<sub>2</sub> Injection and then, by a Hot Waterflood.**

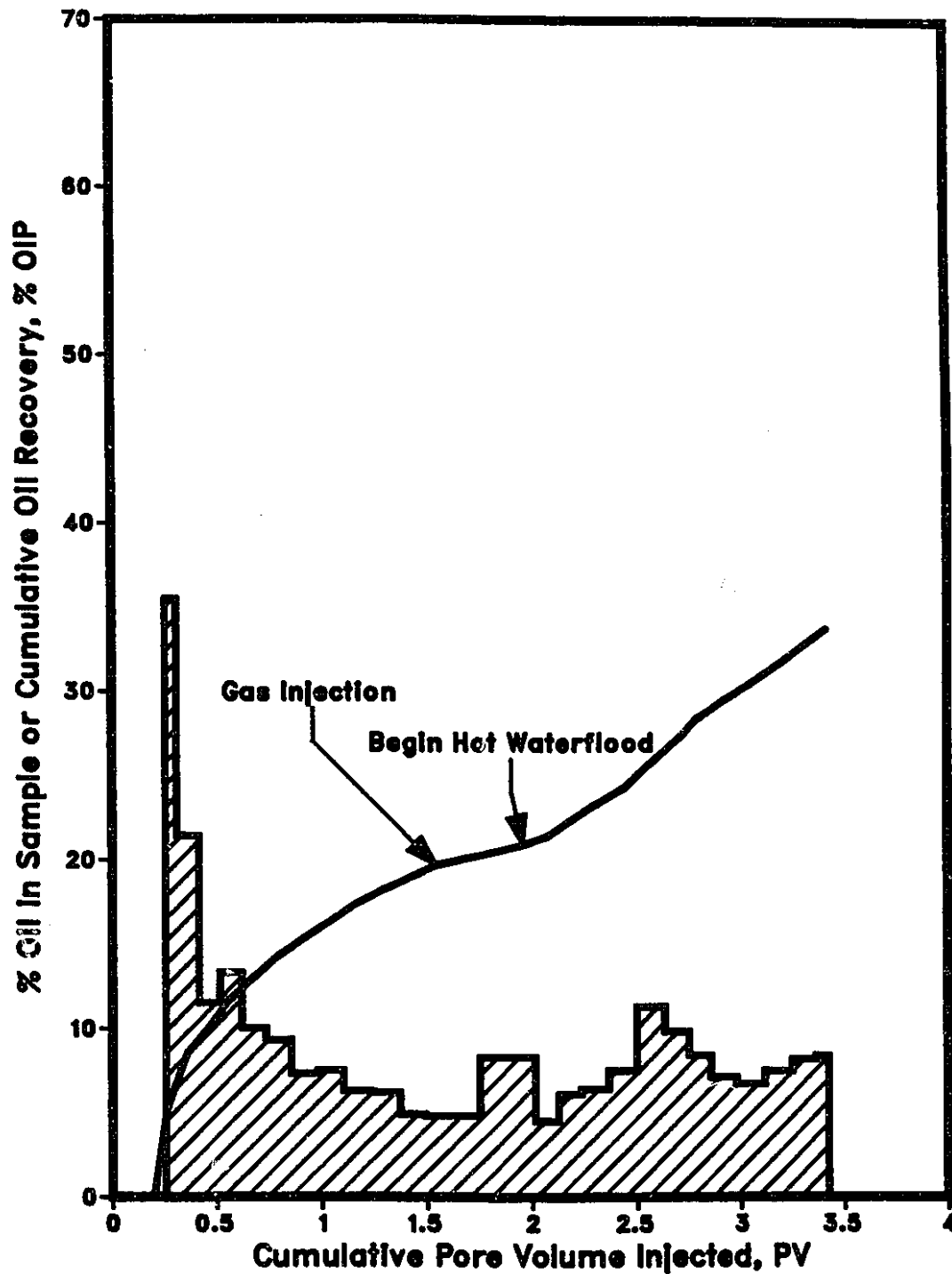
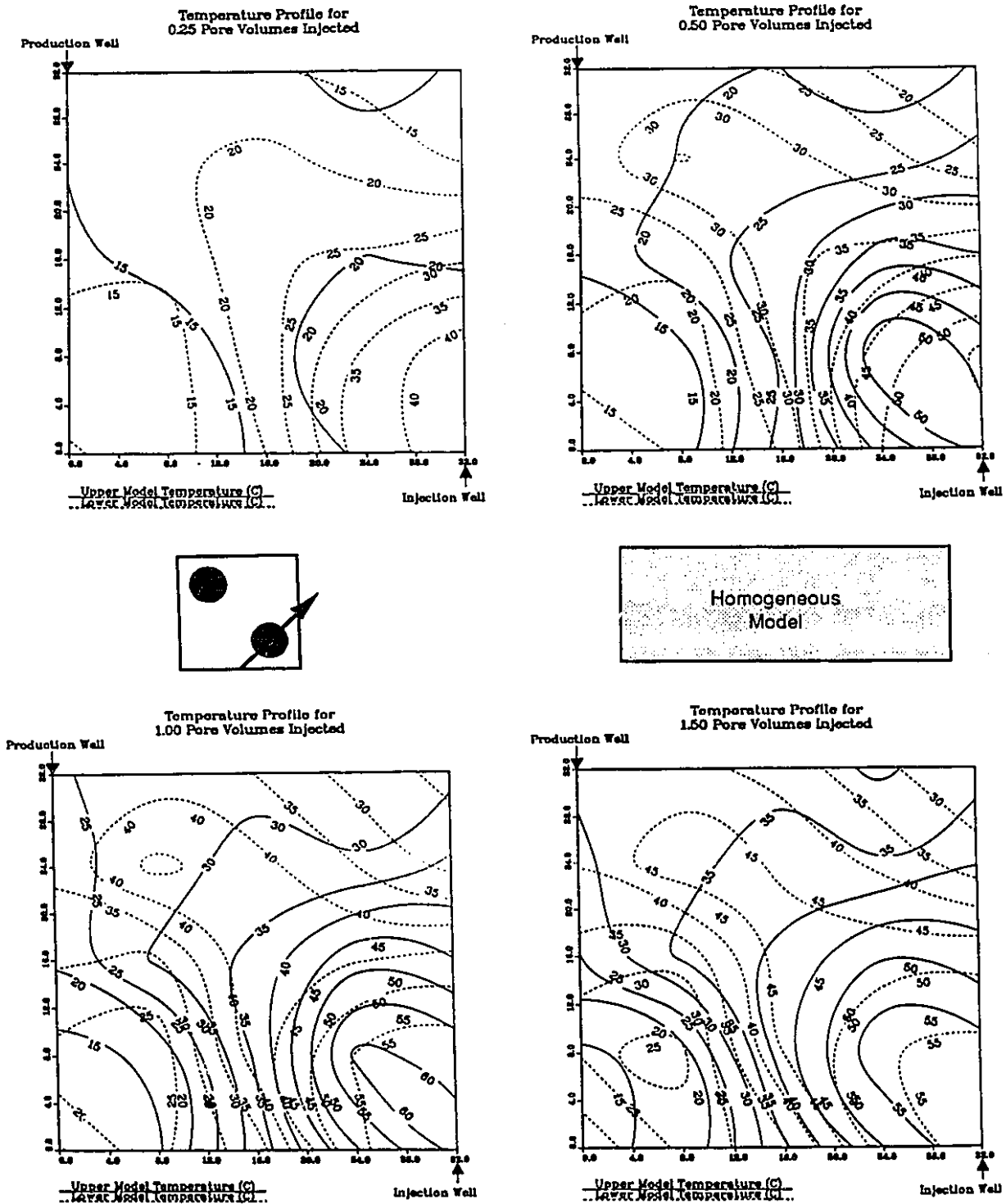




Figure 6.12: Top View Temperature Profiles for Run 72B -- Gas Injection prior to a Hot Waterflood.



previously. It was noted that the nitrogen gas displaced a volume of fluid equal to the volume of the gas zone. Continued gas injection did not cause further fluid production. Instead, it was observed from the production tubing that the gas flowed directly through the channels created during the injection.

#### Thick Bottom Water

The thick bottom water model had a much higher initial gas saturation (44.5%) than the homogeneous case in Run 105B (3%). In Run 95, the positive back pressure created as a result of gas injection caused rapid bottom and formation water production. Under normal conditions, fluid was drawn through the production side solely due to the vacuum pump. In gas injection, nitrogen was injected under 1 psig while the pump was simultaneously extracting the fluid. Hence, a positive pressure was created causing a lower manometer reading. As mentioned previously, no fluid was produced from gas injection after a certain point. Approximately six litres (5615 cc) of steam was injected into the model before oil broke through.

As shown in Figure 6.13, gas injection in the presence of a bottom water layer did improve oil recovery. Initially, only bottom water was produced in the early stages of steam injection for both Run 95 (gas injection) and Run 100 (no gas injection). However, oil breakthrough occurred earlier when gas was injected by approximately 0.25 PV or one prototype year. Temperature contours for Run 95 in Figure 6.14 showed that the gas slug caused the steam zone to advance more rapidly and farther in the formation compared to Run 100, temperature contours for which are shown in Figure 6.15. The significantly higher cumulative oil recovery for Run 95 is attributed to improved displacement efficiency due to the larger gas saturation, which diverted steam away from the water zone.

#### Thin Bottom Water

In Run 96, nitrogen was injected prior to steam injection, in the presence of a thin bottom water zone. Nitrogen caused later oil breakthrough in this case. Figure 6.16

**Figure 6.13: Production History for Steamfloods in 50% Bottom Water—Run 95 (Pre-injection of N<sub>2</sub> Gas) and Run 100 (Continuous Steamflood, No Gas).**

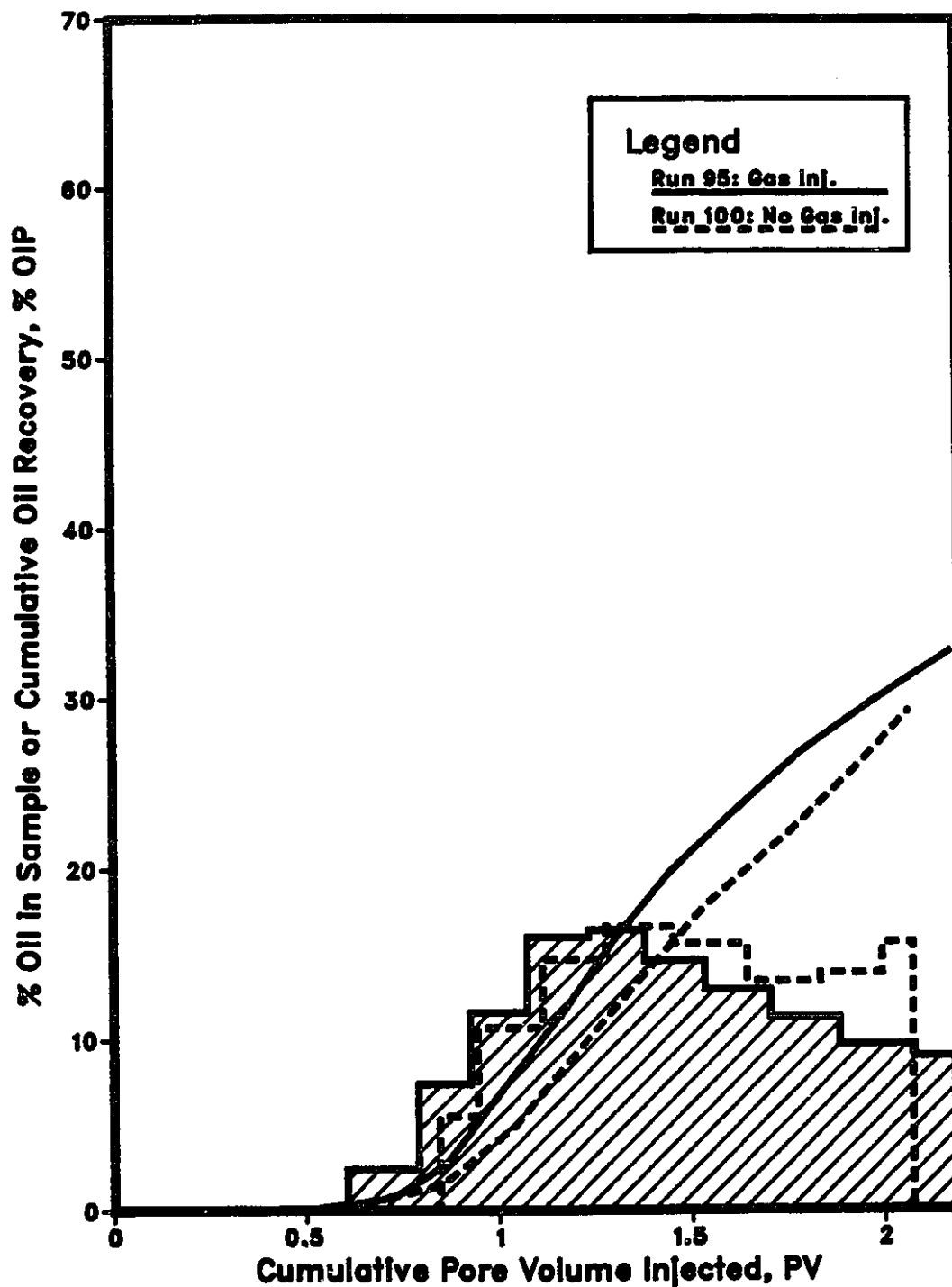


Figure 6.14: Top View Temperature Profiles for Run 95—Gas Injection prior to a Steamflood in a Thick (50%) Bottom Water Model.

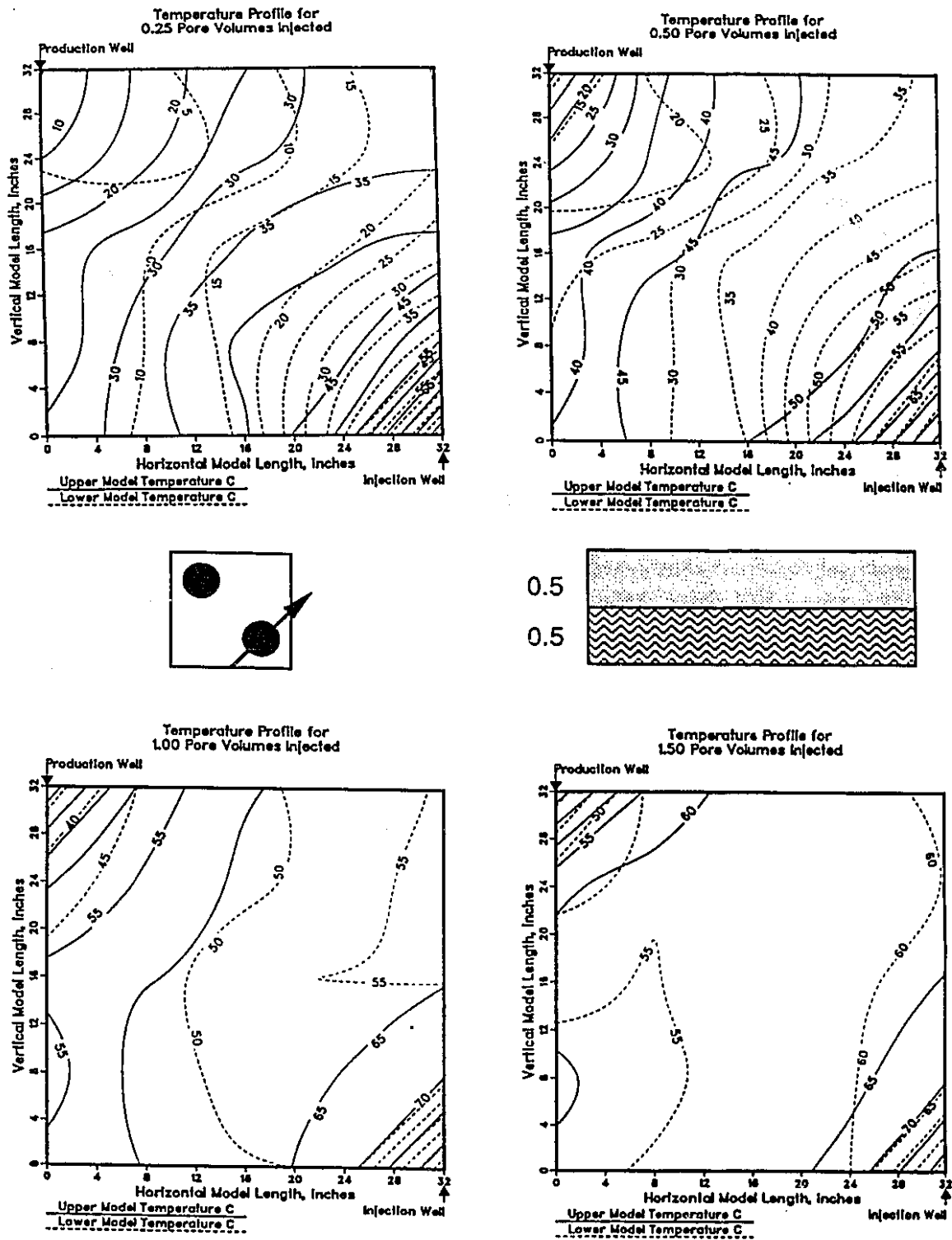
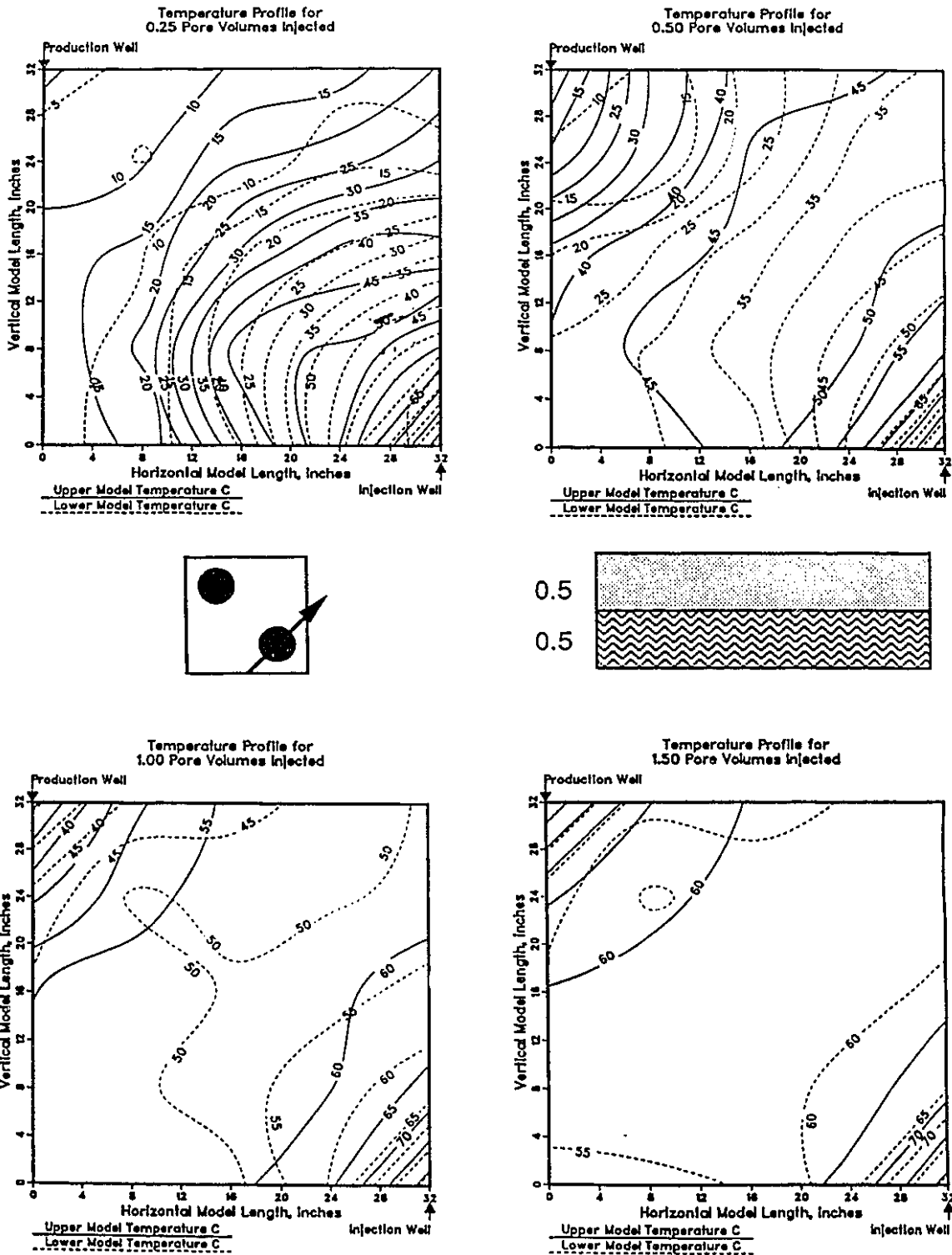


Figure 6.15: Top View Temperature Profiles for Run 100—Steamflood using a Horizontal-Vertical Well Combination in a Thick (50%) Bottom Water Model.



shows that oil breakthrough in Run 96 occurred 0.25 PV later than the conventional steamflood (Run 90), which was the opposite for thick bottom water. Temperature profiles for Run 96, in Figure 6.17, show that steam dispersed farther into the formation than for Run 90 (Figure 6.18, without gas injection). However, there is an additional benefit of conduction heating for gas injection in the thin bottom water case. At 1 PV, oil production from Run 96 starts to exceed that in Run 90. At the conclusion of the experiments, the ultimate oil recovery for Run 96 (50.2%) was greater than that for Run 90 (47.3%), although the difference is of the order of experimental error. It should be noted that in the previous work oil recovery was consistently higher when gas was used<sup>14</sup>.

### **Steamflood in the Presence of Bottom Water**

Figure 6.19 presents the results of four steamfloods conducted in the presence of varying bottom water thicknesses: 0%, 7%, 10% and 50%. Figure 6.19 shows that the initial production for 7% BW was less than that for the homogeneous case, but gradually exceeded that for the homogeneous case as conduction heating effects start to dominate the recovery process. The higher recovery in Run 83 (7% BW) was attributed to increased reservoir heating by conduction through the bottom water zone.

As noted by Proctor et al.<sup>21</sup>, there appears to be some minimum bottom water thickness below which the preferential flow of steam through the basal layer and the concomitant conduction heating would lead to higher ultimate recovery than that for a homogeneous (no bottom water) formation. Figure 6.19 shows that 7% bottom water produced slightly more oil than the homogeneous pack and significantly more than the 10% and 50% BW situations. This suggests that the optimum bottom thickness is less than the 10% value suggested previously.

### **Solvent-Steamfloods**

The purpose of injecting a small solvent slug prior to steamflooding is similar to that for gas injection. The channels created by solvent injection would increase steam

Figure 6.16: Production History for Steamfloods in 10% Bottom Water—Run 96 (Pre-injection of N<sub>2</sub> Gas) and Run 90 (Continuous Steamflood, No Gas).

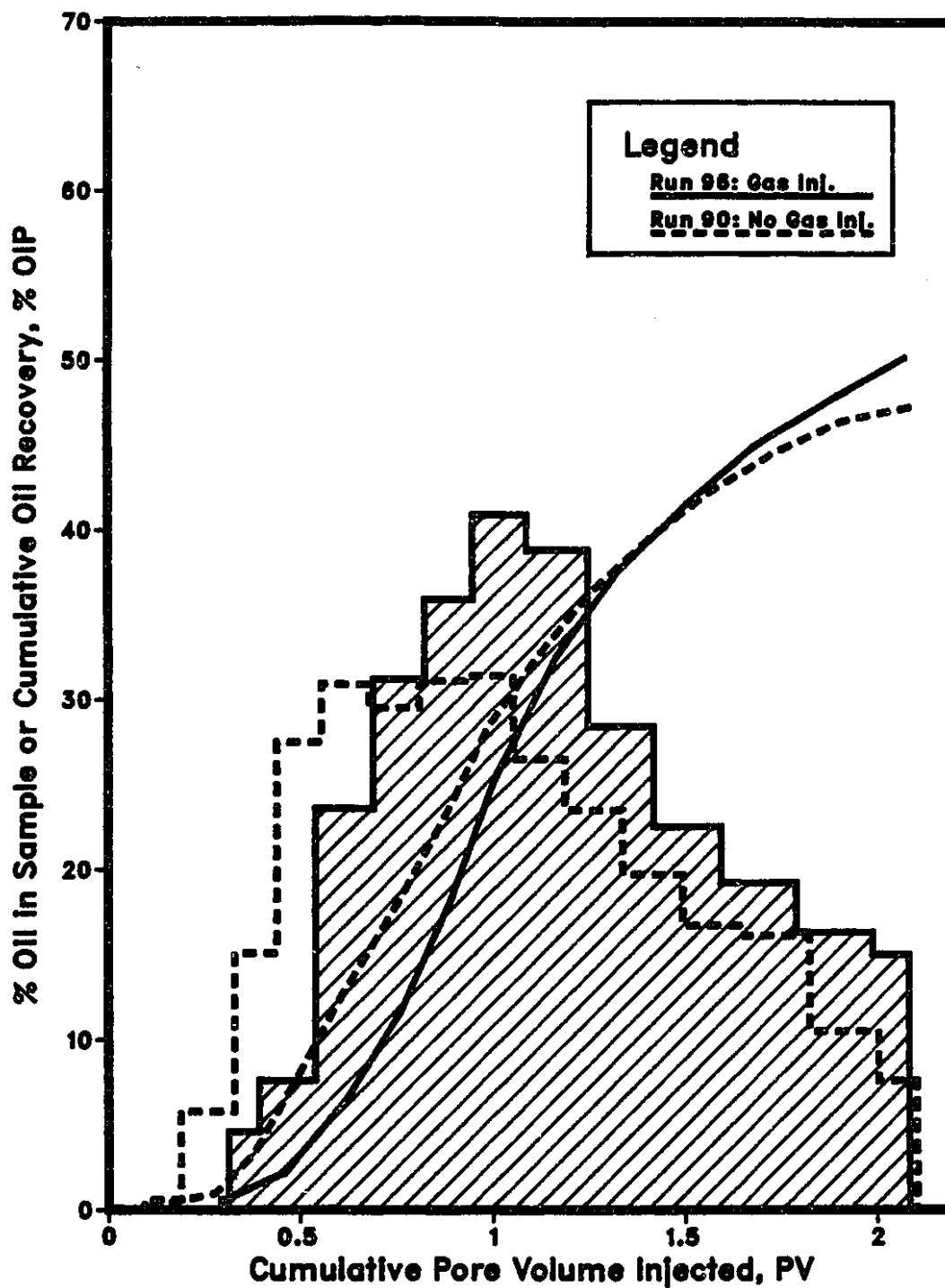


Figure 6.17: Top View Temperature Profiles for Run 96—Gas Injection prior to a Steamflood in a Thin (10%) Bottom Water Model.

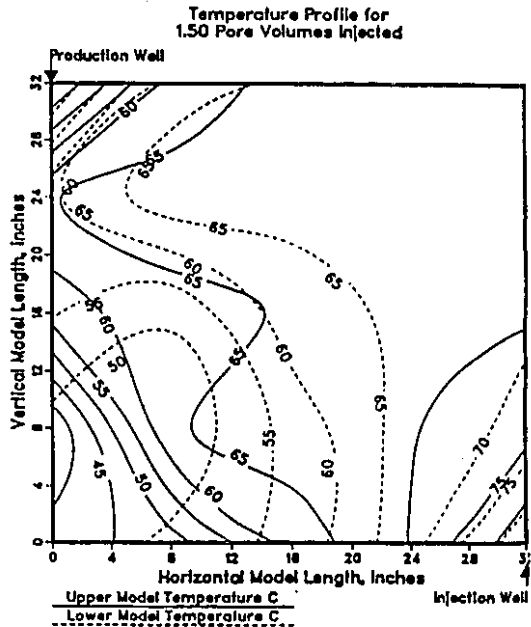
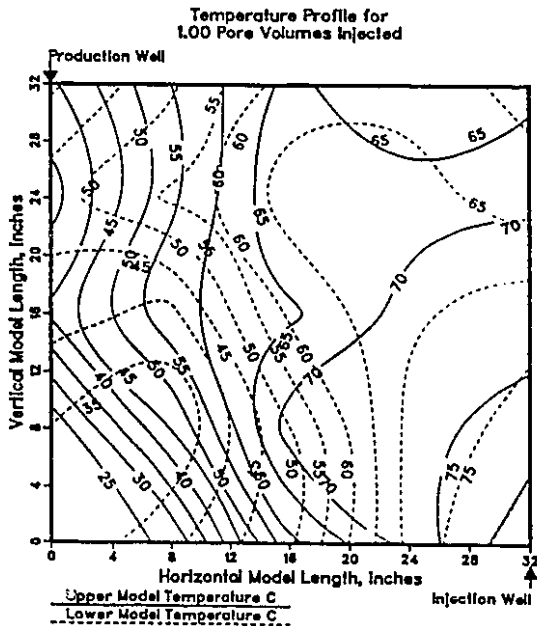
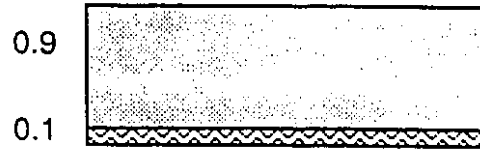
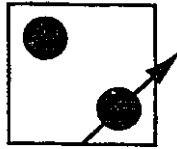
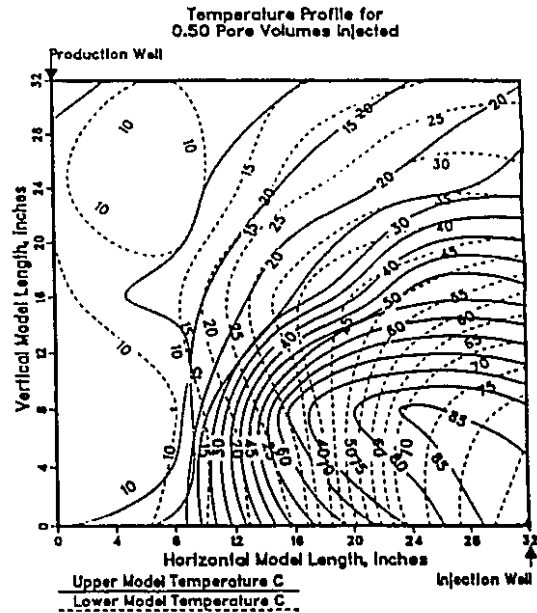
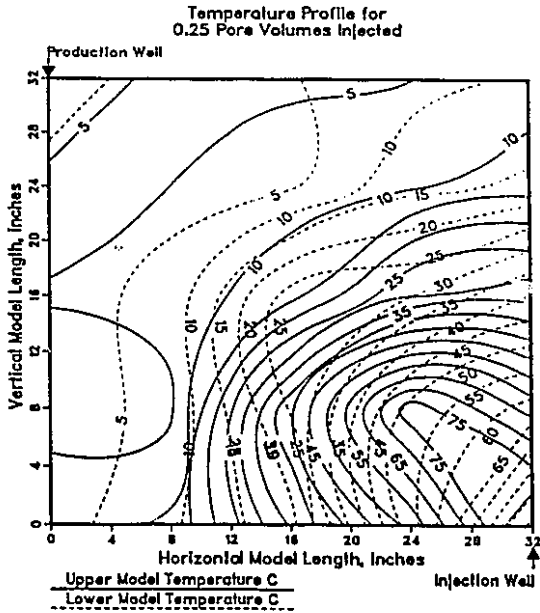
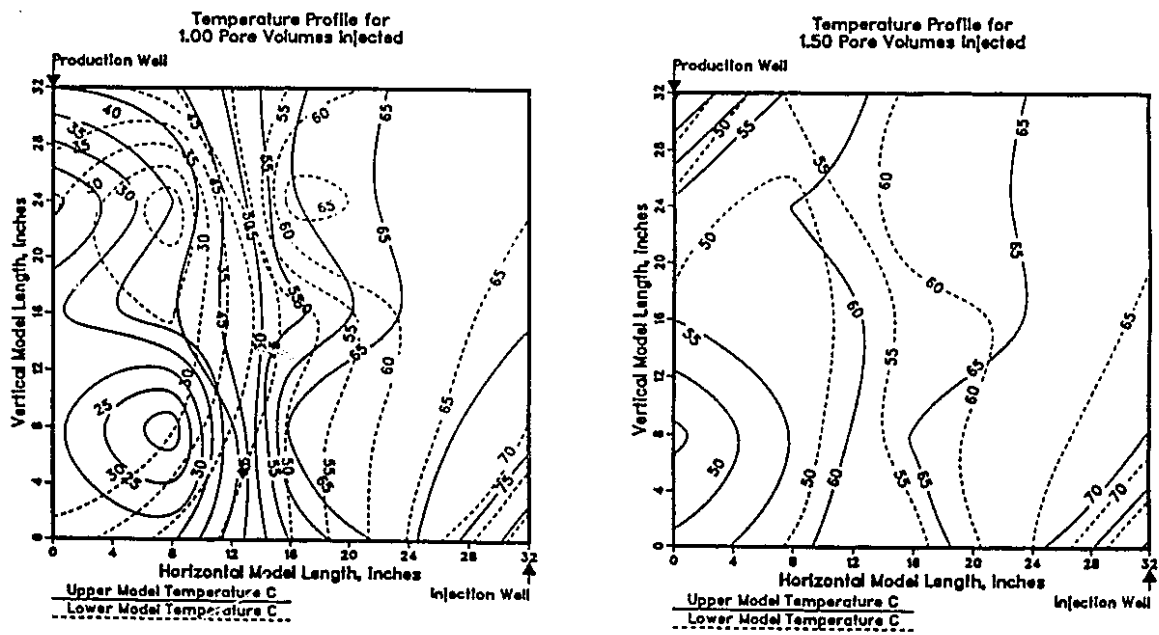
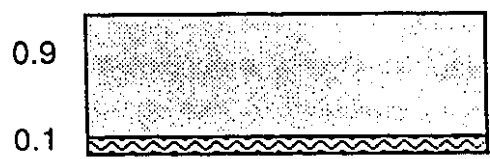
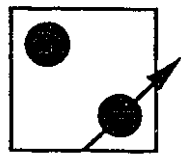
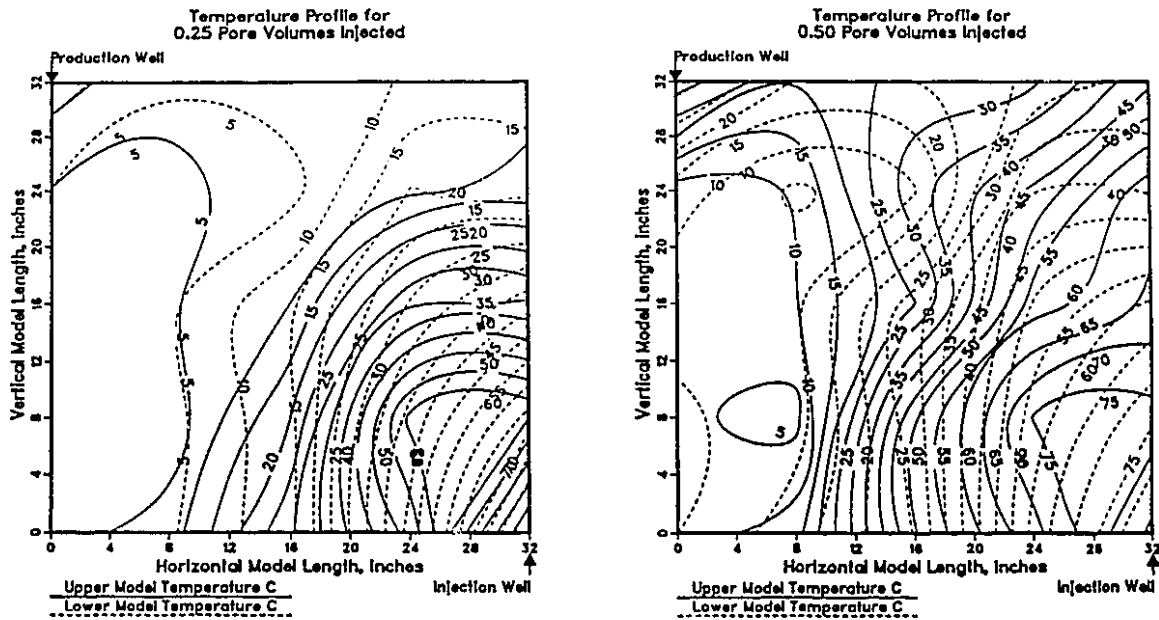
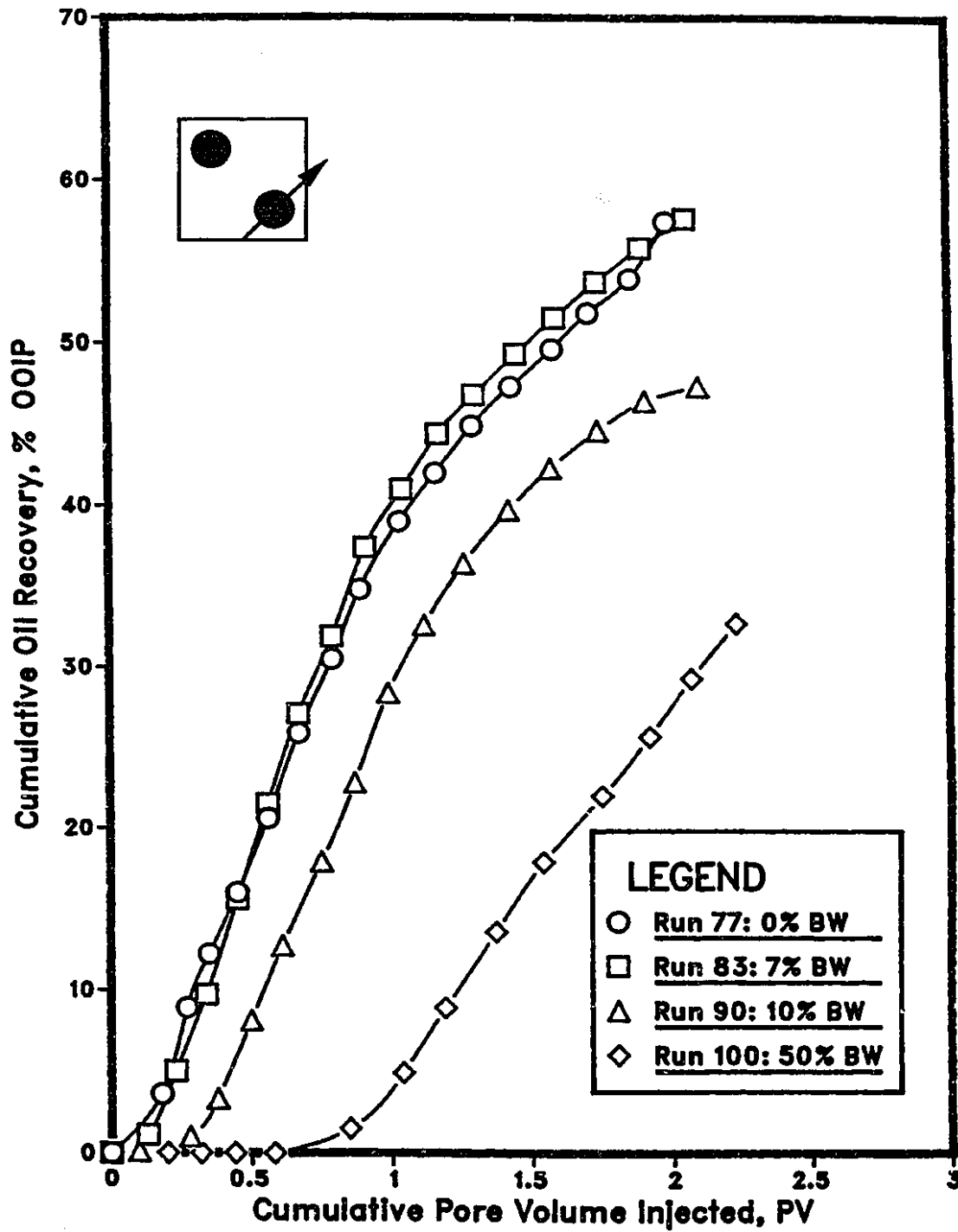




Figure 6.18: Top View Temperature Profiles for Run 90—Steamflood using a Horizontal-Vertical Well Combination in a Thin (10%) Bottom Water Model.



**Figure 6.19: Cumulative Oil Recoveries for Steamfloods using a Vertical Producer and a Vertical Injector as a function of Bottom Water Thickness.**



injectivity by providing the initial steam paths in an otherwise low mobility oil. The solvent is also effective in reducing oil viscosity provided it disperses readily into the oil zone. This is most likely to occur in the form of viscous fingering as a result of the high viscosity of the formation oil and the low viscosity of Heavy Virgin Naphtha (HVN) solvent. Due to increased oil mobility, a larger hydrocarbon (oil and solvent) bank would form and a more stable steam displacement would occur.

The application of solvent injection is particularly useful for bottom water reservoirs because it would divert the steam away from the basal zone. Because the solvent is a non-wetting phase, it would tend to channel only through the oil zone in the upper portion of the reservoir instead of the basal zone.

Too large a solvent slug would create an oil bank in the oil zone leading to a greater pressure drop. The greater flow resistance in the upper portion of the reservoir would cause solvent to channel into the bottom water zone. Asphaltene flocculation would also occur if large volumes of Heavy Virgin Naphtha were injected.

### **Results of Solvent-Steamfloods**

In the following experiments, the effect of the solvent slug size on the overall recovery performance was studied. The objective was to determine the optimal slug size to maximize oil recovery in the presence of thin bottom water formations. Four slug sizes (0%, 10%, 20% and 30%) were preinjected into a 7% bottom water formation prior to a steamflood in Runs 83, 78, 84 and 82, respectively. Individual production results with the accompanying temperature profiles are presented in Figures 6.20 through 6.27. The most noticeable feature of these runs is that approximately 100% of the injected solvent was recovered during the experiment. This was most likely caused by the aforementioned steam distillation effects. The lighter naphtha solvent was carried along with the gaseous steam phase resulting in a higher displacement.

Figure 6.20: Production History for Run 83: No Solvent Injection in a Bottom Water Model, 7% BW, prior to a Continuous Steamflood.

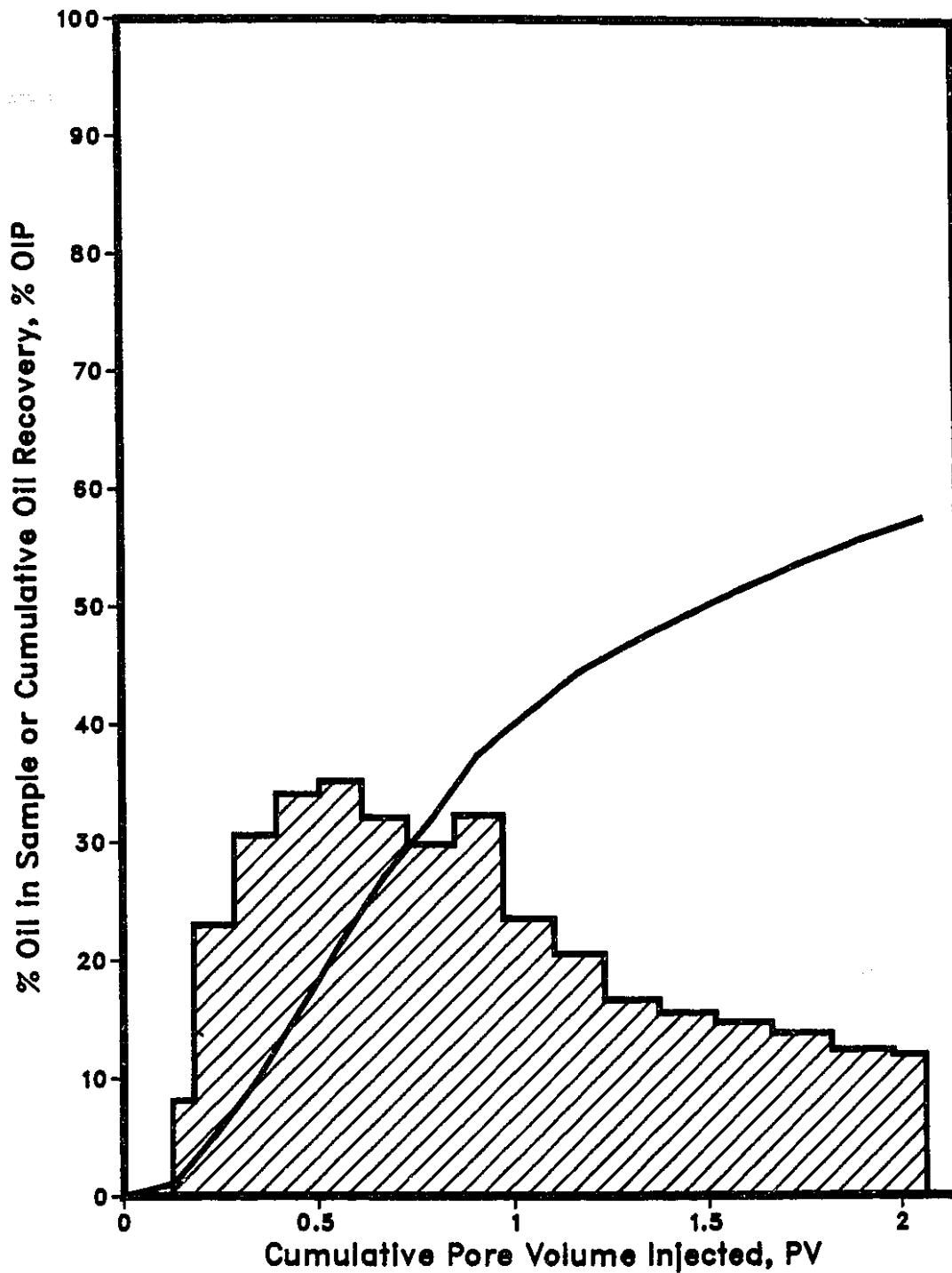


Figure 6.21: Top View Temperature Profiles for Run 83—No Solvent Steamflood in a Thin (7%) Bottom Water Model.

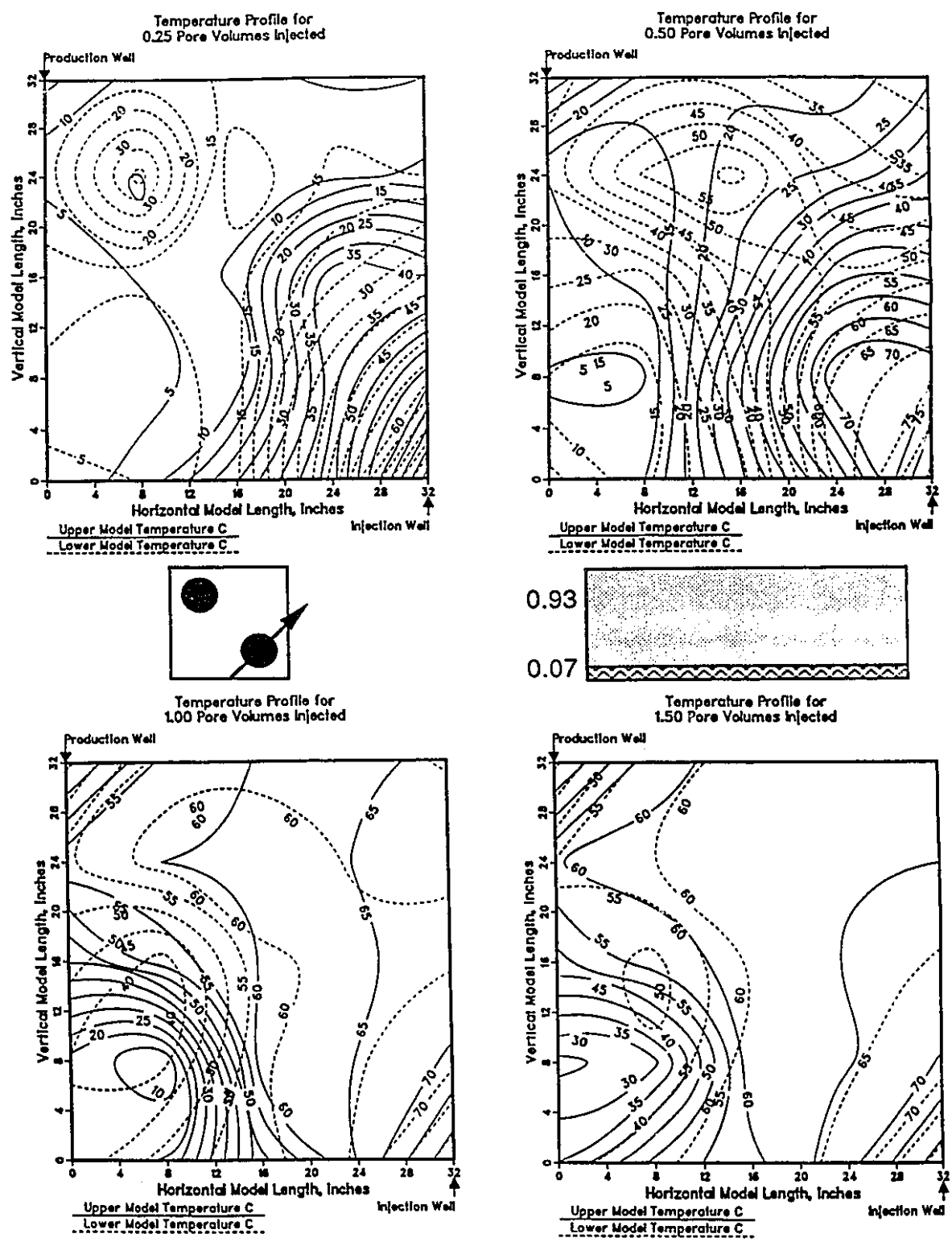


Figure 6.22: Production History for Run 78: Solvent, 10% PV, Injection In a Bottom Water Model, 7% BW, prior to a Continuous Steamflood.

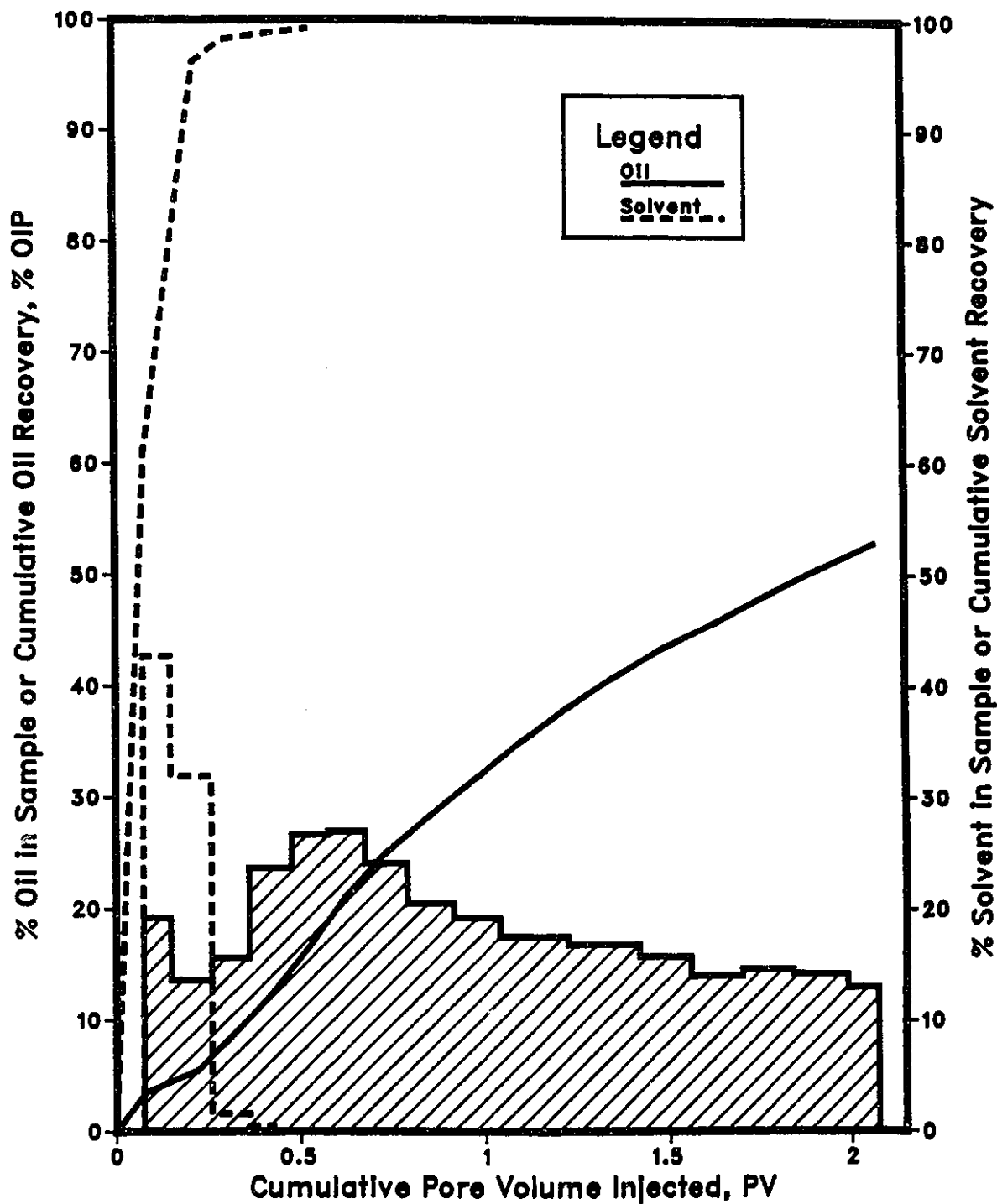


Figure 6.23: Top View Temperature Profiles for Run 78—Solvent (10% PV) Steamflood in a Thin (7%) Bottom Water Model.

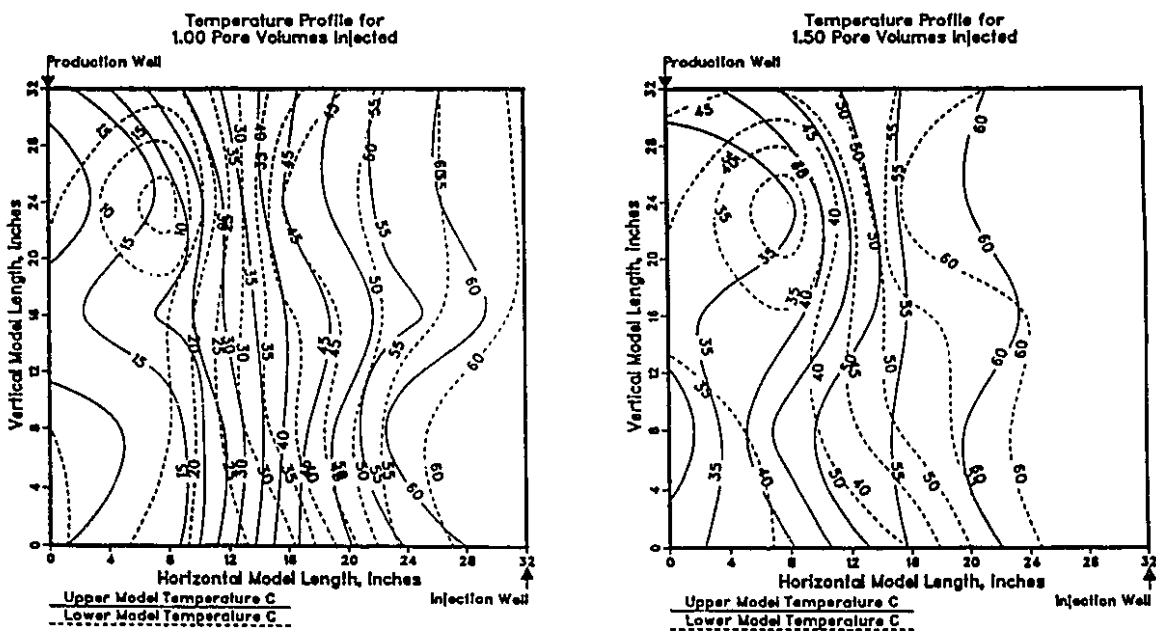
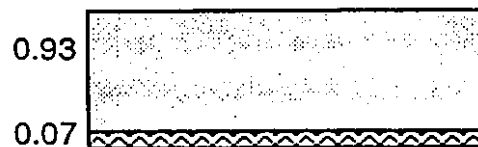
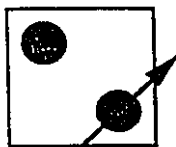
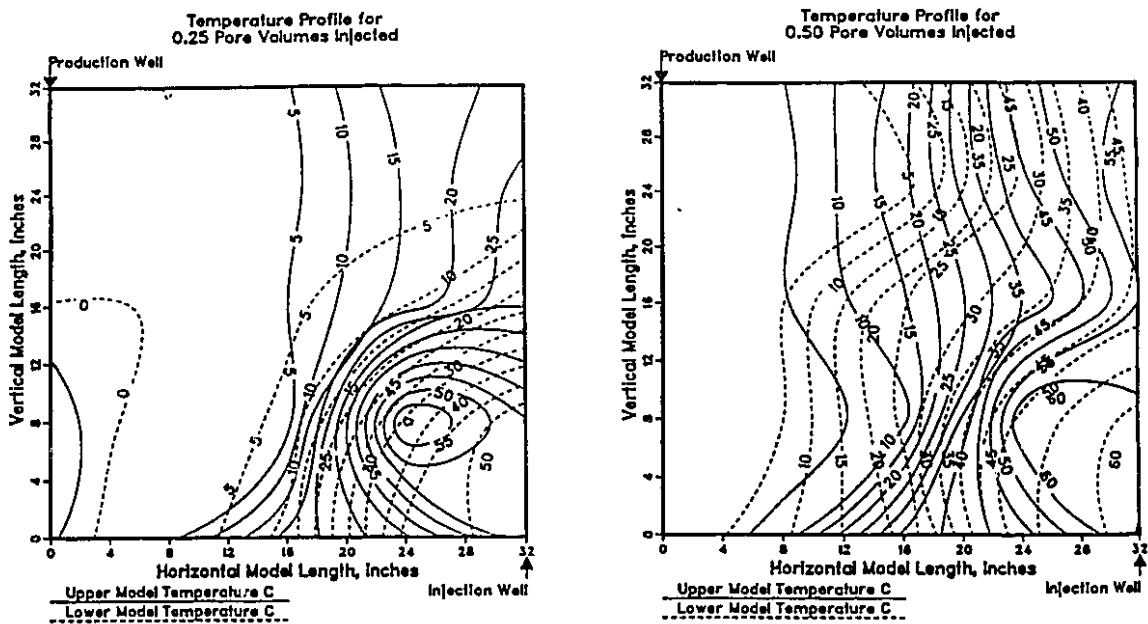


Figure 6.24: Production History for Run 84: Solvent, 20% PV, Injection in a Bottom Water Model, 7% BW, prior to a Continuous Steamflood.

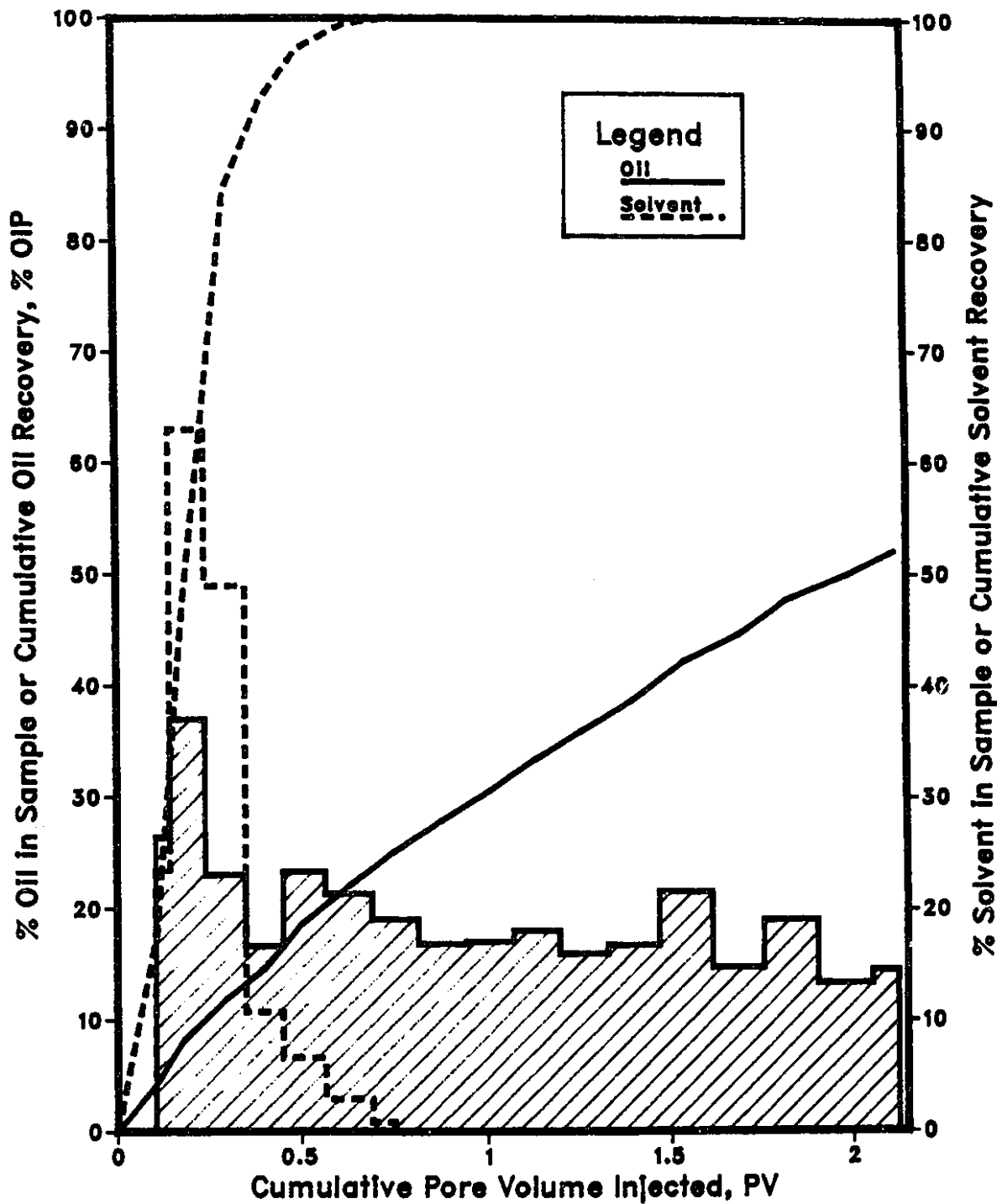




Figure 6.25: Top View Temperature Profiles for Run 84—Solvent (20% PV) Steamflood in a Thin (7%) Bottom Water Model.

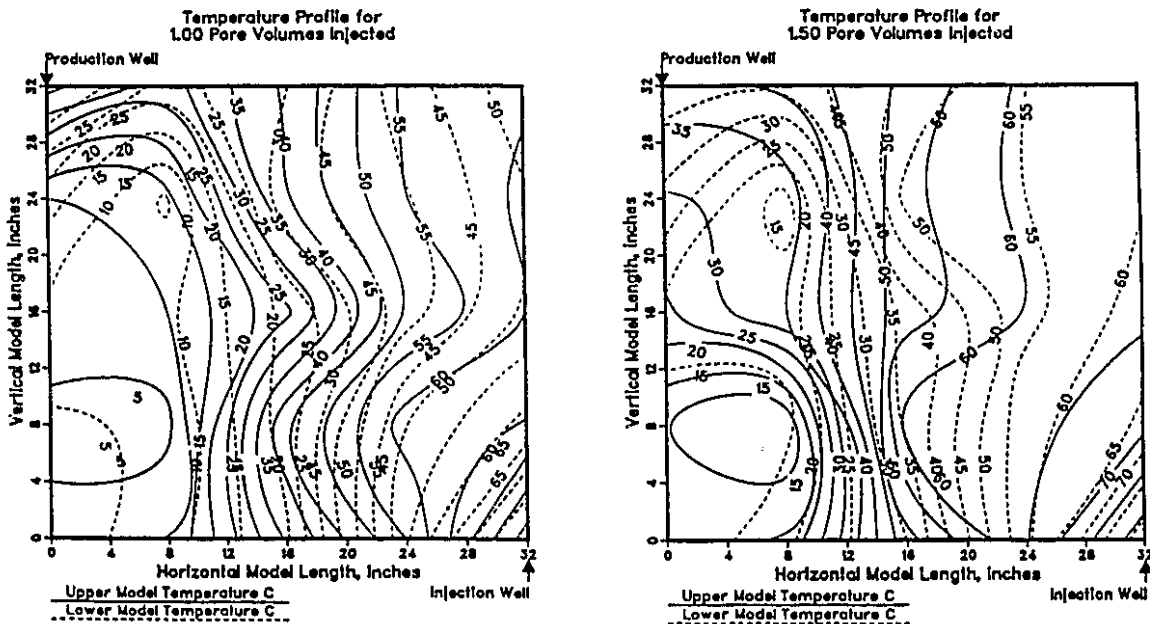
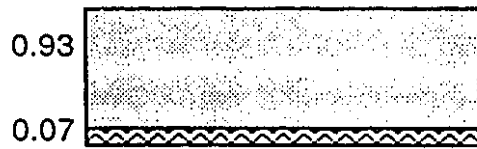
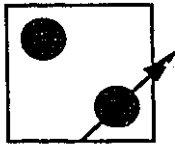
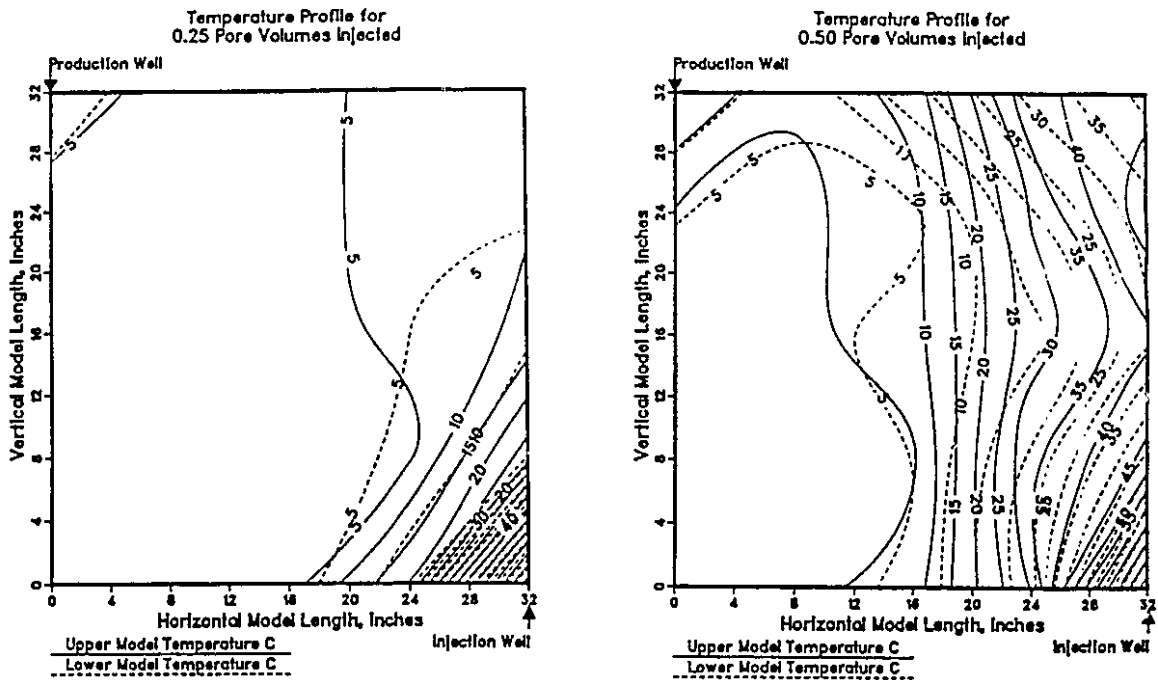


Figure 6.26: Production History for Run 82: Solvent, 30% PV, Injection in a Bottom Water Model, 7% BW, prior to a Continuous Steamflood.

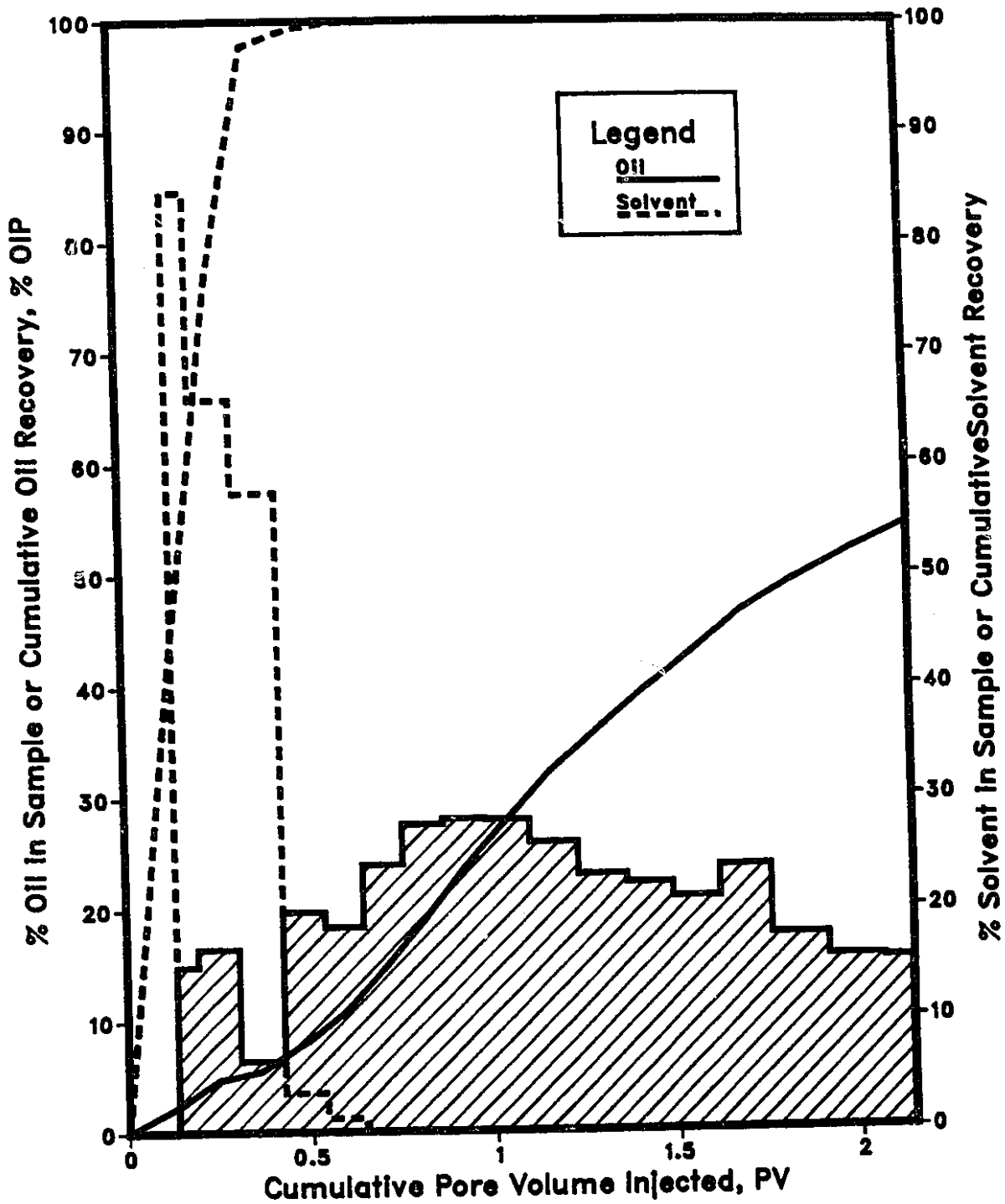
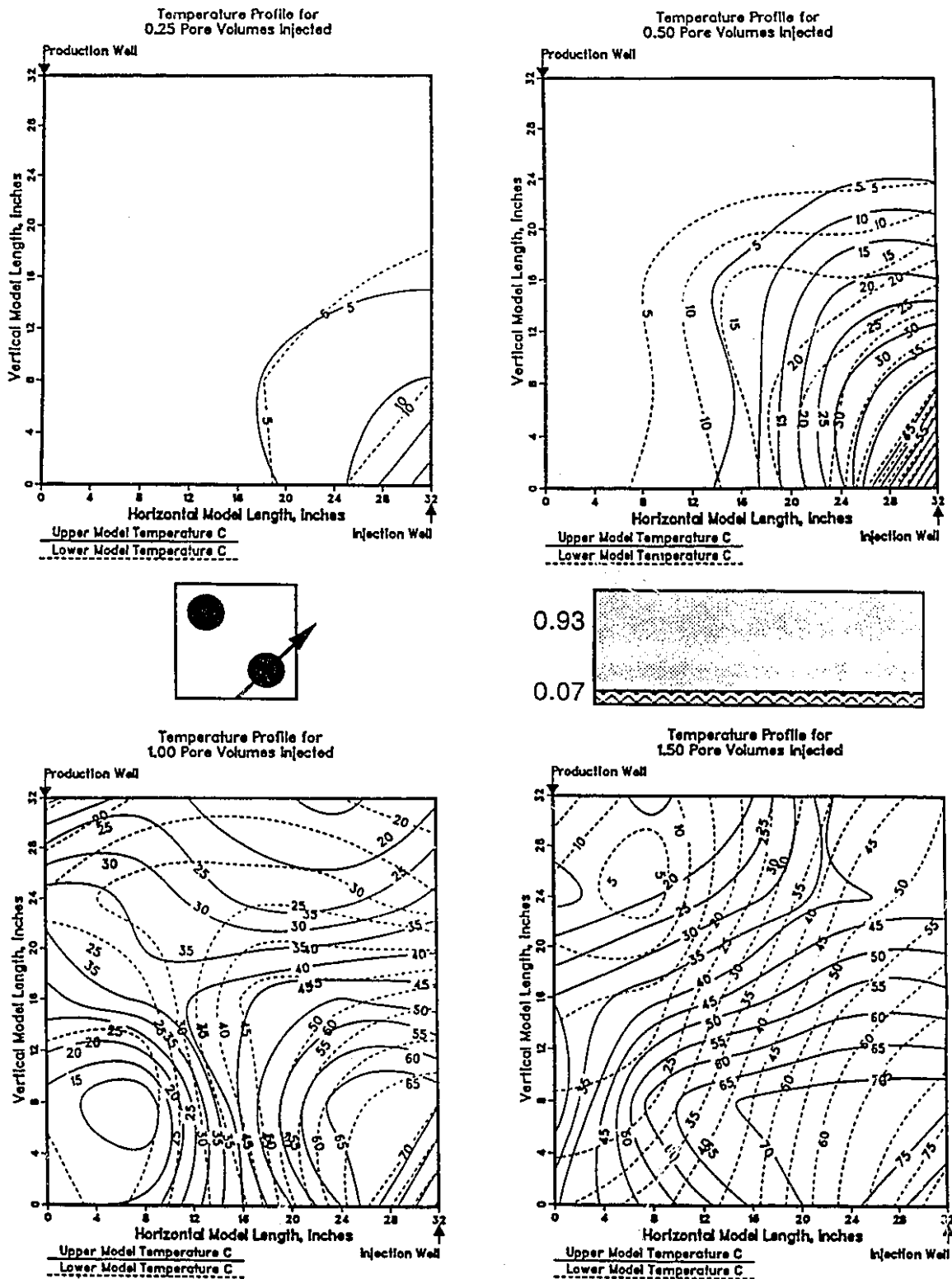


Figure 6.27: Top View Temperature Profiles for Run 82—Solvent (30% PV) Steamflood in a Thin (7%) Bottom Water Model.



Temperature profiles for 0% and 30% solvent, Figures 6.21 and 6.27, respectively, show a radial displacement pattern. In Figure 6.27, the slow development of the initial isotherms was due to the prolonged injection period of the solvent, which was injected at room temperature. However, by 1.5 PV, they were exhibiting the typical radial behaviour. Figures 6.23 and 6.25 (10% and 20% solvent with 52.9% and 52.1% oil recoveries, respectively), on the other hand, show a linear displacement pattern normal to the injection and production sides of the model. Figure 6.28 shows that 0% (56.6%) and 30% (54.3%) solvent slug sizes yielded the greatest recovery. This indicates that a radial displacement may be more favourable than an orthogonal pattern. However, the differences in oil recovery are only slightly above experimental error.

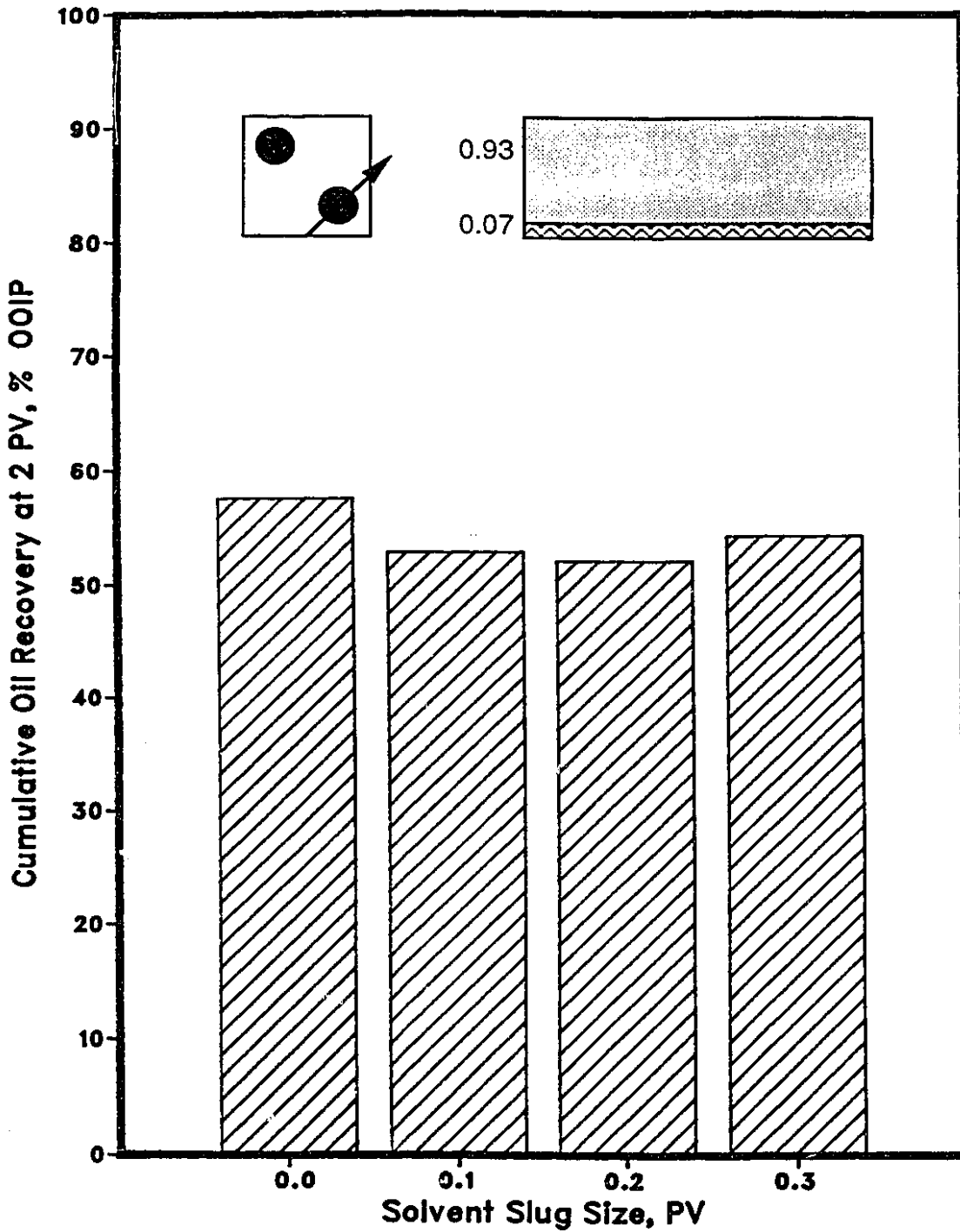
Figure 6.28 reveals that oil recovery was not a strong function of solvent slug size as the runs produced similar results. Although Run 83 (no solvent) had the highest recovery (56.6%), none of the runs was distinctly better than the others. All of the solvent runs had lower recoveries than the continuous (0% solvent) steam case. The results of these experiments suggest that the use of solvent does not improve recovery when the bottom water layer is less than 7%.

By diverting the steam away from the bottom water zone through the use of a solvent slug, the conduction mechanism is forfeited. This is particularly apparent when conduction heating effects through the bottom water zone are dominant. Under these conditions, a continuous steamflood is more beneficial than a solvent-steamflood. The optimum bottom water thickness of 7% also coincides with the results of steam injection in a homogeneous pack for Run 83 as presented in Figure 6.19.

### **Horizontal-Vertical Well Strategies**

Steam injection experiments, employing combinations of horizontal and vertical wells, were performed in the Aberfeldy model. The objective of this study was to develop a viable steamflood process for such thin, heavy oil reservoirs, often with a contiguous

**Figure 6.28: Comparison of Cumulative Oil Recoveries from Continuous Solvent–Steamfloods in Bottom Water Situations, 7% BW, as a function of Solvent Slug Size.**



bottom water zone. Horizontal well runs were carried out for three cases: homogeneous, thin (10%) bottom water and thick (50%) bottom water case: namely, the horizontal producer-vertical injector (HPVI), the horizontal producer-horizontal injector (HPHI) and the vertical producer-horizontal injector (VPHI) combinations. The effect of solvent injection prior to steam injection in a thin (10%) bottom water formation, incorporating horizontal-vertical well strategies, was also investigated. The horizontal wells were placed laterally at the center of the vertical plane (1.25 inches in the scaled model or 5.5 m, prototype length).

#### **Horizontal Producer-Vertical Injector**

Figure 6.29 summarizes the cumulative oil recovery curves for the horizontal producer-vertical injector combination. It is seen from Figure 6.29 that the 50% bottom water cumulative oil recovery (32.4%) was significantly less than that the other two cases. However, the 10% BW curve was not consistently less than the 0% case. Although similar, slightly lower quantities of oil were produced initially than those for the homogeneous case (48.5%). In the latter portion of the run, conduction effects caused the cumulative recovery (53.6%) to exceed that for the homogeneous case.

Temperature profiles for Runs 74 (Figure 6.30, homogeneous model), 87 (Figure 6.31, 10% BW) and 97 (Figure 6.32, 50% BW) show that the steam front was perpendicular to the horizontal producer. It appears, from the contours, that the fluid influx into the producer was relatively uniform. There is no indication that most of the fluid entered only one end of the producer. Gravity override is evident. Notice that at early times (Figure 6.30, 0.25 and 0.50 PV), the steam front in the upper part of the model was approximately radial, although the condensate entering the horizontal well followed a more linear pattern. Possibly the gravity override effect is accentuated by well placement.

Figure 6.29: Cumulative Oil Recoveries for Steamfloods using a Horizontal Producer and a Vertical Injector as a function of Bottom Water Thickness.

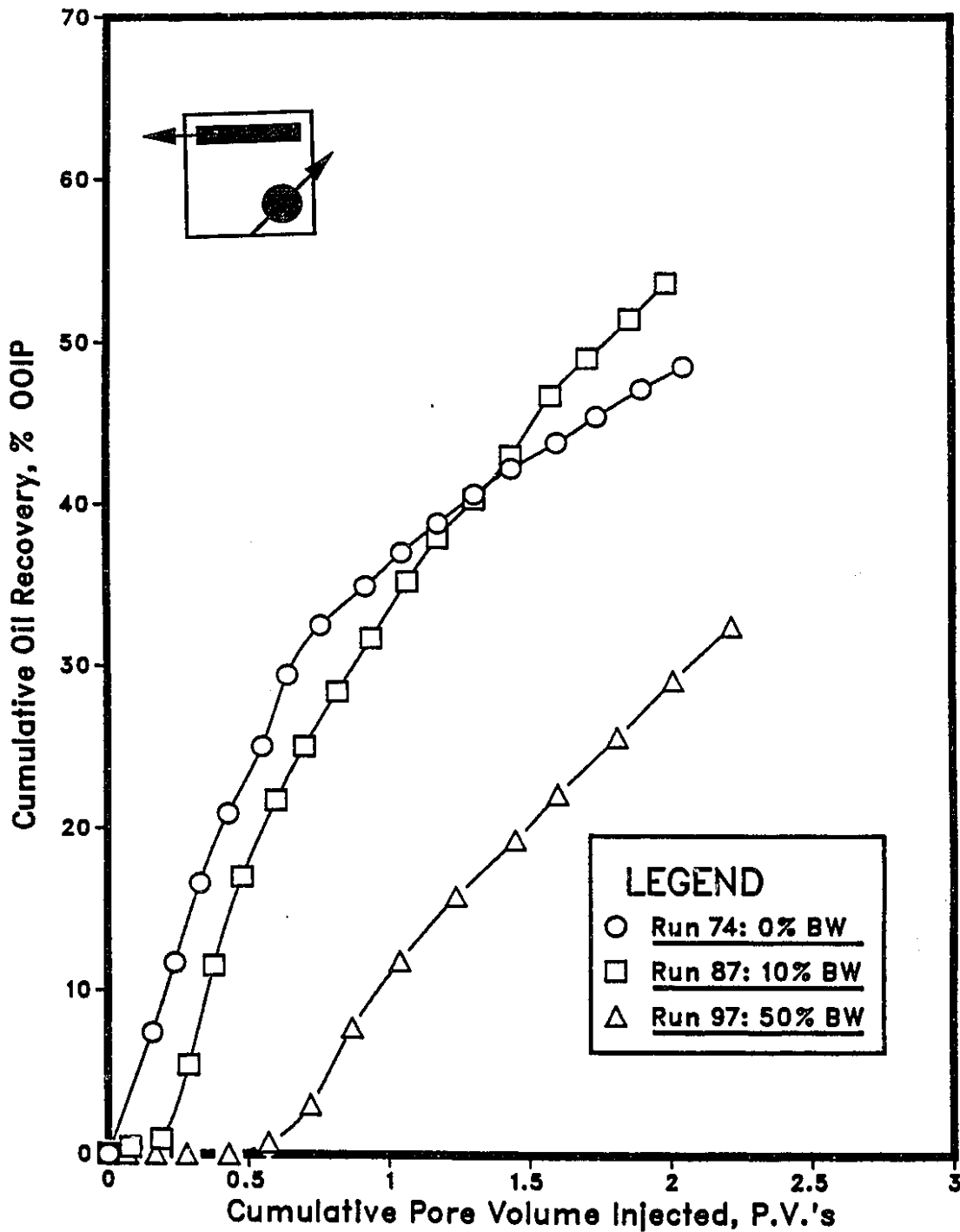


Figure 6.30: Top View Temperature Profiles for Run 74—Steamflood using a Horizontal-Vertical Well Combination in a Homogeneous Model.

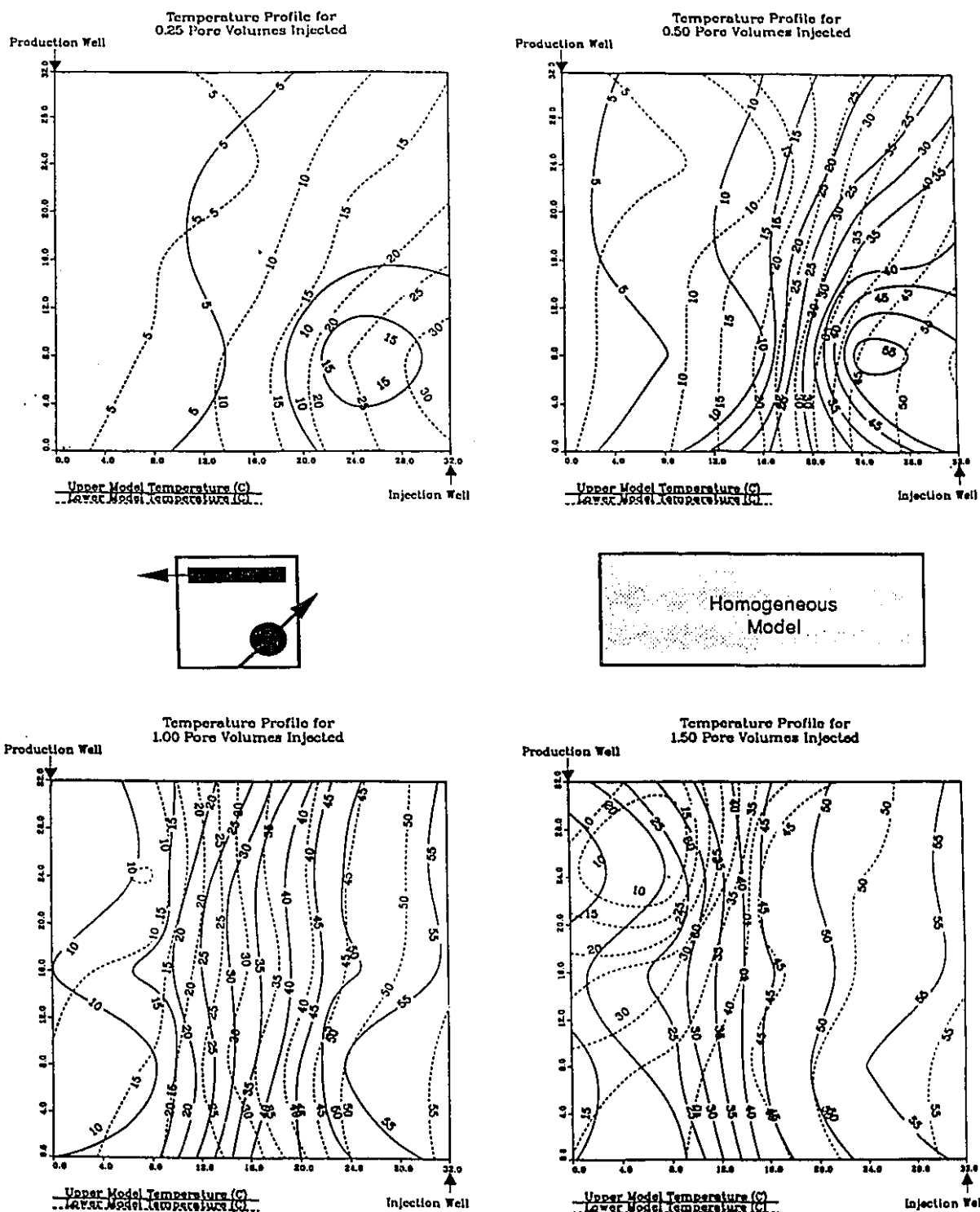




Figure 6.31: Top View Temperature Profiles for Run 87—Steamflood using a Horizontal-Vertical Well Combination in a Thin (10%) Bottom Water Model.

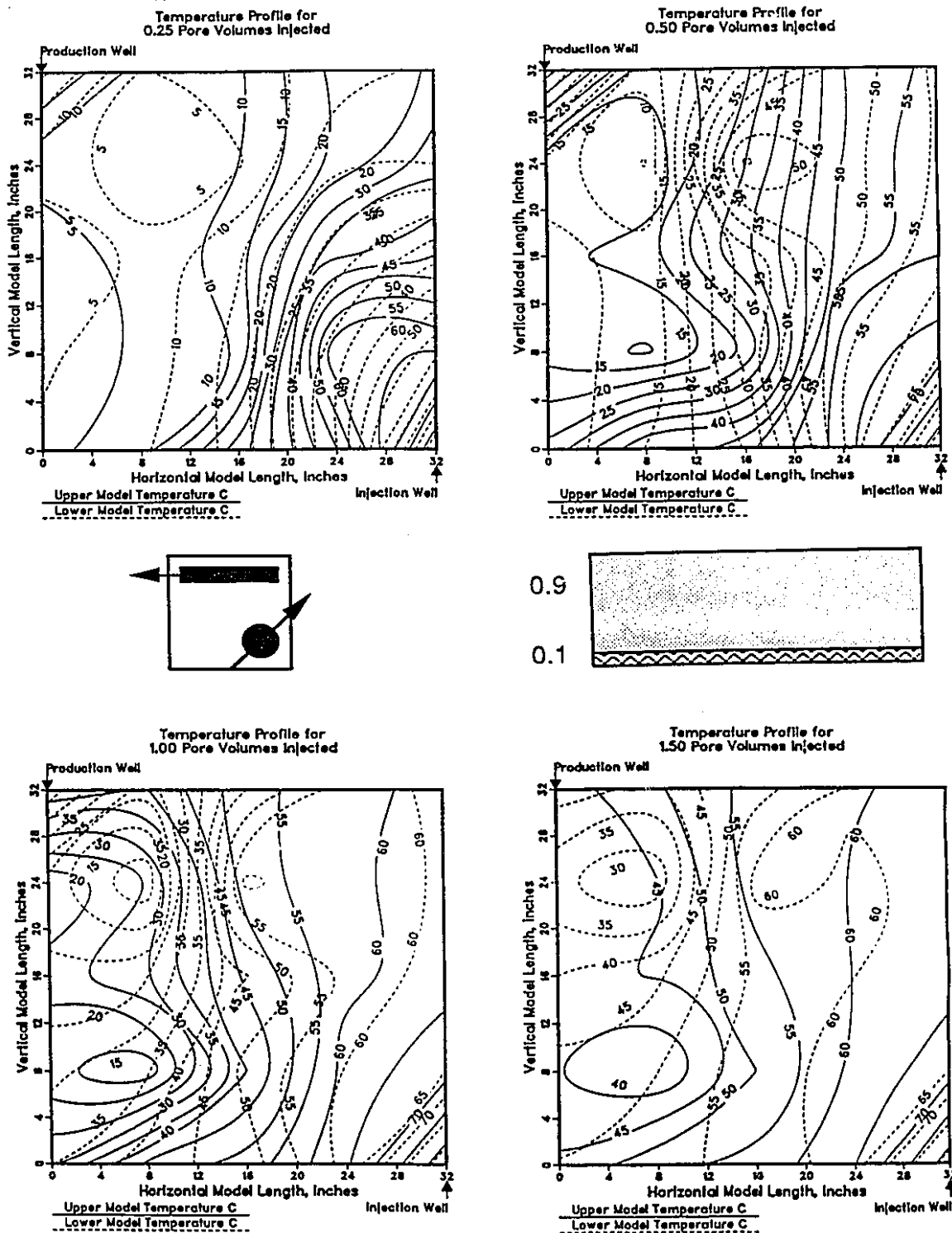
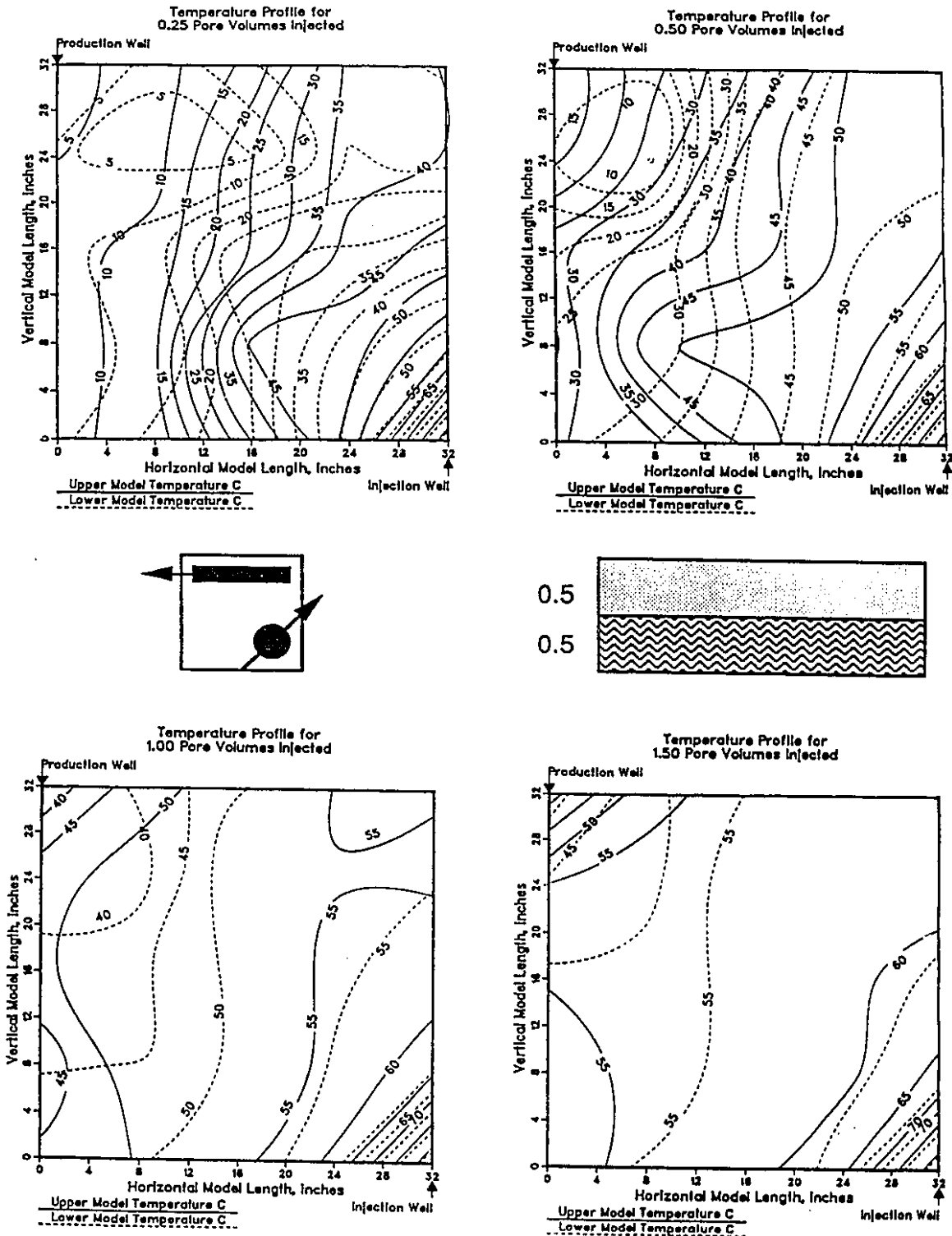


Figure 6.32: Top View Temperature Profiles for Run 97—Steamflood using a Horizontal-Vertical Well Combination in a Thick Bottom (50%) Water Model.



### **Horizontal Producer-Horizontal Injector**

The curves in Figure 6.33 follow a pattern similar to the ones presented in Figure 6.29. Again, high ultimate oil recovery was attributed to conduction effects from the thin bottom water zone. However, the cumulative recoveries are significantly higher for the HPHI than the HPVI combination. Figures 6.34 through 6.36 show that the steam advanced parallel to the horizontal injector and producer. This suggests a linear advance of the steam front because of the horizontal injector. It should be noted that steam was introduced at the midpoint of the horizontal injector. The temperature contours shown in the figures are slightly distorted at the corners, because a thermocouple was installed at one corner and not the other.

### **Vertical Producer-Horizontal Injector**

Figure 6.37 shows that bottom water has an adverse effect on recovery when a vertical producer-horizontal injector combination is used. This is most likely because steam has a strong tendency to be diverted to the bottom water zone when injected vertically in view of the large pressure gradients. When horizontal injectors are used, steam will be injected above the basal zone. This is more effective since heat transport into the mobile water zone will be minimized and hence, process efficiency will increase. It was necessary to establish a line for the position of the horizontal well to consider thick and thin bottom water situations in the same model.

The steam front advanced uniformly in a linear fashion for the three reservoir situations, as shown in Figures 6.38 through 6.40. In the last case, there was some tendency for steam to advance in a radial fashion at the right extremity of the horizontal well, possibly because this was the steam inflow end from the steam generator. In this case, there was no evidence of recovery improvement due to the conduction effects observed previously. Preferential heating of the basal zone, which occurred when steam was injected vertically, did not occur in this instance. The most probable reason is that the

Figure 6.33: Cumulative Oil Recoveries for Steamfloods using a Horizontal Producer and a Horizontal Injector as a function of Bottom Water Thickness.

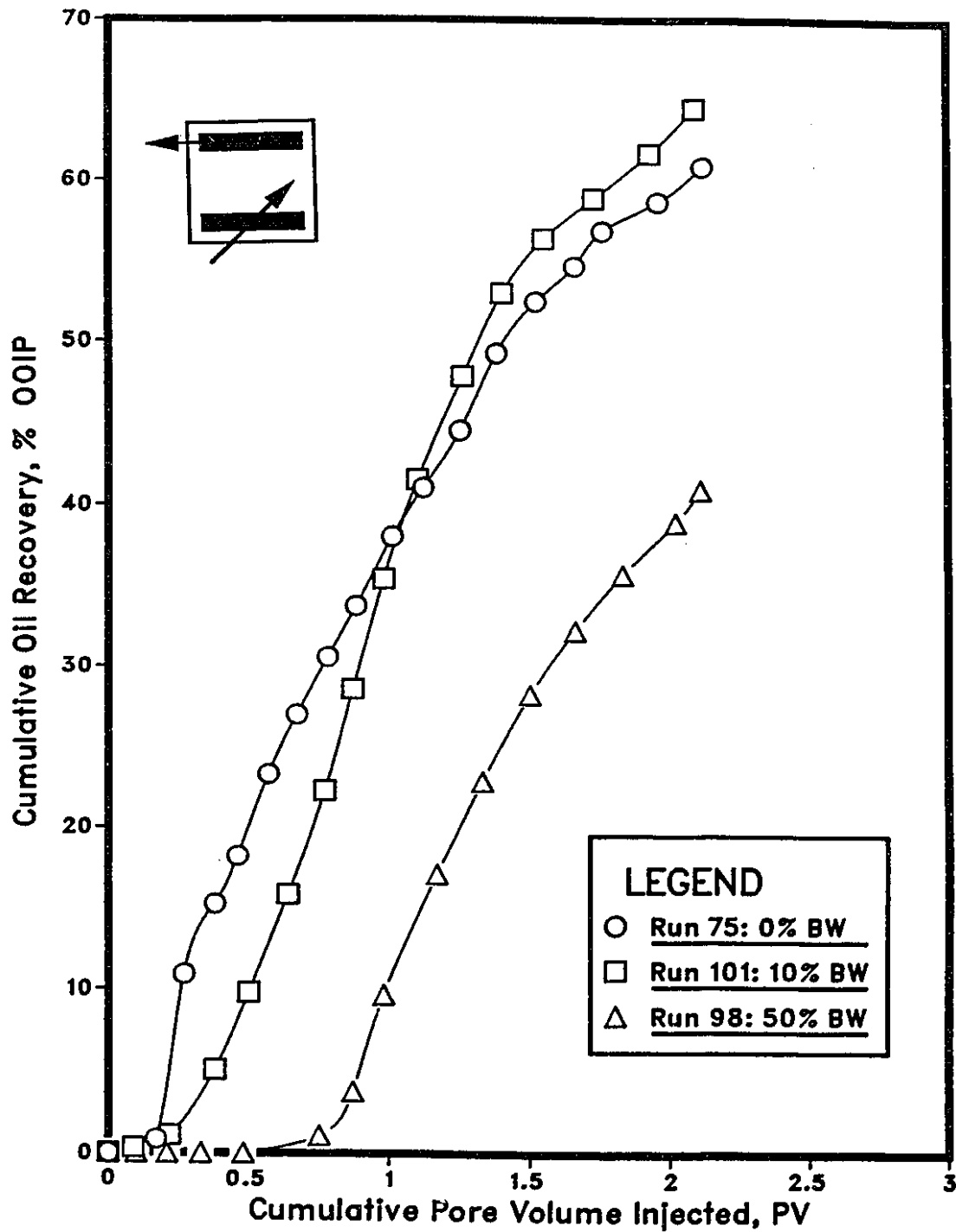


Figure 6.34: Top View Temperature Profiles for Run 75---Steamflood using a Horizontal-Vertical Well Combination in a Homogeneous Model.

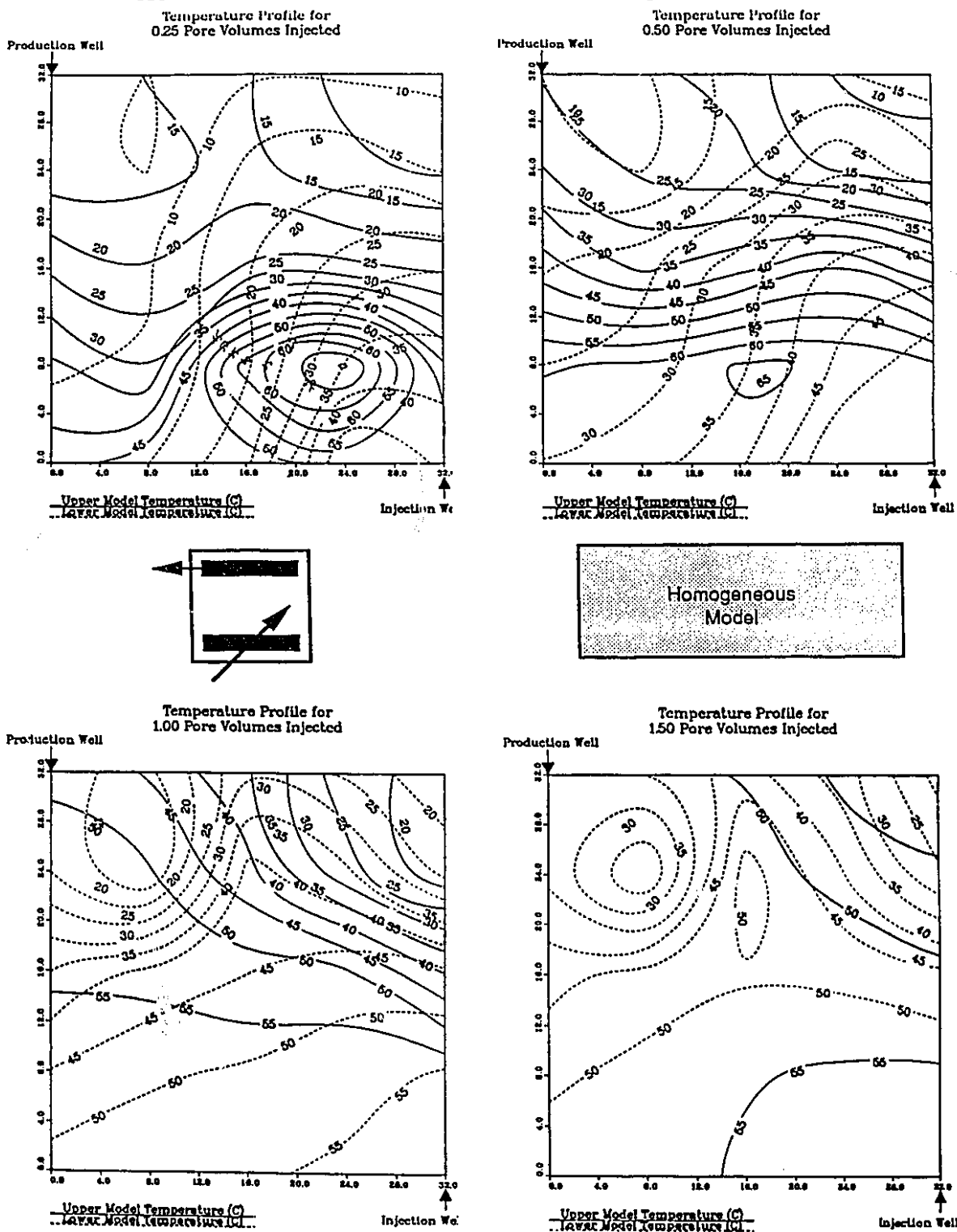


Figure 6.35: Top View Temperature Profiles for Run 101—Steamflood using a Horizontal-Vertical Well Combination in a Thin (10%) Bottom Water Model.

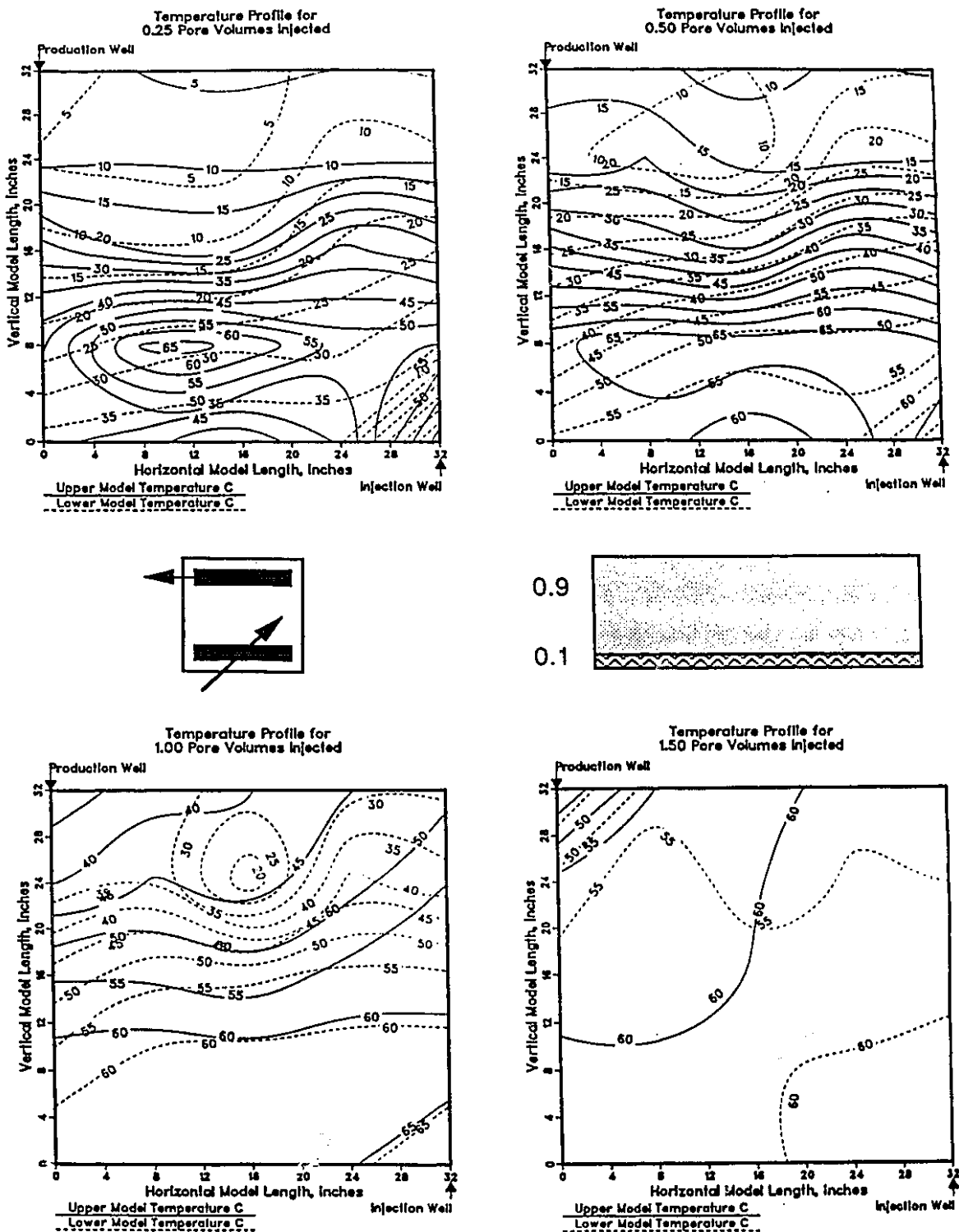


Figure 6.36: Top View Temperature Profiles for Run 98—Steamflood using a Horizontal-Vertical Well Combination in a Thick Bottom (50%) Water Model.

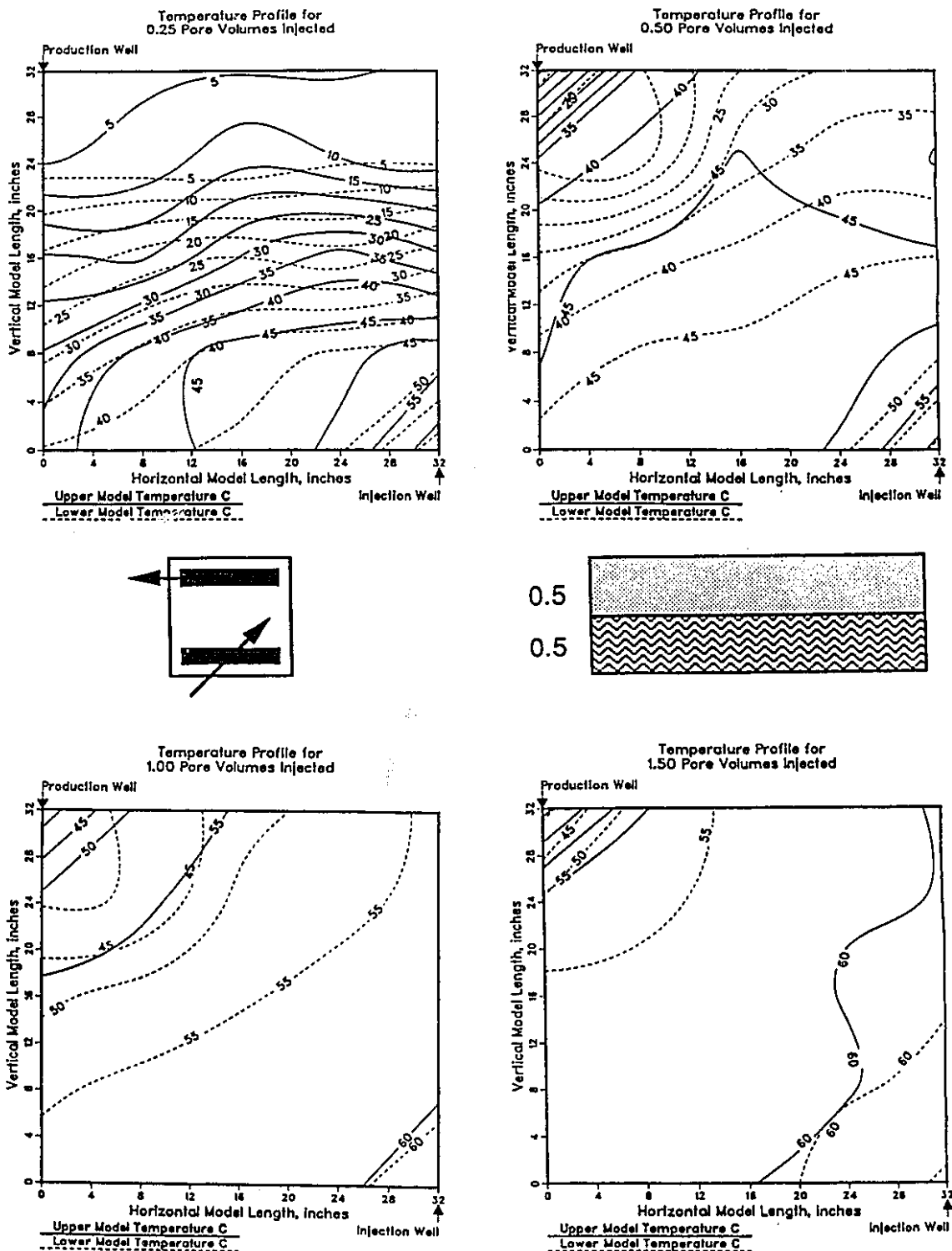


Figure 6.37: Cumulative Oil Recoveries for Steamfloods using a Vertical Producer and a Horizontal Injector as a function of Bottom Water Thickness.

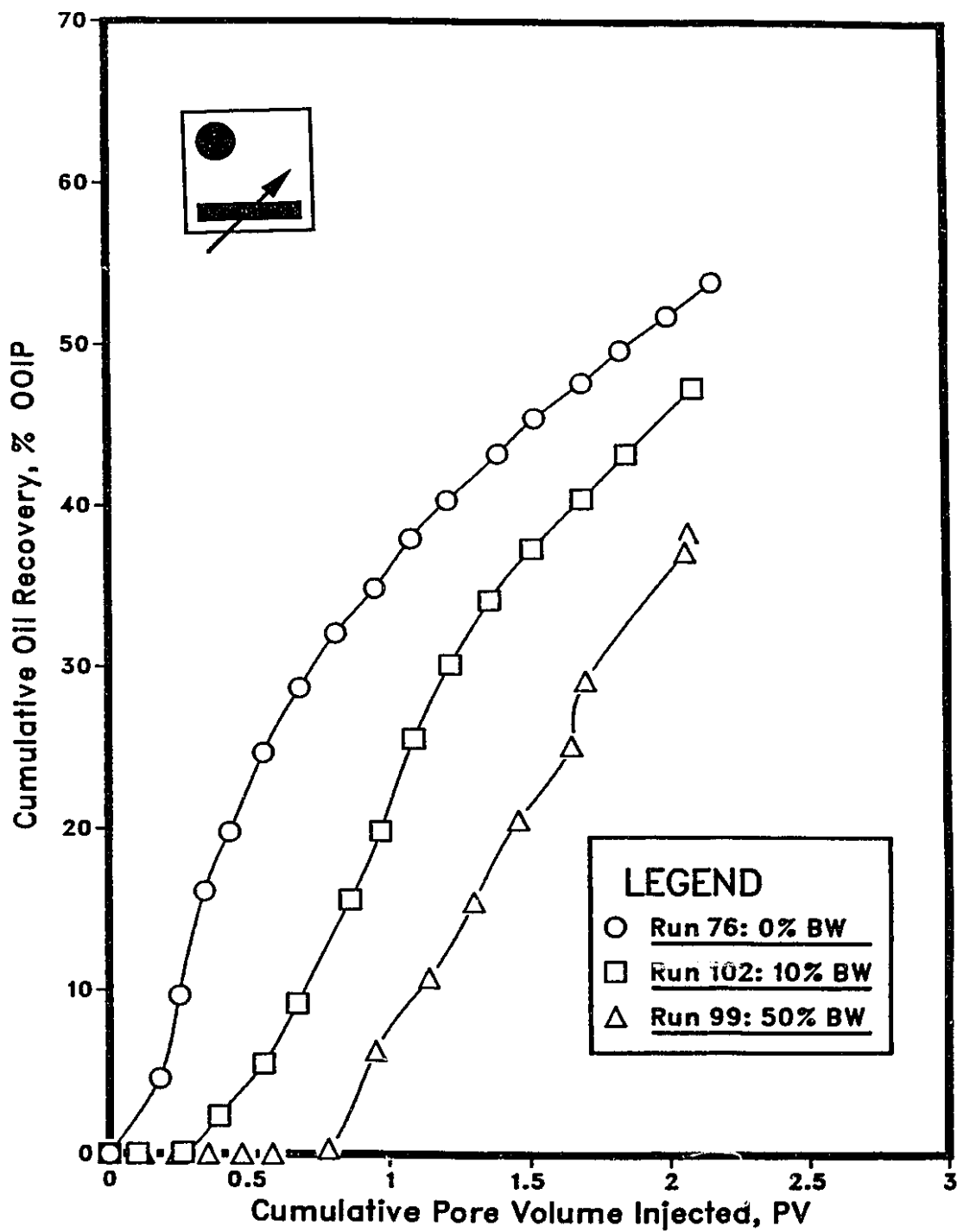




Figure 6.38: Top View Temperature Profiles for Run 76—Steamflood using a Horizontal-Vertical Well Combination in a Homogeneous Model.

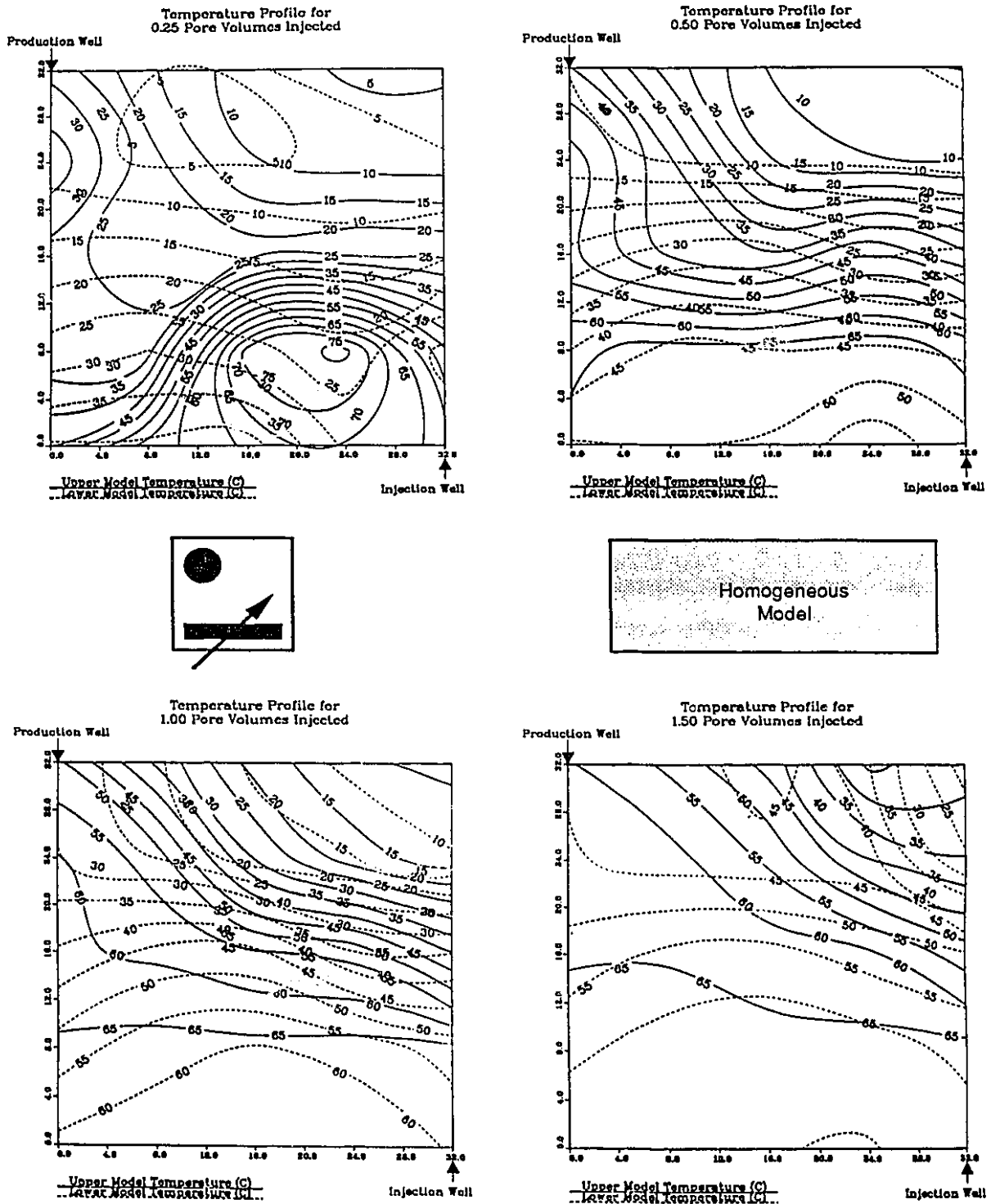


Figure 6.39: Top View Temperature Profiles for Run 102—Steamflood using a Horizontal-Vertical Well Combination in a Thin (10%) Bottom Water Model.

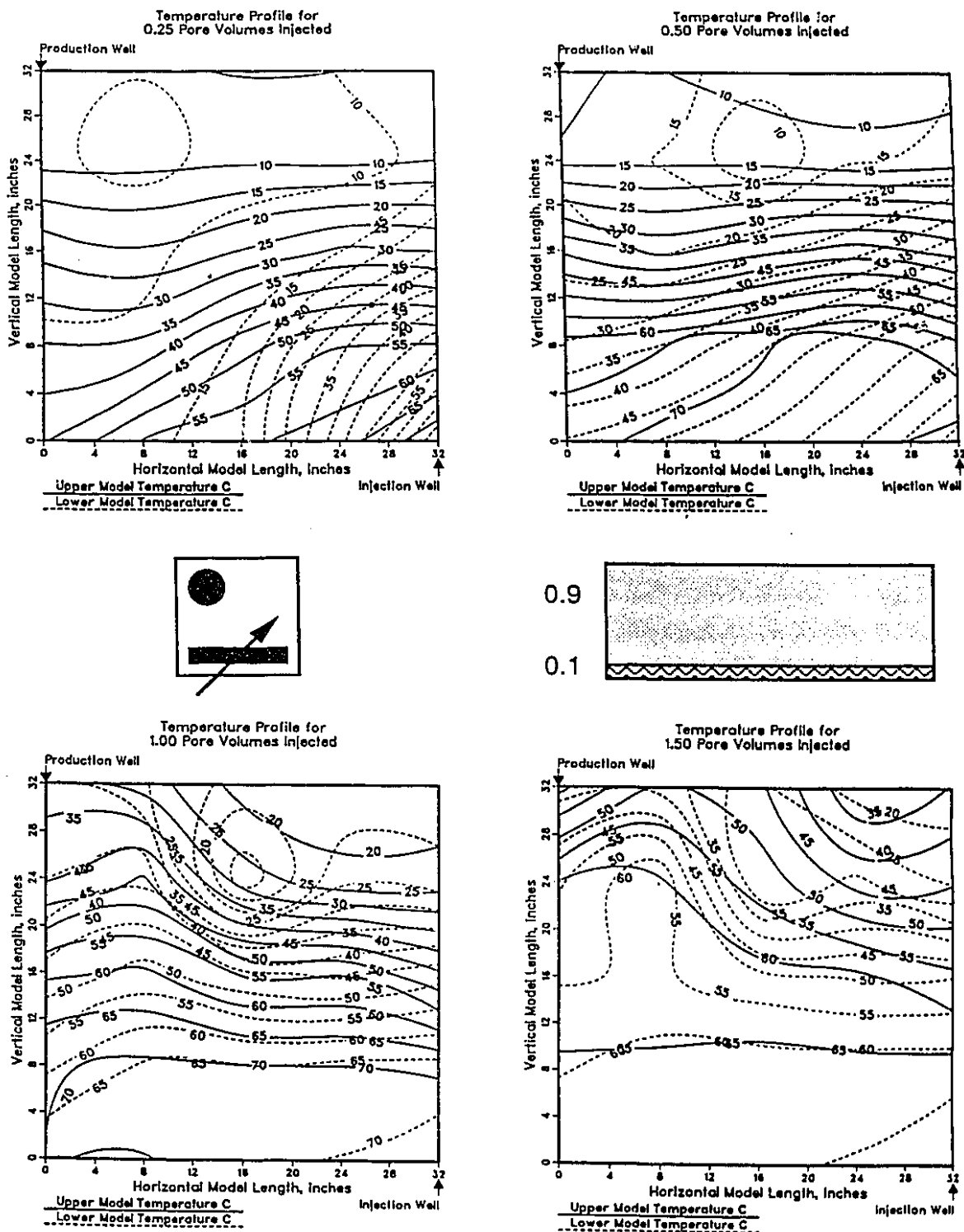
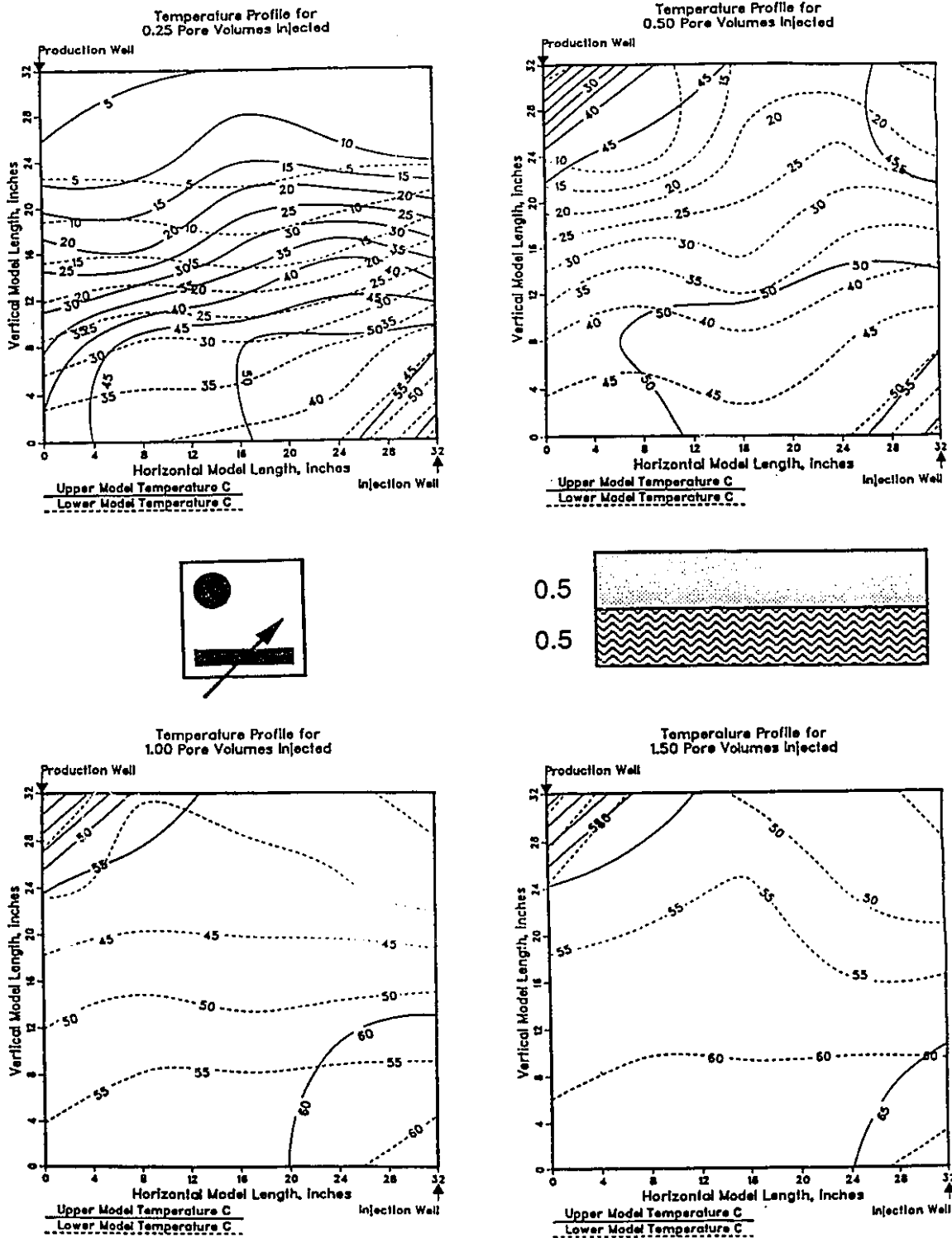


Figure 6.40: Top View Temperature Profiles for Run 99—Steamflood using a Horizontal-Vertical Well Combination in a Thick Bottom (50%) Water Model.



placement of the horizontal injector did not enable the steam to contact the basal zone. However, in Run 101 (Figure 6.33), conduction heating from a horizontal injector seemed to develop because the well was located closer to the basal zone, leading to favourable conditions. Bottom water thawing during saturation generated inaccurate basal zone thicknesses and hence, affected the vertical distance to the well. Thus, based on the results of the experiments, the horizontal injector and the perforations for vertical wells should be placed as close as possible to the basal zones to maximize production from thin bottom water reservoirs.

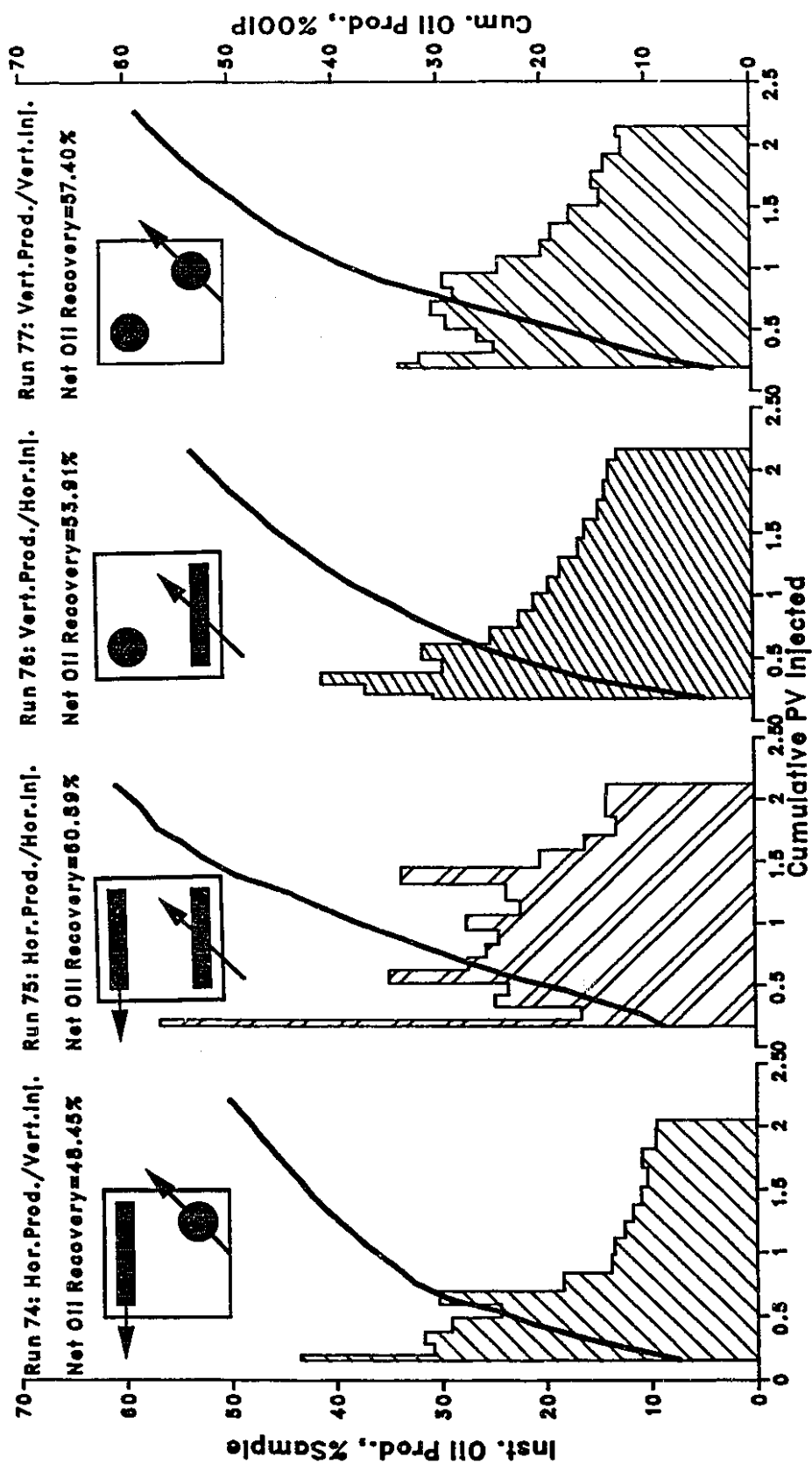
### **Comparison of the Reservoir Situations**

The following sections compare the results of the various vertical-horizontal well situations. An optimal production strategy can be developed for different reservoirs, with and without bottom water.

#### **Homogeneous Case**

As can be seen from Figure 6.41, the horizontal producer-vertical injector combination in Run 74 yielded the lowest ultimate recovery (2.5 PV) of 48.5% while horizontal producer-horizontal injector produced the highest values of 60.9% in Run 75. However, quantitatively speaking, in view of ultimate recovery, the vertical producer-vertical injector combination in Run 77 yielded approximately the same results (57.4%) as Run 75 (HPHI). The primary difference is in instantaneous oil recovery which is shown in Figure 6.41. In all horizontal well combinations (VPVI case is included in all figures for comparison only), initial oil production is high and falls off rapidly after 0.75 to 1.5 PV of steam injection. While initial oil production in the VPVI case was not as high as in the situations incorporating horizontal wells, uniform production is observed to 1.0 PV before oil production rate begins to decline. The cumulative oil recovery plots in Figure 6.41 show the rate of recovery as evidenced by the slope of the curve. This is seen to be the highest in the case of the HPHI arrangement.

**Figure 6.41: Instantaneous and Cumulative Oil Production as a function of Cumulative PV Injected for Steamfloods in Homogeneous Models.**



Temperature distributions tend to show the usual early breakthrough of steam. However, in the case of the HPHI combination, the flow pattern, as shown by temperature profiles resemble a line drive, resulting in a sustained oil cut of about 25% over 1.5 PVs.

#### Thin Bottom Water

Horizontal-vertical well combinations performed better in thin bottom water situations than in the homogeneous case. It can be seen from Figure 6.42 that the HPHI combination again yielded the highest recovery (64.5%), which is about 5% greater than the homogeneous case in Run 75. A horizontal producer-vertical injector combination (Run 87) produced the second highest recovery (53.6%). Again, Run 87 (HPVI) produced approximately 7 percentiles higher than its homogeneous counterpart. However, both vertical production well combinations, VPHI and VPVI, yielded similar results, where ultimate oil production decreased compared to the homogeneous steamfloods in the presence of thin bottom water.

The oil production rate curves shown in Figure 6.42 are somewhat different from those shown in Figure 6.41. The oil production rate builds up from zero to the maximum value over 0.5 to 1 PV of steam injected. This is because the steam initially penetrates the bottom water layer. Subsequently, heat conduction mobilizes the oil above, leading to an increase in the oil cut. At the same time, steam advances into the mobilized oil zone. In the case of the vertical injectors, the wells were completed in the oil zone. Oil recovery was low in the cases involving vertical injectors.

#### Thick Bottom Water

Thick bottom (50% of gross thickness) water adversely affected recoveries in all well combinations by decreasing oil production by about 20 percentiles. In all the instances in Figure 6.43, bottom water production was observed for about 3 to 4 project years (0.75 PV). The most promising results were obtained from the HPHI combination followed closely by a vertical producer-horizontal injector well pair. A VFHI combination works

**Figure 6.42: Instantaneous and Cumulative Oil Production as a function of Cumulative PV Injected for Steamfloods in Thin (10%) Bottom Water Formations.**

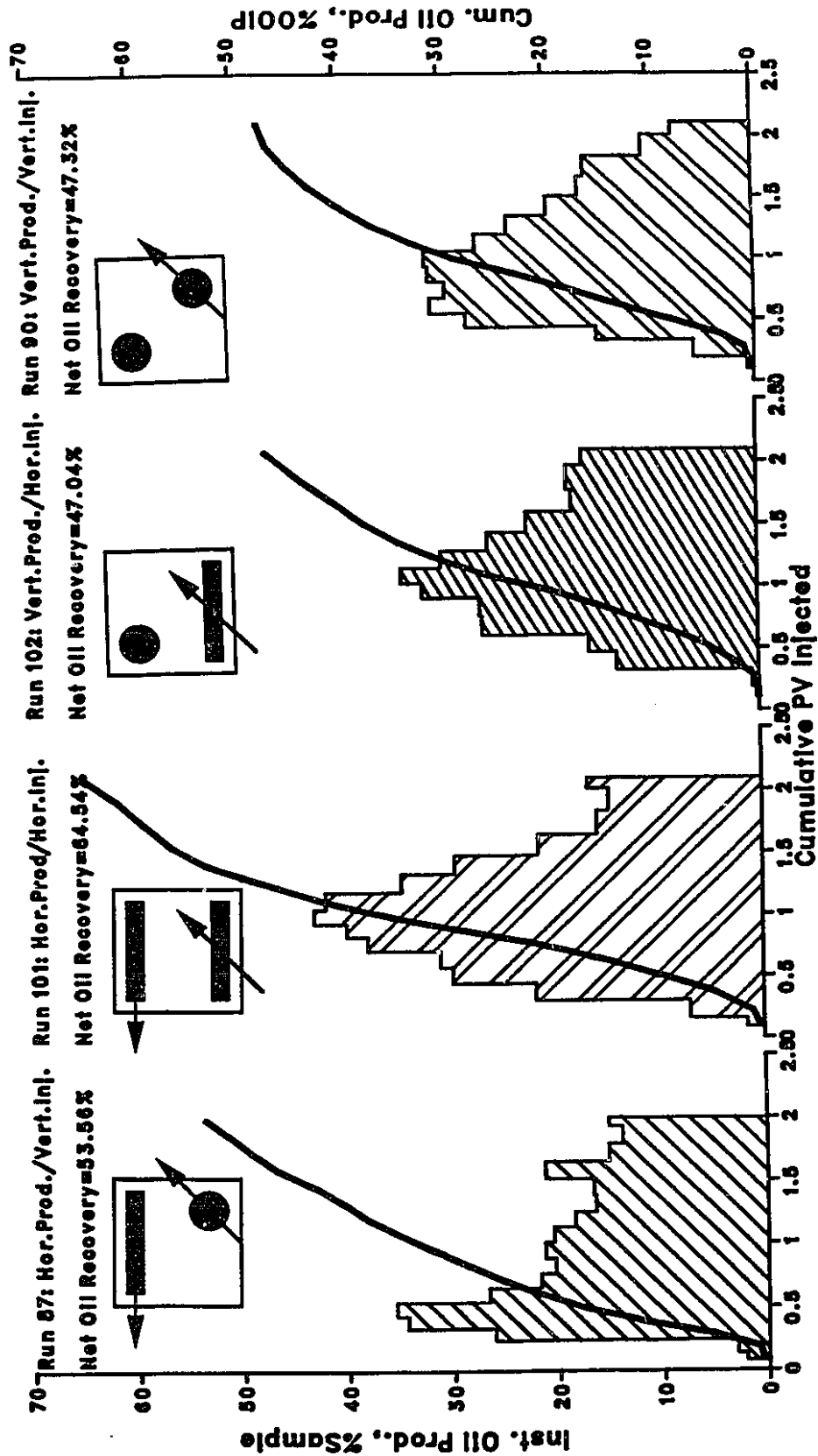
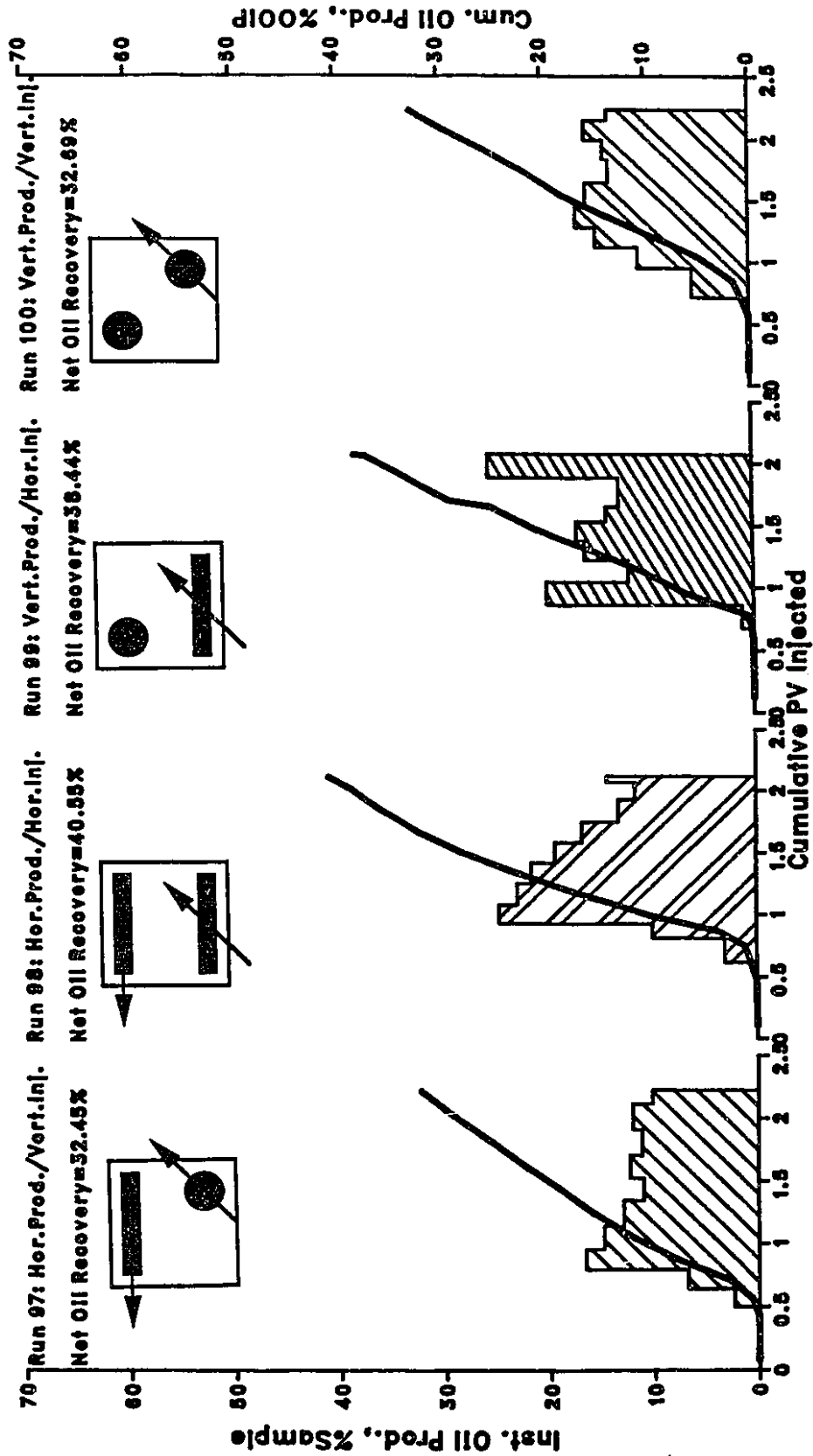


**Figure 6.43: Instantaneous and Cumulative Oil Production as a function of Cumulative PV Injected for Steamfloods In Thick (50%) Bottom Water Formations.**





better in thick bottom water, while a HPHI combination is essential to steamfloods in thin bottom water formations. The experiments that a horizontal injector performs better than a vertical one in a thick bottom water formation. The oil bank breakthrough occurred much later in all cases at 0.5-0.75 PV injected. The temperature profiles tend to show that the injected steam condensed and advanced in the bottom water zone for a considerable time. When the overlying oil was mobilized sufficiently, oil production started while the condensate continued to flow in the bottom water zone.

#### **Application of Horizontal-Vertical Well Strategies in Solvent-Steamfloods**

In a series of runs (Runs 91, 92, 93 and 94), a small slug of solvent (10% PV Heavy Virgin Naphtha, see Table 6.2) was injected in the presence of a thin bottom water (10%) layer through a vertical wellbore ahead of steam. Oracheski et al.<sup>41</sup> suggested that an optimum solvent slug size of 10% seemed to maximize the amount of oil recovered in a solvent-steamflood process when the bottom water thickness is less than 25% of the model thickness. However, the results, as summarized in Figure 6.44, show only a 5% improvement in recovery as a result of preinjection of solvent. No asphaltene flocculation occurred primarily because a small volume of naphtha was used<sup>43</sup>. Approximately 80% of the solvent was recovered in the early stages of the steamflood.

The effect of solvent injection (10% PV) through a horizontal rather than a vertical well was also examined for a 10% bottom water in Run 106. The horizontal producer and horizontal injector combination was selected for this run since it had consistently produced the highest recovery in all other runs. Run 92 (HPHI) yielded the greatest overall recovery of 67.5% in the presence of thin bottom water when the solvent was injected vertically. Temperature contours for HPVI, HPHI, VPHI and VPVI combinations are presented in Figures 6.45 through 6.48, respectively.

Figure 6.49 shows that the type of well through which the solvent is injected affects the cumulative oil recovery. Incremental recovery as a result of solvent injection through a

**Figure 6.44: Instantaneous and Cumulative Hydrocarbon Production as a function of Cumulative PV Injected for Solvent-Steamfloods In Thin (10%) Bottom Water Formations.**

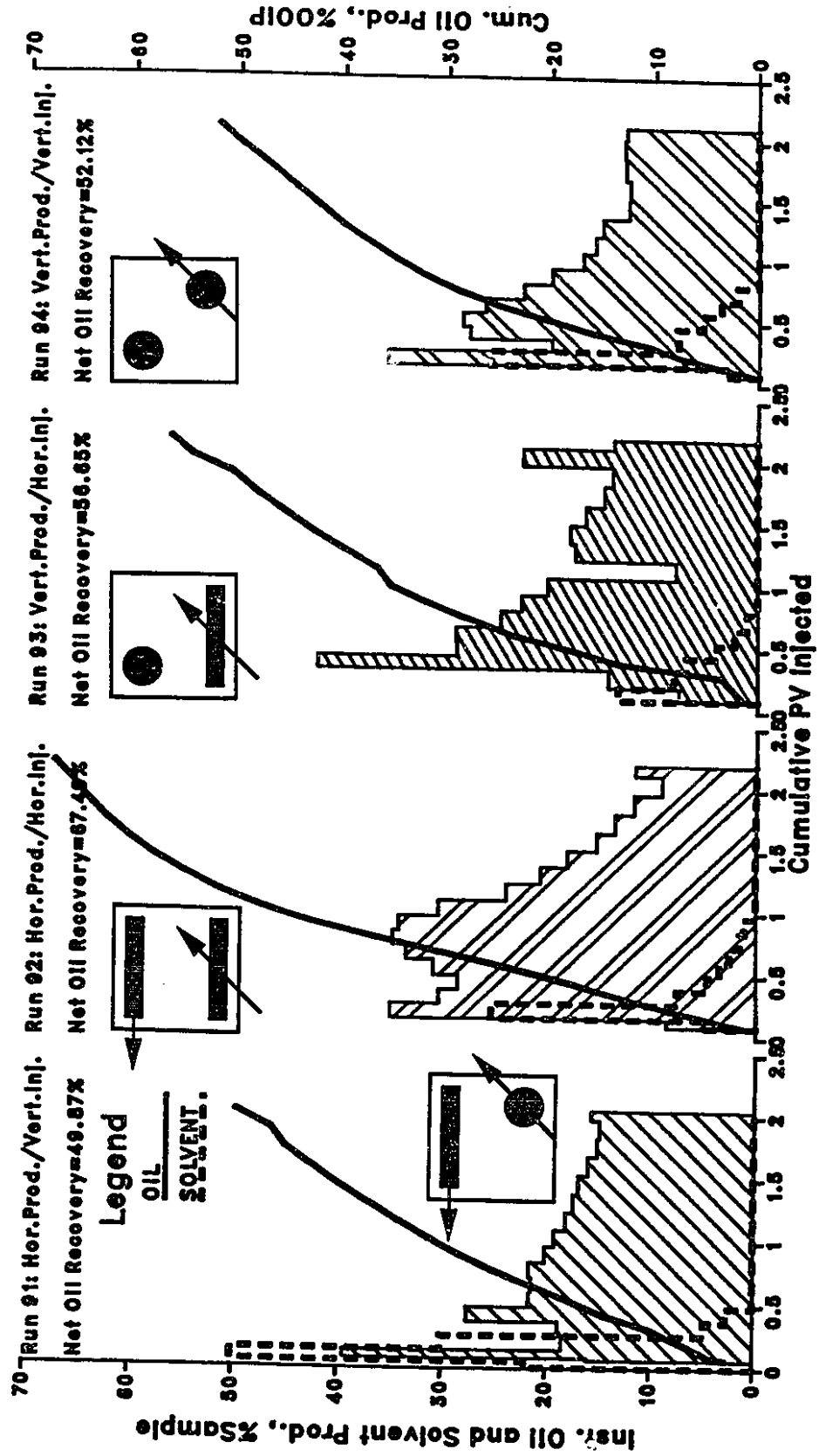


Figure 6.45: Top View Temperature Profiles for Run 91—Solvent (10% PV)-Steamflood using a Horizontal-Vertical Well Combination in a Thin (10%) Bottom Water Model.

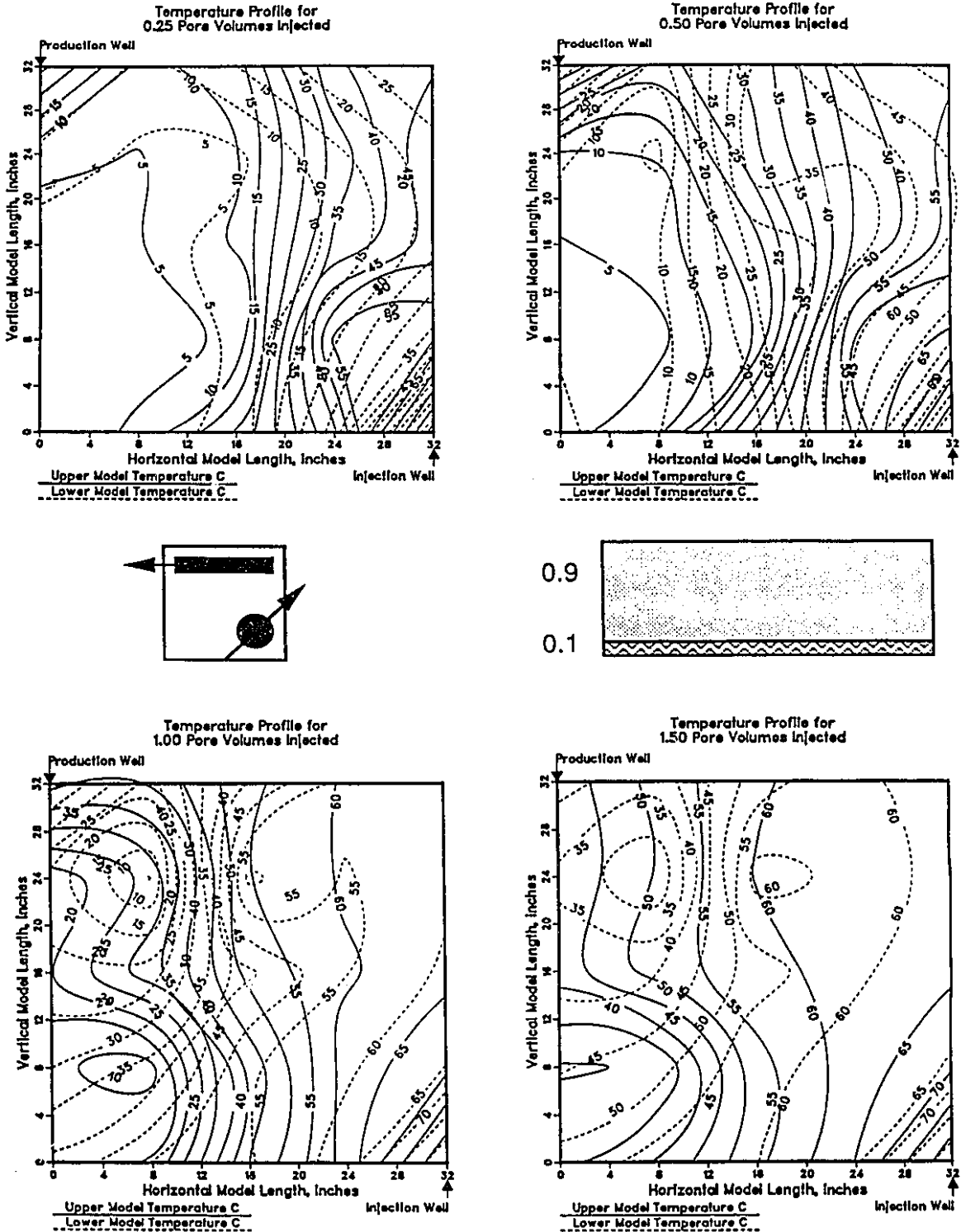


Figure 6.46: Top View Temperature Profiles for Run 92—Solvent (10% PV)-Steamflood using a Horizontal-Vertical Well Combination in a Thin (10%) Bottom Water Model.

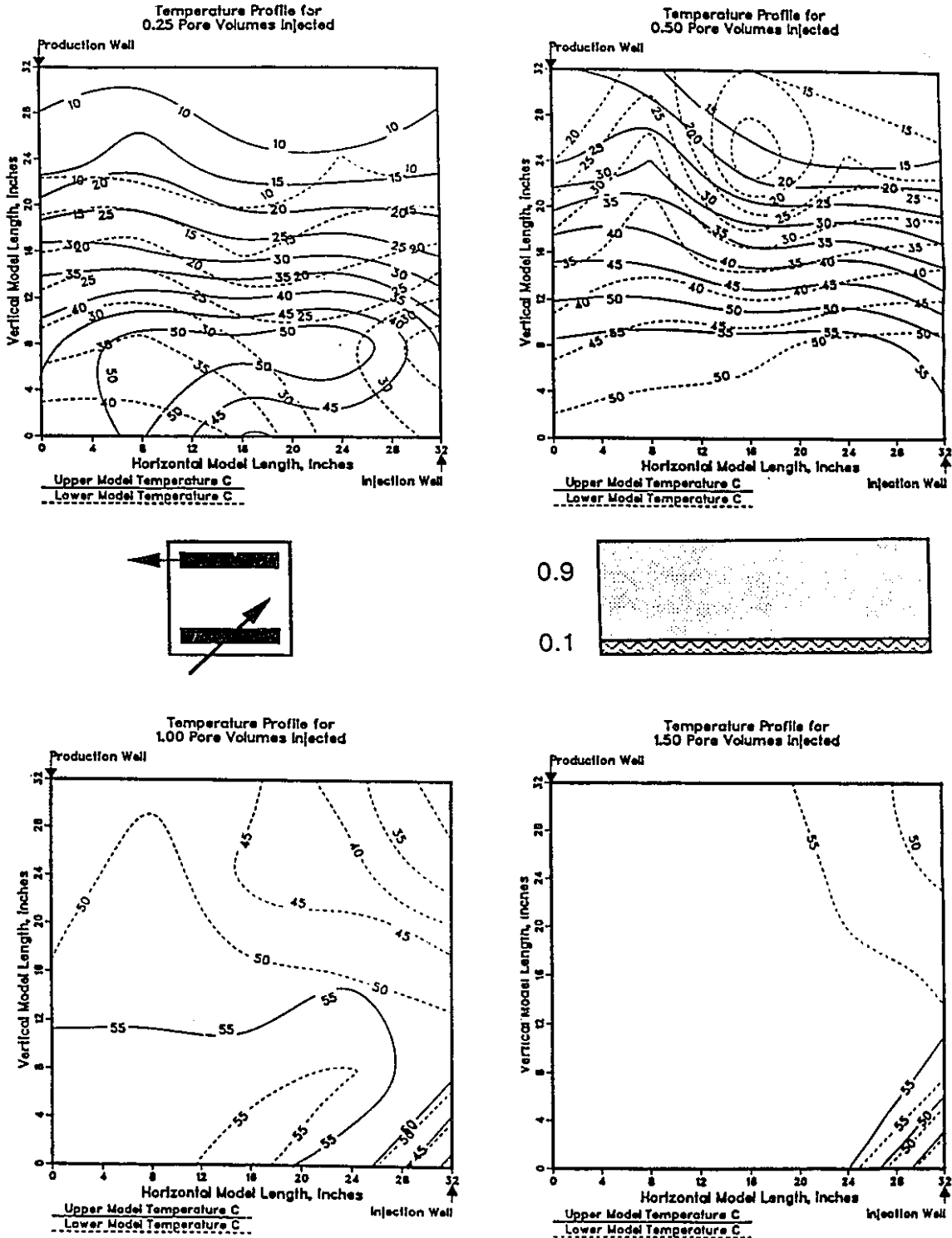


Figure 6.47: Top View Temperature Profiles for Run 93—Solvent (10% PV)-Steamflood using a Horizontal-Vertical Well Combination in a Thin (10%) Bottom Water Model.

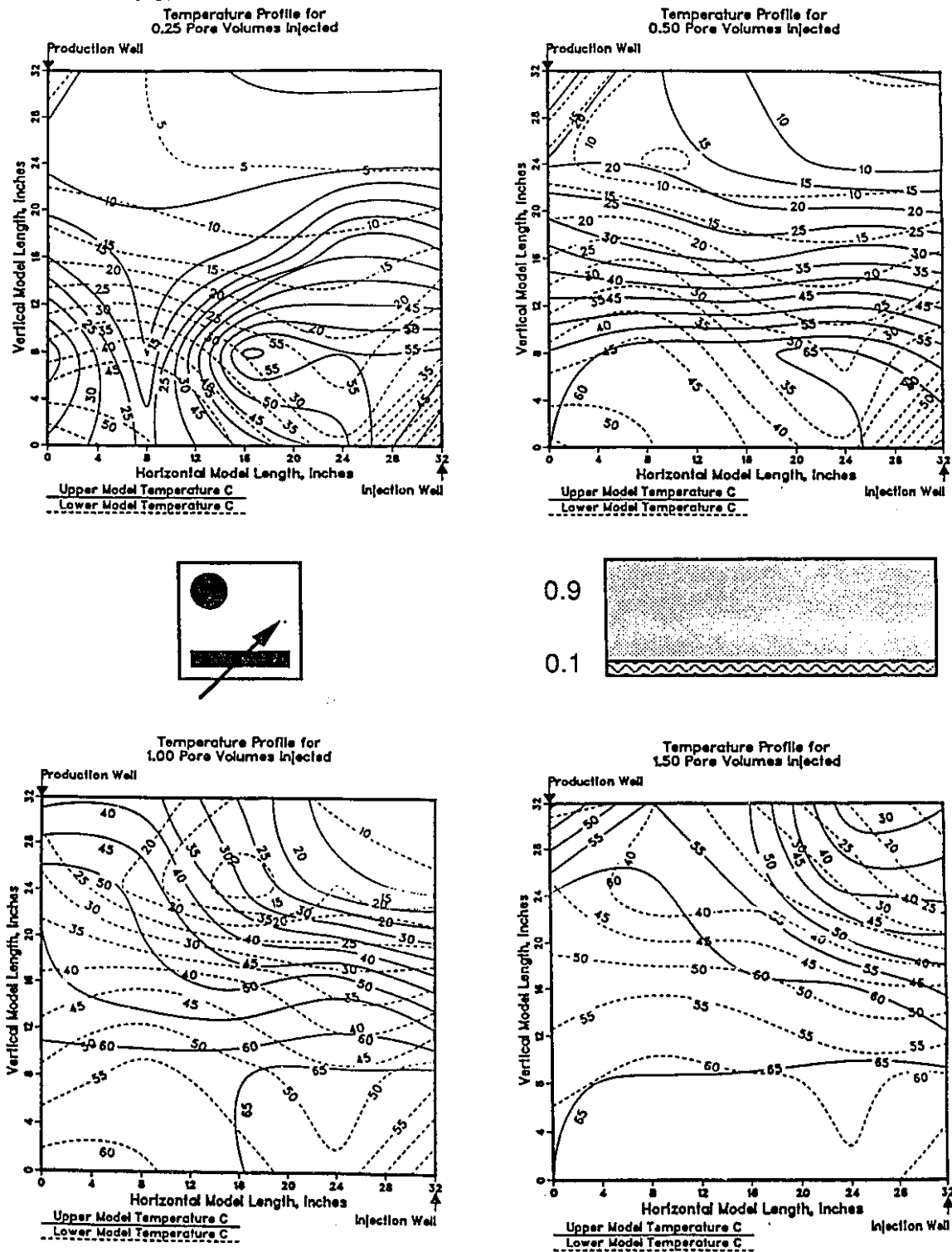
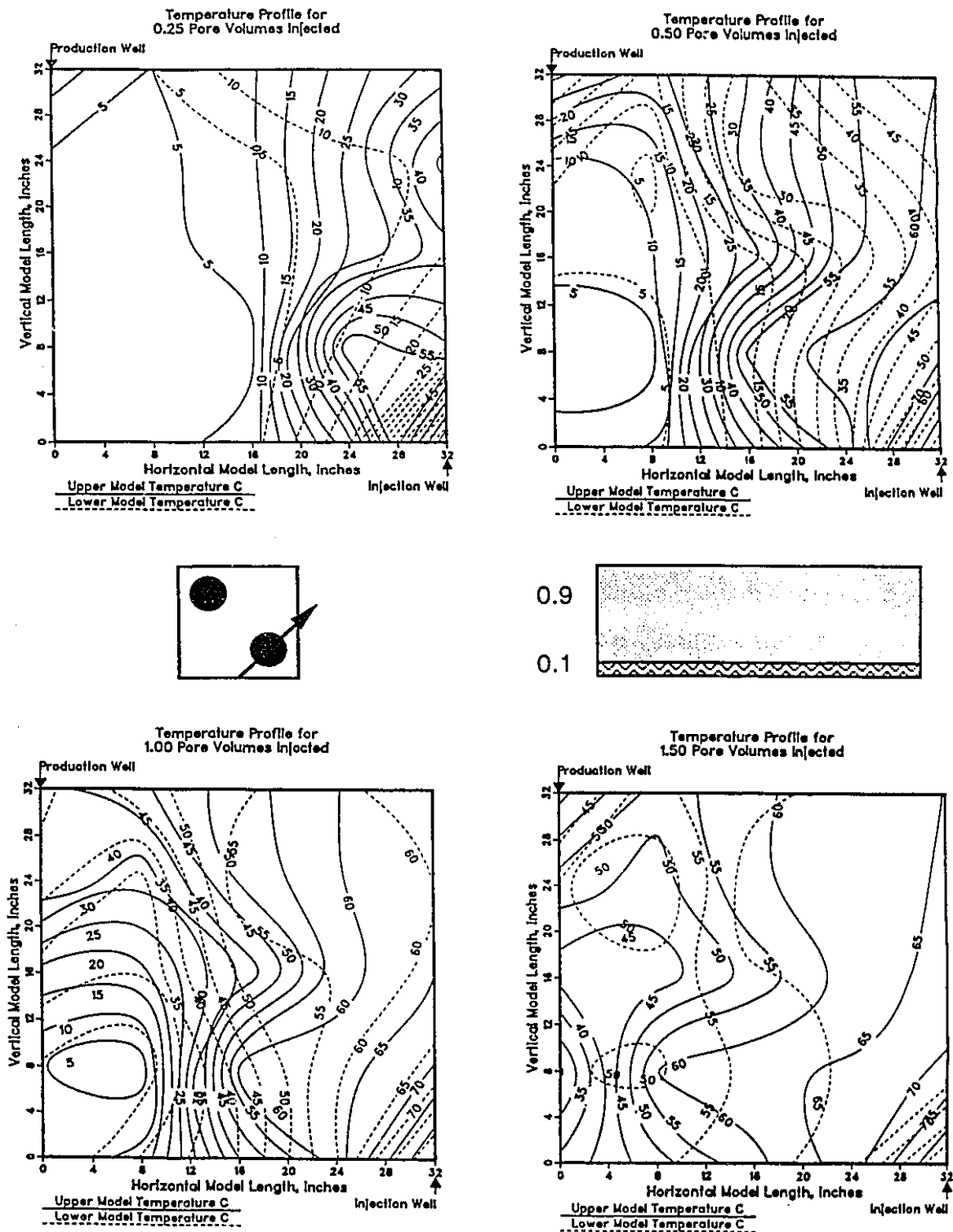
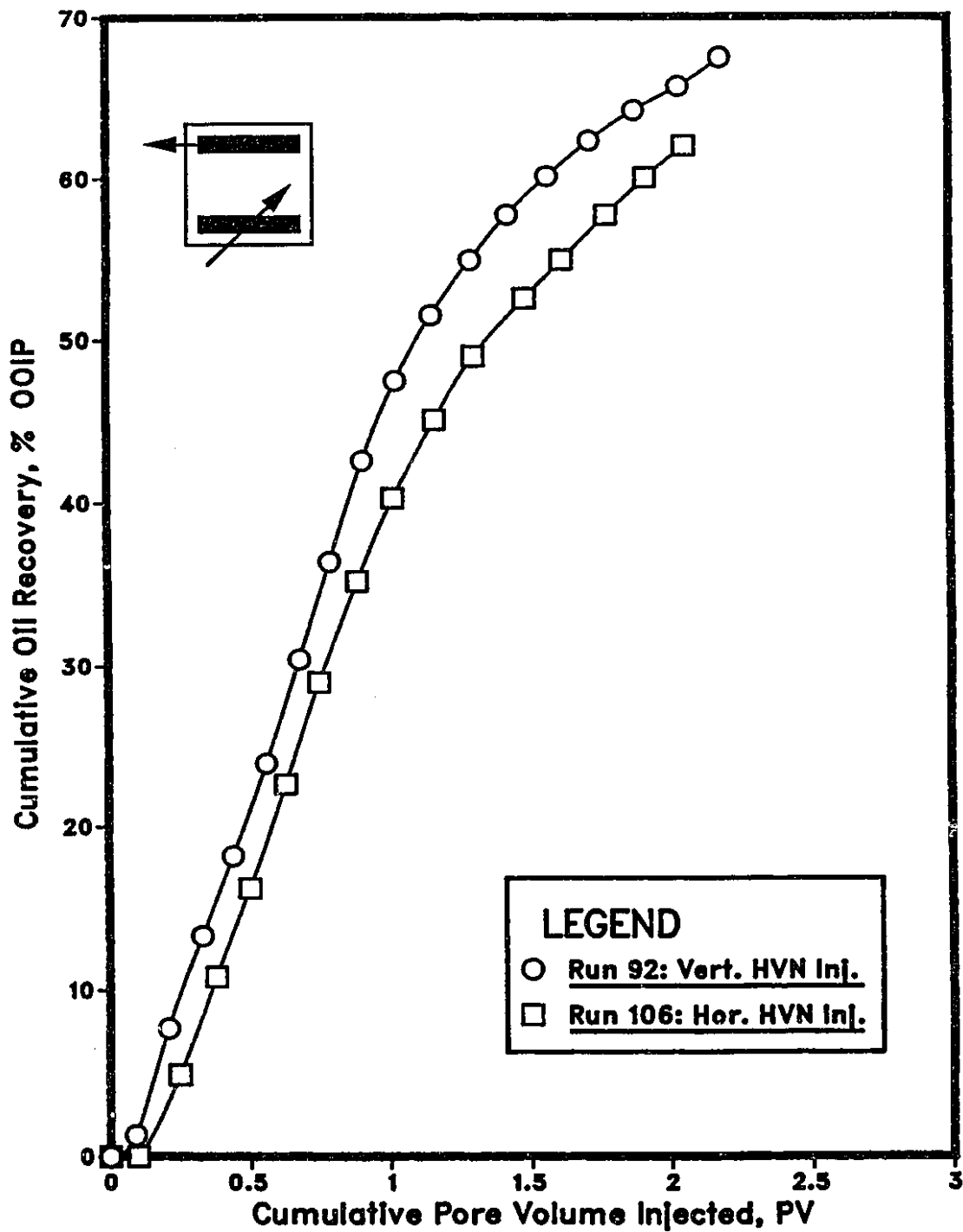


Figure 6.48: Top View Temperature Profiles for Run 94—Solvent (10% PV)-Steamflood using a Horizontal-Vertical Well Combination in a Thin (10%) Bottom Water Model.



**Figure 6.49: Solvent Injection Strategies for Steamfloods using a Horizontal Producer and a Horizontal Injector (10% BW, 10% HVN)**



horizontal wellbore is about 5% less than injection through a vertical well. The results of Run 106 closely resembled those for Run 101 (10% BW, no solvent), which would imply that the use of a horizontal solvent injector in a thin bottom water zone is not beneficial considering performance and cost.

### **Summary of Horizontal-Vertical Well Strategies**

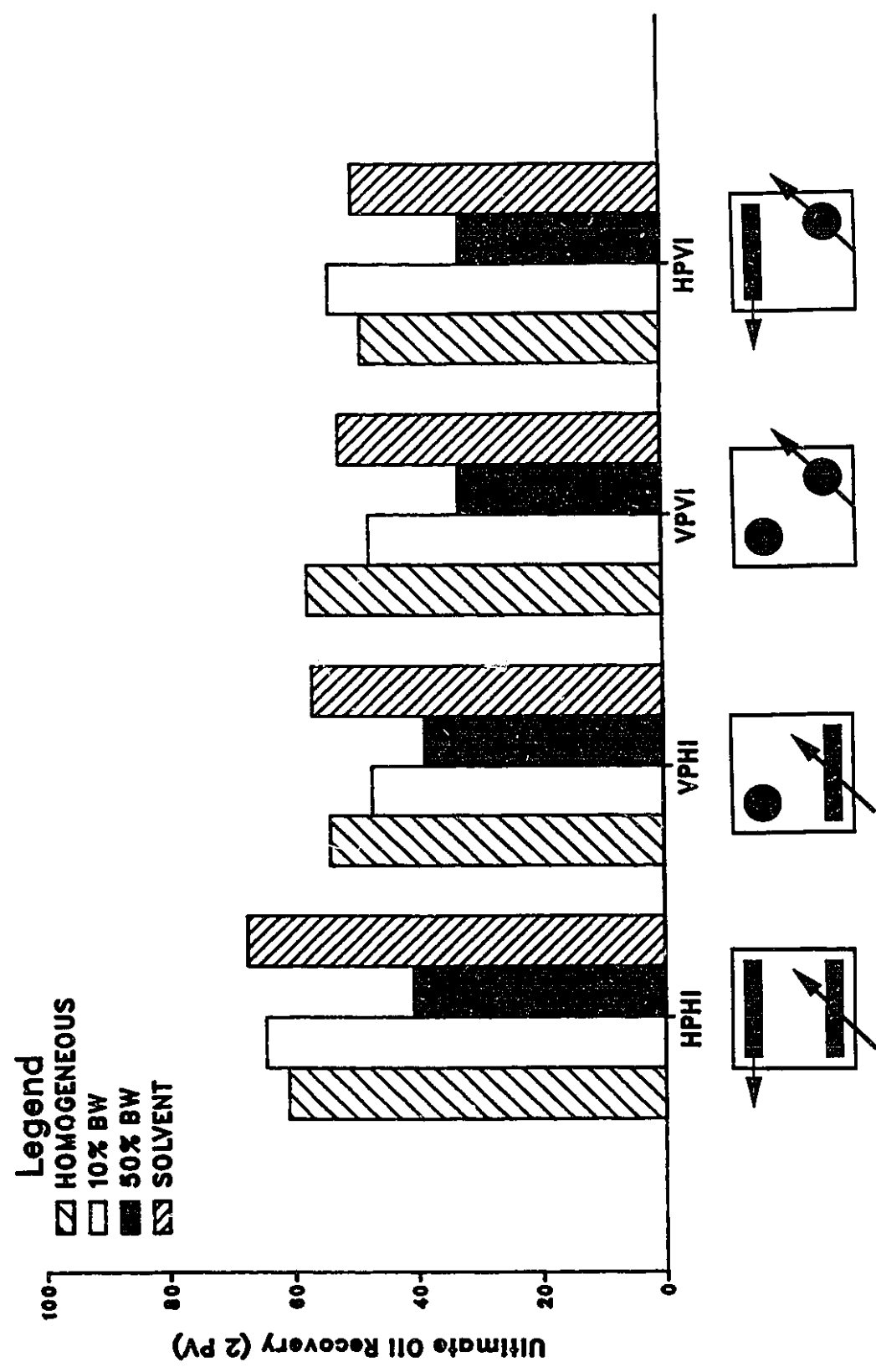
Figure 6.50 provides a comparison of ultimate oil recovery for the different injection-production strategies used, for all cases (with and without solvent). The superiority of the horizontal injection-horizontal production combination is clear. On average, highest recoveries were obtained in thin bottom water cases. The results showed that the horizontal producer-horizontal injector combination worked best for all reservoir situations. While comparing the different bottom water cases, it should be noted that the actual volumes of oil in place differ considerably even though the oil saturations are within experimental error. Thus, the oil recoveries in terms of volume will be quite different even if the percent values are the same.

### **Reproducibility of Results**

Several runs were repeated to test experimental reproducibility. Results in Table 6.1 for Run 86 (Repeat of Run 74, VPHI in a homogeneous pack) and 104 (Repeat of Run 77, VPVI in a homogeneous pack) prove that the experiments could be reproduced within an error of  $\pm 2\%$ .



**Figure 6.50: Comparison of the Various Injection-Production Strategies on Ultimate Oil Recovery, for the Different Bottom Water Cases Investigated.**



## Chapter 7

Conclusions

Steamflood experiments of several types were carried out in an extensively redesigned scaled model, with varying amounts of bottom water present. The following conclusions are reached on the basis of the observed performance in the scaled model:

1. Generally, bottom water has an adverse effect on steamflood performance. However, a thin bottom water zone may help to improve oil recovery. It was found that a 7% bottom water thickness is the optimum value, below which formation heating by conduction is more beneficial than the use of gas or solvent additives, for increasing oil recovery.
2. The implementation of vertical-horizontal well combinations in thin, heavy oil formations led to the following findings:
  - a) A horizontal producer-horizontal injector combination (HPHI) worked best for all reservoir situations, investigated in this work. The oil recovery by HPHI was 10 to 20 percentiles greater than the poorest well combination, characterized by the smallest cumulative oil production.
  - b) Horizontal production wells performed better in thin (10% of gross thickness) bottom water situations than in a homogeneous reservoir with no bottom water. Oil recovery was approximately 4 percentiles higher when steam was injected in the presence of a thin basal water saturation zone.
  - c) In the presence of thick bottom water (50% of gross thickness), all well combinations exhibited similar performance, but a horizontal injector still performed better. The HPHI combination recovered 41% OOIP compared to the 33% recovery by the VPVI combinations

3. A 10% naphtha slug injected ahead of steam improved oil recovery by only 5 percentiles in the presence of a thin bottom water zone, resulting in a maximum oil recovery of 68%.
4. Pre-injection of a slug of solvent or gas was successful in diverting the steam away from the heat scavenging basal water zone. This was proven to be particularly effective in thick bottom water formations, as exhibited by the improved steamflood performance.
5. The precision of the steam quality control governs the outcome of any successful steamflood, in the laboratory or field. This is especially critical in low pressure experiments as the scaled quality is between 5-15%. A plot of the ratio of cumulative production to cumulative injection (CP/CI) vs. cumulative pore volumes injected can verify whether the recovery process is a steamflood or a hot waterflood.

## Chapter 8

**Recommendations for Further Studies**

This study has presented steam injection methods for recovering oil from marginal heavy oil reservoirs in Alberta and Saskatchewan. Of these methods, the use of a gas additive and horizontal wells appear to be the most promising. Laboratory studies in scaled physical models should be continued to devise techniques for increasing the profitability of the present field operations in these reservoirs.

In view of the current shut-in steam projects in Alberta and Saskatchewan, heat scavenging techniques could offer a means of recovering additional oil beyond the current economic limit. Future studies should investigate the viability of using an inert gas additive to partially recover the heat remaining in the formation following a steamflood.

The construction of four vertical injection wells in the model permits the steamflood experiments to be conducted in one-quarter of a nine-spot pattern. The effect of closer well spacing could be considered. In addition, multiple vertical injectors/producers strategies could be studied: one horizontal producer-two vertical injectors and two vertical producers-one horizontal injector.

To complement the current investigation, a thicker model of the Aberfeldy reservoir should be constructed according to the criteria presented here. A thicker model would permit more flexibility in the placement of horizontal wells with respect to the vertical plane, and in bottom water creation. To maintain the same pore volume, yet increase the thickness, the model should be constructed as one-half of its element of symmetry. This could be accomplished in two ways: a rectangular model (one-half the areal size of the present model, which could scale the horizontal wells used in the current study), and a triangular model representing one-eighth of a five spot as opposed to one-quarter (vertical wells could be scaled and the different placement of horizontal wells compared to the rectangular model could be studied). Another alternative is to design a model using a larger

length scale, which would produce a thicker model. Impermeable blocks could be inserted as required to maintain the same pore volume. As in all thermal studies, temperature is a crucial element. Therefore, a thicker model, which would permit more thermocouple leads, should be incorporated into the apparatus.

### References

1. Farouq Ali, S.M. and Redford, D.A.: "Physical Modeling of In Situ Recovery Methods For Oil Sands," presented at the 28th Annual Technical Meeting of the Petroleum Society of CIM, Canada-Venezuela Oil Sands Symposium of 1977, Edmonton (May 1977).
2. Watts, K.G. and Hutchinson, H.L.: "Experimental Investigation of the Steam Drive Process for the Asphalt Ridge Tar Sands Deposit, Utah," SPE 11161 presented at the 57th Annual Fall Technical Conference and Exhibition of the Society of Petroleum Engineers of AIME, New Orleans, September 26-29 (1988).
3. Kimber, K.D., Puttagunta, V.R. and Farouq Ali, S.M.: "New Scaling Criteria and Their Relative Merits for Steam Recovery Experiments," Paper 86-37-22 presented at the 37th Annual Technical Meeting of the Petroleum Society of CIM, Calgary, June 8-11 (1986) 303-318.
4. Doscher, T.M. and Lechtenberg, H.J.: "Scaled Physical Model Studies of the Steam Drive Processes," *U.S. Department of Energy, First Annual Report* (September 1977-September 1978), Report DOE/ET/12075-1.
5. Huygen, H.H.A.: "Laboratory Steamfloods in Half of a Five-Spot," SPE 6171 presented at the 51st Annual Fall Technical Conference and Exhibition of the Society of Petroleum Engineers of AIME, New Orleans, October 3-6 (1976).
6. Pujol, L. and Boberg, T.C.: "Scaling Accuracy of Laboratory Steam Flooding Models," SPE 4191 presented at the SPE California Regional Meeting of the Society of Petroleum Engineers of AIME, Bakersfield, November 8-10 (1972).
7. Pursley, S.A.: "Experimental Studies of Thermal Recovery Processes," presented at the Symposium on Heavy Crude Oil, Maracaibo, Venezuela, July 1-3 (1974).
8. Lo, H.Y.: "Laboratory Model Study of Steam Flood Oil Recovery," *Petroleum Recovery Institute, Interim Report IR-5* (March 1977).
9. Stegemeier, G.L., Laumbach, D.D. and Volek, C.W.: "Representing Steam Processes with Vacuum Models," *SPEJ* (June 1980) 151-174.
10. Singhal, A.K.: "Physical Model Study of Inverted Seven Spot Steamfloods in a Pool Containing Conventional Heavy Oil," Paper 79-30-13 presented at the 30th Annual Technical Meeting of the Petroleum Society of CIM, Banff, May 8-11 (1979).
11. Kimber, K. and Farouq Ali, S.M.: "Application of New Scaling Approaches for Steam Injection Experiments," presented at the 25th National Heat Transfer Conference of AIChE, Houston (1988).

12. Kimber, K.D. and Farouq Ali, S.M.: "Verification of Scaling Approaches for Steam Injection Experiments," Paper 88-39-17 presented at the 39th Annual Technical Meeting of the Petroleum Society of CIM, Calgary, June 12-16 (1988).
13. Prats, M.: "Peace River Steam Drive Scaled Model Experiments," presented at the 28th Annual Technical Meeting of the Petroleum Society of CIM, Canada-Venezuela Oil Sands Symposium of 1977, Edmonton (May 1977).
14. Proctor, M.L.: Steam Injection Experiments in a Scaled Physical Model, M.Sc. Thesis, U. of Alberta (Fall 1985).
15. Yortsos, Y.C. and Gavalas, G.R.: "Analytical Modeling of Oil Recovery by Steam Injection: Part 1 - Upper Bounds," *SPEJ* (April 1981) 162-178.
16. Yortsos, Y.C. and Gavalas, G.R.: "Analytical Modeling of Oil Recovery by Steam Injection: Part 2 - Asymptotic and Approximate Solutions," *SPEJ* (April 1981) 179-190.
17. Hall, A.L. and Bowman, R.W.: "Operation and Performance of the Slocum Thermal Recovery Project," *JPT* (April 1973) 25, 402-408.
18. Ehrlich, R.: "Laboratory Investigation of Steam Displacement in the Wabasca Grand Rapids 'A' Sand," presented at the 28th Annual Technical Meeting of the Petroleum Society of CIM, Canada-Venezuela Oil Sands Symposium of 1977, Edmonton (May 1977).
19. Huygen, H.A. and Lowry Jr., W.E.: "Steamflooding Wabasca Tar Sand Through the Bottom Water Zone - Scaled Lab Experiments," SPE 8398 presented at the 54th Annual Fall Technical Conference and Exhibition of the Society of Petroleum Engineers of AIME, Las Vegas, September 23-26 (1979).
20. Doscher, T.M. and Huang, W.: "Steam-Drive Performance Judged Quickly from Use of Physical Models," *Oil and Gas Journal*, October 22 (1979) 52-57.
21. Proctor, M.L., George, A.E. and Farouq Ali, S.M.: "Steam Injection Strategies for Thin, Bottomwater Reservoirs," SPE paper 16338 presented at the SPE California Regional Meeting, Ventura, April 8-10 (1987).
22. Kasraie, M. and Farouq Ali, S.M.: "Heavy Oil Recovery in the Presence of Bottom Water," Paper 84-35-122 presented at the 35th Annual Technical Meeting of the Petroleum Society of CIM held jointly with the Canadian Association of Drilling Engineers, Calgary, June 10-13 (1984).
23. Joshi, S.D.: "Augmentation of Well Productivity Using Slant and Horizontal Wells," *JPT* (June 1988) 729-739.
24. Joshi, S.D.: "A Review of Horizontal Well Technology," presented at the U.S. Department of Energy Tar Sand Symposium, Jackson, Wyoming, July 7-10 (1986).
25. Muskat, M.: The Flow of Homogeneous Fluids Through Porous Media, Chapter IV, 1st Ed., 2nd. Printing, J.W. Edwards Inc. (1946).

26. Giger, F.M., L.H. Reiss and A.P. Jourdan: "The Reservoir Engineering Aspects of Horizontal Drilling," SPE paper 13024 presented at the 59th Annual Technical Conference and Exhibition, Houston, September 16-19 (1984).
27. Giger, F.M.: "Analytic 2-D Models of Water Cresting Before Breakthrough for Horizontal Wells," SPE paper 15378 presented at the 61st Annual Technical Conference and Exhibition of the Society of Petroleum Engineers, New Orleans, October 5-8 (1986).
28. Borisov, Y.P.: "Oil Field Production Using Horizontal and Multiple-Deviation Wells," French Petroleum Institute Translation Report No. 28 363, revised by J. Combe (August 1980).
29. Economides, M.J. and Nolte, K.G.: Reservoir Stimulation, 2nd Ed. (1989) 19-1 to 19-28.
30. Giger, F.M.: "Low-Permeability Reservoirs Development Using Horizontal Wells," SPE 18334 presented at the SPE/DOE Low Permeability Reservoirs Symposium, Denver, May 18-19 (1987).
31. Goode, P.A. and R.K.M. Thambynayagam: "Pressure Drawdown and Buildup Analysis of Horizontal Wells in Anisotropic Media," *SPE Formation Evaluation* (December 1987) 683-697.
32. Butler, R.M., G.S. McNab and H.Y. Lo: "Theoretical Studies on the Gravity Drainage of Heavy Oil During In-Situ Steam Heating," *The Canadian Journal of Chemical Engineering*, Vol.59 (August 1981) 455-460.
33. Butler, R.M. and Stephens, D.J.: "The Gravity Drainage of Steam-Heated Heavy Oil to Parallel Horizontal Wells," *JCPT* (April-June 1981) 90-96.
34. Joshi, S.D.: "A Laboratory Study of Thermal Oil Recovery Using Horizontal Wells," SPE/DOE Paper No. 14916, Proc. of the Fifth SPE/DOE EOR Conf., Tulsa, April 20-23 (1986) 457-468.
35. Gussis, G.L.: "Simulation of Steam Injection Through Horizontal Wellbores for Viscous Oil Recovery," Paper No. HCTS/CF.3/8.17, Proc. of the Third International Conf. on Heavy Crude and Tar Sands, UNITAR/UNDP, Long Beach, July 22-31 (1985) 699-725.
36. Haston, J.A., Edmunds, N.R., Luhnig, R.W. and Rourke, J.C.: "AOSTRA Underground Test Facility Achievements and Future Development," presented at AOSTRA Oil Sands 2000: Energy-Environment-Enterprise, Edmonton, March 26-28 (1990).
37. Dietrich, J.K.: "The Kern River Horizontal-Well Steam Pilot," *SPE Reservoir Engineering* (August 1988) 935-944.
38. Anon.: "Horizontal Heavy Oil Wells Results Called Encouraging," *Oilweek*, March 28 (1988) 5.
39. Anon.: "Canada Horizontal/Steam Project 'Encouraging'," *Oil and Gas Journal*, September 26 (1988) 32.



40. Dabbs, F.: "Horizontal Wells to Boost Production," *Calgary Sun*, October 17, 1987.
41. Oracheski, D.J., Farouq Ali, S.M. and George, A.E.: "Scaled Model Studies of Solvent-Steam Injection, Under Bottom Water Conditions," Paper 39-40-31 presented at the 40th Annual Technical Meeting of the Petroleum Society of CIM, Banff, May 28-31 (1989).
42. Shu, W.R. and Hartman, K.J.: "Effect of Solvent on Steam Recovery of Heavy Oil," *SPE Reservoir Engineering* (May 1988) 457-465.
43. Farouq Ali, S.M. and Snyder, S.G.: "Miscible Thermal Methods Applied to a Two-Dimensional, Vertical Tar Sand Pack, With Restricted Fluid Entry," *JCPT* (October-December 1973) 20-26.
44. Farouq Ali, S.M. and Abad, B.: "Bitumen Recovery from Oil Sands, Using Solvents in Conjunction with Steam," *JCPT* (July-September 1976) 80-90.
45. Demetre, G.P.: Scaling and Instability of Flow in Porous Media, M.Sc. Thesis, U. of Alberta (Spring 1980).
46. Van Wylen, G.L. and Sonntag, R.E.: Fundamentals of Classical Thermodynamics, 3rd Ed., SI Version, John Wiley & Sons, 1985.
47. Farouq Ali, S.M.: Heavy Oil Recovery, Chapter 5, (1989).
48. Wygal, R.J.: "Construction of Models that Simulate Oil Reservoirs", *SPEJ* (December 1963) 281-286.
49. Marx, J.W. and Langenheim, R.H.: "Reservoir Heating by Hot Fluid Injection," *Trans. AIME* (1959) 312.
50. Mandl, G. and Volek, C.W.: "Heat and Mass Transport in Steam-Drive," *SPEJ* (March 1969) 59-79.
51. Oracheski, D.: Bottom Water Solvent Steam Injection Studies, M.Sc. Thesis, U. of Alberta (Fall 1988).
52. Prats, M.: Thermal Recovery, Monograph Volume 7 SPE Henry L. Doherty Series, Chapters 6 and 7, Society of Petroleum Engineers of AIME (1982).

**Appendix A****Differential Equations in Dimensionless Form**

### Mass Balance for Oil

$$\begin{aligned}
 & \frac{\partial}{\partial x_D} \left( \frac{\rho_{oD} k_{oD}}{\mu_{oD}} \frac{\partial p_{oD}}{\partial x_D} \right) + \left( \frac{\rho_{oR} g_R D_R}{P_{oR}} \right) \frac{\partial}{\partial x_D} \left( \frac{\rho_{oD}^2 k_{oD} g_D}{\mu_{oD}} \frac{\partial D_D}{\partial x_D} \right) \\
 & + \left( \frac{x_R}{y_R} \right)^2 \frac{\partial}{\partial y_D} \left( \frac{\rho_{oD} k_{oD}}{\mu_{oD}} \frac{\partial p_{oD}}{\partial y_D} \right) + \left( \frac{x_R}{y_R} \right)^2 \left( \frac{\rho_{oR} g_R D_R}{P_{oR}} \right) \frac{\partial}{\partial y_D} \left( \frac{\rho_{oD}^2 k_{oD} g_D}{\mu_{oD}} \frac{\partial D_D}{\partial y_D} \right) \\
 & + \left( \frac{x_R}{z_R} \right)^2 \frac{\partial}{\partial z_D} \left( \frac{\rho_{oD} k_{oD}}{\mu_{oD}} \frac{\partial p_{oD}}{\partial z_D} \right) + \left( \frac{x_R}{z_R} \right)^2 \left( \frac{\rho_{oR} g_R D_R}{P_{oR}} \right) \frac{\partial}{\partial z_D} \left( \frac{\rho_{oD}^2 k_{oD} g_D}{\mu_{oD}} \frac{\partial D_D}{\partial z_D} \right) \\
 & + \left( \frac{q_{oR}^* \mu_{oR} X_R^2}{\rho_{oR} k_{oR} P_{oR}} \right) \cdot q_{oD}^* = \left( \frac{\phi_R S_{oR} \mu_{oR} X_R^2}{t_R k_{oR} P_{oR}} \right) \frac{\partial}{\partial t_D} (\phi_D S_{oD} \rho_{oD})
 \end{aligned}$$

### Mass Balance for Gas (Additive)

$$\begin{aligned}
 & \frac{\partial}{\partial x_D} \left( \frac{C_{gAD} \rho_{gD} k_{gD}}{\mu_{gD}} \frac{\partial p_{gD}}{\partial x_D} \right) + \left( \frac{\rho_{gR} g_R D_R}{P_{gR}} \right) \frac{\partial}{\partial x_D} \left( \frac{C_{gAD} \rho_{gD}^2 k_{gD} g_D}{\mu_{gD}} \frac{\partial D_D}{\partial x_D} \right) \\
 & + \left( \frac{x_R}{y_R} \right)^2 \frac{\partial}{\partial y_D} \left( \frac{C_{gAD} \rho_{gD} k_{gD}}{\mu_{gD}} \frac{\partial p_{gD}}{\partial y_D} \right) + \left( \frac{x_R}{y_R} \right)^2 \left( \frac{\rho_{gR} g_R D_R}{P_{gR}} \right) \frac{\partial}{\partial y_D} \left( \frac{C_{gAD} \rho_{gD}^2 k_{gD} g_D}{\mu_{gD}} \frac{\partial D_D}{\partial y_D} \right) \\
 & + \left( \frac{x_R}{z_R} \right)^2 \frac{\partial}{\partial z_D} \left( \frac{C_{gAD} \rho_{gD} k_{gD}}{\mu_{gD}} \frac{\partial p_{gD}}{\partial z_D} \right) + \left( \frac{x_R}{z_R} \right)^2 \left( \frac{\rho_{gR} g_R D_R}{P_{gR}} \right) \frac{\partial}{\partial z_D} \left( \frac{C_{gAD} \rho_{gD}^2 k_{gD} g_D}{\mu_{gD}} \frac{\partial D_D}{\partial z_D} \right) \\
 & + \left( \frac{C_{gAR}^* q_{gR}^* \mu_{gR} X_R^2}{C_{gAR} \rho_{gR} k_{gR} P_{gR}} \right) \cdot q_{gD}^* = \left( \frac{\phi_R S_{gR} \mu_{gR} X_R^2}{t_R k_{gR} P_{gR}} \right) \frac{\partial}{\partial t_D} (\phi_D S_{gD} C_{gAD} \rho_{gD})
 \end{aligned}$$

**Mass Balance for Water**

$$\begin{aligned}
& \frac{\partial}{\partial x_D} \left( \frac{\rho_{wD} k_{wD}}{\mu_{wD}} \frac{\partial p_{wD}}{\partial x_D} \right) + \left( \frac{\rho_{wR} \xi_R D_R}{p_{wR}} \right) \frac{\partial}{\partial x_D} \left( \frac{\rho_{wD}^2 k_{wD} \xi_D}{\mu_{wD}} \frac{\partial D_D}{\partial x_D} \right) \\
& + \left( \frac{C_{gWR} \rho_{gR} k_{gR} p_{gR} \mu_{wR}}{\rho_{wR} k_{wR} p_{wR} \mu_{gR}} \right) \frac{\partial}{\partial x_D} \left( \frac{C_{gWR} \rho_{gD} k_{gD}}{\mu_{gD}} \frac{\partial p_{gD}}{\partial x_D} \right) \\
& + \left( \frac{C_{gWR} \rho_{gR}^2 k_{gR} \xi_R D_R \mu_{wR}}{\rho_{wR} k_{wR} p_{wR} \mu_{gR}} \right) \frac{\partial}{\partial x_D} \left( \frac{C_{gWR} \rho_{gD}^2 k_{gD} \xi_D}{\mu_{gD}} \frac{\partial D_D}{\partial x_D} \right) \\
& + \left( \frac{x_R}{y_R} \right)^2 \frac{\partial}{\partial y_D} \left( \frac{\rho_{wD} k_{wD}}{\mu_{wD}} \frac{\partial p_{wD}}{\partial y_D} \right) + \left( \frac{x_R}{y_R} \right)^2 \left( \frac{\rho_{wR} \xi_R D_R}{p_{wR}} \right) \frac{\partial}{\partial y_D} \left( \frac{\rho_{wD}^2 k_{wD} \xi_D}{\mu_{wD}} \frac{\partial D_D}{\partial y_D} \right) \\
& + \left( \frac{x_R}{y_R} \right)^2 \left( \frac{C_{gWR} \rho_{gR} k_{gR} p_{gR} \mu_{wR}}{\rho_{wR} k_{wR} p_{wR} \mu_{gR}} \right) \frac{\partial}{\partial y_D} \left( \frac{C_{gWR} \rho_{gD} k_{gD}}{\mu_{gD}} \frac{\partial p_{gD}}{\partial y_D} \right) \\
& + \left( \frac{x_R}{y_R} \right)^2 \left( \frac{C_{gWR} \rho_{gR}^2 k_{gR} \xi_R D_R \mu_{wR}}{\rho_{wR} k_{wR} p_{wR} \mu_{gR}} \right) \frac{\partial}{\partial y_D} \left( \frac{C_{gWR} \rho_{gD}^2 k_{gD} \xi_D}{\mu_{gD}} \frac{\partial D_D}{\partial y_D} \right) \\
& + \left( \frac{x_R}{z_R} \right)^2 \frac{\partial}{\partial z_D} \left( \frac{\rho_{wD} k_{wD}}{\mu_{wD}} \frac{\partial p_{wD}}{\partial z_D} \right) + \left( \frac{x_R}{z_R} \right)^2 \left( \frac{\rho_{wR} \xi_R D_R}{p_{wR}} \right) \frac{\partial}{\partial z_D} \left( \frac{\rho_{wD}^2 k_{wD} \xi_D}{\mu_{wD}} \frac{\partial D_D}{\partial z_D} \right) \\
& + \left( \frac{x_R}{z_R} \right)^2 \left( \frac{C_{gWR} \rho_{gR} k_{gR} p_{gR} \mu_{wR}}{\rho_{wR} k_{wR} p_{wR} \mu_{gR}} \right) \frac{\partial}{\partial z_D} \left( \frac{C_{gWR} \rho_{gD} k_{gD}}{\mu_{gD}} \frac{\partial p_{gD}}{\partial z_D} \right) \\
& + \left( \frac{x_R}{z_R} \right)^2 \left( \frac{C_{gWR} \rho_{gR}^2 k_{gR} \xi_R D_R \mu_{wR}}{\rho_{wR} k_{wR} p_{wR} \mu_{gR}} \right) \frac{\partial}{\partial z_D} \left( \frac{C_{gWR} \rho_{gD}^2 k_{gD} \xi_D}{\mu_{gD}} \frac{\partial D_D}{\partial z_D} \right) \\
& + \left( \frac{q_{wR} \mu_{wR} x_R^2}{\rho_{wR} k_{wR} p_{wR}} \right) \cdot q_{wD}^* + \left( \frac{C_{gWR} q_{gR}^* \mu_{wR} x_R^2}{\rho_{wR} k_{wR} p_{wR}} \right) \cdot C_{gWD}^* q_{gD}^* \\
& = \left( \frac{\phi_R S_{wR} \mu_{wR} x_R^2}{t_R k_{wR} p_{wR}} \right) \frac{\partial}{\partial t_D} (\zeta_D S_{wD} \rho_{wD}) + \left( \frac{\phi_R S_{gR} C_{gWR} \rho_{gR} \mu_{wR} x_R^2}{t_R \rho_{wR} k_{wR} p_{wR}} \right) \frac{\partial}{\partial t_D} (\phi_D S_{gD} C_{gWD} \rho_{gD})
\end{aligned}$$

Energy Balance

$$\begin{aligned}
& \left( \frac{k_{hR} T_R \mu_{oR}}{\rho_{oR} k_{oR} h_{oR} p_{oR}} \right) \frac{\partial}{\partial x_D} \left( k_{hD} \frac{\partial T_D}{\partial x_D} \right) + \frac{\partial}{\partial x_D} \left( \frac{\rho_{oD} k_{oD} h_{oD}}{\mu_{oD}} \frac{\partial p_{oD}}{\partial x_D} \right) \\
& + \left( \frac{\rho_{oR} g_R D_R}{p_{oR}} \right) \frac{\partial}{\partial x_D} \left( \frac{\rho_{oD}^2 k_{oD} h_{oD} g_D}{\mu_{oD}} \frac{\partial D_D}{\partial x_D} \right) \\
& + \left( \frac{\rho_{wR} k_{wR} h_{wR} p_{wR} \mu_{oR}}{\rho_{oR} k_{oR} h_{oR} p_{oR} \mu_{wR}} \right) \frac{\partial}{\partial x_D} \left( \frac{\rho_{wD} k_{wD} h_{wD}}{\mu_{wD}} \frac{\partial p_{wD}}{\partial x_D} \right) \\
& + \left( \frac{\rho_{wR}^2 k_{wR} h_{wR} g_R D_R \mu_{oR}}{\rho_{oR} k_{oR} h_{oR} p_{oR} \mu_{wR}} \right) \frac{\partial}{\partial x_D} \left( \frac{\rho_{wD}^2 k_{wD} h_{wD} g_D}{\mu_{wD}} \frac{\partial D_D}{\partial x_D} \right) \\
& + \left( \frac{\rho_{gR} k_{gR} h_{gR} p_{gR} \mu_{oR}}{\rho_{oR} k_{oR} h_{oR} p_{oR} \mu_{gR}} \right) \frac{\partial}{\partial x_D} \left( \frac{\rho_{gD} k_{gD} h_{gD}}{\mu_{gD}} \frac{\partial p_{gD}}{\partial x_D} \right) \\
& + \left( \frac{\rho_{gR}^2 k_{gR} h_{gR} g_R D_R \mu_{oR}}{\rho_{oR} k_{oR} h_{oR} p_{oR} \mu_{gR}} \right) \frac{\partial}{\partial x_D} \left( \frac{\rho_{gD}^2 k_{gD} h_{gD} g_D}{\mu_{gD}} \frac{\partial D_D}{\partial x_D} \right) \\
& + \left( \frac{x_R}{y_R} \right)^2 \left( \frac{k_{hR} T_R \mu_{oR}}{\rho_{oR} k_{oR} h_{oR} p_{oR}} \right) \frac{\partial}{\partial y_D} \left( k_{hD} \frac{\partial T_D}{\partial y_D} \right) + \left( \frac{x_R}{y_R} \right)^2 \frac{\partial}{\partial y_D} \left( \frac{\rho_{oD} k_{oD} h_{oD}}{\mu_{oD}} \frac{\partial p_{oD}}{\partial y_D} \right) \\
& + \left( \frac{x_R}{y_R} \right)^2 \left( \frac{\rho_{oR} g_R D_R}{p_{oR}} \right) \frac{\partial}{\partial y_D} \left( \frac{\rho_{oD}^2 k_{oD} h_{oD} g_D}{\mu_{oD}} \frac{\partial D_D}{\partial y_D} \right) \\
& + \left( \frac{x_R}{y_R} \right)^2 \left( \frac{\rho_{wR} k_{wR} h_{wR} p_{wR} \mu_{oR}}{\rho_{oR} k_{oR} h_{oR} p_{oR} \mu_{wR}} \right) \frac{\partial}{\partial y_D} \left( \frac{\rho_{wD} k_{wD} h_{wD}}{\mu_{wD}} \frac{\partial p_{wD}}{\partial y_D} \right) \\
& + \left( \frac{x_R}{y_R} \right)^2 \left( \frac{\rho_{wR}^2 k_{wR} h_{wR} g_R D_R \mu_{oR}}{\rho_{oR} k_{oR} h_{oR} p_{oR} \mu_{wR}} \right) \frac{\partial}{\partial y_D} \left( \frac{\rho_{wD}^2 k_{wD} h_{wD} g_D}{\mu_{wD}} \frac{\partial D_D}{\partial y_D} \right) \\
& + \left( \frac{x_R}{y_R} \right)^2 \left( \frac{\rho_{gR} k_{gR} h_{gR} p_{gR} \mu_{oR}}{\rho_{oR} k_{oR} h_{oR} p_{oR} \mu_{gR}} \right) \frac{\partial}{\partial y_D} \left( \frac{\rho_{gD} k_{gD} h_{gD}}{\mu_{gD}} \frac{\partial p_{gD}}{\partial y_D} \right)
\end{aligned}$$

**Energy Balance (continued)**

$$\begin{aligned}
& + \left( \frac{x_R}{y_R} \right)^2 \left( \frac{\rho_{gR}^2 k_{gR} h_{gR} g_R D_R \mu_{oR}}{\rho_{oR} k_{oR} h_{oR} p_{oR} \mu_{gR}} \right) \frac{\partial}{\partial y_D} \left( \frac{\rho_{gD}^2 k_{gD} h_{gD} g_D}{\mu_{gD}} \frac{\partial D_D}{\partial x_D} \right) \\
& + \left( \frac{x_R}{z_R} \right)^2 \left( \frac{k_{hR} T_R \mu_{oR}}{\rho_{oR} k_{oR} h_{oR} p_{oR}} \right) \frac{\partial}{\partial z_D} \left( k_{hD} \frac{\partial T_D}{\partial z_D} \right) + \left( \frac{x_R}{z_R} \right)^2 \frac{\partial}{\partial z_D} \left( \frac{\rho_{oD} k_{oD} h_{oD}}{\mu_{oD}} \frac{\partial p_{oD}}{\partial z_D} \right) \\
& + \left( \frac{x_R}{z_R} \right)^2 \left( \frac{\rho_{oR} g_R D_R}{p_{oR}} \right) \frac{\partial}{\partial z_D} \left( \frac{\rho_{oD}^2 k_{oD} h_{oD} g_D}{\mu_{oD}} \frac{\partial D_D}{\partial z_D} \right) \\
& + \left( \frac{x_R}{z_R} \right)^2 \left( \frac{\rho_{wR} k_{wR} h_{wR} p_{wR} \mu_{oR}}{\rho_{oR} k_{oR} h_{oR} p_{oR} \mu_{wR}} \right) \frac{\partial}{\partial z_D} \left( \frac{\rho_{wD} k_{wD} h_{wD}}{\mu_{wD}} \frac{\partial p_{wD}}{\partial z_D} \right) \\
& + \left( \frac{x_R}{z_R} \right)^2 \left( \frac{\rho_{wR}^2 k_{wR} h_{wR} g_R D_R \mu_{oR}}{\rho_{oR} k_{oR} h_{oR} p_{oR} \mu_{wR}} \right) \frac{\partial}{\partial z_D} \left( \frac{\rho_{wD}^2 k_{wD} h_{wD} g_D}{\mu_{wD}} \frac{\partial D_D}{\partial z_D} \right) \\
& + \left( \frac{x_R}{z_R} \right)^2 \left( \frac{\rho_{gR} k_{gR} h_{gR} p_{gR} \mu_{oR}}{\rho_{oR} k_{oR} h_{oR} p_{oR} \mu_{gR}} \right) \frac{\partial}{\partial z_D} \left( \frac{\rho_{gD} k_{gD} h_{gD}}{\mu_{gD}} \frac{\partial p_{gD}}{\partial z_D} \right) \\
& + \left( \frac{x_R}{z_R} \right)^2 \left( \frac{\rho_{gR}^2 k_{gR} h_{gR} g_R D_R \mu_{oR}}{\rho_{oR} k_{oR} h_{oR} p_{oR} \mu_{gR}} \right) \frac{\partial}{\partial z_D} \left( \frac{\rho_{gD}^2 k_{gD} h_{gD} g_D}{\mu_{gD}} \frac{\partial D_D}{\partial z_D} \right) \\
& + \left( \frac{q_{hR}^* \mu_{oR} x_R^2}{\rho_{oR} k_{oR} h_{oR} p_{oR}} \right) \cdot q_{hD}^* - \left( \frac{q_{lR}^* \mu_{oR} x_R^2}{\rho_{oR} k_{oR} h_{oR} p_{oR}} \right) \cdot q_{lD}^* \\
& = \left( \frac{\phi_R S_{oR} U_{oR} \mu_{oR} x_R^2}{t_R k_{oR} h_{oR} p_{oR}} \right) \frac{\partial}{\partial t_D} (\phi_D \rho_{oD} S_{oD} U_{oD}) + \left( \frac{\phi_R \rho_{wR} S_{wR} U_{wR} \mu_{oR} x_R^2}{t_R \rho_{oR} k_{oR} h_{oR} p_{oR}} \right) \frac{\partial}{\partial t_D} (\phi_D \rho_{wD} S_{wD} U_{wD}) \\
& + \left( \frac{\phi_R \rho_{gR} S_{gR} U_{gR} \mu_{oR} x_R^2}{t_R \rho_{oR} k_{oR} h_{oR} p_{oR}} \right) \frac{\partial}{\partial t_D} (\phi_D \rho_{gD} S_{gD} U_{gD}) + \left( \frac{(1-\phi_R) \rho_{rR} U_{rR} \mu_{oR} x_R^2}{t_R \rho_{oR} k_{oR} h_{oR} p_{oR}} \right) \frac{\partial}{\partial t_D} ((1-\phi_D) \rho_{rD} U_{rD})
\end{aligned}$$

**Appendix B**  
Detailed Laboratory Manual

Table of Contents for Appendix B

1. MODEL PREPARATION.....	162
1.1 Preparation of a Homogeneous Model.....	162
1.1.1 Sealing the Model.....	162
1.1.2 Saturating the Model.....	162
1.2 Preparation of a Bottom Water Model.....	164
1.2.1 Introduction.....	164
1.2.2 Bottom Water Calculation.....	164
1.2.3 Formation of a Bottom Water Layer.....	165
2. DATA ACQUISITION SYSTEMS.....	167
2.1 Megadac.....	167
2.1.1 Getting Started.....	167
2.1.2 Megadac Initialization.....	168
2.1.3 Initializing Data Tables.....	169
2.1.4 Recording the Run Data.....	170
2.1.5 Quitting.....	170
2.2 Metrabyte.....	171
3. CLEANING THE MODEL.....	172
3.1 General Procedure.....	172
3.2 Cleaning the Glass Beads.....	173
3.3 Cleaning the Fibreglass Tray.....	173
3.4 Miscellaneous Comments.....	174



## 1. MODEL PREPARATION

### 1.1 Preparation of a Homogeneous Model

#### 1.1.1 Sealing the Model

- a) Place the Wygal<sup>48</sup> particle distributor on top of the frame of the fibreglass model.
  - b) Fill the distributor with approximately 40 litres of 3 mm diameter glass beads using a 2 litre volume beaker.
  - c) Allow beads to pass through a metering board onto the mesh screens in the distributor.
  - d) Trim off excess beads off the model surface using a metal straight edge to ensure a flat surface with no protrusions.
  - e) Apply a thin (1/8" thick), uniform layer of clear silicone sealant (Dow Corning RTV Sealant 732) around the edges of the fibreglass tray.
  - f) Place 1/8" thick Celtite Neoprene Sponge on top of the tray and hence, covering the sealant.
  - g) Place the (overburden) granite block on the tray and clamp the model.
  - h) Turn on the vacuum pump and evacuate the fluid containers.
  - i) Turn injection well off.
  - j) Connect the production well to the the collection system.
  - k) Aim the three way valve towards one of the containers and open the production well in the direction of the up dip saturation ports in order to evacuate the model.
- ~ When the system is completely sealed, it will be indicated by a constant vacuum in excess of 68 cm of Hg which can be read from the adjacent manometer.

#### 1.1.2 Saturating the Model

- a) Once the model is evacuated, tighten the clamps and tilt the model to 45°.
  - b) Immerse the saturation tube in a vessel filled with 16 litres ( $V_{H_2O}$ ) of distilled water.
  - c) Connect the saturation tube to the model.
  - d) Open the injection well by turning it in the direction of the down dip saturation ports.
- ~ Saturation occurs as a result of the suction force of the pump at the production end which draws the water from the down to up dip end of the model.
- e) Close the production well when the model is completely saturated with water which is indicated by water production in the collection flasks.

- f) Record the volume of water displaced during the water saturation process ( $V_1$ ), disconnect the saturation tube and measure the volume of water remaining in the water vessel ( $V_f$ ).
- g) Determine the volume of the pore volume (PV) of the bead pack:

$$\text{Pore Volume} = \left( \frac{\text{Total Initial}}{\text{Water Volume}} \right) - \left( \frac{\text{Amount of Water}}{\text{Displaced}} \right) - \left( \frac{\text{Final Volume}}{\text{of Water Remaining}} \right)$$

$$PV = V_{ii} - V_1 - V_f$$

Since the bulk volume of the model is 42005 cc, the porosity may be obtained:

$$\phi = \left( \frac{PV}{\text{Bulk Volume}} \right) \times 100\% = \frac{PV}{42005 \text{ cc}} \times 100\%$$

- h) Place the saturation tube in a 20 litre pail of Faxam-100 oil and reconnect it to the injection ports.
- i) Open the production wells and collect all fluid production in the pre-evacuated collection flasks.
- j) Close the production saturation port when oil saturation is complete.
- This is signified when water is no longer produced, that is, when the bead pack has reached its irreducible water saturation ( $S_{wi}$ ).
- k) Measure the amount of water displaced during water saturation ( $V_2$ ).
- l) Calculate the hydrocarbon pore volume (HYC PV):

$$\left( \frac{\text{Hydrocarbon}}{\text{Pore Volume}} \right) = (\text{Pore Volume}) - \left( \frac{\text{Amount of Water Displaced}}{\text{During Oil Saturation}} \right)$$

i.e. HYC PV is the amount of oil taken into the model

$$\text{HYC PV} = PV - V_2$$

Thus, the initial oil saturation is

$$S_{oi} = \frac{\text{HYC PV}}{PV} \times 100\%$$

Since the initial gas saturation is assumed to be zero ( $S_{gi}$ ) unless otherwise specified as in the case of a gas run, the irreducible water saturation can be calculated since

$$S_{oi} + S_{wi} + S_{gi} = 1, \text{ but } S_{gi} = 0$$

Hence,  $S_{wi} = 1 - S_{oi}$

- m) Disconnect the saturation tube and production well.
- n) Return the model to the horizontal position.
- o) Push the model into the walk-in cooler.

- p) Turn on the cooler thermostat to 37.5°F (3°C).  
 ~ It takes 24 hours to cool the entire model to 3°C.

## 1.2 Preparation of a Bottom Water Model

### 1.2.1 Introduction

*The primary objectives are:*

- to simulate a bottom water layer using a layer of frozen 5% NaCl solution
- to measure the refractive index of displaced water during the water/oil saturation process and hence, determine the quantity of bottom water remaining as a function of total gross model thickness

### 1.2.2 Bottom Water Calculation

- Express the thickness of bottom water ( $t$ ) required as a percentage of gross model thickness.
- Assume:  $\phi_{avg} = 34\%$ .
- From the *Science Data Book*,  $\rho_{NaCl} = 2.165$  g/cc and  $\rho_{H_2O} = 1.000$  g/cc at 293 K.
- Calculate the average pore volume ( $PV_{avg}$ ) of the model for the given situation:

$$PV_{avg} = \phi_{avg} \times V_b$$

where:  $V_b = 42005$  cc = bulk volume

- Determine the pore volume ( $V_p$ ) that the bottom water of thickness ' $t$ ' occupies:

$$\frac{\text{total model thickness (= 2.5")}}{t} = \frac{PV_{avg}}{V_p}$$

- Include a correction volume in  $V_p$  to account for bottom water loss due to melting during saturation:  $V_p' = V_p + \text{Correction}$
- In order to determine the quantities of NaCl and H<sub>2</sub>O required to make a 5% (by weight) NaCl solution, the following equation is solved by trial and error:

$$V_p' = \frac{m_{H_2O}}{\rho_{H_2O}} + \frac{m_{NaCl}}{\rho_{NaCl}} \quad \text{where } m_p = 0.95m_{H_2O} + 0.05m_{NaCl}$$

#### *Sample Calculation 1. 10% Bottom Water Mixture (10% BW)*

- For 10% BW (% gross model thickness):

$$t = (10\%) \times 2.5" = 0.25"$$

b) Given:  $\phi_{avg} = 34\%$  and  $V_b = 42005 \text{ cc}$ ,

$$PV_{avg} = 34\% \times 42005 \text{ cc} = 14282 \text{ cc}$$

c) The pore volume that the bottom water occupies is:

$$\frac{2.5''}{0.25''} = \frac{14282 \text{ cc}}{V_p}; \quad V_p = 1428 \text{ cc}$$

d) Add a correction factor of 600 cc to the total volume of brine required to compensate for melting:

$$V_p' = 1428 \text{ cc} + 600 \text{ cc} = 2028 \text{ cc}$$

e) If it is assumed that the total mass of the BW required is 2085 g:

$$m_{H_2O} = 0.95 \times 2085 \text{ g} = 1981 \text{ g}$$

$$m_{NaCl} = 0.05 \times 2085 \text{ g} = 104 \text{ g}$$

f) Check to see that the volume calculated using the masses and densities correspond to the required volume of  $V_p'$  which was determined in Step (d):

$$V_{H_2O} = \frac{1981 \text{ g}}{1.000 \text{ g/cc}} = 1981 \text{ cc}; \quad V_{NaCl} = \frac{104 \text{ g}}{2.165 \text{ g/cc}} = 48 \text{ cc}$$

$$\text{Hence, } V_{p \text{ calculated}}' = 1981 \text{ cc} + 48 \text{ cc} = 2029 \text{ cc}$$

g) If  $V_p'$  calculated does not agree with  $V_p'$  required within a  $\pm 10 \text{ cc}$  tolerance then reiterate on Step (e) by assuming another value of total mass required for 10% BW.

### 1.2.3 Formation of a Bottom Water Layer

- Pour the required volume of 5% NaCl solution into the fibreglass model.
- Sprinkle enough glass beads into the tray using a 200 ml beaker to cover the bottom water solution.
- Add an additional thin layer of beads to the brine to compensate for water swelling due to freezing.
- Push the model into the walk-in cooler in preparation for freezing.
- Place 40 litres of dry glass beads into the cooler.
- Close the cooler and adjust the thermostat to  $-30^\circ\text{F}$  ( $-34^\circ\text{C}$ ).
- Freezing generally takes approximately 24 hours for bottom water thickness variations up to 50% of the total gross model thickness.
- When the bottom water is completely frozen, pack the remainder of the model with the frozen beads using the Wygal<sup>48</sup> particle distributor.
- Skim off any excess beads using a straight edge.

- i) Seal and saturate the bottom water model using the same procedure which is applied to the homogeneous model.
- ~ The purpose of using frozen beads and cold water instead of room temperature materials are simply to act as a heat sink by minimizing the thawing effects of the bottom water layer during the saturation process.
- j) Measure the refractive index of each sample to determine the amount of bottom water which has melted using the lever rule.
- ~ A plot of refractive index versus the percentage of NaCl in solution was constructed for various %NaCl combinations. From the linear relationship, which was achieved and is shown below as Figure B.1, it was determined that 0% NaCl corresponded to 0% bottom water and had the refractive index of distilled water, 1.33246 at 25.5°C. Similarly, 5% NaCl corresponded to 100% bottom water and had the refractive index of distilled water, 1.3410 at 25.5°C.

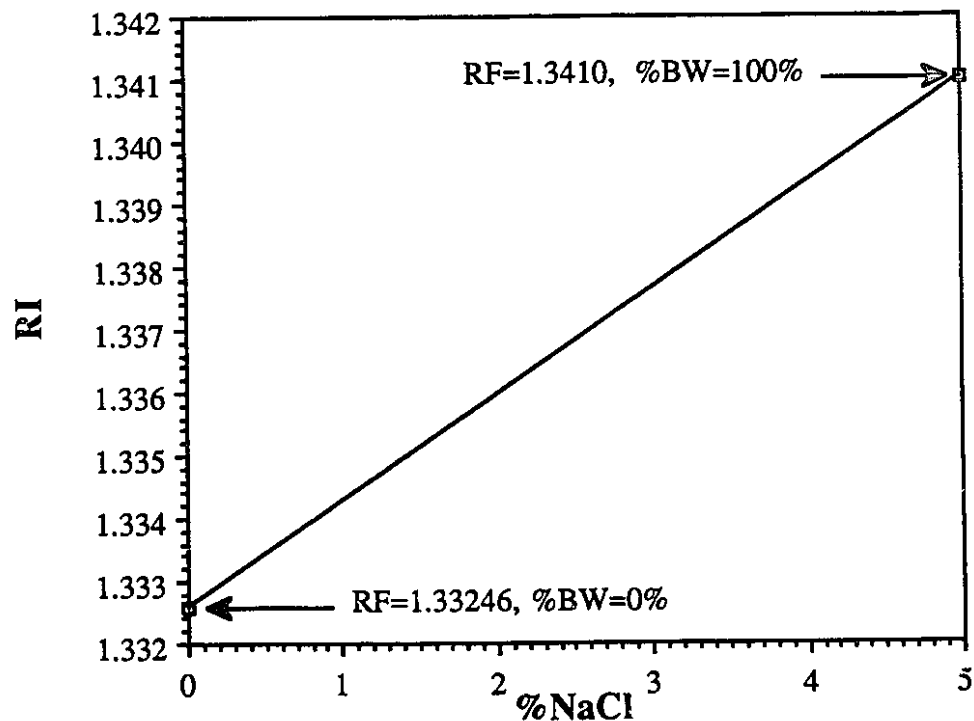


Figure B.1: A Plot of Refractive Index vs. %NaCl.

*Sample Calculation 2. %BW Loss Due to Melting Using Refractive Indices*

- a) Given: RI = 1.3350 at 25.5°C  
 Sample Volume = V = 1200 cc  
 PV = 14000 cc

Volume of Bottom Water Frozen Initially =  $V_p' = 2029$  cc

Find: The volume of BW remaining in the model after this sample is taken.

- b) From Figure B.1, %NaCl = 1.5% at RI = 1.3350. Using the lever rule determine %BW in sample,

$$\frac{\%BW \text{ in Sample}}{100\%BW} = \frac{1.5\%NaCl}{5\%NaCl}$$

$$\text{Thus, \%BW in Sample} = \frac{1.5\%NaCl}{5\%NaCl} \times 100\%BW = 30\%BW$$

- c) Calculate:

$$\begin{aligned} \text{BW Produced} &= \%BW \text{ in Sample} \times \text{Sample Volume} \\ &= 30\% \times 1200 \text{ cc} \\ \text{BW Produced} &= 360 \text{ cc} \end{aligned}$$

- d) Then, solve:

$$\begin{aligned} \text{BW Remaining} &= V_p' - (\text{BW Produced}) \\ &= 2029 \text{ cc} - 360 \text{ cc} \\ \text{BW Remaining} &= 1669 \text{ cc} \end{aligned}$$

- e) Bottom water thickness can now be determined:

$$\frac{2.5''}{t} = \frac{14000 \text{ cc}}{1669 \text{ cc}}$$

$$t = 0.298'' = 11.9\%BW (\% \text{gross model thickness})$$

$$\text{where } \% \text{gross thickness} = \frac{0.298''}{2.5''} \times 100\% = 11.9\%$$

## 2. DATA ACQUISITION SYSTEMS

### 2.1 Megadac

The following procedures are used to generate and record the data from steam injection experiments in a scaled physical model using the Megadac 2000 data acquisition unit. This system has now been replaced by the Metrabyte and Labtech Unit which is described in Section 2.2.

#### 2.1.1 Getting Started

- Turn on the IBM Personal Computer, MEGADAC SYSTEM 2000 and the EPSON Printer.
- To change the directory, type **CD\OPUSHELEN**.
- To run the OPUS software package, type **OPUS**.

d) Press **PF5 (MEASUREMENT USING MEGADAC)** followed by **RETURN**.

~ If the Megadac and IBM screen both have the correct time and date, and no other error message appears on either screen, then go to Step 2.1.3 otherwise go to Step 2.1.2.

### 2.1.2 Megadac Initialization

#### *Part A*

Type **PF9** for initialization instructions which are as follows:

- a) Press **RESET** button on Megadac 2000.
  - b) Press **SETUP** button on Megadac 2000.
  - c) Type **2** to set the mode.
  - d) Type **99**.
  - e) Press **ENTER** button on Megadac 2000.
  - f) Turn off Megadac 2000.
  - g) Turn on Megadac 2000 to establish initial baud rate.
  - h) Wait for the **REMOTE** light on the Megadac panel to appear. Then, press **PF10**.
- ~ If no error is indicated on the IBM screen, then proceed to Step 2.1.3. However, if there is still an error in either the time, date or any other information printed on the screen, then the time and date must also be reset as listed in Step 2.1.2: Part B.

#### *Part B*

- a) Press **RESET** button on MEGADAC 2000.
- b) Press **SETUP** button on MEGADAC 2000.
- c) Press **1** to set the time.
- d) Type the time and date in the following sequence:  
**date month year hour minute seconds or dd mm yy hr mi ss**

~ *Please note:*

- ~ There are no spaces in this character chain.
- ~ Each item consists of two integers.
- ~ Time format is based on 2400 hours.

~ *For example,*

May 19, 1990 at 10:30:35 am is typed in as 190590103035.

October 2, 1990 at 3:45:00 pm is typed in as 021090154500.

- e) Turn off Megadac 2000 to reinitialize baud rate.
- f) Turn on Megadac 2000.
- g) When the **REMOTE** light comes on, press **PF10**.
- ~ If no error message appears on Megadac or on the IBM screen, go to Step 2.1.3.

### 2.1.3 Initializing Data Tables

- a) Press **PF4 (RUN — DATA TO DISK)** and then **RETURN**.
- b) A screen from the **OPTIM USER'S SOFTWARE** is generated to record **SCAN AS PER TABLE**. Type **PREPARE** in the grey box beside the title "Name of Experiment Table". This is done in order to check if the thermocouples are all working.
- c) Press **PF10** to accept the **PREPARE** file.
- d) Suffix to be given to data file: **D\_\_** is shown on the screen. Type in the grey box the suffix number, such as **67** so the data will be recorded as **D67**.
- e) Press **PF10** again to continue in addition to checking the thermocouples and pressure transducers on the model. The Optim User's Software Package converts voltage readings to temperature and pressure units for the respective sensors. White numbers refer to positive values (kPa or °C) while red numbers indicate negative values (kPa or °C). Thermocouple temperatures should be between zero and three degrees Celsius (0 to 3°C). Check and adjust any thermocouple or transducer connections with temperature and pressure readings in excess of a factor of 1000. Possible sources of error are loose connections between the data cable and sensor junction, broken thermocouples or electrical shorts in data cables which connect the sensors with Megadac.
- f) **OPUS** and **Megadac** will continue scanning the thermocouples until all reading are satisfactory. To stop scanning, press **PF8**.
- g) To return to the **OPUS** menu, press **PF10**.
- ~ Once the thermocouples are producing acceptable results, the next stage of the program is to allow **OPUS** to record all the experimental results in the IBM hard drive and print all the transmitted data simultaneously on the **EPSON** printer.
- h) Press **PF4 (RUN — DATA TO DISK)** and **RETURN**.
- i). This time the "Name of Experiment Table" is typed in as **RUNS** instead of **PREPARE** as in Step (b). Then type **RETURN** to accept the table.
- j) The **RUNS** table records the experimental results. To receive a printed copy simultaneously with the displayed results, press **RETURN** to cursor the grey box



to the desired selection: **PRINTED/MEASURED RESULTS**. Type **1** beside **PRINTED/MEASURED RESULTS**. This command will allow the EPSON printer to print one measured result for each one displayed on the IBM terminal.

- k) Press **PF10** to return to the screen.
- l) Press **PF10** to accept the new input data.

#### 2.1.4 Recording the Run Data

~ Record the data only pertinent to the run such as solvent injection and steam injection. Well connection time is ignored.

a) When the solvent inlet is connected to the injection well, begin scanning when solvent injection begins. This is done by pressing **PF10** which stores the run data for each 30 second scan. Record the scan numbers from the IBM screen when solvent injection begins and ends.

b) The solvent port is then disconnected and is replaced by the steam port. The objective is to open the production well approximately half (1/2) a scan before the injection well. First, open the production well and record that scan number. Second, open the injection well on the following scan and record that scan number. It is essential to record the scans at which each sample is collected as well as the instant the pump is shut off (ie. when the experiment ends). Also record additional scans, such as pressure buildup and pore volume injected, as they are helpful when analyzing the results.

~ It is desired to maintain a production pressure between 80 and 90 kPa. If the pressure exceeds this range then the seal will most likely break and destroy the vacuum; the results from the run will then be useless.

d) Other items which should be recorded include the refractive index of the samples, the total volume of the sample and the respective volumes of solvent and oil in the cylinder.

#### 2.1.5 Quitting

- a) To stop scanning and storing the data, press **PF8**.
- b) To return to the OPUS menu, press **PF10**.
- c) To terminate the OPUS program, press **PF10**.
- d) To exit OPUS and return to DOS, press **PF10**.
- e) Finally, type **YES** or **Y** when prompted to exit the OPUS package.

## 2.2 Metrabyte

The Megadac 2000 data acquisition system broke down prior to the initiation of Run 70E. After evaluating situation, it was decided that it would not be economical to repair the Megadac unit or the Optim User's software package. Rather, it was more feasible to replace Megadac with another acquisition system. A Metrabyte data acquisition system was chosen primarily because of its low cost, its ability to interface with the existing IBM personal computer which was used to process Megadac 2000 data, easy accessibility for necessary repairs as well as the availability of consultants. In addition, an integrated data acquisition, control and analysis software package called Labtech Notebook was also purchased.

One of the advantages of choosing Metrabyte is its expansion capability. The central processing unit is an eight channel 12 bit high speed A/D converter and timer/counter board for the IBM PC called the DAS-8 board. The EXP-16 multiplexer offers a relatively inexpensive way to expand the input capabilities of the DAS-8. Each EXP-16 has 16 fully differential inputs that can be multiplexed into a single A/D board input channel. The EXP-16 is ideal for measuring thermocouple inputs because of the temperature sensor on the board which permits the cold junction temperature (CJC) to be monitored. Although it is possible to have a maximum of eight EXP-16 panels attached to one DAS-8 multiplexer, the steam injection experiments require only a maximum of 37 J-type thermocouples and 4 pressure transducers. Therefore, four EXP-16 boards were ordered and were installed according to Figure B.2:

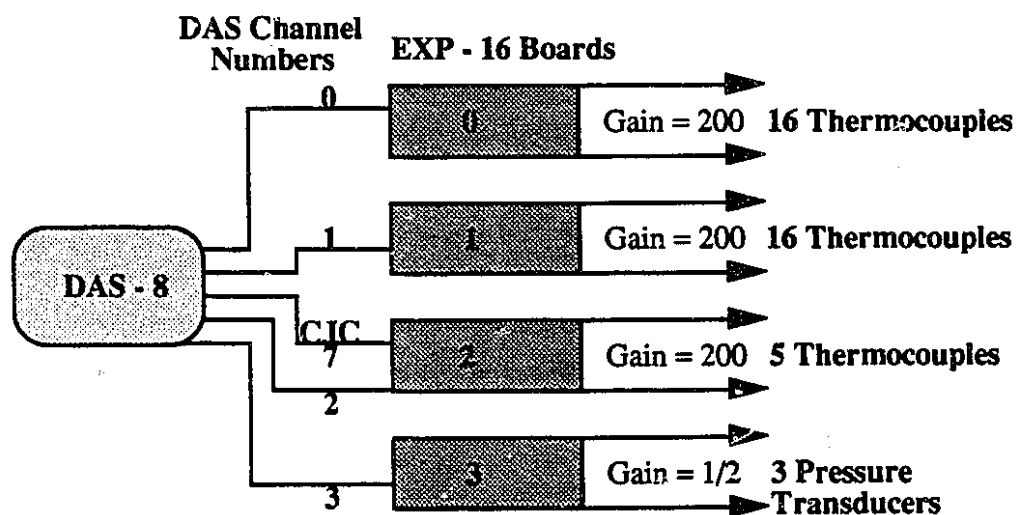


Figure B.2: A Schematic of the Metrabyte Data Acquisition Unit.

Labtech Notebook processes all raw thermocouple (mV) and pressure transducer (mV) measurements and automatically converts them into real values of temperature (degrees Celsius) and pressure (kPa) as a function of real time (seconds or minutes). No programming was required because Labtech is menu driven. To initiate Labtech, simply change the Main directory to the Notebook one by typing the DOS command `cd\nb` followed by `nb` which will execute the program. In addition, Notebook includes foreground/background operations which permits the user to perform other tasks while data is being collected. Furthermore, Labtech Notebook interfaces all data files, which are stored in an ASCII file format, to IBM software packages, such as Lotus 1-2-3 or Lotus Symphony. It is important to note that a hard drive is preferable in order to maximize efficiency due to the large size of this software package. In addition, the hard drive must be referred to as 'C' if it is desired to use Labtech's installation program (Version 4.36), otherwise Notebook must be installed manually.

### **3. CLEANING THE MODEL**

#### **3.1 General Procedure**

- a) Remove the clamps from the model.
- b) Bleed off the vacuum in the model by opening one of the quick-connects. If this is not done, then the top granite block will tend to stick to the Neoprene sheet and consequently, the fibreglass tray as a result of the vacuum created during the run.
- c) Remove the top block using the hydraulic jack.
- d) Pull the cart containing the lower block and tray away from the jack into an open area for cleaning.
- e) Remove the Neoprene sheet.
- f) Shake the sheet to remove any glass beads which may be imbedded in the Neoprene.
- g) Dispose of the Neoprene sheet in a waste container since it will not be reused in future runs.
- h) Scoop out the glass bead pack from the model using a small beaker and place them into several plastic pails.  
~ Try to avoid bending the thermocouples since they break very easily.
- i) Clean the beads as per the instructions in Section 3.2.
- j) Clean the fibreglass model as per the instructions in Section 3.3.

### 3.2 Cleaning the Glass Beads

From past experiences, it is more desirable to clean the glass beads in smaller portions in a 10 litre plastic pail instead of a 20 litre one in order to maximize task efficiency.

- a) Fill one-third (1/3) to half (1/2) of a 10L pail with the glass beads.
  - b) Add approximately 100 to 200 ml of SLIK #5 degreaser to the pail.
  - c) Immerse the beads in hot water.
  - d) Wash the beads in the degreaser-water solution by hand to remove oil and any residual solvent from the beads.
- ~~ SLIK #5 degreaser is water soluble, so it may be poured directly into the sink.
- e) Rinse the beads with hot water and add 50 mL to 100 mL of Sparkleen soap to the pail. Clean the beads and empty the pail.
  - f) Repeat Step (e) and continue to rinse the glass beads until there is no more oil or soap on them.
- ~~ Usually, one wash cycle in degreaser and two wash cycles in Sparkleen followed by four to five rinses in hot water are sufficient.
- ~~ The average time required to clean 5 L to 7 L of beads is approximately 10 to 15 minutes.
- g) Pour the glass beads into the metallic bead driers which are situated on risers.
  - h) Allow any excess water to drain out of the driers in order to expedite the drying period.
  - i) Connect tubing from the driers to the air inlet valve.
  - j) Turn on the air valve and inject air into the bead drier.
- ~~ This process may be left unattended and usually takes between 18 to 24 hours to complete.

### 3.3 Cleaning the Fibreglass Tray

- a) Scrape off the silicone sealant layer using a chisel or sharp metal straight edge, such as a dull knife blade, being careful not to scratch the fibreglass tray.
- b) Remove all trimmings and dispose in waste basket.
- c) Tilt the model 45° using the same the procedure described for model saturation.
- d) Mix 200 mL to 300 mL of degreaser with 4 litres of hot water. Pour half of the solution into the up dip side of the model to remove all traces of oil from the model.
- e) Drain the model using a siphon.

- ~ A siphon is the quickest and most efficient way to remove the liquid waste. This is done by sealing one end of a piece of rubber tubing with one thumb and adding water in the other end until the tubing is completely filled. Then, seal this end immediately trying to eliminate any air bubbles. Place one end in the bottom of the model and the other in a disposal pail on the floor. Remove both thumbs simultaneously. The suction force caused by the height differential and thus, pressure differences between both ends should draw the water and any remaining beads from the model into the waste pail.
- f) Add the remainder of the degreaser solution to the model and drain the waste.
- g) Rinse the model with hot water and drain with siphon. Repeat until there is no more oil in the model.
- h) Dry the model with Kimtuff wipers.
- ~ Kimtuff disposable wipers are used to absorb residual oil and solvents from the model.
- i) Apply Varsol to the fibreglass tray and its edges using a wash bottle.
- j) Wipe the tray and edges with Kimtuff wipers.
- k) Apply acetone to the fibreglass tray and its edges using a wash bottle.
- ~ Both Varsol and acetone are used because some hydrocarbons break down better in Varsol than in acetone and vice-versa. It is hoped that using both solvents can remove all traces of the hydrocarbons used in the experiments, such as Faxam-100 and heavy virgin naphtha. Because the use of toluene is restricted to areas with sufficient ventilation like fume hoods, it is not used in the steam injection experiments which are run in open laboratory conditions.
- l) Dry the tray and edges with the wipers.
- m) Lower the model.
- n) Straighten any bent thermocouples and replace any broken ones.
- ~ New thermocouples are replaced by inserting them through the ferrels and fittings into the fibreglass tray to the desired length. Tighten the fittings and seal all exposed areas with the silicone sealant to ensure that no areas will be potential sources where the vacuum may escape.

### **3.4 Miscellaneous Comments**

- a) Any containers storing solvent must be emptied in a waste receptacle not in the sink as solvent is not water soluble and will corrode the sink and its pipes.

- b) Scrub the glass cylinders, flasks and beakers with beaker brush using Sparkleen detergent and hot water.
- c) Plastic cylinders and beakers are tipped upside down on top of a layer of Kimtuff wipers and allowed to drain out any excess oil. Sparkleen is primarily used for glassware and is not suitable for cleaning plastics. However, common household dishwashing liquid detergent is a very effective and inexpensive way to clean plastic containers of all traces of oil.
- d) Celtite Neoprene sponge is cut in 3'x3' sheets using a utility knife. Epoxy joined portions of the Neoprene roll are cut off as they are often sources of seal leakage and hence, result in vacuum loss. Exact cutting precision is not necessary since the flexible and cushy nature of Neoprene allows it to conform to all situations.

**Appendix C**  
**List of Suppliers and Materials**

Item	Supplier
SIHI Closed Couple Liquid Ring Vacuum Pump (SIHI LRM 10603—1.5 hp close coupled glass filled epoxy resin vacuum pump c/w 208/3/60 teflon motor c/w teflon gaskets)	T.D.H. Fluid Systems Inc. 4634-91 Avenue Edmonton, Alberta, T6B 2L1
Silastic 732 Adhesive Sealant RTV Kintuff wipers Hammond (plain aluminum) panel	Central Stores Materials Management Department The University of Alberta Edmonton, Alberta T6G 2E1 (403) 492-4246
1/8" Celtite Neoprene™ sponge	Continental Petroleum (CP) Rubber Inc.) 9725-62 Avenue Edmonton, Alberta T6G 0E5 (403) 437-1260
Faxam-100	McEwen's Esso 3704-92 Avenue Box 8671, Station L Edmonton, Alberta T8C 4J4 (403) 465-0152
Sparkleen Detergent Parafilm M* Laboratory Film Fisherbrand disposable (flint glass) pasteur pipets Kimwipes wipers Fisherbrand mechanical pump fluid Sodium chloride	Fisher Scientific 10720-178 Street Edmonton, Alberta T5S 1J3 (403) 483-2123
DAS-8—8 channel A/D Board EXP-16—16 channel multiplexer C1800—cables LTN-03—Labtech Notebook	Dycor Industrial Research Ltd. #130, 17303-102 Street Edmonton, Alberta T5S 1J8 (403) 486-0091
Fluke-83 Multimeter	Cardinal Industrial Electronics 10630-172 Street Edmonton, Alberta T5S 1H8 (403)483-6266
0.3 mm fibre plotter pens for the HP plotter (for plotter paper) Graphics plotter paper	Northwest Digital 10640-170 Street Edmonton, Alberta T5S 1P3 (403) 486-3598



Item	Supplier
Industrial glass beads (3 mm diam. (6-8 U.S. mesh) technical quality solid glass spheres)	Rotair Industries 1040-78 Avenue Edmonton, Alberta T6P 1L7 (403) 440-2775
Walk-in cooler/freezer	Edmonton Refrigeration Ltd. 14203-128A Avenue Edmonton, Alberta T5L 4P5 (403) 454-3000
36"x36"x8.5" granite block	DoAll Edmonton Ltd. 9743-45 Avenue Edmonton, Alberta T6E 5V8 (403) 436-0373
Fibreglass tray	Triple M Fibreglass Ltd. 8135 Wagner Road Edmonton, Alberta T6E 4N6 (403) 465-0726
1.5" vacuum traps 1.5" polyethylene trap jar	Tri "S" Dairy Equipment Ltd. 14804-119 Avenue Edmonton, Alberta T5L 2M6
2—4207951506 bushings 2—4207721150 nipples 2—4207721142 nipples 2—4207721130 nipples 4—4206690010 elbows 2—4206900010 female adaptor 2—7436265010 Hayward 1" 3-way ball valve 4—4207500010 hose adaptor	Scepter Manufacturing Co. Ltd. 4225-92 Avenue Edmonton, Alberta T6B 3M7 (403) 468-4444
Slik No.5 medium-duty degreaser (originator: Baroid of Canada Ltd, Calgary, Alberta, (403) 263-8740)	NL Treating Chemicals 1500, 840-7th Avenue S.W. Calgary, Alberta T2P 3G2 (403) 263-8740
Swagelok fittings	Edmonton Valve and Fitting Ltd. 4503-93 Street Edmonton, Alberta T6E 5S9

Item	Supplier
A11-16-J-GSS-15" (miniature quick disconnect small diameter thermocouple, type J316SS sheath	Alltemp Sensors Inc. 9245-34A Avenue
A11-16-J-USS-6" (miniature miniplug type J thermocouple, ungrounded junction)	Edmonton, Alberta T6E 5T6 (403) 463-7035
1237-6-J—connectors mini stripanel (for J-type thermocouples)	
1210-J—mini jack connector	
1260-J—mini plug connector	
640-JX-PC-PC20 (J-thermocouple wire)	

**Appendix D**

**Contour Plotting Programs and Graphing Procedures**

**Table of Contents for Appendix D**

1. INTRODUCTION.....	182
2. CONNECTING TO MTS FROM MICROCOMPUTERS .....	182
2.1 Signing on to MTS via an IBM Personal Computer.....	182
2.2 Signing on to MTS via a Macintosh Computer.....	182
3. GENERATING DISSPLA PLOTS FROM AN IBM TERMINAL.....	183
3.1 Top View Temperature Profiles.....	183
3.2 Cross-Section Temperature Profiles.....	185
4. RUNNING TELL-A-GRAF PLOTS FROM AN IBM .....	186
5. PLOTTING FROM A MACINTOSH TO AN HP DEVICE .....	187
5.1 General Comments .....	187
5.2 Graphing Procedures for DISSPLA Plots using the Macintosh.....	188
5.3 Generating Tell-A-Graf Plots from the Macintosh.....	189
5.4 Cable Schematics .....	190
6. CONTOUR PLOT PROGRAMS.....	190
6.1 Top View Temperature Profiles.....	190
6.2 Injector to Producer Cross-Section Temperature Profiles.....	193
6.3 Macro Program.....	195
6.4 MTS Sigfile.....	196
7. DATA FILE CONSTRUCTION.....	196
7.1 General Procedure .....	196
7.2 Pore Volume Injected.....	197
7.3 Solvent Slug Calculation.....	197
7.4 Top View Data Files.....	198
7.5 Cross-Section Data Files.....	199

## 1. INTRODUCTION

The *DISSPLA* graphics package is used to generate the temperature contours for both the top view of the model and the model cross-section for each run. *DISSPLA* and Tell-A-Graf programs are all compiled in the MTS (Michigan Terminal System) main frame computer system. The Tell-A-Graf software package is used to plot additional experimental results, such as "Cumulative Oil Recovery versus Pore Volume Injected" and "Temperature-Viscosity Profile for Ideal and Actual Model Oil". Additional programs were written in a macro file in MTS to increase the efficiency of generating *DISSPLA* and Tell-A-Graf plots. Appendix B deals with the procedures required to produce many of the plots in this thesis.

## 2. CONNECTING TO MTS FROM MICROCOMPUTERS

### 2.1 Signing on to MTS via an IBM Personal Computer

- a) Turn on IBM Personal Computer screen and hard drive.
- b) Switch "Data Director" switch to position A (MTS).
- c) Type `cd\` to return to the main directory.
- d) Type `ctie`.
- e) Ensure that the Gandalf modem is set to '04' before turning on the switch in order to connect to MTS.
- f) Type `signon CSID` or `sig CSID`.  
 ~ Although MTS recognizes uppercase as well a lower case commands, the *DISSPLA* and Tell-A-Graf packages require all instructions be typed in uppercase letters.
- g) Type 'password' when prompted by MTS.

### 2.2 Signing on to MTS via a Macintosh Computer

- a) Turn on Macintosh computer and its hard drive.
- b) Switch "Data Director" switch to position A (MTS).
- c) Open the communications folder containing the program Mactie by double clicking on the icon.
- d) Open the **MACTIE** application.
- e) Again, as in the case of the IBM, ensure that the Gandalf modem is set to '04' before turning on its switch to connect to MTS.
- f) Type `signon CSID` or `sig CSID`, followed by the 'password'.

### 3. GENERATING DISSPLA PLOTS FROM AN IBM TERMINAL

#### 3.1 Top View Temperature Profiles

- a) Type `cplot` then press RETURN, hereafter denoted as Ret.

*Screen output lists the cplot portion of the Macro file located in Section 6.3:*

ENTER THE NAME OF THE \*DISSPLA FILE:

- b) Type the name of the DISSPLA file in Section 6.1 which will generate a top view profile, TOPVIEW, and enter Ret.

*Screen output is:*

ENTER THE NAME OF THE DATA FILE:

- c) Type the name of the desired data file, such as **R39.025** and press Ret.

*Screen output lists a portion of the TOPVIEW program which can be edited:*

```
CALL HEADIN ('(T)EMPERATURE (P)ROFILE FOR$',100,1.0,4)
CALL HEADIN ('0.25 (P)ORE (V)OLUMES (I)NJECTED$',100,1.0,4)
CALL HEADIN ('$',100,1.0,4)
CALL HEADIN ('$',100,1.0,4)
CALL XNAME ('(H)ORIZONTAL (M)ODEL (L)ENGTH, INCHES',37)
CALL YNAME ('(V)ERTICAL (M)ODEL (L)ENGTH, INCHES',35)
CALL INTAXS
CALL GRAF (0,4,32,0,4,32)
CALL MESSAG ('(F)IGURE 1: (R)UN 39$,100,1.8,7.0)
```

- d) Cursor to the headings in bold letters and edit them as required for each run.  
e) Press **CRTL** and Ret simultaneously to quit the visual edit mode in MTS.

*Screen output is:*

```
$EMPTY -LOAD#
EMPTY -PLOT
EMPTY -PLOTHP
RUN *FORTG SCARDS=TOPVIEW
RUN -LOAD#+*DISSPLA 5=X39.025 9=-PLOT
RUN *PLOTSEE T=5 PAR=-PLOT HP7475F PAGEFILL RETURN
EDIT -PLOTHP D1
```

*Upon the completion of the DISSPLA program, the screen will list the following before the plot file is transferred to the IBM hard drive:*

```
END OF DISSPLA 9.0 -- 4881 VECTORS GENERATED IN 1 PLOT FRAMES,
PROPRIETARY SOFTWARE PRODUCT OF ISSCO,SAN DIEGO,CA. 11608
```

VIRTUAL STORAGE REFERENCES; 7 READS; 0 WRITES.:1 LINE DELETED

File transfer is initiated by the following command:

CONTROL \*MSOURCE\* FT BREP MTS -PLOTHP C:R39.025

Upon the completion of the file transfer from MTS to the IBM, the screen output is:

#:FILE TRANSFER - HOST SIDE NORMAL EXIT

- f) Type **%EX** and **Ret** to exit pctie and to enter DOS.
- g) Turn "Data Director" switch to position B (Hewlett Packard 7550A Plotter).
- h) Type **DIR** and **Ret** to check the remaining amount of disk space in the hard drive and to confirm if the file has been transferred successfully to the main directory. There should be a plotter file in the main directory called **R39.025**.
- i) Type **DOPLOT** and **Ret** to initialize the HP plotter.
- ~~ Doplot and the communications commands are software programs installed in the main directory of the IBM which permit the plotter and computer to interface.

Screen output is:

MODE COM1:9600,N,8,1,P

- j) Type **COPY filename1 COM1** and **Ret**.
  - ~~ In this case, type: **COPY R39.025 COM1**
  - ~~ The HP 7550A should begin plotting the temperature contours immediately. If it does not,
    - i) check the printer -- IBM connection to ensure that it is securely attached
    - ii) check to see if the paper has been fed properly. Usually, the paper needs to be reloaded every time the HP7550A is turned on.
- k) To reload the plotter paper automatically, type **COPY PAGE COM1**. Page is simply a filename in the main directory containing the command "**PG1;**" which will prompt the plotter to feed one sheet of paper through the tray thereby loading the paper. If it is desired to feed two sheets through the plotter, then replace "**PG1;**" by "**PG2;**".
  - ~~ To reload the paper manually, press the **LOAD/UNLOAD** button on the HP plotter.

### 3.2 Cross-Section Temperature Profiles

The procedure for generating injector to producer cross-section profiles is the essentially the same as the one used in Section 3.1 to plot top view temperature profiles, with the exception of a few minor changes listed in this section. For detailed explanations of the of the plot generation commands, please consult Section 3.1.

- a) Type **cplot** then press **RETURN**, hereafter denoted as **Ret**.

Screen output lists the cplot portion of the Macro file located in Section 6.3:

ENTER THE NAME OF THE \*DISSPLA FILE:

- b) Type the name of the *DISSPLA* file in Section 6.2 which will generate a cross-section profile, **XSECTION**, and enter **Ret**.

Screen output is:

ENTER THE NAME OF THE DATA FILE:

- c) Type the name of the desired data file, such as **X74.075** and press **Ret**.

Screen output lists a portion of the XSECTION program which can be edited:

```
CALL HEADIN ('(F)IGURE 7: (R)UN 74 (T)EMP (P)ROFILES$',
+100,1.0,4)
CALL HEADIN ('(I)NJECTOR TO (P)RODUCER (C)ROSS-(S)ECTIONS$',
+-100,-1.0,4)
CALL HEADIN ('0.75 (P)ORE (V)OLUMES (I)NJECTED$',
+100,0.8,4)
CALL HEADIN (' $',100,1.2,4)
CALL XINTAX
CALL GRAF (0.,5.,45.,0.,5,2.5)
```

- d) Cursor to the headings in bold letters and edit them as required for each run.  
e) Press **CRTL** and **Ret** simultaneously to quit the visual edit mode in MTS.

Screen output is:

```
$EMPTY -LOAD#
EMPTY -PLOT
EMPTY -PLOTHP
RUN *FORTG SCARDS=XSECTION
RUN -LOAD#+*DISSPLA 5=X74.075 9=-PLOT
RUN *PLOTSEE T=5 PAR=-PLOT HP7475F PAGEFILL RETURN
EDIT -PLOTHP D1
```



Upon the completion of the DISSPLA program, the screen will list the following before the plot file is transferred to the IBM hard drive:

END OF DISSPLA 9.0 -- 4881 VECTORS GENERATED IN 1 PLOT FRAMES,  
 PROPRIETARY SOFTWARE PRODUCT OF ISSCO,SAN DIEGO,CA. 11608  
 VIRTUAL STORAGE REFERENCES; 7 READS; 0 WRITES.:1 LINE DELETED

File transfer is initiated by the following command:

CONTROL \*MSOURCE\* FT BREP MTS -PLOT HP C:X39.025

Upon the completion of the file transfer from MTS to the IBM, the screen output is:

#:FILE TRANSFER - HOST SIDE NORMAL EXIT

- f) Type **%EX** and **Ret** to exit pctie and to enter DOS.
- g) Turn "Data Director" switch to position B (Hewlett Packard 7550A Plotter).
- h) Type **DIR** and **Ret**. There should be a plotter file in the main directory called **X39.025**.
- i) Type **DOPLOT** and **Ret** to initialize the plotter.
- j) Type **COPY filename1 COM1** and **Ret**.  
 ~ In this case, type: **COPY X74.075 COM1**
- k) To reload the plotter paper automatically, type **COPY PAGE COM1** or press the **LOAD/UNLOAD** button on the HP plotter.

#### 4. RUNNING TELL-A-GRAF PLOTS FROM AN IBM

All Tell-A-Graf plots are generated through MTS. The signon procedure is the same as the one described in Section 1.

- a) If the computer terminal has graphics capability, such as a video card for the IBM or is a Macintosh computer, the Tell-A-Graf plot may be viewed on the computer screen through MTS prior to sending it to the plotter. This is done by typing **%T4010** to enter the graphics mode.
- b) Type **TAG** to run the Tell-A-Graf program.  
 ~ TAG is a source file listed Section 6.3.  
 ~ If the TAG is not available in the Macro program, then it is necessary to type:  
**RUN \*TELLAGRAF.**
- c) Type **include "plot name"**. Then **Ret**.
- d) Press **Ret** again.
- e) Type **send**.

Output is:

- 9 was referenced, but unit is not set.  
 Enter a new file/device name, "CANCEL", or "HELP".  
 ?  
 Type -AA and Ret (-AA is a temporary file to which the plot is sent).  
 f) Type quit. and Ret.

Output is:

END OF TELLAGRAF 4.0 -- 3312 VECTORS GENERATED IN 2 PLOT  
 FRAMES.  
 PROPRIETARY SOFTWARE PRODUCT OF ISSCO, SAN DIEGO, CA.  
 #08:07:23 T=1.234 RC=0

- g) Press CTRL and ESC to return to the MTS write screen.  
 h) Type the following:  
**RUN \*PLOTSEE T=5 PAR=-AA HP7475f PAGEFILL RETURN** and  
 then press Ret.

Output is:

...For information about the placement of HP7475 plots,  
 ...see the file "LEEN:PLOTSEE.NOTE".  
 #08:11:05  
 End of plot file  
 #08:11:12 T=0.0462 RC=0

- i) Type **EDIT -PLOTHP DEL 1** and Ret.  
 j) Type **%FT BREP MTS -PLOTHP C:plot name** and then Ret.  
 k) Type **%EX** to exit MTS.  
 l) Turn "Data Director" switch to position B (Plotter).  
 m) Type **DOPLOT** for plotter initialization.  
 n) Type **COPY plot name COM1** to print the graph.  
 o) Type **COPY PAGE COM1** to reload the paper.

## 5. PLOTTING FROM A MACINTOSH TO AN HP DEVICE

### 5.1 General Comments

To plot any graphs using a Hewlett Packard plotter, one requires a copy of the "File to HP7475" plotting program (which is available through the University of Alberta Computing Services), a MacWrite application (Version 5.01 and up) and a cable with the

same internal components as an Imagewriter cable are required in order to be able to plot graphs from the Macintosh to an HP plotter.

The "mock" Imagewriter cable, as shown schematically in Section 5.4, connects the Macintosh to the plotter and attempts to generate the illusion to the Macintosh that the HP plotter is really an Imagewriter. Thus, to plot a graph, one chooses the Imagewriter printer device and then opens the "File to HP7475" application which will allow the user to open the desired plot file, and then print the MacWrite document. The computer believes that it is printing a MacWrite document using an Imagewriter when in reality it is sending the material to an HP the plotter. Although the programs are written for the HP7475, they have also been tested successfully on the HP7550A and HP7470A.

MACPLOT is a macro program in MTS which will automatically compile and transfer any *DISSPLA* program to a Macintosh computer. MACPLOT is the Macintosh equivalent to the CPLOT program used for the IBM. Tell-A-Graf plots are first generated using the TAG macro and can be transferred using the TELPLOT macro. To avoid redundancy, the Macintosh commands are listed briefly in Section 5.2 and 5.3 without any detailed comments. All of the macros are listed in Section 6.3.

The primary difference between plotting from an IBM or Macintosh is that the IBM transfers the plot file in binary code (BREP) whereas the Macintosh appends the file (BAPP) during any transfer. In addition, sometimes the Mactie will prompt the user for a device, at which time "HP7475" will be typed. Hence, the command used to transfer a \*plotsee file is

```
%FT BAPP MTS -PLOTHP {filename}
```

To send an MTS file via Mactie to the LaserWriter, simply type:

```
%FT MTS {MTS file to be printed} {Name of the printer file}
```

One will then quit Mactie, without necessarily signing off, and open the printer file, which is formatted as a MacWrite document, and print the file in the normal manner.

## 5.2 Graphing Procedures for *DISSPLA* Plots using the Macintosh

- a) Type **macplot** then press **Ret.**

- b) Type the name of the *DISSPLA* file when prompted, TOPVIEW for top view temperature contour profiles and X-SECTION for a cross-section profile, followed by entering **Ret**.
  - c) Type the name of the desired data file, such as **X74.075** and press **Ret**.
  - d) Cursor to the headings in bold letters and edit them as required for each run.
  - e) Press **command** and **Ret** simultaneously to quit the visual edit mode in MTS. The \*plotsee program and the file transfer commands are sourced automatically from the Macplot macro in Section 6.3 so there is no need to type any additional command.
- ~ Occasionally, MTS asks: "What type of device are you on?". If this occurs, type: HP7475.

*The file transfer is initiated by the following command:*

```
CONTROL *MSOURCE* FT BAPP MTS -PLOTHP X39.025
```

- f) Type **%EX** and **Ret** or select quit to exit Mactie.
  - g) Choose Imagewriter printer device.
  - h) Open File to **HP7475** application.
  - i) Select and open the desired plot file when prompted, in this case, X39.025 which is now in a MacWrite document.
- ~ The Hewlett Packard plotter should begin plotting immediately otherwise check cable connections and open the plot file in MacWrite to ensure that the file was transferred properly and its contents are complete.

### 5.3 Generating Tell-A-Graf Plots from the Macintosh

- a) The Tell-A-Graf plot may be viewed on the computer screen through MTS prior to sending it to the plotter by selecting or typing **%T4010** to enter the graphics mode.
- b) Type **TAG** to run the Tell-A-Graf program.
- c) Type include "*plot name*". Then **Ret**.
- d) Press **Ret** again.
- e) Type **send**.
- f) Type **quit**. and **Ret**.
- g) Press **command** and **Ret** to return to the MTS write screen.
- h) Type **source sigfile**.
- i) Type **TELPLOT** which will source the following commands:

Output is:

TYPE THE NAME OF THE \*TELLAGRAF FILE TO BE TRANSFERRED:

- j) Type any name, for simplicity the title of the Tell-A-Graf file, which will correspond the file name in MacWrite to which the data will be transferred.

The resulting output will be:

```
RUN *PLOTSEE T=5 PAR=-AA HP7475f PAGEFILL RETURN
EDIT -PLOTHP DEL 1
%FT BAPP MTS -PLOTHP *TELLAGRAFILE
```

- k) Type %EX or command Q to exit MTS.  
l) Repeat Steps (h) and (i) in Section 5.2 to send file to HP plotter.

**5.4 Cable Schematics**

Because the objective used in sending Tell-A-Graf and *DISSPLA* plots to an HP plotter is to mislead the Macintosh computer into believing that the HP plotter is really an Imagewriter, certain cables must be constructed in the manner described in Figure D.1.

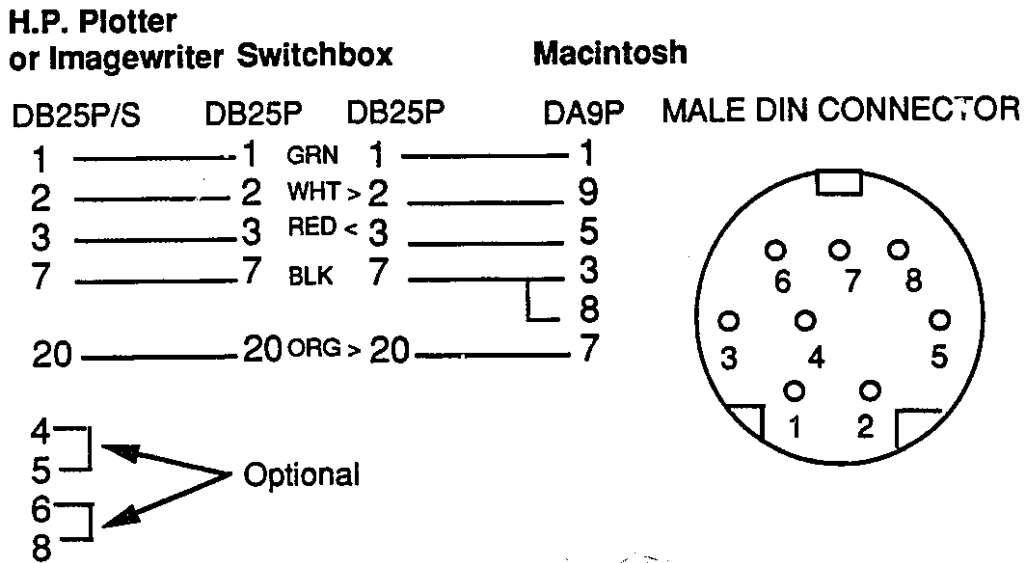
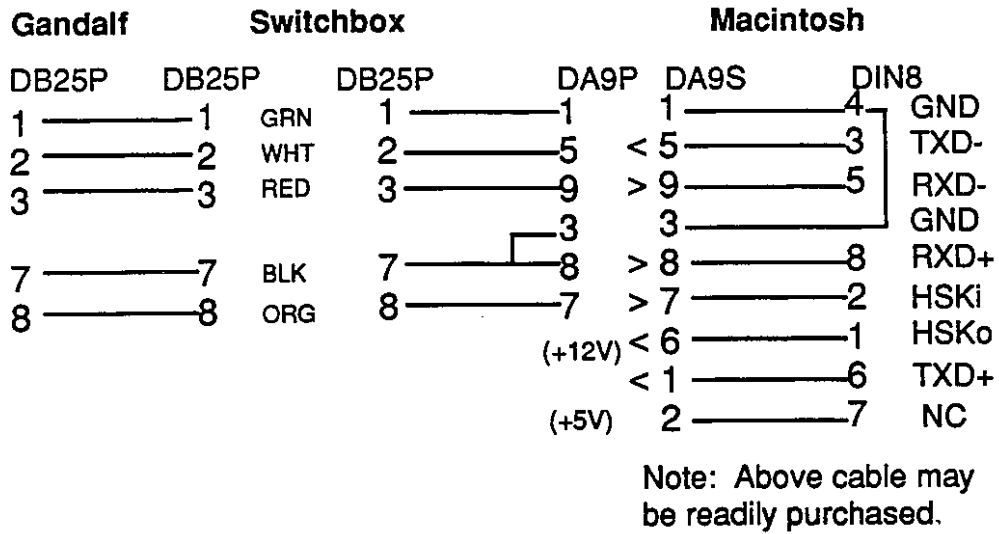
**6. CONTOUR PLOT PROGRAMS****6.1 Top View Temperature Profiles**

C The following DISSPLA program is used to generate a contour plot of two sets of  
C X, Y, Z data, with Z representing the temperature at the given (X, Y) coordinates.  
C

```
LOGICAL *1 FREE (1) /*'/
DIMENSION ZMAT (5,5)
DIMENSION IPAK (1000)
REAL DUMMY (2) /0.,0./
COMMON WORK (20000)
CALL PAGE (8.5,11.)
CALL PHYSOR (2.0,2.5)
CALL AREA2D (5.5,5.5)
CALL FRAME
CALL DUPLX
CALL BASALF ('L/CSTD')
CALL MIXALF ('STANDARD')
```

C  
C The following commands are used to generate both the text material and the plot  
C axes:  
C

```
CALL HEADIN ('(T)EMPERATURE (P)ROFILE FOR$',100,1.0,4)
CALL HEADIN ('1.50 (P)ORE (V)OLUMES (I)NJECTED$',100,1.0,4)
```



Cable schematics reprinted with the permission of:  
 R.K. Stefaniuk, E.E.T., U of Alberta Technical Services  
 1990-01-10

Figure D.1: Cable Schematics for Macintosh Computer to Modem/Plotter.

```

CALL HEADIN ('$',100,1.0,4)
CALL HEADIN ('$',100,1.0,4)
CALL XNAME ('(H)ORIZONTAL (M)ODEL (L)ENGTH, INCHES',37)
CALL YNAME ('(V)ERTICAL (M)ODEL (L)ENGTH, INCHES',35)
CALL INTAXS
CALL GRAF (0,4,32,0,4,32)
CALL MESSAG ('(F)IGURE 4: (R)UN 104$,100,1.8,7.0)
CALL MESSAG ('(S)TEAMFLOOD OF (B)OTTOM (W)ATER (M)ODELS',
+100,1.0,6.7)

```

C  
C  
C

These DISSPLA commands are used to label the injection points:

```

CALL HEIGHT (0.12)
CALL MESSAG ('(I)NJECTION (W)ELLS$', 100,4.4,-0.7)
CALL MESSAG ('(P)RODUCTION (W)ELLS$',100,0.0,5.775)

```

C  
C  
C  
C

These series of routines draw arrows from the two labels described above to the injection and production wells, respectively:

```

CALL VECTOR (5.5,-.5,5.5,-.25,2201)
CALL VECTOR (0.0,5.75,0.0,5.5,2201)

```

C  
C  
C

The following series generates legend text material:

```

CALL LINE$P (2.0)
CALL LINE$ ('(U)PPER (M)ODEL (T)EMPERATURE (C)$',IPAK,1)
CALL LINE$ ('(L)OWER (M)ODEL (T)EMPERATURE (C)$',IPAK,2)
CALL BGNMAT (5,5)
DO 20 J=1,2
  READ (5,FREE) N
  DO 10 I=1,N
    READ (5,FREE) X,Y,Z
    Z=Z+3.0
10  CALL GETMAT (X,Y,Z,1,0)
    CALL ENDMAT (ZMAT,0)

```

C  
C  
C

Contouring routines:

```

CALL BCOMON (10000)
CALL CONMAK (ZMAT,5,5,5.)
CALL CONMIN (1.5)
CALL CONDIG (0)
IF (J.EQ.2) GO TO 15
CALL SETCLR ('BLUE')
CALL CONLIN (0,'SOLID','LABELS',1,10)
GO TO 16
15  CALL SETCLR ('RED')
    CALL CONLIN (0,'DASH','LABELS',1,9)
16  CONTINUE
    CALL RASPLN (0.2)
    CALL CONTUR (1,'LABELS','DRAW')

```

C  
20  
C

CONTINUE

C The following commands generate a legend with the appropriate colour markers:  
C

```
CALL SPCMOD
CALL LEGLIN
CALL CURVE (DUMMY,DUMMY,2,0)
CALL CURVE (DUMMY,DUMMY,2,0)
CALL MYLEGN (' ',1)
CALL LEGEND (IPAK,2,0.,-1.)
CALL ENDPL (0)
CALL DONEPL
STOP
END
```

C This subroutine is used to define different textures between the line types and  
C colours:  
C

```
1 SUBROUTINE MYSPEC (IENTRY)
GO TO (1,2) , IENTRY
1 CALL SETCLR ('BLUE')
RETURN
2 CALL DASH
CALL SETCLR ('RED')
RETURN
END
```

## 6.2 Injector to Producer Cross-Section Temperature Profiles

C The following DISSPLA program is used to generate a temperature profile through  
C a cross-section of the model from the injection well to the production well.  
C

```
LOGICAL *1 FREE (1) /**/
DIMENSION ZMAT (7,7)
DIMENSION IPAK (400)
COMMON WORK (20000)
CALL DSPDEV ('PLOTTER')
CALL PAGE (11.,8.5)
CALL PHYSOR (1.8,2)
CALL AREA2D (7.5,4.)
CALL FRAME
CALL DUPLX
CALL BASALF ('L/CSTD')
CALL MIXALF ('STANDARD')
CALL XNAME (('D)ISTANCE, INCHES$',100)
CALL YNAME (('V)ERT. (S)CALE = 10X (H)OR. (S)CALES$',100)
CALL HEADIN (('F)IGURE 3: (R)UN 74 (T)EMP (P)ROFILES$',
+100,1.0,4)
CALL HEADIN (('I)NJECTOR TO (P)RODUCER (C)ROSS-(S)ECTIONS$',
+-100,-1.0,4)
CALL HEADIN ('0.75 (P)ORE (V)OLUMES (I)NJECTED$',
+100,0.8,4)
CALL HEADIN ('$',100,1.2,4)
CALL XINTAX
CALL GRAF (0.,5.,45.,0.,5,2.5)
```



C  
C  
C  
C

The following commands generate arrows and text material which label the injection and production points:

```
CALL HEIGHT (0.12)
CALL MESSAG ('(I)NJECTION (W)ELLS', 100,0.0,-0.7)
CALL MESSAG ('(P)RODUCTION (W)ELLS',100,6.2,-0.7)
CALL VECTOR (0.0,-0.5,0.0,-0.25,2201)
CALL VECTOR (7.5,-0.5,7.5,-0.25,2201)
```

C  
C  
C  
C  
C  
C  
C  
C  
C  
C

The next section of commands read in the data. Note that the X-coordinates were measured from the top view temperature profile described in Section 6.1 using an Engineers scale. The 1:60 scale was chosen so that the length from the injection well to the production well was 46.2 units. Thus, there was no need to modify the X-coordinates since the actual model length was 45.2548 inches. In other words, 1 unit (on a 1:60 Engineers scale)  $\approx$  1 inch (on the model).

The Z-coordinates are 0.8333 and 1.6667 inches for the lower and upper layer of thermocouples, respectively.

```
CALL BGNMAT (7,7)
  READ (5,FREE) N
  DO 10 I=1,N
    READ (5,FREE) X,Y,Z
10  CALL GETMAT (X,Y,Z,1,0)
    CALL ENDMAT (ZMAT,0)
```

C  
C  
C

Contouring routines:

```
CALL BCOMON (10000)
CALL CONMAK (ZMAT,7,7,5.)
CALL CONMIN (1.5)
CALL CONDIG (0)
CALL SETCLR ('RED')
CALL CONLIN (0,'SOLID','LABELS',1,10)
CALL RASPLN (0.2)
CALL CONTUR (1,'LABELS','DRAW')
CALL ENDPL (0)
CALL DONEPL
STOP
END
```

### 6.3 Macro Program

```
1 TAG          1000
2 BANK         1100
3 CPLOT        1200
4 MACPLOT      1300
5 TELPLOT      1400
6 /END
1000 MACRO TAG
1001 >*
1002 >*      The tag macro invokes the Tellagraf program
```

```

1003 >*
1004 $RUN NEW:TELLAGRAF
1005 ENDMACRO
1100 MACRO BANK
1101 >*
1102 >*   The bank macro invokes the Tellabank program
1103 >*
1104 $RUN NEW:TELLABANK
1105 ENDMACRO
1200 MACRO CPLOT
1201 >*
1201 >*   The cplot macro prompts for the Fortran DISSPLA file and a data file for
1203 >*   contouring. It then compiles the DISSPLA program which produces a plot
1204 >*   file in '-plot'. The '-plot' file is then converted to an HPGL plot file for the
1205 >*   HP7475A plotter using the '*plotsee' program. Then, the first line of this
1206 >*   file is deleted so that it can be transferred to the HP7550 or any HP plotters
1207 >*   other than the HP7475A. The resulting file, '-plothp', is then sent to the
1208 >*   IBM PC to the 'C:' drive under the name of the data file.
1209 >*
1210 define dispfile
1211 define datafile
1212     write "ENTER THE NAME OF THE *DISSPLA FILE:"
1213     read dispfile from *source*
1214     write "ENTER THE NAME OF THE DATA FILE:"
1215     read dispfile from *source*
1216 $EDIT {dispfile} V18
1217 IF FILE ("-LOAD#") EXISTS, $EMPTY -LOAD#
1218 IF FILE ("-PLOT") EXISTS, $EMPTY -PLOT
1219 IF FILE ("-PLOTHP") EXISTS, $EMPTY -PLOTHP
1220 $RUN *FORTG SCARDS={dispfile}
1221 IF RUNRC > 0, EXIT
1222 $RUN -LOAD#+*DISSPLA 5={datafile} 9=-PLOT
1223 $RUN *PLOTSEE T=5 PAR=-PLOT HP7475F PAGEFILL RETURN
1224 $EDIT -PLOTHP D1
1225 $CONTROL *MSOURCE* FT BREP MTS -PLOTHP C:{datafile}
1226 >ENDMACRO
1300 MACRO MACPLOT
1301 >*
1301 >*   The macplot macro prompts for the Fortran DISSPLA file and a data file for
1303 >*   contouring. This program is the Macintosh equivalent of the CPLOT (IBM)
1304 >*   macro program which is used to run and transfer the contour plot file
1305 >*   generated from the '*plotsee' program to the HP7550 plotter. The resulting
1306 >*   file, -plothp, is sent to the Macintosh hard drive in the form of a MacWrite
1307 >*   document file which uses the same title as the datafile. To run the program
1308 >*   successfully, one must have MacWrite as well as the corresponding cables.
1309 >*
1310 define dispfile
1311 define datafile
1312     write "ENTER THE NAME OF THE *DISSPLA FILE:"
1313     read dispfile from *source*
1314     write "ENTER THE NAME OF THE DATA FILE:"
1315     read dispfile from *source*
1316 $EDIT {dispfile} V18
1317 IF FILE ("-LOAD#") EXISTS, $EMPTY -LOAD#

```

```

1318 IF FILE ("-PLOT") EXISTS, $EMPTY -PLOT
1319 IF FILE ("-PLOTHP") EXISTS, $EMPTY -PLOTHP
1320 $RUN *FORTG SCARDS={dispfile}
1321 IF RUNRC > 0, EXIT
1322 $RUN -LOAD#+*DISSPLA 5={datafile} 9=-PLOT
1323 $RUN *PLOTSEE T=5 PAR=-PLOT HP7475F PAGEFILL RETURN
1324 $EDIT -PLOTHP D1
1325 $CONTROL *MSOURCE* FT BAPP MTS -PLOTHP {datafile}
1326 >ENDMACRO
1400 MACRO TELPLOT
1401 >*
1401 >* The telplot macro will transfer the compiled tellagraf program resulting
1403 >* from the tag macro to a MacWrite document located in the Macintosh
1404 >* hard drive in order to be sent to a HP plotter.
1405 define tellagrafile
1406 write "ENTER THE NAME OF THE TELLAGRAF FILE TO BE
1407 TRANSFERRED:"
1408 >*
1409 $RUN *PLOTSEE T=5 PAR=-PLOT HP7475F PAGEFILL RETURN
1410 $EDIT -PLOTHP D1
1411 $CONTROL *MSOURCE* FT BAPP MTS -PLOTHP {tellagrafile}
1412 >*
1413 >ENDMACRO

```

#### **6.4 MTS Sigfile**

In order to be able to access the Macro file from MTS, it is essential to include the following commands in the MTS sigfile:

```

SET MACROS=OFF
SET MACROS=OFF
SET MACROS=ON
>SET VAR MACLIB(1)="MACLIB"

```

where MACLIB(1) = refers to the macrolibrary file 1 to be called  
MACLIB = the name of the macrolibrary file 1 containing the  
programs to be called and are listed in Section 6.3

### **7. DATA FILE CONSTRUCTION**

#### **7.1 General Procedure**

Lotus 1-2-3 is used to analyze the experimental data generated from Labtech Notebook. The following types of data calculations which serve the basis for contour plots are explained in detail in this section:

- 7.2 Pore Volume Injected Calculations
- 7.3 Solvent Slug Calculations based on %PV Injected

- 7.4 Top View Temperature Contour Data File Formulation  
 7.5 Injector to Producer Temperature Cross-Section Contour Data File Formulation

## 7.2 Pore Volume Injected

The objective of this section is to examine the procedure used to calculate the time corresponding to a specified injected pore volume.

**Let:**

%PV	=	the amount of pore volume injected at a certain time, t
V	=	the pore volume of the bead pack, cc
q	=	total steam injection rate, cc/min
t	=	the time at which %PV pore volume injected is obtained, minutes

**Assume:** V, q and %PV are given.  
 where, %PV is chosen arbitrarily at an interval where a contour plot is desired, such as %PV = 0.75 PV or %PV = 1.50 PV.

Thus, t can be determined: 
$$t = \frac{(\%PV) \times (V)}{q}$$

After calculating the time it takes to reach a desired pore volume, simply extract the thermocouple temperature values from Lotus 1-2-3 at that time to obtain the necessary information for the temperature profiles.

### Sample Calculation 1:

**Given:**

%PV	=	0.25
V	=	15150 cc
q	=	230.1 cc/min

**Find:** t at 0.25 PV steam injected

$$t = \frac{(\%PV) \times V}{q_{\text{total}}} = \frac{(0.25) \times (15150 \text{ cc})}{230.1 \text{ cc / min}} = 16.26 \text{ minutes} \cong 16.5 \text{ min.}$$

The calculated time value is rounded up to the next 0.5 minutes since the data in the steamflood experiments was formatted to record data every 30 seconds.

## 7.3 Solvent Slug Calculation

In solvent slug calculations, the objective is to determine the time required to inject a specified amount of solvent into the physical model which is measured as a percentage of the total pore volume of the model. The amount of solvent that is required to be injected is calculated using the method described in Section 7.2.

Let:            %SPV =        the percentage of solvent injected into the pore volume of the model  
                      V        =        the pore volume of the bead pack, cc  
                       $q_{\text{solvent}}$  =        solvent flow rate, cc/min  
                       $t_{\text{solvent}}$  =        the time at which %SPV is injected into the model, min

Assume:        %SPV, V and  $q_{\text{solvent}}$

Thus,  $t_{\text{solvent}}$  can be determined:      $t_{\text{solvent}} = \frac{(\%SPV) \times (V)}{q_{\text{solvent}}}$

#### Sample Calculation 2:

Given:            V            = 15340 cc  
                       $q_{\text{solvent}}$  = 200 cc/min  
                      %SPV     = 10%  
Find:             $t_{\text{solvent}}$  at 10% PV injected

$$t = \frac{(0.10) \times (15340 \text{ cc})}{200 \text{ cc / min}} = 7.67 \text{ minutes} \cong 8.0 \text{ min.}$$

### 7.4 Top View Data Files

Selected experimental data from Lotus-1-2-3 are transferred to the Michigan Terminal System (MTS) manually. Top view data files are typed in R##.### files in the following format:

# thermocouples in

TOP layer of model, I2

x-coordinate of

TOP thermocouples, F6.3

y-coordinate of

TOP thermocouples, F6.3

MEGADAC value as

listed in RUNS D.##, F6.3

# thermocouples in

BOTTOM layer of model, I2

x-coordinate of

BOTTOM thermocouples, F6.3

y-coordinate of

BOTTOM thermocouples, F6.3

MEGADAC value as

listed in RUNS D.##, F6.3

1

-----

10

-----

20

-----

Column

N.B: \*Do not double space the data.

Sample of Top Profile Data File

18		
32.000	0.0000	103.4
23.63	8.50	50.0
15.75	9.00	38.2
7.50	8.75	2.2
4.00	7.50	2.1
8.125	4.00	1.6
13.125	12.5	13.4
8.438	20.0	2.9
13.305	27.725	2.3
3.75	24.375	3.6
12.125	18.375	11.2
20.000	24.063	6.4
28.063	24.125	4.1
25.125	28.000	3.5
19.250	20.000	11.8
24.625	12.250	15.7
18.750	4.00	13.9
0.000	32.000	4.0
17		
32.000	0.0000	103.4
28.000	7.3750	99.7
20.063	7.563	14.1
12.125	7.188	39.2
13.375	3.750	13.2
8.313	12.0	17.1
13.375	20.313	20.0
8.305	28.0	1.8
4.00	28.00	2.8
7.75	23.5	3.9
15.75	23.5	5.5
28.000	28.00	3.1
19.250	28.00	4.2
25.125	20.000	17.1
18.438	12.125	36.9
24.000	4.000	84.3
0.000	32.000	4.0

7.5 Cross-Section Data Files

Injector to producer temperature cross-section data files are denoted by the format X##.### in MTS and are inputted as follows:

\*Total number of  
 data readings from top  
 view temperature plot, I2



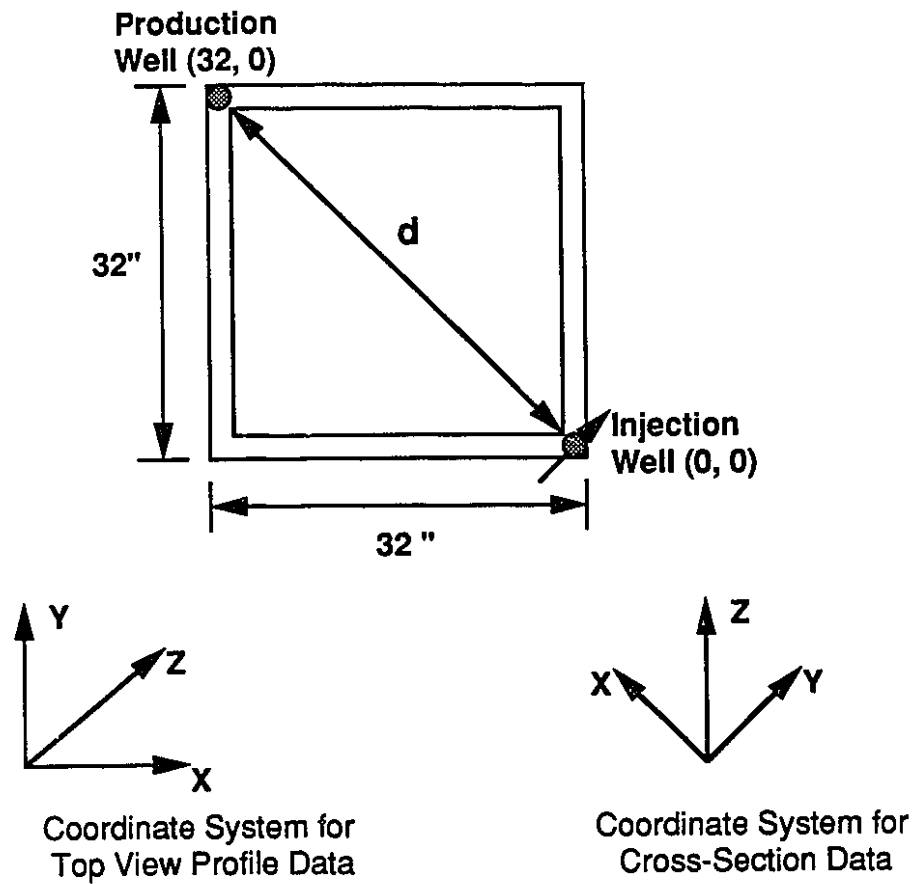


Figure D.2: A Schematic of the Top View of the Aberfeldy Model Showing the Coordinate Systems used for the DISSPLA data files.



8.3	0.8333	70.0
9.4	0.8333	65.0
10.7	0.8333	60.0
11.9	0.8333	55.0
13.0	0.8333	50.0
14.2	0.8333	45.0
15.3	0.8333	40.0
16.6	0.8333	35.0
17.8	0.8333	30.0
20.5	0.8333	25.0
24.4	0.8333	20.0
26.8	0.8333	15.0
29.0	0.8333	10.0
32.6	0.8333	5.0

Additional Comments:

- ~ Do not double space the data.
- ~ According to the XSECTION program listed in Section 6.2, an Engineers Scale was chosen such that the diagonal length from the injection to production well is 46.2 inches, which was the closest approximation to the actual model diagonal length of 45.25 inches. By trial and error, the only scale that satisfies this criteria is the 1:60 Engineers Scale. In other words, since  $d^2 = (32 \text{ in.})^2 + (32 \text{ in.})^2$ , the hypotenuse is therefore,  $d = 45.2548 \text{ in.}$  Hence, the best fit scale is the 1:60 scale:  
 $d = 46.2 \text{ units} \cong 45.2548 \text{ inches}$
- ~ Figure D.2 is a schematic diagram of the physical model shows the method used to determine the correct engineering scale used in the cross-section plots. The coordinates are written as (X, Z) because the Y coordinate is zero for all injector to producer temperature contour plots; that is, since  $(X, Y, Z) = (X, 0, Z)$ , for simplicity, let  $(X, 0, Z) = (X, Z)$ .

**Appendix E**

**Production Histories of Experiments Conducted**

Table E.1

## Run 70A: Waterflood prior to a Steamflood in a Homogeneous Model.

HC Pore Volume:	11700 cc	Type of Oil Used:	Faxam-100
Pore Volume:	13310 cc	Initial Model Temperature:	3°C
Bulk Volume:	42005 cc	Water Feed Flow Rate:	230.2 cc/min
Porosity:	31.7%	Initial Oil Saturation:	87.9%
Water Vol. Injected:	27818 cc (2.09 PV)	Initial Water Saturation:	12.1%

Net Oil Recovery : 27.7%      Final Oil Saturation: 63.6%

Cylinder No.	Total Vol. Produced (cc)	Instantaneous Oil Prod. (cc)	Cumulative Oil Recovery (cc)	Cum. Oil Rec. %OoIP	Instantaneous Produced WOR		Sample Vol. Oleic Phase	Cum. PV Injected
					Produced WOR	Oleic Phase		
1	1630	860	860	7.4	0.9	52.8	0.31	
2	2330	460	1320	11.3	4.1	19.7	0.41	
3	1955	295	1615	13.8	5.6	15.1	0.54	
4	2200	300	1915	16.4	6.3	13.6	0.96	
5	2110	230	2145	18.3	8.2	10.9	0.85	
6	1670	160	2305	19.7	9.4	9.6	0.96	
7	1810	155	2460	21.0	10.7	8.6	1.11	
8	1820	160	2620	22.4	10.4	8.8	1.25	
9	1960	230	2850	24.4	7.5	11.7	1.63	
10	1930	140	2990	25.6	12.8	7.3	1.79	
11	1970	140	3130	26.8	13.1	7.1	1.95	
12	1940	110	3240	27.7	16.6	5.7	2.09	

Table E.2

## Run 70B: Steamflood following a Waterflood in a Homogeneous Model.

HC Pore Volume:	7960 cc	Type of Oil Used:	Faxam-100
Pore Volume:	13310 cc	Initial Model Temperature:	3°C
Bulk Volume:	42005 cc	Water Feed Flow Rate:	213.21 cc/min
Porosity:	31.7%	Boiler Feed Flow Rate:	28.68 cc/min
Initial Oil Saturation:	59.8%	Total Flow Rate of Steam:	241.89 cc/min
Initial Water Saturation:	40.2%	Steam Volume Injected:	27951 cc (2.10 PV)

Net Oil Recovery: 11.43%      Final Oil Saturation: 52.97%

Cylinder No.	Total Vol. Produced (cc)	Instantaneous Oil Prod. (cc)	Cumulative Oil Recovery (cc)	Cum. Oil Rec. %OIP	Instantaneous Produced WOR	% Sample Oleic Phase	Cum. PV Injected
1	1990	10	10	0.1	198.0	0.5	2.44
2	1540	10	20	0.2	153.0	0.6	2.54
3	1640	20	40	0.3	81.0	1.2	2.64
4	1680	20	60	0.5	83.0	1.2	2.75
5	2400	40	100	0.9	59.0	1.7	2.92
6	1900	30	130	1.1	62.3	1.6	3.04
7	1880	40	170	1.5	46.0	2.1	3.19
8	1930	50	220	1.9	37.6	2.6	3.33
9	1850	70	290	2.5	25.4	3.8	3.47
10	1910	120	410	3.5	14.9	6.3	3.65
11	1950	120	530	4.5	15.3	6.2	3.80
12	1900	120	650	5.6	14.8	6.3	3.93
13	1810	130	780	6.7	12.9	7.2	4.09
14	1830	130	910	7.8	13.1	7.1	4.19

Table E.3

## Run 71: Gas injection followed by a Waterflood in a Homogeneous Model.

HC Pore Volume: 12970 cc      Type of Oil Used: Faxam-100  
 Pore Volume: 14382 cc      Initial Model Temperature: 3°C  
 Bulk Volume: 42005 cc      Water Feed Flow Rate: 241.89 cc/min  
 Porosity: 34.2%      N2 gas injection pressure: 1 psig  
 Initial Oil Saturation: 90.2%      Initial Gas Saturation: 2.43% (350 cc)  
 Initial Water Saturation: 7.4%      Water Volume Injected: 29269 cc (2.04 PV)

Net Oil Recovery: 19.51%      Final Oil Saturation: 72.59%

Cylinder No.	Total Vol. Produced (cc)	Instantaneous Oil Prod. (cc)	Cumulative Oil Recovery (cc)	%OOIP	Instantaneous Produced WOR	Sample Vol.	
						Oleic Phase	Cum. PV Injected
1	1280	495	495	3.8	1.6	38.7	0.49
2	1470	285	780	6.0	4.2	19.4	0.59
3	1740	265	1045	8.1	5.6	15.2	0.71
4	1855	270	1315	10.1	5.9	14.6	0.85
5	1895	215	1530	11.8	7.8	11.3	0.98
6	1750	180	1710	13.2	8.7	10.3	1.12
7	1800	160	1870	14.4	10.3	8.9	1.24
8	1700	125	1995	15.4	12.6	7.4	1.38
9	1780	140	2135	16.5	11.7	7.9	1.51
10	1580	120	2255	17.4	12.2	7.6	1.63
11	1750	90	2345	18.1	18.4	5.1	1.77
12	1740	100	2445	18.9	16.4	5.7	1.90
13	1705	85	2530	19.5	19.1	5.0	2.04

**Table E.4****Run 72A: Waterflood in a Homogeneous Model.**

HC Pore Volume:	12580 cc	Type of Oil Used:	Faxam-100
Pore Volume:	14100 cc	Initial Model Temperature:	3°C
Bulk Volume:	42005 cc	Water Feed Flow Rate:	213.21 cc/min
Porosity:	33.6%	N2 Gas Injection Pressure:	1 psig
Initial Oil Saturation:	89.2%	Water Volume Injected:	21747 cc (1.54 PV)
Initial Water Saturation:	10.8%		

**Net Oil Recovery: 19.67%****Final Oil Saturation: 71.67%**

Cylinder No.	Total Vol. Produced (cc)	Instantaneous Oil Prod. (cc)	Cumulative Oil Recovery (cc)	Cum. Oil Rec. %OOIP	Instantaneous Produced WOR	% Sample Vol. Oleic Phase	Cum. PV Injected
1	1860	660	660	5.2	1.8	35.5	0.26
2	1985	425	1085	8.6	3.7	21.4	0.36
3	1690	195	1280	10.2	7.7	11.5	0.47
4	1430	190	1470	11.7	6.5	13.3	0.56
5	1800	180	1650	13.1	9.0	10.0	0.68
6	1610	150	1800	14.3	9.7	9.3	0.79
7	1920	140	1940	15.4	12.7	7.3	0.92
8	1665	125	2065	16.4	12.3	7.5	1.04
9	1900	120	2185	17.4	14.8	6.3	1.16
10	1950	120	2305	18.3	15.3	6.2	1.30
11	2030	100	2405	19.1	19.3	4.9	1.44
12	1460	70	2475	19.7	19.9	4.8	1.54

**Table E.5**

**Run 72B: N2 Injection followed by Hot Water Injection in a Homogeneous Model which was Initially Waterflooded.**

HC Pore Volume:	10105 cc	Type of Oil Used:	Faxam-100
Pore Volume:	14100 cc	Initial Model Temperature:	12.25°C
Bulk Volume:	42005 cc	Water Feed Flow Rate:	213.21 cc/min
Porosity:	33.6%	Boiler Feed Rate:	28.68 cc/min
Initial Oil Saturation:	71.7%	Total Flow Rate of Hot H2O:	241.89 cc/min
Initial Water Saturation:	27.2%	N2 Gas Injection Pressure:	1 psig
Initial Gas Saturation:	1.1% (150 cc)	Total Water Volume Injected:	48257 cc (3.42 PV)
		Hot Water Volume Injected:	23584 cc (1.61 PV)

**Net Oil Recovery: 33.82%**      **Final Oil Saturation: 59.04%**

Cylinder No.	Total Vol. Produced (cc)	Instantaneous Oil Prod. (cc)	Cumulative Recovery (cc)	%OOIP	Oil Rec. Produced WOR	Instantaneous % Sample Vol. Oleic Phase	Cum. PV Injected
1	1800	150	150	20.9	11.0	8.3	1.96
2	1570	70	220	21.4	21.4	4.5	2.07
3	1800	110	330	22.3	15.4	6.1	2.18
4	1730	110	440	23.2	14.7	6.4	2.29
5	1860	140	580	24.3	12.3	7.5	2.44
6	1600	180	760	25.7	7.9	11.3	2.56
7	1930	190	950	27.3	9.2	9.8	2.71
8	1670	140	1090	28.4	10.9	8.4	2.79
9	1980	140	1230	29.5	13.1	7.1	2.92
10	1780	120	1350	30.4	13.8	6.7	3.04
11	2120	160	1510	31.7	12.3	7.5	3.19
12	1700	140	1650	32.8	11.1	8.2	3.31
13	1550	130	1780	33.8	10.9	8.4	3.42

Table E.6

## Run 73: Steamflood in a Homogeneous Model.

HC Pore Volume:	12550 cc	Type of Oil Used:	Faxam-100
Pore Volume:	13470 cc	Initial Model Temperature:	3°C
Bulk Volume:	42005 cc	Total Flow Rate of Steam:	230.0 cc/min
Porosity:	32.1%	Steam Quality, fst:	0.40
Initial Oil Saturation:	93.2%	Total Steam Volume Injected:	28175 cc (2.09 PV)
Initial Water Saturation:	6.8%		

Final Oil Saturation: 43.50%

Net Oil Recovery: 53.31%

Cylinder No.	Total Vol. Produced (cc)	Instantaneous Oil Prod. (cc)	Cumulative Oil Recovery (cc)	Cum. Oil Rec. %OOIP	Instantaneous Produced WOR	% Sample Vol. Oleic Phase	Cum. PV Injected
1	1880	720	720	5.7	1.6	38.3	0.26
2	1780	400	1120	8.9	3.5	22.5	0.36
3	2030	810	1930	15.4	1.5	39.9	0.47
4	1640	640	2570	20.5	1.6	39.0	0.57
5	1730	650	3220	25.7	1.7	37.6	0.68
6	1740	560	3780	30.1	2.1	32.2	0.80
7	1780	550	4330	34.5	2.2	30.9	0.92
8	1660	440	4770	38.0	2.8	26.5	1.06
9	1870	420	5190	41.4	3.5	22.5	1.21
10	1700	330	5520	44.0	4.2	19.4	1.37
11	1990	340	5860	46.7	4.9	17.1	1.55
12	1750	290	6150	49.0	5.0	16.6	1.71
13	2000	290	6440	51.3	5.9	14.5	1.91
14	1850	250	6690	53.3	6.4	13.5	2.09



Table E.7

**Run 74: Steam Injection of a Homogeneous Model using a Vertical Injector and a Horizontal Producer.**

HC Pore Volume:	12260 cc	Type of Oil Used:	Faxam-100
Pore Volume:	13460 cc	Initial Model Temperature:	3°C
Bulk Volume:	42005 cc	Total Flow Rate of Steam:	226.50 cc/min
Porosity:	32.0%	Steam Quality, fst:	0.10
Initial Oil Saturation:	91.1%	Total Steam Volume Injected:	27572 cc (2.05 PV)
Initial Water Saturation:	8.9%		

**Net Oil Recovery: 48.45%**      **Final Oil Saturation: 46.95%**

Cylinder No.	Total Vol. Produced (cc)	Instantaneous Oil Prod. (cc)	Cumulative Oil Recovery (cc)	Cum. Oil Rec. %OOIP	Instantaneous Produced WOR	% Sample Vol. Oleic Phase	Cum. PV Injected
1	2090	910	910	7.4	1.3	43.5	0.16
2	1720	530	1440	11.7	2.2	30.8	0.24
3	1860	590	2030	16.6	2.2	31.7	0.33
4	1820	530	2560	20.9	2.4	29.1	0.43
5	2090	510	3070	25.0	3.1	24.4	0.55
6	1780	540	3610	29.4	2.3	30.3	0.64
7	2010	370	3980	32.5	4.4	18.4	0.76
8	2180	300	4280	34.9	6.3	13.8	0.92
9	1920	260	4540	37.0	6.4	13.5	1.05
10	1760	220	4760	38.8	7.0	12.5	1.18
11	1880	220	4980	40.6	7.5	11.7	1.31
12	1750	190	5170	42.2	8.2	10.9	1.44
13	1950	200	5370	43.8	8.8	10.3	1.60
14	1860	200	5570	45.4	8.3	10.8	1.74
15	2100	200	5770	47.1	9.5	9.5	1.90
16	1800	170	5940	48.5	9.6	9.4	2.05

**Table E.8****Run 75: Steam Injection of a Homogeneous Model using a Horizontal Injector and a Horizontal Producer.**

HC Pore Volume:	12990 cc	Type of Oil Used:	Faxam-100
Pore Volume:	14200 cc	Initial Model Temperature:	3°C
Bulk Volume:	42005 cc	Total Flow Rate of Steam:	297.7 cc/min
Porosity:	33.8%	Steam Quality, fst:	0.10
Initial Oil Saturation:	91.5%	Total Steam Volume Injected:	30068 cc (2.12 PV)
Initial Water Saturation:	8.5%		

**Net Oil Recovery:** 60.89%      **Final Oil Saturation:** 35.77%

Cylinder No.	Total Vol. Produced (cc)	Instantaneous Oil Prod. (cc)	Cumulative Oil Recovery (cc)	%OOIP	Instantaneous Produced WOR	% Sample Vol. Oleic Phase	Cum. PV Injected
1	1990	1130	1130	8.7	0.8	56.8	0.17
2	1700	280	1410	10.9	5.1	16.5	0.27
3	2260	560	1970	15.2	3.0	24.8	0.38
4	1700	400	2370	18.2	3.3	23.5	0.46
5	1890	660	3030	23.3	1.9	34.9	0.57
6	1760	480	3510	27.0	2.7	27.3	0.67
7	1800	460	3970	30.6	2.9	25.6	0.78
8	1720	420	4390	33.8	3.1	24.4	0.88
9	2040	560	4950	38.1	2.6	27.5	1.01
10	1750	390	5340	41.1	3.5	22.3	1.12
11	1940	460	5800	44.6	3.2	23.7	1.25
12	1780	600	6400	49.3	2.0	33.7	1.38
13	2060	420	6820	52.5	3.9	20.4	1.52
14	1800	290	7110	54.7	5.2	16.1	1.66
15	2140	280	7390	56.9	6.6	13.1	1.76
16	1700	240	7630	58.7	6.1	14.1	1.96
17	2000	280	7910	60.9	6.1	14.0	2.12

Table E.2

**Run 76. Steam Injection of a Homogeneous Model using a Horizontal Injector and a Vertical Producer.**

HC Pore Volume:	12910 cc	Type of Oil Used:	Faxam-100
Pore Volume:	14250 cc	Initial Model Temperature:	3°C
Bulk Volume:	42005 cc	Total Flow Rate of Steam:	227.28 cc/min
Porosity:	33.9%	Steam Quality, fst:	0.10
Initial Oil Saturation:	90.6%	Total Steam Volume Injected:	30796 cc (2.16 PV)
Initial Water Saturation:	9.4%		

**Net Oil Recovery: 53.91%      Final Oil Saturation: 41.75%**

Cylinder No.	Total Vol. Produced (cc)	Instantaneous Oil Prod. (cc)	Cumulative Oil Recovery (cc)	Cum. Oil Rec. %OOIP	Instantaneous Produced WOR	% Sample Vol. Oleic Phase	Cum. PV Injected
1	1970	600	600	4.6	2.3	30.5	0.18
2	1760	650	1250	9.7	1.7	36.9	0.25
3	2020	830	2080	16.1	1.4	41.1	0.34
4	1620	480	2560	19.3	2.4	29.6	0.43
5	2000	630	3190	24.7	2.2	31.5	0.55
6	2040	510	3700	28.7	3.0	25.0	0.68
7	1980	440	4140	32.1	3.5	22.2	0.81
8	1920	400	4540	35.2	3.8	20.8	0.95
9	2060	400	4940	38.3	4.2	19.4	1.08
10	1690	310	5250	40.7	4.5	18.3	1.21
11	2300	380	5630	43.6	5.1	16.5	1.39
12	1760	280	5910	45.8	5.3	15.9	1.52
13	1990	290	6200	48.0	5.9	14.6	1.69
14	1780	250	6450	50.0	6.1	14.0	1.83
15	2060	280	6730	52.1	6.4	13.6	2.00
16	1800	230	6960	53.9	6.8	12.8	2.16

Table E.10

**Run 77: Steam Injection of a Homogeneous Model using a Vertical Injector and a Vertical Producer.**

HC Pore Volume:	12560 cc	Type of Oil Used:	Faxam-100
Pore Volume:	13620 cc	Initial Model Temperature:	3°C
Bulk Volume:	42005 cc	Total Flow Rate of Steam:	227.28 cc/min
Porosity:	32.4%	Steam Quality, fst:	0.10
Initial Oil Saturation:	92.2%	Total Steam Volume Injected:	29205 cc (2.14 PV)
Initial Water Saturation:	7.8%		

**Net Oil Recovery: 57.40%      Final Oil Saturation: 39.28%**

Cylinder No.	Total Vol. Produced (cc)	Instantaneous Oil Prod. (cc)	Cumulative Oil Recovery (cc)	Cum. Oil Rec. %OOIP	Instantaneous Produced WOR	% Sample Vol. Oleic Phase	Cum. PV Injected
1	1340	450	450	3.6	2.0	33.6	0.18
2	2120	670	1120	8.9	2.2	31.6	0.27
3	1695	415	1535	12.2	3.1	24.5	0.35
4	1840	480	2015	16.0	2.8	26.1	0.45
5	1960	570	2585	20.6	2.4	29.1	0.56
6	2100	640	3225	25.7	2.3	30.5	0.67
7	2150	610	3835	30.5	2.5	28.4	0.79
8	1800	530	4365	34.8	2.4	29.4	0.89
9	2200	530	4895	39.0	3.2	24.1	1.03
10	1880	375	5270	42.0	4.0	19.9	1.16
11	1925	365	5635	44.9	4.3	19.0	1.29
12	1740	300	5935	47.3	4.8	17.2	1.43
13	2100	300	6235	49.6	6.0	14.3	1.58
14	1830	275	6510	51.8	5.7	15.0	1.71
15	1900	265	6775	53.9	6.2	13.9	1.86
16	1640	200	6975	55.5	7.2	12.2	1.99
17	1870	235	7210	57.4	7.0	12.6	2.14

**Table E.11**

**Run 78: Solvent-Steamflood in a Bottom Water Model.**

HC Pore Volume:	11645 cc	Type of Oil Used:	Faxam-100
Pore Volume:	14611 cc	Initial Model Temperature:	3°C
Bulk Volume:	42005 cc	Total Flow Rate of Steam:	227.28 cc/min
Porosity:	34.8%	Steam Quality, fst:	0.10
Initial Oil Saturation:	79.7%	Solvent Flow Rate:	200.00 cc/min
Initial Water Saturation:	20.3%	Steam Volume Injected:	30228 cc (2.07 PV)
Bottom Water Thickness:	7.6% (% Gross Thickness)	Solvent Volume Injected:	1500 cc (0.11 PV)

**Net Oil Recovery: 52.92%      Solvent Recovery: 99.20%      Final Oil Saturation: 37.53%**

Cyl. No.	Solvent Conc. %	Total Vol. Prod. (cc)	Inst. HC Prod. (cc)	Inst. Oil Prod.(cc)	Cumulative Solv. Rec. (%)		Cumulative Oil Rec. (cc)		Inst. Prod. WOR	Inst. HC Prod %Sample	Cum. PV Injected
					(cc)	(%)	(cc)	%OIP			
1	69	2150	1330	412	918	61.2	412	3.5	2.0	61.9	0.08
2	70	1650	750	225	1443	96.2	637	5.5	4.0	45.5	0.22
3	9	1920	330	300	1472	98.2	938	8.1	5.3	17.2	0.30
4	2	2110	510	500	1483	98.8	1437	12.3	3.2	24.2	0.42
5	1	2020	540	535	1488	99.2	1972	16.9	2.8	26.7	0.53
6	0	1780	480	480	1488	99.2	2452	21.1	2.7	27.0	0.62
7	0	1910	460	460	1488	99.2	2912	25.0	3.2	24.1	0.73
8	0	1950	400	400	1488	99.2	3312	28.4	3.9	20.5	0.85
9	0	2080	400	400	1488	99.2	3712	31.9	4.2	19.2	0.98
10	0	1870	370	370	1488	99.2	4082	35.1	4.1	19.8	1.10
11	0	1940	340	340	1488	99.2	4422	38.0	4.7	17.5	1.22
12	0	1960	330	330	1488	99.2	4752	40.8	4.9	16.8	1.35
13	0	1980	310	310	1488	99.2	5062	43.5	5.4	15.7	1.49
14	0	1860	260	260	1488	99.2	5322	45.7	6.2	14.0	1.63
15	0	1990	290	290	1488	99.2	5612	48.2	5.9	14.6	1.77
16	0	1900	270	270	1488	99.2	5882	50.5	6.0	14.2	1.91
17	0	2160	280	280	1488	99.2	6162	52.9	6.7	13.0	2.07

**Table E.12**

**Run 79: Solvent-Steamflood in a Homogeneous Model.**

HC Pore Volume:	12410 cc	Type of Oil Used:	Faxam-100
Pore Volume:	13655 cc	Initial Model Temperature:	3°C
Bulk Volume:	42005 cc	Total Flow Rate of Steam:	227.28 cc/min
Porosity:	32.5%	Steam Quality, fst:	0.10
Initial Oil Saturation:	50.9%	Solvent Flow Rate:	200.00 cc/min
Initial Water Saturation:	9.1%	Steam Volume Injected:	29092 cc (2.13 PV)
		Solvent Volume Injected:	2200 cc (0.15 PV)

**Net Oil Recovery: 57.51%**      **Solvent Recovery: 99.93%**      **Final Oil Saturation: 38.62%**

Cyl. No.	Solvent Conc. %	Total Vol. Prod. (cc)	Inst. HC Prod. (cc)	Inst. Oil Prod.(cc)	Cumulative Solv. Rec. (%)		Cumulative Oil Rec. (cc)	%OOIP	Inst. Prod. Prod. WOR	Inst HC Prod %Sample	Cum. PV Injected
					(cc)	(%)					
1	69	1920	1920	595	1325	60.2	595	4.8	0.0	100.0	0.10
2	76	1660	1060	254	2130	96.8	850	6.8	2.4	63.9	0.14
3	8	1865	605	557	2179	99.0	1406	11.3	2.3	32.4	0.18
4	3	1800	560	543	2196	99.8	1949	15.7	2.3	31.1	0.28
5	1	2100	580	577	2199	99.9	2527	20.4	2.6	27.6	0.40
6	0	1880	480	480	2199	100.0	3007	24.2	2.9	25.5	0.50
7	0	1880	460	460	2199	100.0	3467	27.9	3.1	24.5	0.62
8	0	1995	455	455	2199	100.0	3922	31.6	3.4	22.8	0.74
9	0	2040	430	430	2199	100.0	4352	35.1	3.7	21.1	0.87
10	0	1820	350	350	2199	100.0	4702	37.9	4.2	19.2	0.98
11	0	2035	355	355	2199	100.0	5057	40.7	4.7	17.4	1.12
12	0	1800	320	320	2199	100.0	5377	43.3	4.6	17.8	1.25
13	0	1930	310	310	2199	100.0	5687	45.8	5.2	16.1	1.39
14	0	2060	330	330	2199	100.0	6017	48.5	5.2	16.0	1.54
15	0	2000	310	310	2199	100.0	6327	51.0	5.5	15.5	1.68
16	0	1780	260	260	2199	100.0	6587	53.1	5.8	14.6	1.81
17	0	2080	270	270	2199	100.0	6857	55.2	6.7	13.0	1.98
18	0	1880	280	280	2199	100.0	7137	57.5	5.7	14.9	2.13

Table E.13

## Run 82: Solvent-Steamflood in a Bottom Water Model.

HC Pore Volume:	12590 cc	Type of Oil Used:	Faxam-100
Pore Volume:	13865 cc	Initial Model Temperature:	3°C
Bulk Volume:	42005 cc	Total Flow Rate of Steam:	227.28 cc/min
Porosity:	33.0%	Steam Quality, fst:	0.10
Initial Oil Saturation:	90.8%	Solvent Flow Rate:	200.00 cc/min
Initial Water Saturation:	9.2%	Steam Volume Injected:	25650 cc (1.85 PV)
Bottom Water Thickness:	7.2% (% Gross Thickness)	Solvent Volume Injected:	3850 cc (0.28 PV)
<b>Net Oil Recovery:</b>	<b>54.31%</b>	<b>Solvent Recovery:</b>	<b>99.95%</b>
		<b>Final Oil Saturation:</b>	<b>41.49%</b>

Cyl. No.	Solvent Conc. %	Total Vol. Prod. (cc)	Inst. HC Prod. (cc)	Inst. Oil Prod.(cc)	Cumulative Solv. Rec. (%)		Cumulative Oil Rec. (cc)		Inst. Prod. WOR	Inst HC Prod %Sample	Cum. PV Injected
					(%)	(%)	(cc)	%OOIP			
1	85	2080	2070	311	1760	45.7	311	2.5	0.0	99.5	0.14
2	80	1810	1490	298	2952	76.7	609	4.8	1.1	82.3	0.25
3	90	1410	900	90	3762	97.7	699	5.5	5.7	63.8	0.36
4	15	1720	400	340	3822	99.3	1039	8.2	3.9	23.3	0.49
5	7	1655	325	304	3843	99.8	1342	10.7	4.4	19.6	0.59
6	1	2060	500	495	3848	99.9	1837	14.6	3.2	24.3	0.70
7	0	1960	540	540	3848	99.9	2377	18.9	2.6	27.6	0.81
8	0	2100	590	590	3848	99.9	2967	23.6	2.6	28.1	0.92
9	0	2000	560	560	3848	99.9	3527	28.0	2.6	28.0	1.04
10	0	2065	535	535	3848	99.9	4062	32.3	2.9	25.9	1.16
11	0	2220	510	510	3848	99.9	4572	36.3	3.4	23.0	1.30
12	0	1980	440	440	3848	99.9	5012	39.8	3.5	22.2	1.43
13	0	1820	380	380	3848	99.9	5392	42.8	3.8	20.9	1.55
14	0	1980	470	470	3848	99.9	5862	46.6	3.2	23.7	1.69
15	0	2000	350	350	3848	99.9	6212	49.3	4.7	17.5	1.83
16	0	2285	355	355	3848	99.9	6567	52.2	5.4	15.5	2.00
17	0	1760	270	270	3848	99.9	6837	54.3	5.5	15.3	2.14

**Table E.14**

**Run 83: Solvent-Steamflood in a Bottom Water Model.**

HC Pore Volume:	12810 cc	Type of Oil Used:	Faxam-100
Pore Volume:	14039 cc	Initial Model Temperature:	3°C
Bulk Volume:	42005 cc	Total Flow Rate of Steam:	227.28 cc/min
Porosity:	33.4%	Steam Quality, fst:	0.10
Initial Oil Saturation:	91.2%	Solvent Flow Rate:	200.00 cc/min
Initial Water Saturation:	8.8%	Steam Volume Injected:	28865 cc (2.06 PV)
Bottom Water Thickness:	7.0% (% Gross Thickness)	Solvent Volume Injected:	0 cc (0.00 PV)

**Net Oil Recovery: 56.60%**      **Solvent Recovery: 0.00%**      **Final Oil Saturation: 39.60%**

Cyl. No.	Solvent Conc. %	Total Vol. Prod. (cc)	Inst. HC Prod. (cc)	Inst. Oil Prod.(cc)	Cumulative Solv. Rec. (%)		Cumulative Oil Rec. (cc)		Inst. Prod. WOR	Inst HC Prod %Sample	Cum. PV Injected
					(cc)	(%)	(cc)	%OOIP			
1	0	1735	140	140	0	0.0	140	1.1	11.4	8.1	0.13
2	0	2130	490	490	0	0.0	630	5.0	3.3	23.0	0.23
3	0	1945	595	595	0	0.0	1225	9.7	2.3	30.6	0.34
4	0	2170	740	740	0	0.0	1965	15.6	1.9	34.1	0.45
5	0	2100	740	740	0	0.0	2705	21.5	1.8	35.2	0.56
6	0	2210	710	710	0	0.0	3415	27.1	2.1	32.1	0.67
7	0	1995	595	595	0	0.0	4010	31.9	2.4	29.8	0.79
8	0	2150	695	695	0	0.0	4705	37.4	2.1	32.3	0.91
9	0	1935	455	455	0	0.0	5160	41.0	3.3	23.5	1.04
10	0	2075	425	425	0	0.0	5585	44.4	3.9	20.5	1.17
11	0	1865	310	310	0	0.0	5895	46.8	5.0	16.6	1.30
12	0	2035	315	315	0	0.0	6210	49.3	5.5	15.5	1.45
13	0	1900	280	280	0	0.0	6490	51.5	5.8	14.7	1.59
14	0	1960	270	270	0	0.0	6760	53.7	6.3	13.8	1.74
15	0	2090	260	260	0	0.0	7020	55.8	7.0	12.4	1.90
16	0	1920	230	230	0	0.0	7250	57.6	7.3	12.0	2.06



**Table E.15**

**Run 84: Solvent-Steamflood in a Bottom Water Model.**

HC Pore Volume:	11615 cc	Type of Oil Used:	Faxam-100
Pore Volume:	13614 cc	Initial Model Temperature:	3°C
Bulk Volume:	42005 cc	Total Flow Rate of Steam:	227.28 cc/min
Porosity:	32.4%	Steam Quality, fst:	0.10
Initial Oil Saturation:	85.3%	Solvent Flow Rate:	200.00 cc/min
Initial Water Saturation:	14.7%	Steam Volume Injected:	26137 cc (1.93 PV)
Bottom Water Thickness:	7.67% (% Gross Thickness)	Solvent Volume Injected:	2529 cc (0.19 PV)

**Net Oil Recovery: 52.05%**      **Solvent Recovery: 100.00%**      **Final Oil Saturation: 40.91%**

Cyl. No.	Solvent Conc. %	Total Vol. Prod. (cc)	Inst. HC Prod. (cc)	Inst. Oil Prod.(cc)	Cumulative Solv. Rec. (%)		Cumulative Oil Rec. (cc)		Inst. Prod. WOR	Inst HC Prod %Sample	Cum. PV Injected
					(cc)	(%)	(cc)	%OOIP			
1	47	1950	970	514	456	18.0	514	4.4	1.9	49.7	0.11
2	63	1175	1175	435	1196	47.3	949	8.2	0.0	100.0	0.18
3	68	1925	1385	443	2138	84.6	1392	12.0	1.2	71.9	0.30
4	39	1850	505	308	2335	92.4	1700	14.6	4.4	27.3	0.40
5	22	1825	545	425	2455	97.1	2125	18.3	3.0	29.9	0.50
6	12	2070	500	440	2515	99.5	2565	22.1	3.6	24.2	0.63
7	4	1820	360	346	2529	100.0	2911	25.1	4.2	19.8	0.75
8	0	1995	335	335	2529	100.0	3246	27.9	5.0	16.8	0.88
9	0	1795	305	305	2529	100.0	3551	30.6	4.9	17.0	1.01
10	0	1890	340	340	2529	100.0	3891	33.5	4.6	18.0	1.14
11	0	1760	280	280	2529	100.0	4171	35.9	5.3	15.9	1.26
12	0	1980	330	330	2529	100.0	4501	38.7	5.0	16.7	1.40
13	0	1840	395	395	2529	100.0	4896	42.2	3.7	21.5	1.54
14	0	1900	280	280	2529	100.0	5176	44.6	5.8	14.7	1.69
15	0	1895	360	360	2529	100.0	5536	47.7	4.3	19.0	1.8
16	0	2030	270	270	2529	100.0	5806	50.0	6.5	13.3	1.99
17	0	1660	240	240	2529	100.0	6046	52.1	5.9	14.5	2.12

Table E.16

## Run 85: Continuous Steamflood in a Bottom Water Model.

HC Pore Volume:	11235 cc	Type of Oil Used:	Faxam-100
Pore Volume:	13836 cc	Initial Model Temperature:	3°C
Bulk Volume:	42005 cc	Total Flow Rate of Steam:	227.28 cc/min
Porosity:	32.9%	Steam Quality, fst:	0.10
Initial Oil Saturation:	81.2%	Steam Volume Injected:	27955 cc (2.02 PV)
Initial Water Saturation:	18.8%		
Bottom Water Thickness:	9.1% (% Gross Thickness)		

Net Oil Recovery: 49.18%      Final Oil Saturation: 41.27%

Cylinder No.	Total Vol. Produced (cc)	Instantaneous Oil Prod. (cc)	Cumulative Oil Recovery (cc)	Cum. Oil Rec.		Instantaneous Produced WOR	% Sample Vol. Oleic Phase	Cum. PV Injected
				%OOIP	Produced WOR			
1	1885	20	20	0.2	93.3	1.1	0.08	
2	1680	35	55	0.5	47.0	2.1	0.24	
3	1825	245	300	2.7	6.4	13.4	0.32	
4	2225	525	825	7.3	3.2	23.6	0.44	
5	1720	540	1365	12.1	2.2	31.4	0.53	
6	1890	595	1960	17.4	2.2	31.5	0.64	
7	1835	515	2475	22.0	2.6	28.1	0.75	
8	2030	525	3000	26.7	2.9	25.9	0.86	
9	1620	380	3380	30.1	3.3	23.5	0.96	
10	1870	280	3660	32.6	5.7	15.0	1.08	
11	1770	310	3970	35.3	4.7	17.5	1.21	
12	1800	290	4260	37.9	5.2	16.1	1.33	
13	1820	260	4520	40.2	6.0	14.3	1.47	
14	1870	260	4780	42.5	6.2	13.9	1.60	
15	1840	240	5020	44.7	6.7	13.0	1.75	
16	1990	255	5275	47.0	6.8	12.8	1.90	
17	1570	250	5525	49.2	5.3	15.9	2.02	

**Table E.17****Run 86: Steam Injection of a Homogeneous Model using a Vertical Injector and a Horizontal Producer.**

HC Pore Volume:	12885 cc	Type of Oil Used:	Faxam-100
Pore Volume:	14175 cc	Initial Model Temperature:	3°C
Bulk Volume:	42005 cc	Total Flow Rate of Steam:	227.28 cc/min
Porosity:	33.7%	Steam Quality, fst:	0.10
Initial Oil Saturation:	90.9%	Total Steam Volume Injected:	29774 cc (2.10 PV)
Initial Water Saturation:	8.9%		

**Net Oil Recovery: 51.87%**      **Final Oil Saturation: 43.75%**

Cylinder No.	Total Vol. Produced (cc)	Instantaneous Oil Prod. (cc)	Cumulative Oil Recovery (cc)	%OOIP	Instantaneous Produced WOR	% Sample Vol. Cleic Phase	Cum. PV Injected
1	1550	690	690	5.4	1.2	44.5	0.17
2	1960	640	1330	10.3	2.1	32.7	0.26
3	1800	690	2020	15.7	1.6	38.3	0.34
4	2045	755	2775	21.5	1.7	36.9	0.44
5	1700	480	3255	25.3	2.5	28.2	0.54
6	1830	435	3690	28.6	3.2	23.8	0.64
7	1670	337	4027	31.3	4.0	20.2	0.75
8	1900	355	4382	34.0	4.4	18.7	0.87
9	1815	330	4712	36.6	4.5	18.2	1.00
10	1855	295	5007	38.9	5.3	15.9	1.13
11	1760	270	5277	41.0	5.5	15.3	1.26
12	1900	270	5547	43.1	6.0	14.2	1.40
13	1777	237	5784	44.9	6.5	13.3	1.55
14	1855	240	6024	46.8	6.7	12.9	1.68
15	1670	210	6234	48.4	7.0	12.6	1.81
16	1900	240	6474	50.2	6.9	12.6	2.04
17	1690	210	6684	51.9	7.0	12.4	2.10

**Table E.18****Run 87: Steam Injection of a Bottom Water Model using a Vertical Injector and a Horizontal Producer.**

HC Pore Volume:	10820 cc	Type of Oil Used:	Faxam-100
Pore Volume:	13719 cc	Initial Model Temperature:	3°C
Bulk Volume:	42005 cc	Total Flow Rate of Steam:	227.28 cc/min
Porosity:	32.7%	Steam Quality, fst:	0.10
Initial Oil Saturation:	78.9%	Total Steam Volume Injected:	27274 cc (1.99 PV)
Initial Water Saturation:	21.1%		
Bottom Water Thickness:	9.94% (% Gross Thickness)		

**Net Oil Recovery: 53.56%**      **Final Oil Saturation: 36.63%**

Cylinder No.	Total Vol. Produced (cc)	Instantaneous Oil Prod. (cc)	Cumulative Oil Recovery (cc)	Cum. Oil Rec. %OOIP	Instantaneous Produced WOR	% Sample Vol. Oleic Phase	Cum. PV Injected
1	1870	40	40	0.4	45.8	2.1	0.08
2	1990	60	100	0.9	32.2	3.0	0.19
3	1840	480	580	5.4	2.8	26.1	0.29
4	1920	660	1240	11.5	1.9	34.4	0.38
5	1675	595	1835	17.0	1.8	35.5	0.48
6	1920	510	2345	21.7	2.8	26.6	0.60
7	1685	365	2710	25.0	3.6	21.7	0.70
8	1770	360	3070	28.4	3.9	20.3	0.82
9	1710	365	3435	31.7	3.7	21.3	0.94
10	1810	370	3805	35.2	3.9	20.4	1.07
11	1600	295	4100	37.9	4.4	18.4	1.18
12	1615	265	4365	40.3	5.1	16.4	1.31
13	1750	290	4655	43.0	5.0	16.6	1.44
14	1890	400	5055	46.7	3.7	21.2	1.58
15	1660	250	5305	49.0	5.6	15.1	1.71
16	1890	260	5565	51.4	6.3	13.8	1.86
17	1520	230	5795	53.6	5.6	15.1	1.99

**Table E.12****Run 90: Steam Injection of a Bottom Water Model using a Vertical Injector and a Vertical Producer.**

HC Pore Volume:	11950 cc	Type of Oil Used:	Faxam-100
Pore Volume:	14291 cc	Initial Model Temperature:	3°C
Bulk Volume:	42005 cc	Total Flow Rate of Steam:	227.28 cc/min
Porosity:	34.0%	Steam Quality, fst:	0.10
Initial Oil Saturation:	83.6%	Total Steam Volume Injected:	30001 cc (2.10 PV)
Initial Water Saturation:	16.4%		
Bottom Water Thickness:	8.51% (% Gross Thickness)		

**Net Oil Recovery: 47.32%**      **Final Oil Saturation: 44.05%**

Cylinder No.	Total Vol. Produced (cc)	Instantaneous Oil Prod. (cc)	Cumulative Oil Recovery (cc)	Cum. Oil Rec. %OIP	Instantaneous Produced WOR	% Sample Vol. Oleic Phase	Cum. PV Injected
1	1800	10	10	0.1	179.0	0.6	0.10
2	1825	105	115	1.0	16.4	5.8	0.28
3	1860	280	395	3.3	5.6	15.1	0.38
4	2090	575	970	8.1	2.6	27.5	0.50
5	1765	545	1515	12.7	2.2	30.9	0.61
6	2120	625	2140	17.9	2.4	29.5	0.75
7	1900	590	2730	22.8	2.2	31.1	0.87
8	2100	660	3390	28.4	2.2	31.4	0.99
9	1890	500	3890	32.6	2.8	26.5	1.12
10	1975	465	4355	36.4	3.2	23.5	1.26
11	1955	385	4740	39.7	4.1	19.7	1.42
12	1860	310	5050	42.3	5.0	16.7	1.57
13	1705	275	5325	44.6	5.2	16.1	1.74
14	2040	215	5540	46.4	8.5	10.5	1.91
15	1515	115	5655	47.3	12.2	7.6	2.10

**Table E.20**

**Run 91: Solvent-Steamflood in a Bottom Water Model using a Vertical Injector and a Horizontal Producer.**

HC Pore Volume:	11820 cc	Type of Oil Used:	Faxam-100
Pore Volume:	14258 cc	Initial Model Temperature:	3°C
Bulk Volume:	42005 cc	Total Flow Rate of Steam:	227.28 cc/min
Porosity:	33.9%	Steam Quality, fst:	0.10
Initial Oil Saturation:	2.9%	Solvent Flow Rate:	200.00 cc/min
Initial Water Saturation:	17.1%	Steam Volume Injected:	27615 cc (1.94 PV)
Bottom Water Thickness:	9.2% (% Gross Thickness)	Solvent Volume Injected:	1400 cc (0.10 PV)

**Net Oil Recovery: 49.87%      Solvent Recovery: 95.00%      Final Oil Saturation: 41.56%**

Cyl. No.	Solvent Conc. %	Total Vol. Prod. (cc)	Inst. HC Prod. (cc)	Inst. Oil Prod.(cc)	Cumulative Solv. Rec. (%)		Cumulative Oil Rec. (cc)		Inst. Prod. WOR	Inst HC Prod %Sample	Cum. PV Injected
					(cc)	(%)	(cc)	%OOIP			
1	58	1960	745	313	432	30.9	313	2.6	3.9	38.0	0.07
2	56	475	425	187	670	47.9	500	4.2	0.3	89.5	0.09
3	62	1710	830	315	1185	84.6	815	6.9	2.8	48.5	0.20
4	20	2110	495	396	1284	91.7	1211	10.2	4.1	23.5	0.32
5	9	1790	540	494	1330	95.0	1705	14.4	2.5	30.2	0.42
6	0	2080	450	450	1330	95.0	2155	18.2	3.6	21.6	0.55
7	0	1870	400	400	1330	95.0	2555	21.6	3.7	21.4	0.66
8	0	1965	425	425	1330	95.0	2980	25.2	3.6	21.6	0.78
9	0	1845	370	370	1330	95.0	3350	28.3	4.0	20.1	0.90
10	0	1820	350	350	1330	95.0	3700	31.3	4.2	19.2	1.03
11	0	1820	330	330	1330	95.0	4030	34.1	4.5	18.1	1.16
12	0	2010	350	350	1330	95.0	4380	37.1	4.7	17.4	1.31
13	0	1950	330	330	1330	95.0	4710	39.9	4.9	16.9	1.45
14	0	2090	335	335	1330	95.0	5045	42.7	5.2	16.0	1.61
15	0	1860	280	280	1330	95.0	5325	45.1	5.6	15.1	1.75
16	0	1940	290	290	1330	95.0	5615	47.5	5.7	14.9	1.90
17	0	1780	280	280	1330	95.0	5895	49.9	5.4	15.7	2.04

Table E.21

**Run 92: Solvent-Steamflood in a Bottom Water Model using a Horizontal Injector and a Horizontal Producer.**

HC Pore Volume:	12055 cc	Type of Oil Used:	Faxam-100
Pore Volume:	14348 cc	Initial Model Temperature:	3°C
Bulk Volume:	42005 cc	Total Flow Rate of Steam:	227.28 cc/min
Porosity:	34.2%	Steam Quality, fsi:	0.10
Initial Oil Saturation:	84.0%	Solvent Flow Rate:	200.00 cc/min
Initial Water Saturation:	16.0%	Steam Volume Injected:	29887 cc (2.09 PV)
Bottom Water Thickness:	8.8% (% Gross Thickness)	Solvent Volume Injected:	1380 cc (0.10 PV)

**Net Oil Recovery: 67.49%      Solvent Recovery: 79.64%      Final Oil Saturation: 27.31%**

Cyl. No.	Solvent Conc. %	Total Vol. Prod. (cc)	Inst. HC Prod. (cc)	Inst. Oil Prod.(cc)	Cumulative Solv. Rec. (%)		Cumulative Oil Rec. (cc)		Inst. Prod. WOR	Inst HC Prod %Sample	Cum. PV Injected
					(cc)	(%)	(cc)	%OPIP			
1	36	1795	240	154	86	6.3	154	1.3	10.1	13.4	0.09
2	42	2190	1330	771	645	46.7	925	7.7	1.1	60.7	0.21
3	20	2230	850	680	815	59.1	1605	13.3	2.0	38.1	0.33
4	14	2040	680	585	910	66.0	2190	18.2	2.3	33.3	0.44
5	10	2230	770	693	987	71.5	2883	23.9	2.1	34.5	0.56
6	7	2320	840	781	1046	75.8	3664	30.4	1.9	36.2	0.68
7	4	2055	750	720	1076	78.0	4384	36.4	1.8	36.5	0.79
8	3	2170	770	747	1099	79.6	5131	42.6	1.9	35.5	0.91
9	0	1960	600	600	1099	79.6	5731	47.5	2.3	30.6	1.03
10	0	1995	480	480	1099	79.6	6211	51.5	3.2	24.1	1.16
11	0	1950	405	405	1099	79.6	6616	54.9	3.8	20.8	1.30
12	0	1895	345	345	1099	79.6	6961	57.7	4.5	18.2	1.43
13	0	1815	280	280	1099	79.6	7241	60.1	5.5	15.4	1.57
14	0	2015	275	275	1099	79.6	7516	62.3	6.3	13.6	1.72
15	0	1860	220	220	1099	79.6	7736	64.2	7.5	11.8	1.88
16	0	2080	190	190	1099	79.6	7926	65.7	9.9	9.1	2.04
17	0	1800	210	210	1099	79.6	8136	67.5	7.6	11.7	2.19

Table E.22

**Run 93: Solvent-Steamflood in a Bottom Water Model using a Horizontal Injector and a Vertical Producer.**

HC Pore Volume:	11575 cc	Type of Oil Used:	Faxam-100
Pore Volume:	13711 cc	Initial Model Temperature:	3°C
Bulk Volume:	42005 cc	Total Flow Rate of Steam:	227.28 cc/min
Porosity:	32.6%	Steam Quality, fsi:	0.10
Initial Oil Saturation:	84.4%	Solvent Flow Rate:	200.00 cc/min
Initial Water Saturation:	15.6%	Steam Volume injected:	28410 cc (2.07 PV)
Bottom Water Thickness:	9.96% (% Gross Thickness)	Solvent Volume Injected:	1310 cc (0.10 PV)

Net Oil Recovery: 56.65%      Solvent Recovery: 84.96%      Final Oil Saturation: 36.60%

Cyl. No.	Solvent Conc. %	Total Vol. Prod. (cc)	Inst. HC Prod. (cc)	Inst. Oil Prod.(cc)	Cumulative Solv. Rec. (%)		Cumulative Oil Rec. (cc)		Inst. Prod. WOR	Inst HC Prod %Sample	Cum. PV Injected
					(cc)	(%)	(cc)	%OOIP			
1	64	1940	410	148	262	20.0	148	1.3	10.4	21.1	0.09
2	36	1750	395	253	405	30.9	400	3.5	5.4	22.6	0.28
3	14	2715	1340	1152	592	45.2	1553	13.4	1.2	49.4	0.38
4	12	1930	635	559	668	51.0	2112	18.2	2.3	32.9	0.49
5	7	2080	650	605	714	54.5	2716	23.5	2.4	31.3	0.60
6	4	2170	560	538	736	56.2	3254	28.1	3.0	25.8	0.74
7	1	1995	460	455	741	56.6	3709	32.0	3.4	23.1	0.87
8	3	1940	405	393	753	57.5	4102	35.4	3.9	20.9	0.99
9	0	1960	155	155	753	57.5	4257	36.8	11.6	7.9	1.14
10	0	1965	345	345	753	57.5	4602	39.8	4.7	17.6	1.28
11	0	1880	340	340	753	57.5	4942	42.7	4.5	18.1	1.42
12	0	1900	315	315	753	57.5	5257	45.4	5.0	16.6	1.57
13	0	2060	305	305	753	57.5	5562	48.1	5.8	14.8	1.72
14	0	2210	310	310	753	57.5	5872	50.7	6.1	14.0	1.90
15	0	1875	425	425	753	57.5	6297	54.4	3.4	22.7	2.03
16	0	1870	260	260	753	57.5	6557	56.6	6.2	13.9	2.18



Table E.23

**Run 94: Solvent-Steamflood in a Bottom Water Model using a Vertical Injector and a Vertical Producer.**

HC Pore Volume:	11380 cc	Type of Oil Used:	Faxam-100
Pore Volume:	14080 cc	Initial Model Temperature:	3°C
Bulk Volume:	42005 cc	Total Flow Rate of Steam:	227.28 cc/min
Porosity:	33.5%	Steam Quality, fst:	0.10
Initial Oil Saturation:	80.8%	Solvent Flow Rate:	200.00 cc/min
Initial Water Saturation:	19.2%	Steam Volume Injected:	27921 cc (1.98 PV)
Bottom Water Thickness:	10.41% (% Gross Thickness)	Solvent Volume Injected:	1310 cc (0.093 PV)
<b>Net Oil Recovery:</b>	<b>52.12%</b>	<b>Solvent Recovery:</b>	<b>87.71%</b>
		<b>Final Oil Saturation:</b>	<b>38.70%</b>

Cyl. No.	Solvent Conc. %	Total Vol. Prod. (cc)	Inst. HC Prod. (cc)	Inst. Oil Prod.(cc)	Cumulative Solv. Rec. (%)		Cumulative Oil Rec. (cc)	%OOIP	Inst. Prod. WOR	Inst HC Prod %Sample	Cum. PV Injected
					(cc)	(%)					
1	50	1940	115	58	58	4.4	58	0.5	31.7	5.9	0.08
2	42	2140	1320	766	612	46.7	823	7.2	1.1	61.7	0.21
3	28	1995	555	400	767	58.6	1223	10.7	3.6	27.8	0.31
4	22	1960	700	546	921	70.3	1769	15.5	2.3	35.7	0.40
5	16	1910	650	546	1025	78.3	2315	20.3	2.3	34.0	0.51
6	12	2100	630	554	1101	84.0	2869	25.2	2.7	30.0	0.63
7	8	1825	450	414	1137	86.8	3283	28.8	3.3	24.7	0.74
8	3	1940	400	388	1149	87.7	3671	32.3	4.0	20.6	0.87
9	0	1760	300	300	1149	87.7	3971	34.9	4.9	17.0	0.99
10	0	1900	300	300	1149	87.7	4271	37.5	5.3	15.8	1.13
11	0	1920	290	290	1149	87.7	4561	40.1	5.6	15.1	1.27
12	0	2110	265	265	1149	87.7	4826	42.4	7.0	12.6	1.43
13	0	1795	225	225	1149	87.7	5051	44.4	7.0	12.5	1.57
14	0	2560	330	330	1149	87.7	5381	47.3	6.8	12.9	1.77
15	0	1995	260	260	1149	87.7	5641	49.6	6.7	13.0	1.92
16	0	2270	290	290	1149	87.7	5931	52.1	6.8	12.8	2.10

**Table E.24****Run 95: Steam Injection of a Thick Bottom Water Model  
subsequent to N2 Gas Injection.**

HC Pore Volume:	6735 cc	Type of Oil Used:	Faxam-100
Pore Volume:	12627 cc	Initial Model Temperature:	3°C
Bulk Volume:	42005 cc	Total Flow Rate of Steam:	227.28 cc/min
Porosity:	30.1%	Steam Quality, fst:	0.10
Initial Oil Saturation:	53.3%	Total Steam Volume Injected:	27501 cc (2.18 PV)
Initial Water Saturation:	46.7%	Length of Gas Injection:	1 prototype year (12 min)
Bottom Water Thickness:	49.71% (% Gross Thickness)		

**Net Oil Recovery: 32.81%**      **Final Oil Saturation: 35.84%**

Cylinder No.	Total Vol. Produced (cc)	Instantaneous Oil Prod. (cc)	Cumulative Oil Recovery (cc)	Cum. Oil Rec. %OOIP	Instantaneous Produced WOR	Sample Vol.		Cum. PV Injected
						%Oleic	Phase	
1	1900	0	0	0.0	-	0.0	-	-
2	2155	0	0	0.0	-	0.0	-	-
3	1560	0	0	0.0	-	0.0	-	-
4	2220	0	0	0.0	-	0.0	0.39	0.39
5	1945	0	0	0.0	-	0.0	0.49	0.49
6	2070	50	50	0.7	40.4	2.4	0.72	0.72
7	1760	130	180	2.7	12.5	7.4	0.86	0.86
8	2200	255	435	6.5	7.6	11.6	0.99	0.99
9	2100	335	770	11.4	5.3	16.0	1.16	1.16
10	1915	315	1085	16.1	5.1	16.4	1.31	1.31
11	1750	255	1340	19.9	5.9	14.6	1.45	1.45
12	1895	245	1585	23.5	6.7	12.9	1.62	1.62
13	2030	230	1815	26.9	7.8	11.3	1.79	1.79
14	2060	200	2015	29.9	9.3	9.7	1.98	1.98
15	2165	195	2210	32.8	10.1	9.0	2.18	2.18

Table E.25

**Run 96: Steam Injection of a Thin Bottom Water Model  
subsequent to N2 Gas Injection.**

HC Pore Volume:	11390 cc	Type of Oil Used:	Faxam-100
Pore Volume:	13792 cc	Initial Model Temperature:	3°C
Bulk Volume:	42005 cc	Total Flow Rate of Steam:	227.28 cc/min
Porosity:	32.8%	Steam Quality, fst:	0.10
Initial Oil Saturation:	53.3%	Total Steam Volume Injected:	28637 cc (2.08 PV)
Initial Water Saturation:	46.7%	Length of Gas Injection:	1 prototype year (12 min)
Bottom Water Thickness:	10.38% (% Gross Thickness)		

**Net Oil Recovery: 50.22%**      **Final Oil Saturation: 41.11%**

Cylinder No.	Total Vol. Produced (cc)	Instantaneous Oil Prod. (cc)	Cumulative Oil Recovery (cc)	Cum. Oil Rec. %OOIP	Instantaneous Produced WOR		Cum. PV Injected
					Produced	Oleic Phase	
1	1650	10	10	0.1	164.0	0.6	-
2	2065	95	105	0.9	20.7	4.6	0.33
3	1840	140	245	2.2	12.1	7.6	0.46
4	2120	500	745	6.5	3.2	23.6	0.62
5	1860	580	1325	11.6	2.2	31.2	0.76
6	2060	740	2065	18.1	1.8	35.9	0.89
7	2040	835	2900	25.5	1.4	40.9	1.01
8	2100	815	3715	32.6	1.6	38.8	1.17
9	2010	570	4285	37.6	2.5	28.4	1.33
10	2000	450	4735	41.6	3.4	22.5	1.51
11	1980	380	5115	44.9	4.2	19.2	1.68
12	2115	345	5460	47.9	5.1	16.3	1.90
13	1730	260	5720	50.2	5.7	15.0	2.08

Table E.26

**Run 97: Steam Injection of a Bottom Water Model using a Vertical Injector and a Horizontal Producer.**

HC Pore Volume:	6595 cc	Type of Oil Used:	Faxam-100
Pore Volume:	13126 cc	Initial Model Temperature:	3°C
Bulk Volume:	42005 cc	Total Flow Rate of Steam:	227.28 cc/min
Porosity:	31.2%	Steam Quality, fst:	0.10
Initial Oil Saturation:	50.2%	Total Steam Volume Injected:	29092 cc (2.22 PV)
Initial Water Saturation:	49.8%		
Bottom Water Thickness:	48.51% (% Gross Thickness)		

**Net Oil Recovery:** 32.45%      **Final Oil Saturation:** 33.94%

Cylinder No.	Total Vol. Produced (cc)	Instantaneous Oil Prod. (cc)	Cumulative Oil Recovery (cc)	%OOIP	Oil Rec. Produced WOR	Instantaneous % Sample Vol. Oleic Phase	Cum. PV Injected
1	1715	0	0	0.0	N/A	0.0	0.07
2	2150	0	0	0.0	N/A	0.0	0.17
3	1905	0	0	0.0	N/A	0.0	0.28
4	2100	0	0	0.0	N/A	0.0	0.43
5	1850	45	45	0.7	40.1	2.4	0.57
6	2200	150	195	3.0	13.7	6.8	0.72
7	1870	310	505	7.7	5.0	16.6	0.87
8	1820	270	775	11.8	5.7	14.8	1.04
9	2060	265	1040	15.8	6.8	12.9	1.24
10	2100	230	1270	19.3	8.1	11.0	1.45
11	1540	190	1460	22.1	7.1	12.3	1.60
12	2070	230	1690	25.6	8.0	11.1	1.81
13	1910	230	1920	29.1	7.3	12.0	2.01
14	2170	220	2140	32.4	8.9	10.1	2.22

**Table E.27****Run 98: Steam Injection of a Bottom Water Model using a Horizontal Injector and a Horizontal Producer.**

HC Pore Volume:	6670 cc	Type of Oil Used:	Faxam-100
Pore Volume:	13387 cc	Initial Model Temperature:	3°C
Bulk Volume:	42005 cc	Total Flow Rate of Steam:	227.28 cc/min
Porosity:	31.9%	Steam Quality, fst:	0.10
Initial Oil Saturation:	49.8%	Total Steam Volume Injected:	28183 cc (2.11 PV)
Initial Water Saturation:	50.2%		
Bottom Water Thickness:	49.81% (% Gross Thickness)		

**Net Oil Recovery: 40.55%**      **Final Oil Saturation: 29.62%**

Cylinder No.	Total Vol. Produced (cc)	Instantaneous Oil Prod. (cc)	Cumulative Recovery (cc)	Oil Rec. %OOIP	Instantaneous Produced WOR	% Sample Vol. Oleic Phase	Cum. PV Injected
1	2130	0	0	0.0	N/A	0.0	0.10
2	2170	0	0	0.0	N/A	0.0	0.21
3	2220	0	0	0.0	N/A	0.0	0.33
4	2340	0	0	0.0	N/A	0.0	0.48
5	2430	75	75	1.1	31.4	3.1	0.75
6	1750	175	250	3.8	9.0	10.0	0.87
7	1580	390	640	9.7	3.1	24.7	0.98
8	2140	490	1130	17.1	3.4	22.9	1.17
9	1760	380	1510	22.9	3.6	21.6	1.33
10	1840	355	1865	28.3	4.2	19.3	1.50
11	1590	265	2130	32.3	5.0	16.7	1.66
12	1740	230	2360	35.8	6.6	13.2	1.83
13	1810	210	2570	39.0	7.6	11.6	2.02
14	945	135	2705	41.0	6.0	14.3	2.11

**Table E.28**

**Run 99: Steam Injection of a Bottom Water Model using a Horizontal Injector and a Vertical Producer.**

HC Pore Volume:	6010 cc	Type of Oil Used:	Faxam-100
Pore Volume:	13424 cc	Initial Model Temperature:	3°C
Bulk Volume:	42005 cc	Total Flow Rate of Steam:	227.28 cc/min
Porosity:	32.0%	Steam Quality, fst:	0.10
Initial Oil Saturation:	44.8%	Total Steam Volume Injected:	27842 cc (2.07 PV)
Initial Water Saturation:	55.2%		
Bottom Water Thickness:	54.85% (% Gross Thickness)		

**Net Oil Recovery: 38.44%      Final Oil Saturation: 27.56%**

Cylinder No.	Total Vol. Produced (cc)	Instantaneous Oil Prod. (cc)	Cumulative Oil Recovery (cc)	%OOIP	Cum. Oil Rec.	Instantaneous Produced WOR	% Sample Vol. Oteic Phase	Cum. PV Injected
1	2180	0	0	0.0	0.0	N/A	0.0	0.12
2	2180	0	0	0.0	0.0	N/A	0.0	0.24
3	1800	0	0	0.0	0.0	N/A	0.0	0.35
4	2200	0	0	0.0	0.0	N/A	0.0	0.47
5	1810	0	0	0.0	0.0	N/A	0.0	0.58
6	1850	20	20	0.3	0.3	91.5	1.1	0.78
7	1820	360	380	6.3	6.3	4.1	19.8	0.95
8	2270	270	650	10.8	10.8	7.4	11.9	1.14
9	1740	280	930	15.5	15.5	5.2	16.1	1.30
10	1830	310	1240	20.6	20.6	4.9	16.9	1.46
11	1960	275	1515	25.2	25.2	6.1	14.0	1.65
12	1875	240	1755	29.2	29.2	6.8	12.8	1.70
13	2200	480	2235	37.2	37.2	3.6	21.8	2.06
14	295	75	2310	38.4	38.4	2.9	25.4	2.07

**Table E.22**

**Run 100: Steam Injection of a Bottom Water Model using a Vertical Injector and a Vertical Producer.**

HC Pore Volume:	6470 cc	Type of Oil Used:	Faxam-100
Pore Volume:	12809 cc	Initial Model Temperature:	3°C
Bulk Volume:	42005 cc	Total Flow Rate of Steam:	227.28 cc/min
Porosity:	30.5%	Steam Quality, fst:	0.10
Initial Oil Saturation:	50.5%	Total Steam Volume Injected:	28524 cc (2.23 PV)
Initial Water Saturation:	49.5%		
Bottom Water Thickness:	49.18% (% Gross Thickness)		

**Net Oil Recovery: 32.69%      Final Oil Saturation: 34.00%**

Cylinder No.	Total Vol. Produced (cc)	Instantaneous Oil Prod. (cc)	Cumulative Oil Recovery (cc)	Cum. Oil Rec. %OIP	Instantaneous Produced WOR	% Sample Vol. Oleic Phase	Cum. PV Injected
1	1780	0	0	0.0	N/A	0.0	0.11
2	2190	0	0	0.0	N/A	0.0	0.20
3	2005	0	0	0.0	N/A	0.0	0.32
4	2150	0	0	0.0	N/A	0.0	0.44
5	2090	0	0	0.0	N/A	0.0	0.58
6	1830	100	100	1.5	17.3	5.5	0.85
7	2060	220	320	4.9	8.4	10.7	1.04
8	1735	255	575	8.9	5.8	14.7	1.19
9	1835	305	880	13.6	5.0	16.6	1.37
10	1795	280	1160	17.9	5.4	15.6	1.54
11	1975	265	1425	22.0	6.5	13.4	1.75
12	1685	235	1660	25.7	6.2	13.9	1.92
13	1500	235	1895	29.3	5.4	15.7	2.07
14	1630	220	2115	32.7	6.4	13.5	2.23

**Table E.30****Run 101: Steam Injection of a Bottom Water Model using a Horizontal Injector and a Horizontal Producer.**

HC Pore Volume:	11365 cc	Type of Oil Used:	Faxam-100
Pore Volume:	13928 cc	Initial Model Temperature:	3°C
Bulk Volume:	42005 cc	Total Flow Rate of Steam:	227.28 cc/min
Porosity:	33.2%	Steam Quality, fst:	0.10
Initial Oil Saturation:	81.6%	Total Steam Volume Injected:	29092cc (2.09 PV)
Initial Water Saturation:	18.4%		
Bottom Water Thickness:	10.04% (% Gross Thickness)		

**Net Oil Recovery:** 64.54%      **Final Oil Saturation:** 28.93%

Cylinder No.	Total Vol. Produced (cc)	Instantaneous Oil Prod. (cc)	Cumulative Oil Recovery (cc)	Cum. Oil Rec. %OOIP	Instantaneous Produced WOR	% Sample Vol. Oleic Phase	Cum. PV Injected
1	1930	30	30	0.3	63.3	1.6	0.09
2	1400	100	130	1.1	13.0	7.1	0.22
3	2090	455	585	5.1	3.6	21.8	0.38
4	1765	525	1110	9.8	2.4	29.7	0.50
5	2220	685	1795	15.8	2.2	30.9	0.64
6	1960	740	2535	22.3	1.6	37.8	0.77
7	1795	715	3250	28.6	1.5	39.8	0.87
8	1840	790	4040	35.5	1.3	42.9	0.98
9	1650	690	4730	41.6	1.4	41.8	1.10
10	2060	710	5440	47.9	1.9	34.5	1.26
11	1970	580	6020	53.0	2.4	29.4	1.40
12	1795	385	6405	56.4	3.7	21.4	1.55
13	1840	290	6695	58.9	5.3	15.8	1.73
14	2170	320	7015	61.7	5.8	14.7	1.93
15	1920	320	7335	64.5	5.0	16.7	2.09



**Table E.31****Run 102: Steam Injection of a Bottom Water Model using a Horizontal Injector and a Vertical Producer.**

HC Pore Volume:	11310 cc	Type of Oil Used:	Faxam-100
Pore Volume:	14156 cc	Initial Model Temperature:	3°C
Bulk Volume:	42005 cc	Total Flow Rate of Steam:	227.28 cc/min
Porosity:	33.7%	Steam Quality, fst:	0.10
Initial Oil Saturation:	79.9%	Total Steam Volume Injected:	29546 cc (2.09 PV)
Initial Water Saturation:	20.1%		
Bottom Water Thickness:	10.00% (% Gross Thickness)		

**Net Oil Recovery: 47.04%**      **Final Oil Saturation: 42.32%**

Cylinder No.	Total Vol. Produced (cc)	Instantaneous Oil Prod. (cc)	Cumulative Oil Recovery (cc)	%OOIP	Oil Rec. Produced WOR	Instantaneous Produced WOR	% Sample Vol. Oleic Phase	Cum. PV Injected
1	2040	0	0	0.0	0.0	N/A	0.0	0.10
2	1640	10	10	0.1	0.1	163.0	0.6	0.26
3	1840	250	260	2.3	2.3	6.4	13.6	0.39
4	2220	360	620	5.5	5.5	5.2	16.2	0.55
5	1600	420	1040	9.2	9.2	2.8	26.3	0.67
6	2720	720	1760	15.6	15.6	2.8	26.5	0.86
7	1530	490	2250	19.9	19.9	2.1	32.0	0.97
8	1880	640	2890	25.6	25.6	1.9	34.0	1.09
9	1720	520	3410	30.2	30.2	2.3	30.2	1.22
10	1790	460	3870	34.2	34.2	2.9	25.7	1.36
11	1615	355	4225	37.4	37.4	3.5	22.0	1.51
12	2010	355	4580	40.5	40.5	4.7	17.7	1.69
13	1760	320	4900	43.3	43.3	4.5	18.2	1.85
14	2510	420	5320	47.0	47.0	5.0	16.7	2.09

Table E.32

## Run 104: A Continuous Steamflood in a Homogeneous Model.

HC Pore Volume:	12475 cc	Type of Oil Used:	Faxam-100
Pore Volume:	13790 cc	Initial Model Temperature:	3°C
Bulk Volume:	42005 cc	Total Flow Rate of Steam:	227.28 cc/min
Porosity:	32.8%	Steam Quality, fst:	0.10
Initial Oil Saturation:	90.5%	Total Steam Volume Injected:	29433 cc (2.13 PV)
Initial Water Saturation:	9.5%		

Net Oil Recovery: 57.80%      Final Oil Saturation: 38.18%

Cylinder No.	Total Vol. Produced (cc)	Instantaneous Oil Prod. (cc)	Cumulative Oil Recovery (cc)	Cum. Oil Rec. %OOIP	Instantaneous Produced WOR	% Sample Vol. Oleic Phase	Cum. PV Injected
1	1050	680	680	5.5	0.5	64.8	0.16
2	1970	190	870	7.0	9.4	9.6	0.33
3	2320	540	1410	11.3	3.3	23.3	0.48
4	2240	670	2080	16.7	2.3	29.9	0.65
5	1770	710	2790	22.4	1.5	40.1	0.77
6	2050	920	3710	29.7	1.2	44.9	0.87
7	1770	640	4350	34.9	1.8	36.2	0.99
8	2320	760	5110	41.0	2.1	32.8	1.16
9	1850	490	5600	44.9	2.8	26.5	1.31
10	2120	460	6060	48.6	3.6	21.7	1.50
11	1740	260	6320	50.7	5.7	14.9	1.66
12	2120	380	6700	53.7	4.6	17.9	1.85
13	1880	310	7010	56.2	5.1	16.5	2.03
14	1200	200	7210	57.8	5.0	16.7	2.13

**Table E.33**

**Run 105A: A Continuous Waterflood in a Homogeneous Model.**

HC Pore Volume:	13025 cc	Type of Oil Used:	Faxam-100
Pore Volume:	14045 cc	Initial Model Temperature:	3°C
Bulk Volume:	42005 cc	Total Flow Rate of Water:	227.28 cc/min
Porosity:	33.4%	Steam Quality, fst:	0.00
Initial Oil Saturation:	92.7%	Total Water Volume Injected:	25796 cc (1.84 PV)
Initial Water Saturation:	7.3%		

**Net Oil Recovery: 18.39%**      **Final Oil Saturation: 75.69%**

Cylinder No.	Total Vol. Produced (cc)	Instantaneous Oil Prod. (cc)	Cumulative Oil Recovery (cc)	Cum. Oil Rec. %OoIP	Instantaneous Produced WOR	% Sample Vol. Oleic Phase	Cum. PV Injected
1	530	230	230	1.8	1.3	43.4	0.17
2	1840	450	680	5.2	3.1	24.5	0.32
3	2370	340	1020	7.8	6.0	14.3	0.49
4	1680	220	1240	9.5	6.6	13.1	0.62
5	1675	205	1445	11.1	7.2	12.2	0.76
6	1760	185	1630	12.5	8.5	10.5	0.91
7	1820	140	1770	13.6	12.0	7.7	1.06
8	1680	120	1890	14.5	13.0	7.1	1.21
9	1740	140	2030	15.6	11.4	8.0	1.37
10	1660	125	2155	16.5	12.3	7.5	1.52
11	1590	110	2265	17.4	13.5	6.9	1.67
12	1870	130	2395	18.4	13.4	7.0	1.84

**Table E.34**

**Run 105B: A Continuous Steamflood in a Homogeneous Model following a Waterflood (Run 105A).**

HC Pore Volume:	10630 cc	Type of Oil Used:	Faxam-100
Pore Volume:	14045 cc	Initial Model Temperature:	5.8°C
Bulk Volume:	42005 cc	Total Flow Rate of Steam:	227.28 cc/min
Porosity:	33.4%	Steam Quality, fst:	0.10
Initial Oil Saturation:	75.7%	Total Steam Volume Injected:	28296 cc (2.01 PV)
Initial Water Saturation:	24.3%		

**Net Oil Recovery: 42.84%**      **Final Oil Saturation: 38.77%**

Cylinder No.	Total Vol. Produced (cc)	Instantaneous Oil Prod. (cc)	Cumulative Oil Recovery (cc)	%OOIP	Instantaneous Produced WOR	% Sample Vol. Oleic Phase	Cum. PV Injected
1	1800	100	100	0.8	17.0	5.6	0.12
2	1580	130	230	1.8	11.2	8.2	0.27
3	1850	370	600	4.6	4.0	20.0	0.42
4	2100	560	1160	8.9	2.8	26.7	0.57
5	1960	660	1820	14.0	2.0	33.7	0.71
6	2110	800	2620	20.1	1.6	37.9	0.86
7	2010	740	3360	25.8	1.7	36.8	1.00
8	2000	585	3945	30.3	2.4	29.3	1.17
9	1920	460	4405	33.8	3.2	24.0	1.34
10	1640	320	4725	36.3	4.1	19.5	1.50
11	1700	260	4985	38.3	5.5	15.3	1.67
12	1890	305	5290	40.6	5.2	16.1	1.84
13	1830	290	5580	42.8	5.3	15.8	2.01

Table E.35

**Run 106: Solvent-Steamflood in a Bottom Water Model  
using a Horizontal Injector and Horizontal Producer.  
(Solvent Injected from a Horizontal Well.)**

HC Pore Volume:	11370 cc	Type of Oil Used:	Faxam-100
Pore Volume:	14450 cc	Initial Model Temperature:	3°C
Bulk Volume:	42005 cc	Total Flow Rate of Steam:	227.28 cc/min
Porosity:	34.4%	Steam Quality, fst:	0.10
Initial Oil Saturation:	78.7%	Solvent Flow Rate:	200.00 cc/min
Initial Water Saturation:	21.3%	Steam Volume Injected:	28183 cc (1.95 PV)
Bottom Water Thickness:	11.7% (% Gross Thickness)	Solvent Volume Injected:	1400 cc (0.10 PV)

**Net Oil Recovery: 61.98%**      **Solvent Recovery: 86.29%**      **Final Oil Saturation: 29.92%**

Cyl. No.	Solvent Conc. %	Total Vol. Prod. (cc)	Inst. HC Prod. (cc)	Inst. Oil Prod.(cc)	Cumulative Solv. Rec. (%)		Cumulative Oil Rec. (cc)		Inst. Prod. WOR	Inst. HC Prod %Sample	Cum. PV Injected
					(cc)	(%)	(cc)	%OIP			
1	0	1640	0	0	0	0.0	0	0.0	N/A	0.0	0.10
2	50	2370	1105	553	553	39.5	553	4.9	2.3	46.6	0.25
3	29	2150	950	679	823	58.8	1232	10.8	1.8	44.2	0.38
4	18	1880	740	607	956	68.3	1839	16.2	1.9	39.4	0.50
5	12	2005	825	726	1055	75.4	2565	22.6	1.6	41.1	0.63
6	9	2000	810	737	1128	80.6	3302	29.0	1.6	40.5	0.75
7	6	1930	740	696	1173	83.8	3997	35.2	1.7	38.3	0.89
8	4	1790	610	586	1197	85.5	4583	40.3	2.0	34.1	1.02
9	2	1960	560	549	1208	86.3	5132	45.1	2.6	28.6	1.17
10	0	1775	435	435	1208	86.3	5567	49.0	3.1	24.5	1.31
11	0	2040	400	400	1208	86.3	5967	52.5	4.1	19.6	1.49
12	0	1550	280	280	1208	86.3	6247	54.9	4.5	18.1	1.62
13	0	1810	310	310	1208	86.3	6557	57.7	4.8	17.1	1.78
14	0	1670	270	270	1208	86.3	6827	60.0	5.2	16.2	1.92
15	0	1600	220	220	1208	86.3	7047	62.0	6.3	13.8	2.06

Table E.36

## Run 107: A Continuous Steamflood in a Homogeneous Model.

HC Pore Volume:	11640 cc	Type of Oil Used:	Faxam-100
Pore Volume:	13760 cc	Initial Model Temperature:	3°C
Bulk Volume:	42005 cc	Total Flow Rate of Steam:	247.49 cc/min
Porosity:	32.8%	Steam Quality, fst:	0.10
Initial Oil Saturation:	84.6%	Total Steam Volume Injected:	27520 cc (2.00 PV)
Initial Water Saturation:	15.4%		

Net Oil Recovery: 59.84% Final Oil Saturation: 33.98%

Cylinder No.	Total Vol. Produced (cc)	Instantaneous Oil Prod. (cc)	Cumulative Oil Recovery (cc)	Cum. Oil Rec. %OOIP	Instantaneous Produced WOR	% Sample Vol. Oleic Phase	Cum. PV Injected
1	1620	480	480	4.1	2.4	29.6	0.20
2	2015	820	1300	11.2	1.5	40.7	0.29
3	1840	905	2205	18.9	1.0	49.2	0.38
4	1900	800	3005	25.8	1.4	42.1	0.48
5	1740	490	3495	30.0	2.6	28.2	0.58
6	1880	445	3940	33.8	3.2	23.7	0.70
7	1830	370	4310	37.0	3.9	20.2	0.83
8	1875	385	4695	40.3	3.9	20.5	0.95
9	1815	295	4990	42.9	5.2	16.3	1.08
10	1900	315	5305	45.6	5.0	16.6	1.22
11	1930	330	5635	48.4	4.8	17.1	1.37
12	1810	310	5945	51.1	4.8	17.1	1.50
13	1760	260	6205	53.3	5.8	14.8	1.65
14	1815	275	6480	55.7	5.6	15.2	1.79
15	1945	325	6805	58.5	5.0	16.7	1.93
16	890	160	6965	59.8	4.6	18.0	2.00